

AD-A174 001

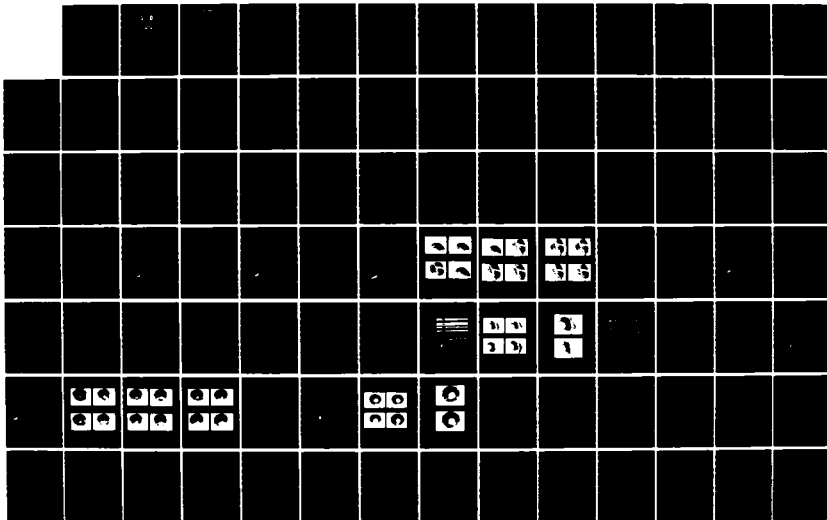
SCALED CENTRIFUGAL COMPRESSOR PROGRAM(U) GARRETT  
TURBINE ENGINE CO PHOENIX AZ G CARGILL ET AL.  
31 OCT 86 21-5464 NASA-CR-174912 NAS3-23277

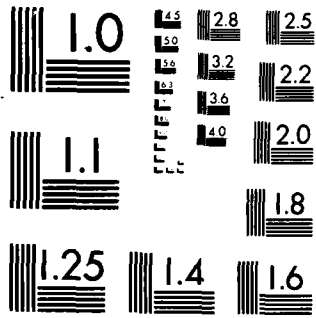
1/3

UNCLASSIFIED

F/G 21/5

NL





MICROCOPY RESOLUTION TEST CHART  
NATIONAL BUREAU OF STANDARDS-1963-A

2

NASA CR-174912  
USAAVSCOM TR-85-C-13  
GARRETT REPORT 21-5464

DTIC  
ELECTE  
NOV 07 1988  
S D  
D. *[Handwritten mark]*

**NASA**

**FINAL REPORT  
FOR**

**SCALED CENTRIFUGAL COMPRESSOR  
PROGRAM**

AD-A174 001

**GARRETT TURBINE ENGINE COMPANY  
A DIVISION OF THE GARRETT CORPORATION  
111 SOUTH 34TH STREET — P.O. BOX 5217  
PHOENIX, ARIZONA 85010**

This document has been approved  
for public release and sale; its  
distribution is unlimited.

PREPARED FOR

**NATIONAL AERONAUTICS AND SPACE ADMINISTRATION**

**NASA LEWIS RESEARCH CENTER  
CONTRACT NAS3-23277**

DTIC FILE COPY

1. Report No. NASA CR-174912 USAAVSCOM-TR-85-C-13		2. Government Accession No. <i>AD-A174001</i>		3. Recipient's Catalog No.	
4. Title and Subtitle  FINAL REPORT FOR SCALED CENTRIFUGAL COMPRESSOR PROGRAM				5. Report Date October 31, 1986	
7. Author(s)  G. CARGILL C. LINDER				6. Performing Organization Code	
9. Performing Organization Name and Address  GARRETT TURBINE ENGINE COMPANY 111 S. 34th Street Phoenix, AZ 85282				8. Performing Organization Report No. Garrett 21-5464	
12. Sponsoring Agency Name and Address U.S. Army Aviation Research and Technology Activity- AVSCOM, Propulsion Directorate, Lewis Research Center, Cleveland, Ohio 44135 and NASA Lewis Research Center, Cleveland, Ohio 44135.				10. Work Unit No. 1L162209AH76 535-05-12	
				11. Contract or Grant No. NAS3-23277	
15. Supplementary Notes  Project Manager, Gary J. Skoch, Propulsion Directorate, U.S. Army Aviation Research and Technology Activity - AVSCOM, Lewis Research Center.				13. Type of Report and Period Covered Contrator Report Final	
16. Abstract  The Scaled Centrifugal Compressor Program (NASA Contract NAS3-23277) has been part of an overall NASA strategy to improve small compressors in turbo-shaft, turbofan, and turboprop engines used in rotorcraft; fixed-wing general aviation, and cruise missile aircraft. Included in this strategy has been an effort to improve performance, durability, and reliability while reducing both initial and life-cycle costs of components for advanced small gas turbine engines. Of particular interest has been the potential of scaling as a means of applying advanced technologies developed for large gas turbine engines to small gas turbine engines. <i>The program has provided NASA with</i>				14. Sponsoring Agency Code	
<p>The Garrett Turbine Engine Company supported this NASA strategy by fulfilling the program objectives of providing centrifugal compressors that can be used to evaluate the effects of direct scaling, and establishing methodology for design adjustments when direct scaling is not mechanically feasible.</p> <p>These objectives were accomplished by the following approaches: (1)</p> <ul style="list-style-type: none"> <li>o Scaling the existing high-performance centrifugal compressor of Contract NAS3-22431 from 10-lb/sec to 2-lb/sec flow size</li> <li>o Making the necessary adjustments to the 2-lb/sec flow size compressor to make it mechanically acceptable</li> <li>o Directly scaling the final 2-lb/sec flow size compressor to 10-lb/sec flow size</li> <li>o Fabricating the resulting 10-lb/sec and 2-lb/sec flow size compressors for testing in the NASA-Lewis Compressor Facilities.</li> </ul>					
17. Key Words (Suggested by Author(s))  CENTRIFUGAL COMPRESSOR SCALE TEST RIG			18. Distribution Statement  Unclassified - unlimited STAR Category 07		
19. Security Classif. (of this report)  UNCLASSIFIED		20. Security Classif. (of this page)  UNCLASSIFIED		21. No. of Pages  189	22. Price*  A

\* For sale by the National Technical Information Service, Springfield, Virginia 22161

## TABLE OF CONTENTS

	<u>Page</u>
SUMMARY	1
SECTION I	
1.0 INTRODUCTION	3
1.1 Background	3
1.2 Relevance and Significance of the Program	3
1.3 Scope of the Program	4
1.4 Purpose of the Program	5
1.5 Overview of the Technical Approach	5
SECTION II	
2.0 AERODYNAMIC SCALING AND ANALYSIS	8
2.1 Baseline Compressor	8
2.2 Design Approach	8
2.3 Mechanical Design Criteria	8
2.4 Aerodynamic Design Criteria	8
2.5 Detailed Aerodynamic Design of the 2-Lb/Sec Impeller	10
2.6 2-Lb/Sec Diffuser Design	16
2.7 Surface Finish Study	23
2.8 10-Lb/Sec Compressor Design	26
SECTION III	
3.0 2-LB/SEC IMPELLER MECHANICAL DESIGN	28
3.1 Impeller Mechanical Blading Design	28
3.2 Impeller Blade Holographic and Acoustic Analyses	28
3.3 Rough-Cut Impeller Blade Holographic and Acoustic Analyses	44
3.4 Impeller Backplate Vibration Analysis	53
3.5 Impeller Backplate Holographic Test Results	53
3.6 Rough-Cut Impeller Backplate Holographic Test Results	60
SECTION IV	
4.0 2-LB/SEC ROTATING COMPONENT ANALYSIS	64
4.1 2-Lb/Sec Impeller Stress and Burst Speed Analysis	64
4.2 Calculation of Moment of Inertia	74
4.3 2-Lb/Sec Test Rig Rotor Dynamics Analysis	74
4.4 2-Lb/Sec Impeller Weight Study	80

TABLE OF CONTENTS (Contd)

	<u>Page</u>
SECTION V	
5.0 2-LB/SEC STATIC COMPONENT ANALYSIS	95
SECTION VI	
6.0 2-LB/SEC TEST RIG DESCRIPTION	99
SECTION VII	
7.0 2-LB/SEC TEST RIG MECHANICAL INTEGRITY	109
7.1 Test Rig Operating Conditions	109
7.2 Hardware Inspection	110
7.3 Balance Results	110
7.4 Test Rig Instrumentation Calibrations	124
SECTION VIII	
8.0 10-LB/SEC ROTATING COMPONENT ANALYSIS	132
8.1 Rotor Burst Speed Calculation	132
8.2 Rotor Cyclic Life Calculation	137
8.3 Calculation of Moment of Inertia	137
8.4 Backplate Vibration Analysis	137
8.5 Compressor Rig Compatibility	141
8.6 Impeller Holographic Test	141
SECTION IX	
9.0 10-LB/SEC STATIC COMPONENT ANALYSIS	153
9.1 Component Definition	153
9.2 Baseline (25-Lb/Sec) Shroud Thermal Analysis	153
9.3 10-Lb/Sec Shroud Thermal Design	155
9.4 Shroud Mechanical Design	160
9.5 10-Lb/Sec LDV Diffuser Design	167

TABLE OF CONTENTS (Contd)

	<u>Page</u>
<b>SECTION X</b>	
<b>10.0 10-LB/SEC HARDWARE MECHANICAL INTEGRITY</b>	<b>179</b>
10.1 Hardware Inspection	179
10.2 Impeller Balance	179
<b>SECTION XI</b>	
<b>11.0 CONCLUSIONS AND RECOMMENDATIONS</b>	<b>188</b>
<b>REFERENCES</b>	<b>189</b>
<b>DISTRIBUTION LIST</b>	<b>190</b>

Accession For	
NTIS GRA&I	<input checked="" type="checkbox"/>
DTIC TAB	<input type="checkbox"/>
Unannounced	<input type="checkbox"/>
Justification	
By	
Distribution/	
Availability Codes	
Dist. Special	

A-1



## LIST OF FIGURES

<u>Figure</u>	<u>Title</u>	<u>Page</u>
1	Modified NASA 2-Lb/Sec Centrifugal Compressor Test Rig Layout	6
2	Iterative Design Logic Flow Chart	12
3	Final Blade Loadings for Shroud Showing Near Duplication of Baseline	13
4	Final Mean Blade Loadings Showing Near Duplication of Baseline	14
5	Final Blade Loadings for Hub Showing Near Duplication of Baseline	15
6	Flow Path for Baseline and Final 2-Lb/Sec Design	17
7	Final 2-Lb/Sec Blade Angle Distributions Adjusted to Control Blade Loading (Carpet Plot)	18
8	Main Blade Normal Thickness Change for 2-Lb/Sec Impeller	19
9	Splitter Blade Normal Thickness Change for 2-Lb/Sec Impeller	20
10	Impeller Surface Angles and Thickness	21
11	Vane Shape Change for 2-Lb/Sec Diffuser	24
12	Change in Loss Shown as a Function of Reynolds Number Change	27
13	Full-Blade Effective Stress Distribution, 110-Percent Speed	29
14	Full-Blade Campbell Diagram	30
15	Splitter-Blade Effective Stress Distribution, 110-Percent Speed	31
16	Splitter-Blade Campbell Diagram	32
17	NASA 2-Lb/Sec Scaled Compressor Main Blade Holography Campbell Diagram	34

LIST OF FIGURES (CONTD)

<u>Figure</u>	<u>Title</u>	<u>Page</u>
18	NASA 2-Lb/Sec Scaled Compressor Blade Mode Shapes	35
19	NASA 2-Lb/Sec Scaled Compressor Blade Mode Shapes	36
20	NASA 2-Lb/Sec Scaled Compressor Blade Mode Shapes	37
21	NASA 2-Lb/Sec Scaled Compressor Acoustic Test Results	40
22	Probe and Strut Circumferential Locations	41
23	Pressure Drop Versus Circumferential Angle At Blade Leading Edge	42
24	NASA 2-Lb/Sec Scaled Compressor Steady-State Stress - 81,319 rpm	45
25	NASA 2-Lb/Sec Compressor Normalized Vibratory Stress	46
26	NASA 2-Lb/Sec Rough-Cut Impeller Acoustic Test Results	49
27	NASA 2-Lb/Sec Rough-Cut Impeller Blade Mode Shapes	50
28	NASA 2-Lb/Sec Rough-Cut Impeller Blade Mode Shapes	51
29	NASA 2-Lb/Sec Rough-Cut Impeller Holography Test Results.	52
30	NASA 2-Lb/Sec Impeller Backplate Vibration Model	54
31	NASA 2-Lb/Sec Compressor Backplate Vibration Campbell Diagram	55
32	NASA 2-Lb/Sec Impeller Backplate Holography Results	56
33	NASA 2-Lb/Sec Scaled Compressor Holography Test Results	57
34	NASA 2-Lb/Sec Scaled Compressor Holography Test Results	58
35	NASA 2-Lb/Sec Scaled Compressor Holography Test Results	59

LIST OF FIGURES (CONTD)

<u>Figure</u>	<u>Title</u>	<u>Page</u>
36	NASA 2-Lb/Sec Rough-Cut Impeller Backplate Vibration Campbell Diagram	61
37	NASA 2-Lb/Sec Rough-Cut Impeller Holography Test Results	62
38	NASA 2-Lb/Sec Rough-Cut Impeller Holography Test Results	63
39	NASA 2-Lb/Sec Impeller Finite Element Model	65
40	Temperature Distribution of 10-Lb/Sec Scaled Impeller	66
41	NASA 2-Lb/Sec Scaled Compressor: 105-Percent Speed Effective Distribution	68
42	NASA 2-Lb/Sec Scaled Compressor: 105-Percent Speed Tangential Stress Distribution	69
43	NASA 2-Lb/Sec Scaled Compressor: 105-Percent Speed Radial Stress Distribution	70
44	NASA 2-Lb/Sec Scaled Compressor: 105-Percent Speed Two-Dimensional Hubline Deflection	72
45	NASA 2-Lb/Sec Scaled Compressor: 100-Percent Speed Three-Dimensional Blade Displacement, 81,319 rpm	73
46a	2-Lb/Sec Compressor Rig Rotor Dynamics Schematic	77
46b	2-Lb/Sec Compressor Rig Rotor Dynamic Analysis Model	77
47	Structural Stiffness Versus Critical Speed	78
48	Deflection Versus Axial Distance, Modes 1 to 4	79
49	Unbalance Condition Load Versus Speed, In-Phase	81
50	Unbalance Condition Displacement Versus Speed, In-Phase	82
51	Unbalance Condition Load Versus Speed, Out-Of-Phase	83

LIST OF FIGURES (CONTD)

<u>Figure</u>	<u>Title</u>	<u>Page</u>
52	Unbalance Condition Displacement Versus Speed, Out-Of-Phase	84
53	Unbalance Condition Load Versus Speed, Out-Of-Phase	85
54	Unbalance Condition Displacement Versus Speed, Out-Of-Phase	86
55	Unbalance Condition Load Versus Speed, In-Phase	87
56	Unbalance Condition Displacement Versus Speed, In-Phase	88
57	2-Lb/Sec Compressor Rig; Effect of Mass and Inertia on Critical Speed	90
58	NASA 2-Lb/Sec Compressor Rig Unbalance Response With 1.5 Times Nominal Impeller Mass	91
59	NASA 2-Lb/Sec Compressor Rig Unbalance Response with Nominal Impeller Mass	92
60	NASA 2-Lb/Sec Compressor Rig Unbalance Response with One-Half Nominal Impeller Mass	93
61	NASA 2-Lb/Sec Compressor Rig; Effect of Mass and Inertia on Maximum Bearing Load	94
62	2-Lb/Sec Test Rig Static Structure Finite Element Model	96
63	2-Lb/Sec Test Rig Static Structure Thermal Distribution at 100-Percent Speed	97
64	Magnified Thermal Deflection of 2-Lb/Sec Test Rig Static Structure (100-Percent Speed)	98
65	Test Rig Instrumentation Summary	100
66	Total Temperature Performance Rakes	101
67	Total Pressure Performance Rakes	102
68	Modified NASA 2-Lb/Sec Centrifugal Compressor Test Rig Layout	103

LIST OF FIGURES (CONTD)

<u>Figure</u>	<u>Title</u>	<u>Page</u>
69	Spring Cage Design	105
70	Compressor Bearing Hydraulic Mount Design	106
71	NASA 2-Lb/Sec Scaled Compressor Test Rig	108
72	2-Lb/Sec Shroud Contour Inspection Results (P/N 3554662-1)	111
73	2-Lb/Sec Diffuser Inspection Results (P/N 3554663-1)	112
74	2-Lb/Sec Impeller Inspection Results (P/N 3554664-1) Hub and Shroud Profile	113
75	Vane Diffuser Throat Area	114
76	NASA 2-Lb/Sec Impeller	116
77	NASA 2-Lb/Sec Diffuser Prior to Braze	117
78	2-Lb/Sec Impeller Balance Plane Locations	118
79	NASA Drive Turbine Rotor Balance Results	120
80	NASA 2-Lb/Sec Rotating Group	121
81	NASA 2-Lb/Sec Rotating Group Runouts	122
82	NASA 2-Lb/Sec Rotating Group Balance Plane Locations	123
83	Strain Gage Installation Information Sheet	125
84	Thrust Ring Strain Gage Calibration	126
85	Forward Bently Probe Calibration - Vertical	127
86	Forward Bently Probe Calibration - Horizontal	128
87	Aft Bently Probe Calibration - Vertical	129
88	Aft Bently Probe Calibration - Horizontal	130
89	Finite-Element Model	133
90	Tangential Stress Distribution at 105-Percent Speed	134

LIST OF FIGURES (CONTD)

<u>Figure</u>	<u>Title</u>	<u>Page</u>
91	Effective Stress Distribution at 105-Percent Speed	135
92	Titanium 6-4 Life Diagram	138
93	Backplate Model Vibration Analysis	140
94	10-Lb/Sec Compressor Rig Unbalance Response with Original 10-Lb/Sec Compressor	142
95	10-Lb/Sec Compressor Rig Unbalance Response with 10-2-10-Lb/Sec Scaled Compressor	143
96	Full-Blade Campbell Diagram from Holographic Testing	144
97	NASA 10-Lb/Sec Impeller Holographic Blade Modes	146
98	NASA 10-Lb/Sec Impeller Holographic Blade Modes	147
99	NASA 10-Lb/Sec Impeller Holographic Blade Modes	148
100	Back Plate Campbell Diagram From Holographic Testing	149
101	NASA 10-Lb/Sec Impeller Holography Results	150
102	NASA 10-Lb/Sec Impeller Holography Results	151
103	NASA 10-Lb/Sec Impeller Holography Results	152
104	Baseline (25-Lb/Sec) Shroud and Inlet Duct Metal Temperatures (F)	154
105	Baseline (25-Lb/Sec) Shroud and Fluid Stream Temperatures (F)	156
106	Shroud Heat Flux, Baseline Compressor (25-Lb/Sec)	157
107	Thermal Scaling of Compressor Rotor and Shroud	158
108	Comparison of Shroud and Rotor Heat Flux Rates for a Similar GTEC Centrifugal Compressor	159
109	Comparison of the Shroud (25-Lbm/Sec and P/N 3553028 10-Lbm/Sec) Conductivity	161
110	Bulk-Fluid Temperature Rise Due to Shroud Conductivity	162

LIST OF FIGURES (CONTD)

<u>Figure</u>	<u>Title</u>	<u>Page</u>
111	Metal and Fluid Temperature Comparison of the Two Shrouds	163
112	Thermal Design Process	164
113	Metal Temperature Comparison Between Baseline 25-Lb/Sec Shroud and Thermally Scaled 10-Lb/Sec Shroud (P/N 3553145)	165
114	10-Lb/Sec Performance Shroud (P/N 3553145) Stress Distribution	166
115	LDV Shroud Design Model	168
116	LDV Shroud Cross Section	169
117	LDV Shroud Deflection (P/N 3553146)	170
118	10-Lb/Sec LDV Diffuser (P/N 3553147-2)	171
119	Campbell Diagram for Cantilevered Vane	173
120	Campbell Diagram for Cantilevered Splitter	174
121	Cantilevered Vane Mode Shapes	177
122	Cantilevered Splitter Mode Shapes	178
123	NASA 10-Lb/Sec Impeller (P/N 3553144-1)	180
124	10-Lb/Sec Impeller Inspection Results (P/N 3553144-1) Hub and Shroud Contour	181
125	Diffuser Inspection Results	182
126	10-Lb/Sec LDV Diffuser Prior to Braze	183
127	Performance Shroud and Diffuser Assembly	185
128	10-Lb/Sec Balance Plane Results	187

LIST OF TABLES

<u>Table</u>	<u>Title</u>	<u>Page</u>
1	Comparison of 2-Lb/Sec Design with Baseline	22
2	Acoustic Test Results: NASA 2-Lb/Sec Scaled Compressor, All Blades and Backplate Damped Except Blade Under Test	38
3	Fourier Analysis of the NASA 2-Lb/Sec Rig Inlet Strut and Probe Configuration	43
4	2-Lb/Sec Rough-Cut Impeller Blade Frequencies Obtained During Acoustic and Holography Tests	48
5	NASA 2-Lb/Sec Compressor Disk Actual and Allowable Stress Levels	71
6	Computer Mechanical Analysis NASA Schedule 2-Lb/Sec Impeller	75
7	Test Rig Service Conditions	109
8	Summary of Measured Throat Widths	115
9	Thermocouple Calibration Results	131
10	Impeller Disk Stress Margins	136
11	Inertia Properties Computer Printout	139
12	Summary of Vibration Analysis	172
13	Holography Results	176
14	Performance Shroud Contour Inspection (P/N 3553145-1)	184
15	10-Lb/Sec LDV Shroud (P/N 3553146-1) Flow Path Inspection Results	186

## SUMMARY

The Scaled Centrifugal Compressor Program (NASA Contract NAS3-23277) has been part of an overall NASA strategy to improve small compressors in turboshaft, turbofan, and turboprop engines used in rotorcraft, fixed-wing general aviation, and cruise missile aircraft. Included in this strategy has been an effort to improve performance, durability, and reliability while reducing both initial and life-cycle costs of components for advanced small gas turbine engines. Of particular interest has been the potential of scaling as a means of applying advanced technologies developed for large gas turbine engines to small gas turbine engines.

The Garrett Turbine Engine Company supported this NASA strategy by fulfilling the program objectives of (1) providing centrifugal compressors that can be used to evaluate the effects of direct scaling, and (2) establishing methodology for design adjustments when direct scaling is not mechanically feasible.

These objectives were accomplished by the following approaches:

- o Scaling the existing high-performance centrifugal compressor of Contract NAS3-22431 from 10-lb/sec to 2-lb/sec flow size
- o Making the necessary adjustments to the 2-lb/sec flow size compressor to make it mechanically acceptable
- o Directly scaling the final 2-lb/sec flow size compressor to 10-lb/sec flow size

- o Fabricating the resulting 10-lb/sec and 2-lb/sec flow size compressors for testing in the NASA-Lewis Compressor Facilities.

Garrett performed complete design studies and analyses for the modified 2-lb/sec test rig. This test rig has been designed to operate at maximum air pressures and temperatures of 126 psia and 686F, respectively. The test rig shafting was designed to operate smoothly throughout a speed range up to 140,000 rpm.

The 10-lb/sec hardware supplied under this contract (two shrouds, two diffusers, one impeller) is interchangeable with existing test rig hardware supplied to NASA under Contract NAS3-22431). Both 10-lb/sec shrouds are thermal scales of a baseline 25-lb/sec shroud designed for the U.S. Air Force under contract F33615-74-C-2006. One of the new shrouds supplied under this contract will be for aerodynamic performance evaluation. The other is for Laser Doppler Velocimeter (LDV) activities. The 10-lb/sec impeller is an exact scale of the 2-lb/sec impeller.

Both the 2-lb/sec and the 10-lb/sec hardware furnished under this contract should facilitate the acquisition of meaningful test data that will fulfill the overall program objectives.

## 1.0 INTRODUCTION

This document is submitted by the Garrett Turbine Engine Company (GTEC), a division of The Garrett Corporation. It presents the Final Report for the Scaled Centrifugal Compressor Program, which was conducted from February 18, 1982, through February 18, 1985, for the NASA-Lewis Research Center (NASA-LeRC) under Contract NAS3-23277.

### 1.1 Background

NASA-LeRC is active in developing large and small flow-class compressors. The Scaled Centrifugal Compressor Program has provided NASA-LeRC with a modified 2-lb/sec flow-class compressor test rig that will facilitate complete and varied testing of compressors in this flow class. Additionally, a 10-lb/sec impeller, two 10-lb/sec shrouds, and two 10-lb/sec diffusers were supplied to be used to further investigate the effects of scaling. This 10-lb/sec hardware is capable of being tested in the 10-lb/sec test rig supplied under Contract NAS3-22431.

### 1.2 Relevance and Significance of the Program

The Scaled Centrifugal Compressor Program has been part of an overall NASA strategy to improve small compressors in turbo-shaft, turbofan, and turboprop engines used in rotorcraft, fixed-wing general aviation, and cruise-missile aircraft. Included in this strategy has been an effort to improve performance, durability, and reliability while reducing both initial and life-cycle costs of components for advanced, small gas turbine engines. Of particular interest has been the potential of scaling as a means of applying advanced technologies developed for large gas turbine engines to small gas turbine engines.

The Scaled Centrifugal Compressor Program supported this NASA strategy by providing a scaled centrifugal compressor stage (or, impeller\*) and an appropriate test rig capable of evaluating the effects of scaling on aerodynamic performance. The program also provided NASA with 10-lb/sec test rig capabilities for characterizing the flow within blade passages by the use of Laser Anemometry (LA) measurements.

### 1.3 Scope of the Program

GTEC furnished all labor, services, and materials to design, fabricate, and assemble the modified 2-lb/sec test rig and the 10-lb/sec hardware. The statement of work consisted of the following tasks:

<u>Task No.</u>	<u>Activity</u>
I	Preliminary design of the 2-lb/sec compressor
II	Final design of the 2-lb/sec compressor
III	Final design of the 10-lb/sec compressor
IV	Fabrication/procurement of the 10-lb/sec compressor
V	Program management and reporting
VI	Fabrication/procurement of the 2-lb/sec compressor
VII	2-lb/sec test rig modification design
VIII	Fabrication/procurement of the 2-lb/sec test rig modifications

---

\*Hereafter, the centrifugal compressor stages are referred to as impellers. For simplicity, "compressor" is used to refer to the larger system which includes the impeller.

#### 1.4 Purpose of the Program

This program has two objectives: (1) to provide centrifugal compressors that can be used to evaluate the effects of direct scaling, and (2) to establish methodology for design adjustments when direct scaling is not mechanically feasible.

These objectives were accomplished by the following approach:

- o Scale the existing high-performance centrifugal compressor of Contract NAS3-22431 from 10-lb/sec to 2-lb/sec flow size
- o Make the necessary adjustments to the 2-lb/sec flow size compressor to make it mechanically acceptable
- o Directly scale the final 2-lb/sec flow size compressor to 10-lb/sec flow size
- o Fabricate the resulting 10-lb/sec and 2-lb/sec flow size compressors for testing in the NASA-Lewis compressor facilities.

#### 1.5 Overview of the Technical Approach

The NASA 2-lb/sec test rig (Figure 1), which will operate in a vertical position, is a modification of a previous NASA compressor rig. It is a two-bearing arrangement with the centrifugal compressor overhung on the forward (top) side and a single-stage drive turbine overhung on the aft (bottom) side of the bearings. A thrust balance system is used to maintain a constant load in the compressor direction on the thrust (aft) bearing. Instrumentation locations are provided to monitor impeller-to-shroud clearance, thrust load, shaft excursion, compressor speed,

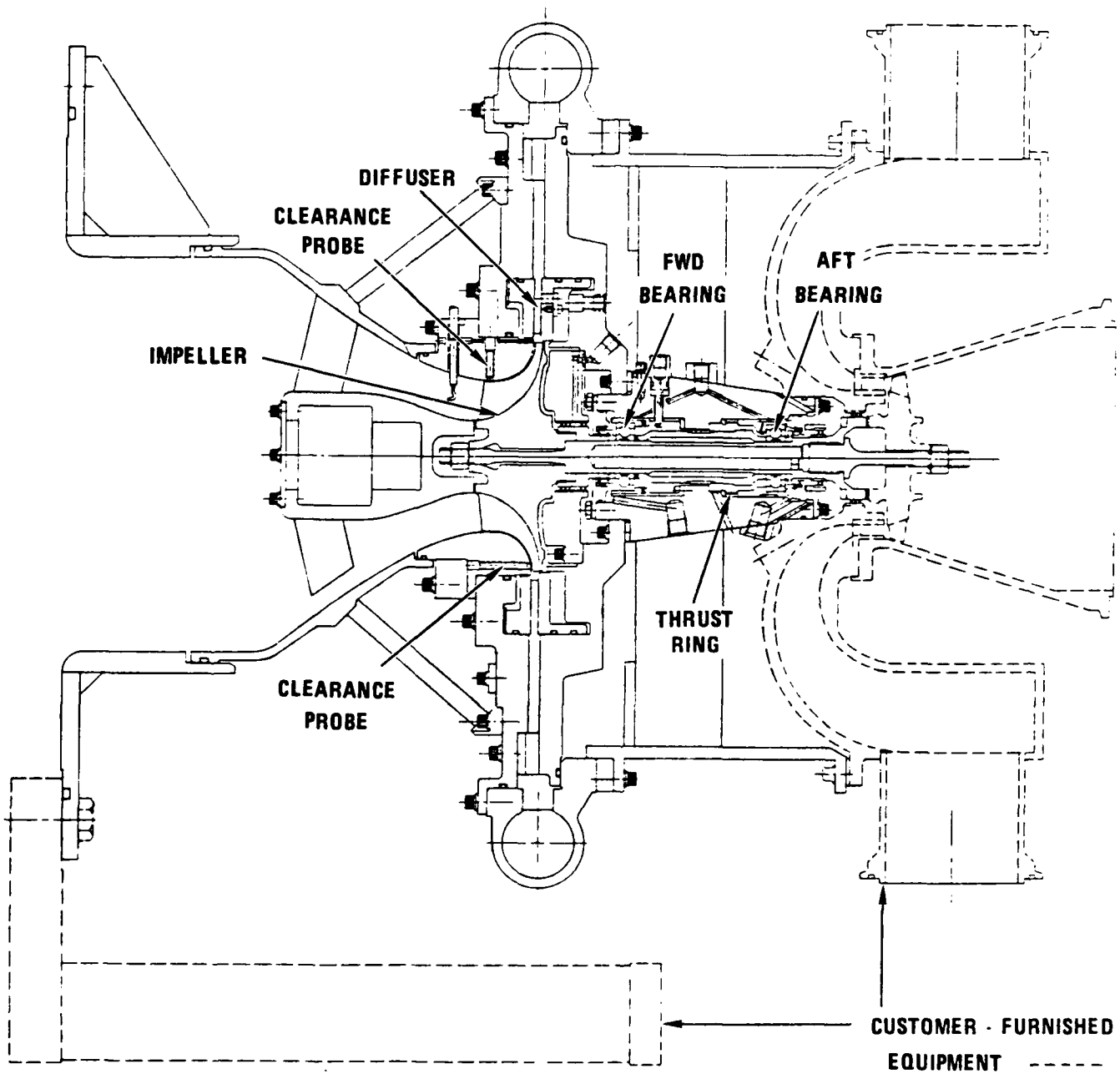


Figure 1. Modified NASA 2-lb/Sec Centrifugal Compressor Test Rig Layout.

bearing outer race temperatures, flow path static pressures, and air-seal pressures. Compressor performance is determined by total temperature and total pressure performance rakes located at the diffuser exit.

#### 1.5.1 Aerodynamic Scaling

The baseline compressor for this effort was the existing 10-lb/sec high performance centrifugal compressor fabricated under NASA contract NAS3-22431. This baseline compressor was an exact scale from the cold shape coordinates of the 25-lb/sec compressor, designed for the U.S. Air Force under Contract F33615-74-C-2006 and GTEC R&D.

The configuration of the NASA 2-lb/sec impeller was generated by applying a scaling factor to the manufacturing coordinates (cold shape) of the baseline impeller. The resulting coordinates were then adjusted to make the impeller mechanically acceptable. The impeller-to-shroud running clearance was scaled by the same factor. This scaling factor, which is equal to 0.4472, was calculated by taking the square root of the ratio of the scaled compressor air flow to the baseline compressor air flow.

To define the aerodynamic flow path geometry for the 10-lb/sec version of the 2-lb/sec modified compressor, all flow path coordinates of the aerodynamic components of the 2-lb/sec compressor were multiplied by a linear scale factor of  $10/2 = 2.2361$ .

## 2.0 AERODYNAMIC SCALING AND ANALYSIS

### 2.1 Baseline Compressor

The baseline compressor for this effort was the existing 10-lb/sec high performance centrifugal compressor fabricated under NASA Contract NAS3-22431. This baseline compressor was in turn an exact scale from the cold shape coordinates of the 25-lb/sec compressor, designed for the U.S. Air Force under Contract F33615-74-C-2006 and GTEC R&D.

### 2.2 Design Approach

The aerodynamic design approach focused on the following goals:

- o The establishment of manufacturing design criteria with respect to minimum blade thickness, minimum diffuser vane thickness, and dimensional tolerance based on normal production fabrication methods.
- o Definition of a 2-lb/sec compressor stage scaled as closely as possible to the baseline compressor, while conforming to the design criteria.
- o Modify the defined configuration to achieve aerodynamic similarity with the baseline compressor while preserving the mechanical characteristics of the baseline design.
- o Exactly scale the modified 2-lb/sec configuration scaled up to 10-lb/sec through use of a linear scale factor of  $\sqrt{10/2} = 2.2361$ .
- o Determine a surface finish for the scaled compressor and establish the Reynolds number effects.

### 2.3 Mechanical Design Criteria

Scaling the baseline 10-lb/sec compressor by a linear factor of  $\sqrt{2/10}$  would result in a minimum blade thickness approaching 0.007 inch. To determine the practicality of this blade thickness, discussions were conducted with vendors, the GTEC manufacturing engineering department, and NASA personnel.

Taking into consideration material deflections, machine limitations, required tolerances, and resistance to foreign object damage (FOD) and handling, it was concluded that a minimum practical normal thickness for the impeller and the vaned diffuser blading would be 0.012 inch for the 2-lb/sec design. It was also concluded that a blade contour tolerance of  $\pm 0.002$  inch could be held in the thinnest blade areas. Thus, a modification of the exact scaled baseline impeller to incorporate the relatively thicker blading was required. In addition, current manufacturing technology does not permit a radius less than 0.040 inch. This was the minimum fillet radius specified on the 2-lb/sec compressor.

### 2.4 Aerodynamic Design Criteria

The criteria for the redesign of the 2-lb/sec compressor were as follows:

- o The work input  $\Delta T/T$  of the impeller was set equal to that of the baseline.
- o The exit blade angles (backward curvature) of the baseline were retained.
- o Design axial running clearance was scaled from the baseline.

- o The cold fixed-shroud contour was an exact scale of the cold baseline-shroud contour.
- o The baseline blade relative velocity distributions were duplicated as closely as possible within the developed constraints.
- o The impeller throat area of the new design was set to provide at least as much choke margin as that of the baseline.
- o Blade stress levels and vibratory characteristics approximated those of the baseline.
- o The leading-edge incidence was set using the same design criteria rules as applied to the baseline.
- o The splitter leading edge was adjusted by the same technique as for the baseline to minimize incidence and diffusion losses.

## 2.5 Detailed Aerodynamic Design of the 2-Lb/Sec Impeller

During the detailed design of the impeller the question was raised as to whether the 2-lb/sec compressor should be optimized for the Reynolds Number regime associated with its size. This would mean that boundary-layer blockages and friction-loss models would be modified from the baseline values.

At NASA's request, the detailed design was carried out with blockage and loss models retained from the baseline in order to provide a truer measure of the effects of scaling from 10-lb/sec to 2-lb/sec.

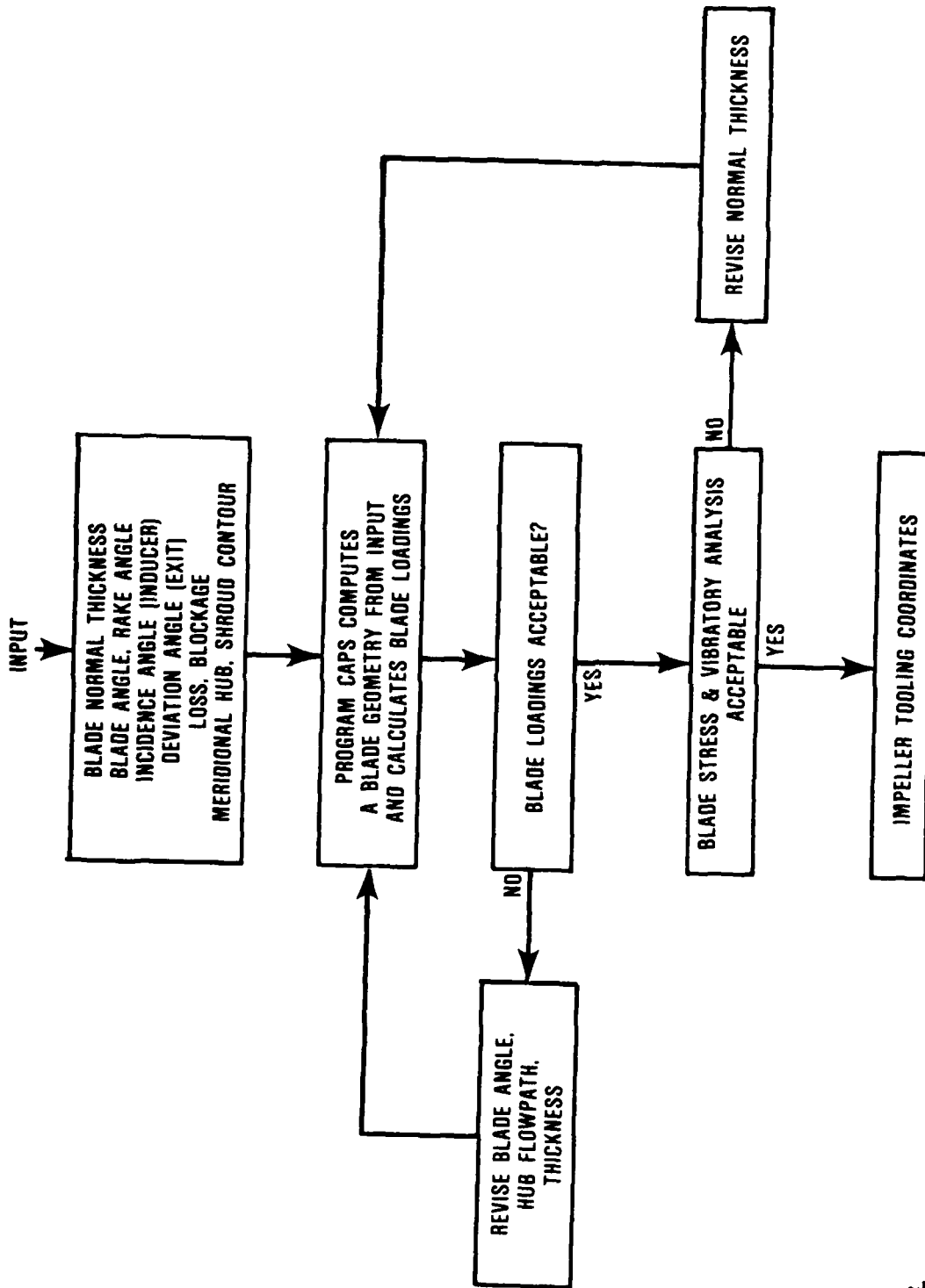
The modification was initiated by adding 0.005 inch to all normal thickness values of a direct scale of the baseline impeller. A mechanical analysis of the resulting geometry indicated a need to increase blade thickness in the trailing-edge hub region to reduce stress levels and to decrease thickness in the inducer region to achieve a blade frequency of 3.5/rev as in the baseline.

Blade thickness was modified as required, and the leading-edge of the blade was adjusted to match the baseline incidence rules. Based on a preliminary design analysis, the exit blade height was increased slightly to retain the baseline work level ( $\Delta T/T$ ).

The iterative design logic used in the many modification combinations evaluated in the design process is detailed in Figure 2. The aerodynamic flow solution for these initial changes showed a need to adjust the flow area to better match baseline loadings. A combination of thickness modifications and hub recontour was made (upstream of the splitter leading edge) to improve the loading match. An acceptable aerodynamic solution was then achieved.

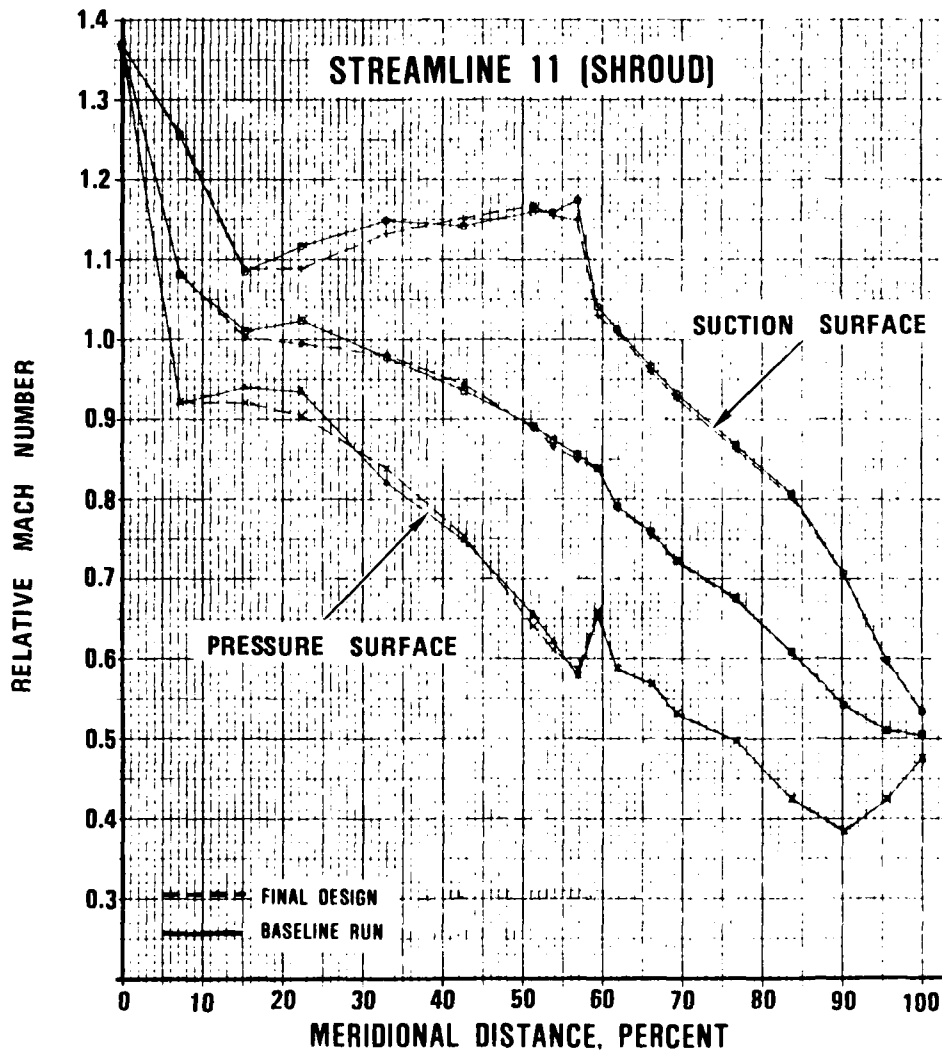
The splitter and main blade had been treated as being identical up to this point in the calculation. To make the splitter similar to the baseline design, the splitter blade thickness was reduced (from the main blade) by the same difference used for the baseline impeller (down to the 0.012 min. thickness allowed). The hub contour was also adjusted to compensate for the average blade thickness change in the splitter region. The splitter leading edge was subsequently shifted, using the identical procedure followed for the baseline, to give a 50/50 flow split.

Final blade loadings, based on the average thickness of splitter and main blade, are shown in Figures 3, 4, and 5 for



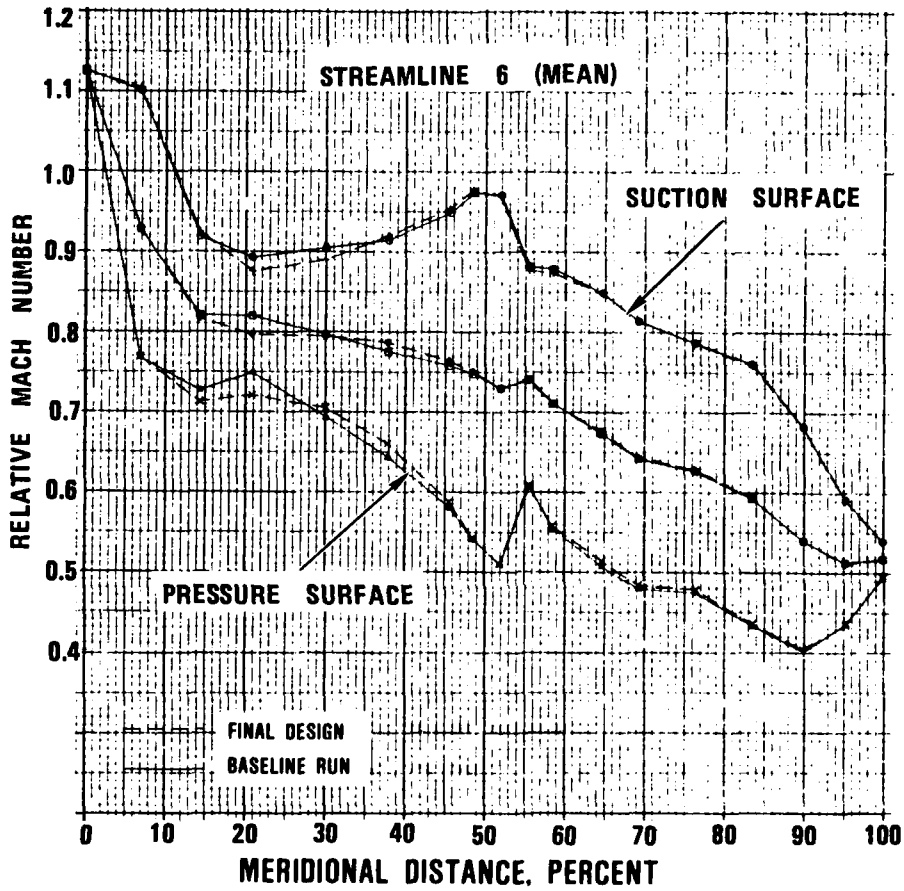
82-12-1482

Figure 2. Iterative Design Logic Flow Chart.



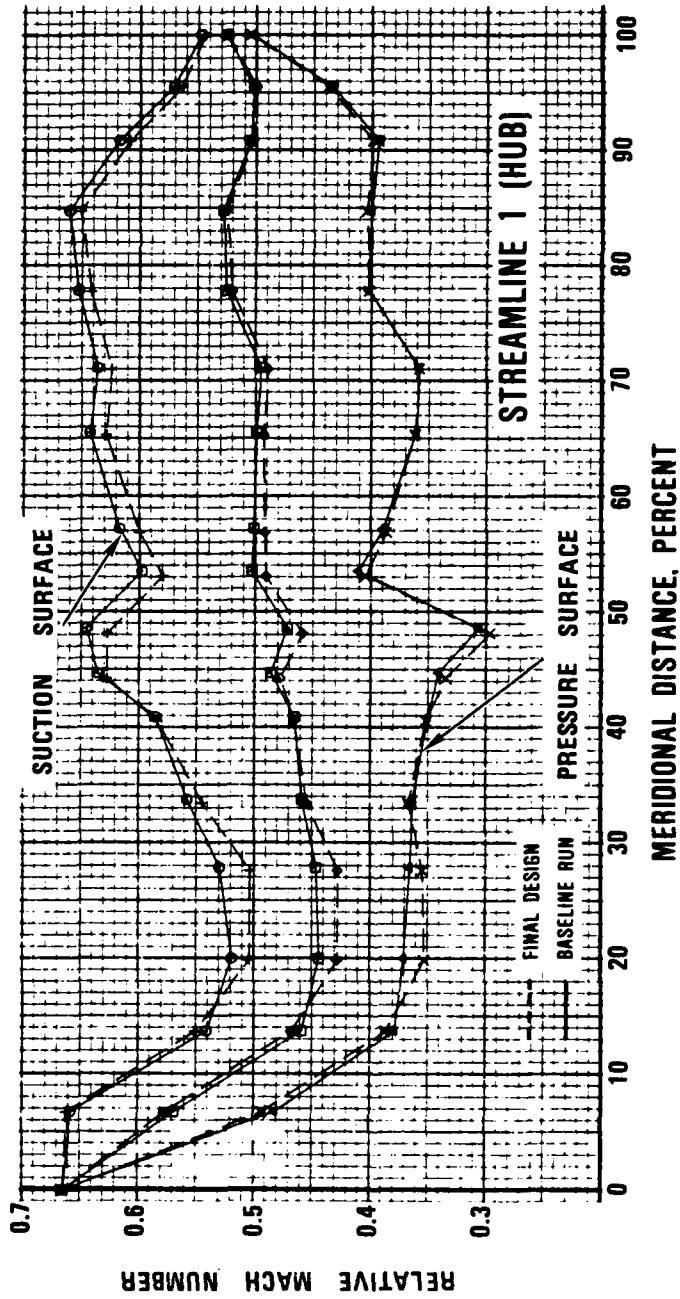
82-12-1491

Figure 3. Final Blade Loadings for Shroud Showing Near Duplication of Baseline.



82-12-1485

Figure 4. Final Mean Blade Loadings Showing Near Duplication of Baseline.



82-12-1490

Figure 5. Final Blade Loadings for Hub Showing Near Duplication of Baseline.

hub, mean, and shroud. All mechanical requirements for this blade design were met.

Impeller clearances were scaled, as well as blade geometry to maintain comparable performance. The 25-lb/sec AFAPL compressor was tested with an impeller axial running clearance value of 0.015 inch. Scaling to 10 lb/sec results in an axial clearance value of 0.0094 inch. Further scaling to 2 lb/sec implies the impeller axial clearance must be 0.0043 inch. These clearances were included in the design of the corresponding shroud contours.

Comparison of the flow path for baseline and final 2-lb/sec design is shown in Figure 6. Blade angle plots of the redesign are shown in Figure 7. The only blade angle difference from the baseline occurs in the leading edge region where an adjustment was made for the increased thickness. A comparison of the normal thicknesses is shown for main blade and splitters in Figures 8 and 9, respectively.

Because of the exaggerated scale used in the thickness plot of Figure 8, it appears that an abrupt change in thickness occurs at about 55 percent of the meridional length, which could cause a discontinuity. Figure 10, which is plotted with a true scale, indicates that the blade is still smooth.

The close agreement between blade relative velocity distributions for the 2-lb/sec final design and the baseline should guarantee aerodynamic equivalence. Performance differences between the two impellers should represent true size or scale effects.

## 2.6 2-Lb/Sec Diffuser Design

In the design of the vaned diffuser, an attempt was made to retain all important parameters from the baseline design, with the exception of the leading-edge thickness of the main and splitter vanes. This was set at a minimum of 0.012 inch in accordance with the mechanical design criteria.

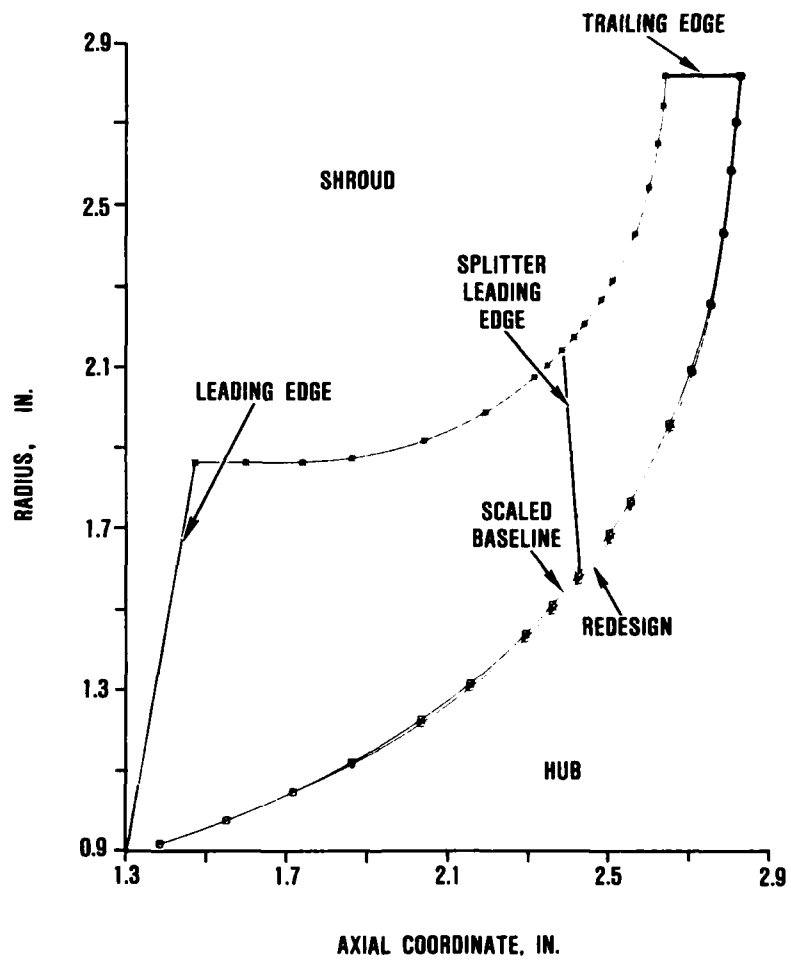
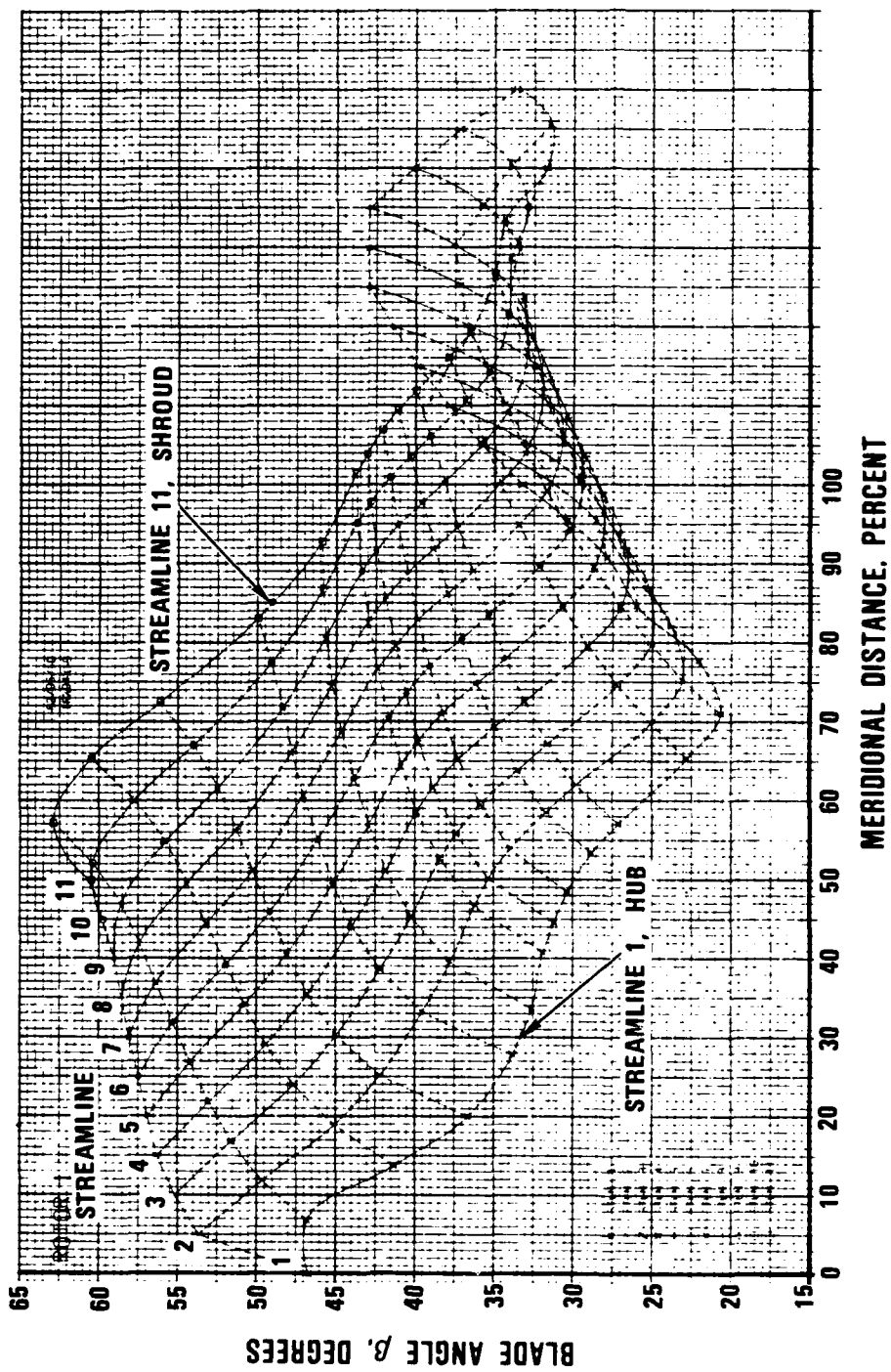
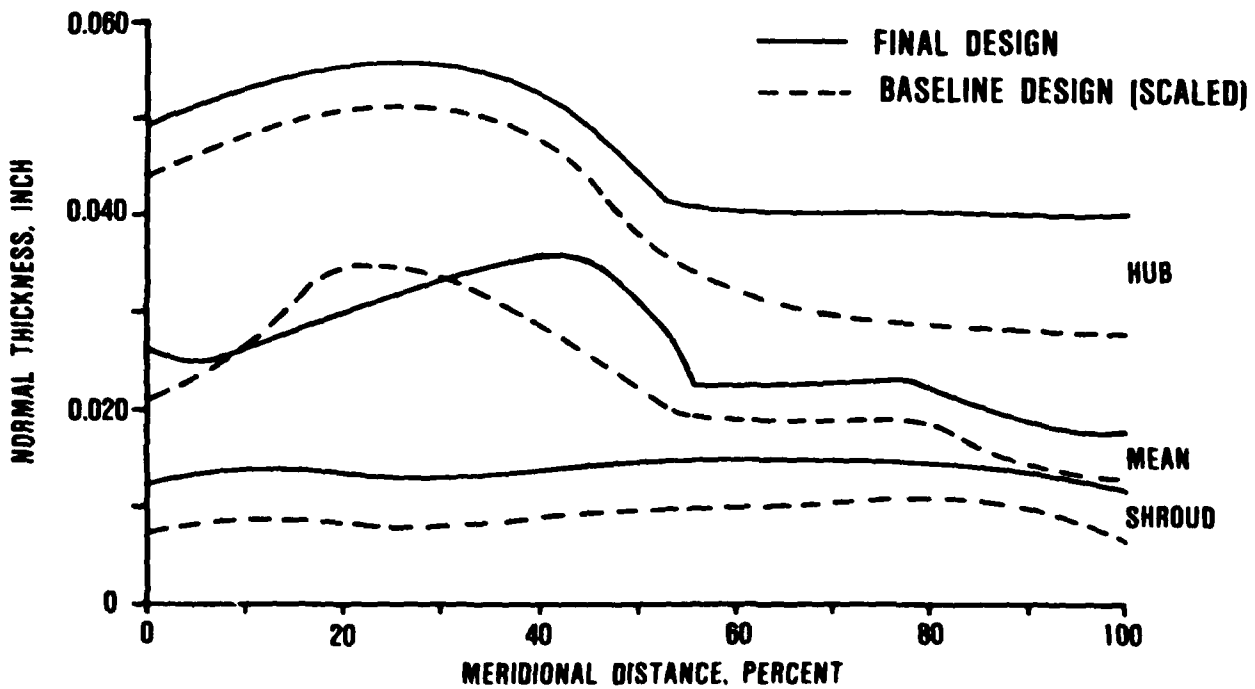


Figure 6. Flow Path for Baseline and Final 2-lb/Sec Design.



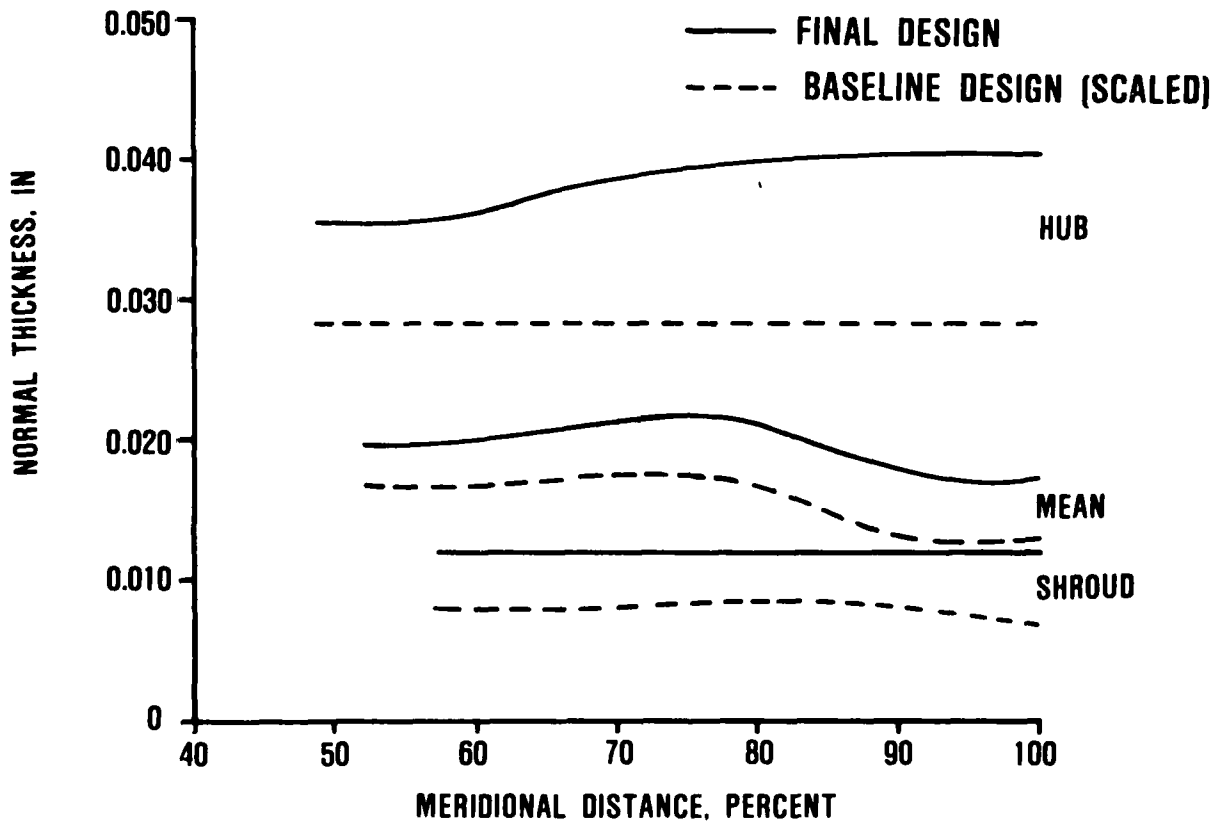
82-12.1487

Figure 7. Final 2-lb/Sec Blade Angle Distributions Adjusted to Control Blade Loading (Carpet Plot.)



82-12-1484

Figure 8. Main Blade Normal Thickness Change for 2-lb/Sec Impeller.



82-12-1486

Figure 9. Splitter Blade Normal Thickness Change for 2-lb/Sec Impeller.

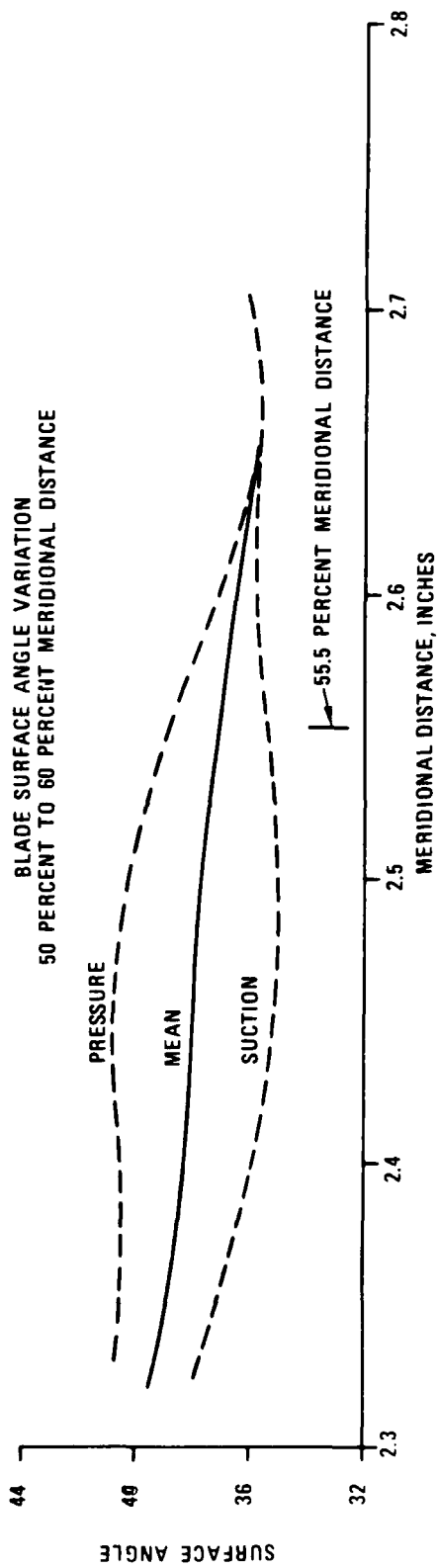
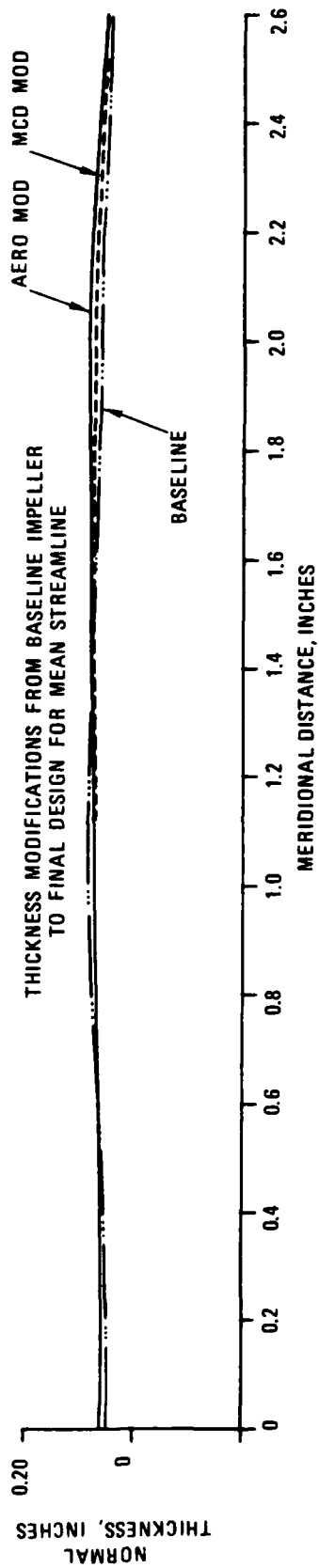


Figure 10. Impeller Surface Angles and Thickness.

TABLE 1. COMPARISON OF 2-LB/SEC DESIGN WITH BASELINE.

Parameter	2-lb/sec	Baseline Design (Scaled)
Vane Number: Full Vanes	21	21
Splitter Vanes	21	21
Vane Inlet Radius, Inches	3.030	3.030
Vane Exit Radius, Inches	3.734	3.734
Splitter L.E. Radius, Inches	3.186	3.186
Passage Height, Inches	0.1766	0.173
Total Throat-to-Capture Ratio	1.215	1.215
Upper Throat	0.1602	0.164
Lower Throat	0.1577	0.161
Full Vane Leading Edge Incidence Angle, Degrees	-5.38 (mean)	-5.38
Total Throat Area, Square Inches	1.179	1.181
Upper Channel Divergence Angle (2θ)	6.7	7.07
Lower Channel Divergence Angle (2θ)	4.4	4.4
Main Blade L.E. Thickness, Inches	0.012	0.006
Splitter Blade L.E. Thickness, Inches	0.012	0.006
Main Blade T.E. Thickness, Inches	0.040	0.028
Splitter Blade T.E. Thickness, Inches	0.040	0.024
Vane Inlet Air Angle, Degrees	73.22	72.78

Table 1 shows the degree to which the parameters were retained. (In comparing the 2-lb/sec design with the baseline design in Table 1, linear dimensions from the baseline were scaled by  $\sqrt{2/10}$ , and areas were reduced by 2/10.)

In order to maintain the important design features while increasing the leading edge thickness, considerable modification was required of the main and splitter vane because of the blade height change required in the impeller to retain  $\Delta T/T$ . The throat openings were slightly reduced in order to maintain the total throat area of the baseline shapes.

The final 2-lb/sec diffuser configuration is presented in Figure 11.

The degree of retention of the important aerodynamic features ensures that only scaling should affect performance.

### 2.7 Surface Finish Study

Of significant concern was the possible need to scale the surface finish of the NASA 2-lb/sec impeller and diffuser to retain hydraulic similarity to the baseline compressor; consequently, a surface-finish study was conducted. Based upon the work of Schlichting (Ref. 1), it was recognized that, to have a hydraulically smooth surface, the magnitude of the surface finish must be less than that which corresponds to the maximum allowable surface protuberance height ( $K_{adm}$ ) for a given velocity and density,

where 
$$K_{adm} \leq \frac{\text{Kinematic Viscosity}}{\text{Free Stream Velocity}} \times 10^2.$$

Since the relationship between  $K_{adm}$  and rms surface finish is a function of the shape of the surface waveform (Ref.2), three surface waveforms typical of machined surfaces were used to determine the required surface finish for the value of  $K_{adm}$  calculated from the above equation.



- o For the NASA impeller, the minimum value of  $K_{adm}$  is 136.8  $\mu$ inch; this occurs at the leading edge of the impeller and generally increases as the flow proceeds through the impeller blades. Using sinusoidal, saw-tooth, and intersecting arc waveforms, this minimum impeller  $K_{adm}$  translated to an rms surface finish of 40 to 48  $\mu$ inch.
- o Similarly, for the NASA diffuser, 61.3  $\mu$ inch was calculated as a minimum value of  $K_{adm}$ . (This value also changes significantly as the flow passes through the diffuser, rising to 183.6  $\mu$ inch at the diffuser exit.) In turn, this required an rms surface finish of 18 to 22  $\mu$ inch.

Inasmuch as geometric scaling changes Reynolds number only by changing the diameter,  $K_{adm}$  remains unchanged since neither kinematic viscosity nor free-stream velocity changes. Therefore, as concluded by Schlichting (Ref. 1), if the surface finish were hydraulically smooth for the large scale, it also would be hydraulically smooth in the smaller scale (even though the reference Reynolds number changed significantly).

A relationship between loss and Reynolds number was correlated by GTEC. In the correlation, Reynolds number is given by the equation,

$$Rey = \frac{\rho_{01} D_T U_T}{\mu_{01}}$$

where:

- Rey = Reynolds number
- $\rho_{01}$  = Inlet stagnation density
- $\mu_{01}$  = Inlet stagnation viscosity
- $D_T$  = Tip diameter
- $U_T$  = Tip speed.

As shown by Figure 12, for a hydraulically smooth surface finish, changing the Reynolds number causes the loss to change according to the solid line. For a hydraulically rough surface finish, a similar change of Reynolds number causes the loss to remain unchanged (dashed line). To test the effect of a hydraulically rough surface finish, a second 2-lb/sec impeller was fabricated with an rms surface finish of 50 to 80  $\mu$  inch.

The solid line in Figure 12 can be represented by the equation,

$$\left(\frac{1-\eta}{1-\eta}\right)_{\text{Baseline}} = \left(\frac{\text{ReyBaseline}}{\text{Rey}}\right)^N$$

where:  $\eta$  = Efficiency.

Two test-data points taken on the 25-lb/sec compressor at suppressed inlet conditions gave a value of 0.1385 for N. This exponent was lower than the 0.2 power expected from turbulent boundary layer theory, since several contributors to compressor loss (such as clearance, shock, and dump losses) were not Reynolds-number-dependent.

The measured surface finish of the 25-lb/sec impeller was 30 to 50  $\mu$  inches. It was concluded that, since the scaled compressor surface finish will be the same as the baseline compressor, hydraulic similarity is established. The relationship between Reynolds number and loss is the same for both compressors.

## 2.8 10-Lb/Sec Compressor Design

To define the aerodynamic flowpath geometry for the 10-lb/sec version of the 2-lb/sec modified compressor, all flow path coordinates of the aerodynamic components of the 2-lb/sec compressor were multiplied by a linear scale factor of  $\sqrt{10/2} = 2.2361$ .

The running clearances of the two compressors should be related by the same ratio to ensure accurate determination of scaling effects.

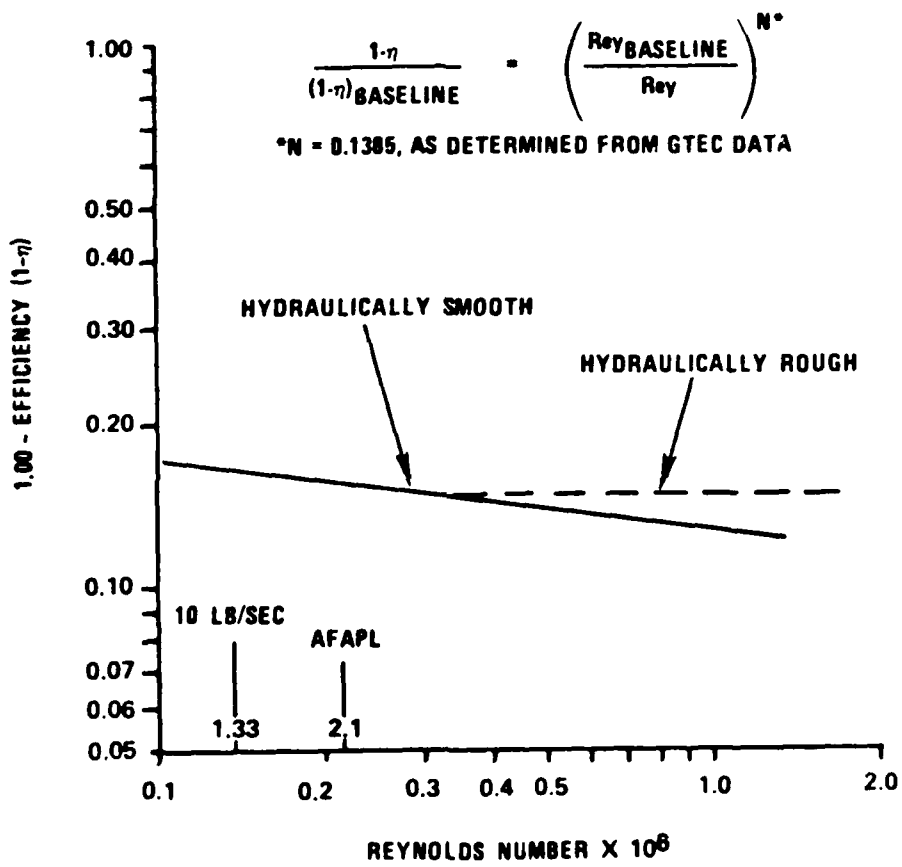


Figure 12. Change in Loss Shown as a Function of Reynolds Number Change.

### 3.0 2-LB/SEC IMPELLER MECHANICAL DESIGN

#### 3.1 Impeller Mechanical Blading Design

A three-dimensional stress analysis was performed on the 2-lb/sec blade. Preliminary two-dimensional impeller hubline deflections were added as boundary conditions to the root of the blade. A "worst case" tolerance condition was evaluated by adding 0.002 inch to the nominal tip thickness along the discharge of the blade (the final 1/3 meridional length) and subtracting 0.002 inch from the nominal hub thickness of the blade along the same discharge length.

The maximum effective stress at 110-percent speed (89,450 rpm) is 65.4 ksi in the inducer region on the pressure side of the full blade. Figure 13 shows the full-blade effective stress distribution for this speed and thickness distribution. A fixed rotor hub vibration analysis revealed the fundamental mode to be at 3.9/rev at 100-percent speed, as shown in Figure 14. The 4/rev excitation crossing is at 97.2-percent speed. Figure 15 shows the splitter-blade maximum effective stress of 62.3 ksi on the suction surface. The vibration analysis Campbell diagram for the splitter blade is shown in Figure 16.

#### 3.2 Impeller Blade Holographic and Acoustic Analyses

Both holographic and acoustic analyses were performed on the 2-lb/sec impeller to verify the analytical predictions of the compressor blade natural frequencies. The procedure was as follows: Holographic tests were performed on one blade without neighboring blade or disk damping. The blades were excited from 0-30,000 Hz by four evenly spaced piezo-electric crystals mounted on the disk.

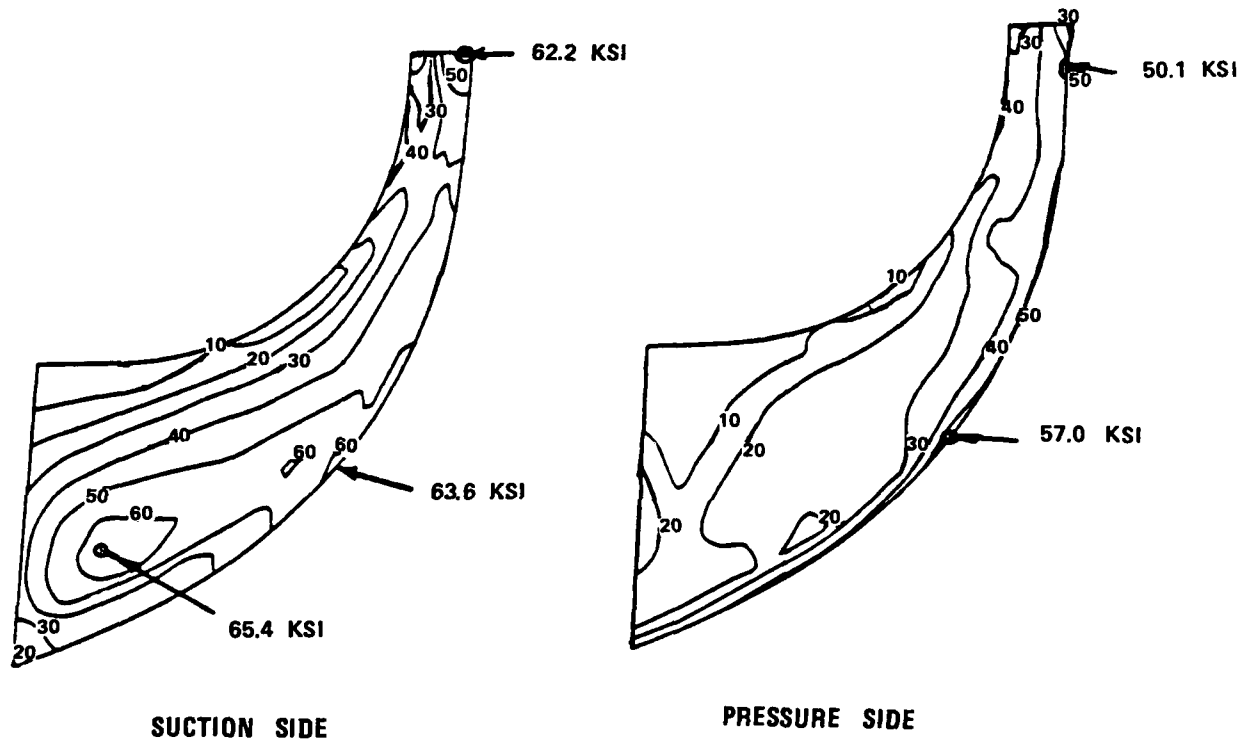


Figure 13. Full-Blade Effective Stress Distribution, 110-Percent Speed.

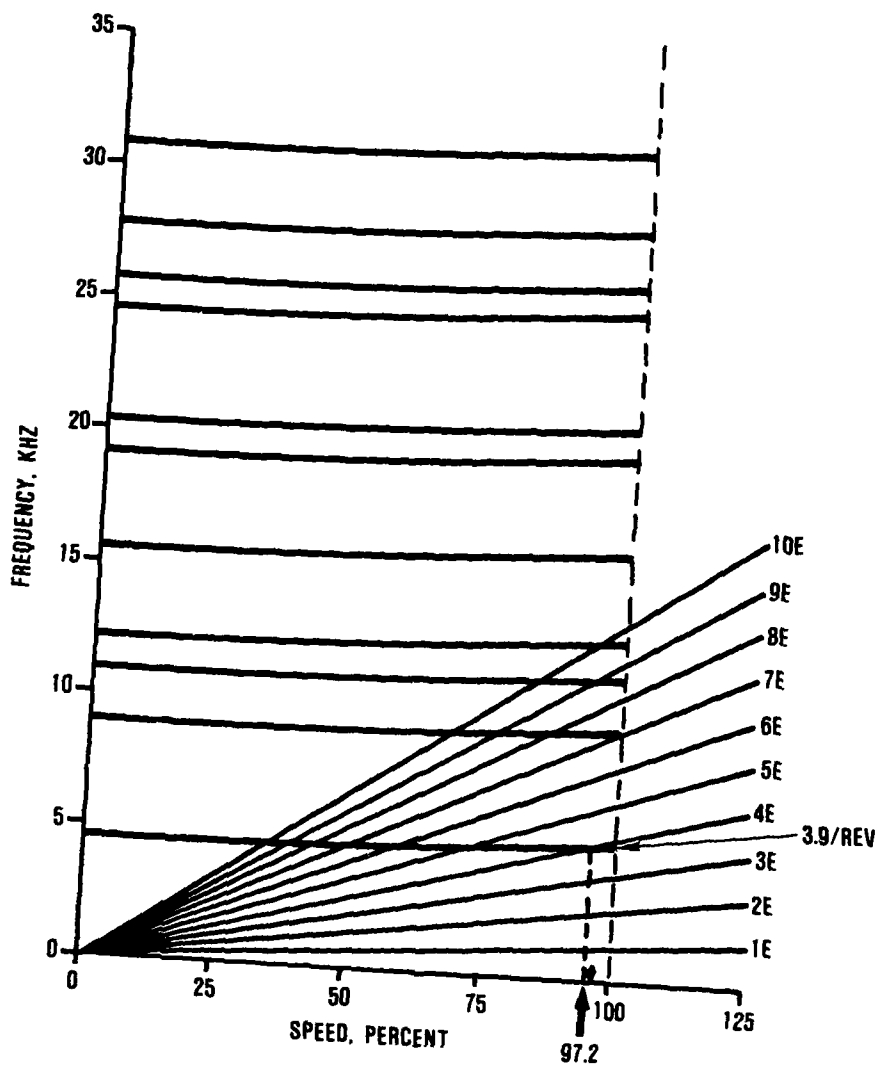


Figure 14. Full-Blade Campbell Diagram.

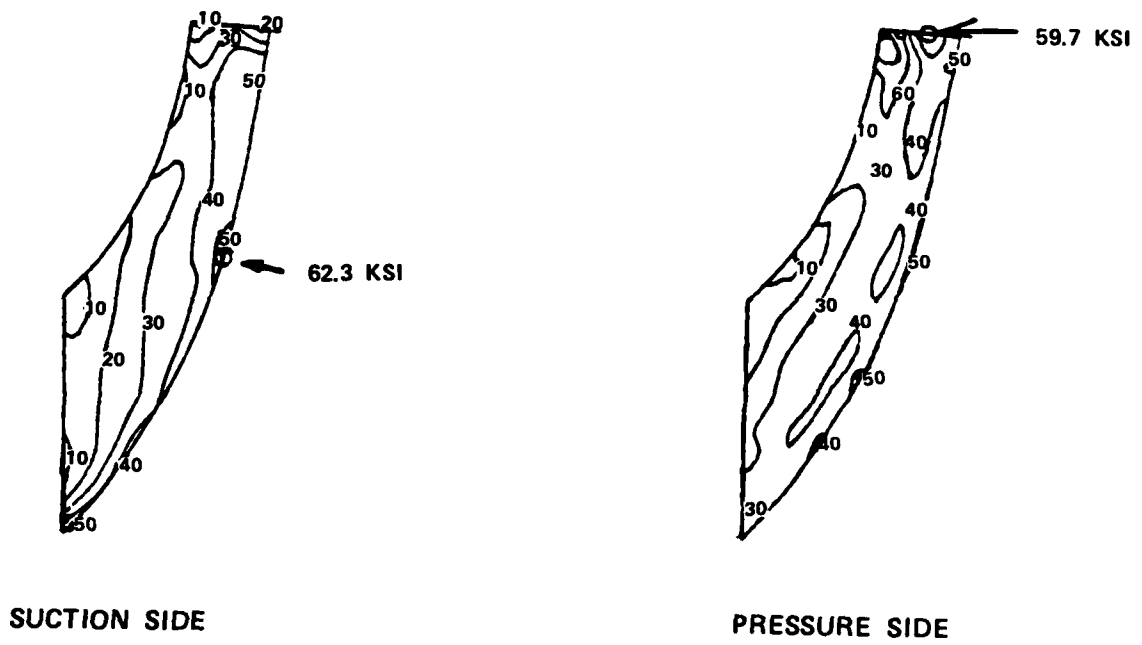


Figure 15. Splitter-Blade Effective Stress Distribution, 110-Percent Speed.

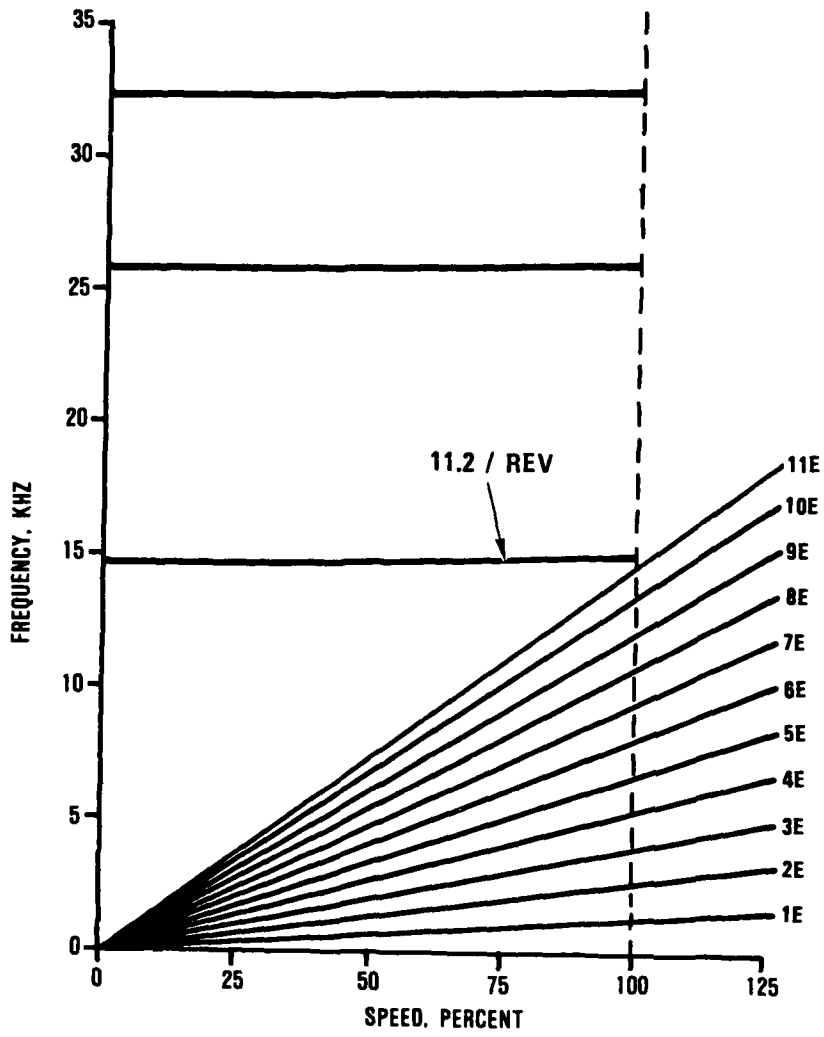


Figure 16. Splitter-Blade Campbell Diagram.

Acoustic testing was performed on each full blade with neighboring blade and disk damping.

The holographic testing showed a wide scatter in the blade natural frequencies as well as a substantial amount of disk activity forcing the blades. The results are summarized in Figure 17. The dark bars on the left side of the Campbell diagram represent the frequency range each mode was excited in laboratory conditions. This data has been corrected to operating conditions by adjusting the holographic testing results with the calculated frequency difference between 0 rpm at 70F and 100-percent speed operating conditions (81,319 rpm and 560F). Analytical predictions for 100-percent speed operating conditions are shown on the Campbell diagram as a triangle on the 100-percent speed line.

The wide frequency range obtained in the holography test can be attributed to, in part, the strong influence of the backplate on the blade response. An examination of the blade photographs from the test will show significant backplate movement that is due to backplate modes excited at or near the blade resonant frequencies.

Photographs of typical blade modes obtained during testing are shown in Figures 18, 19, and 20.

The second mode excited during testing was not predicted in the analysis performed on the blade. This mode was determined to be a backplate mode that was forcing the blade. The vibration analysis considered a fixed hub blade, and therefore did not consider any backplate coupling. The blade should not be excited at this mode by aerodynamic forces, and the disk mode responsible for this action will not occur until 133-percent speed. This has been confirmed by the acoustic test. The acoustic test separated the disk and blade modes by comparing blade and disk resonance in damped and undamped conditions. Table 2 contains the acoustic

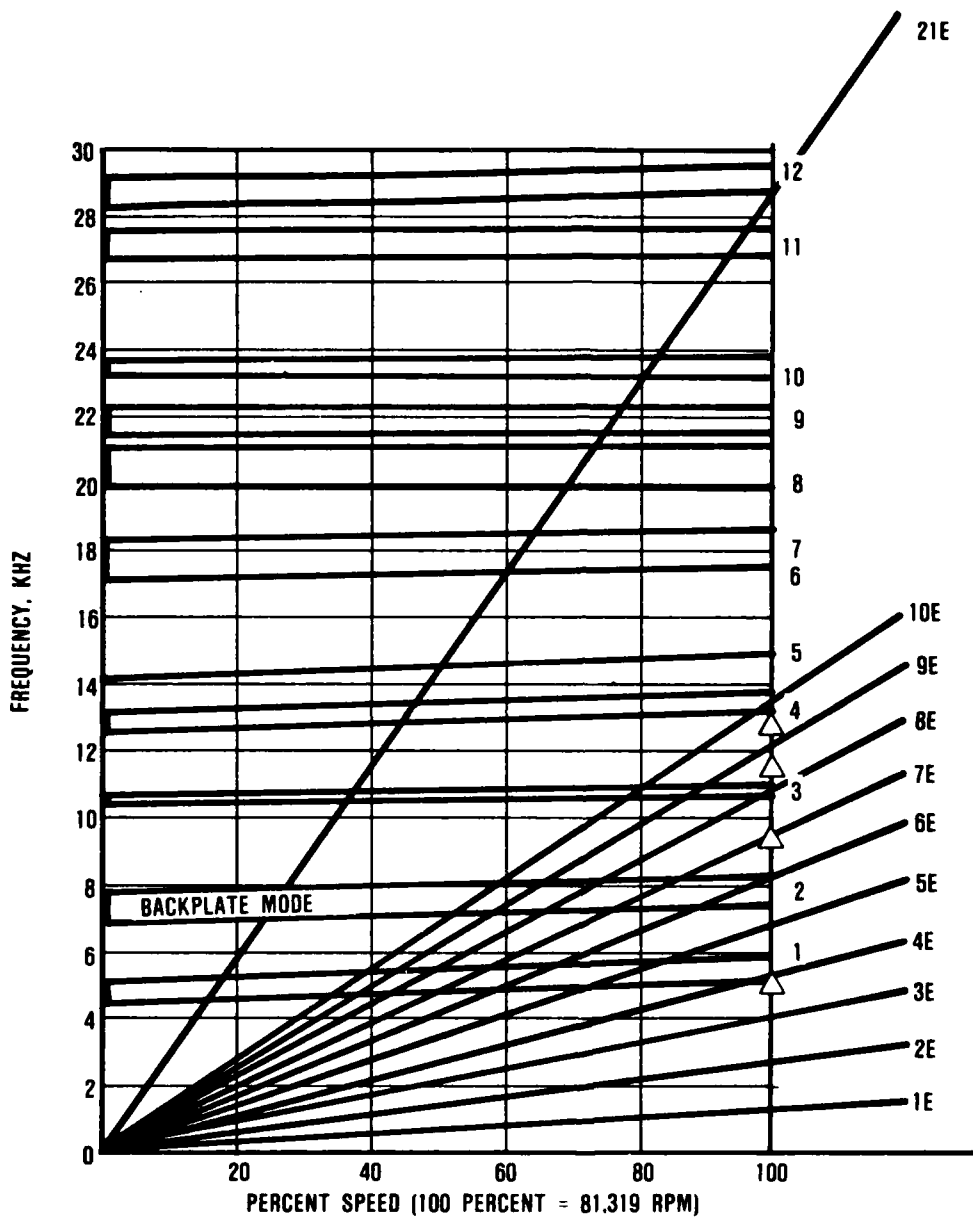
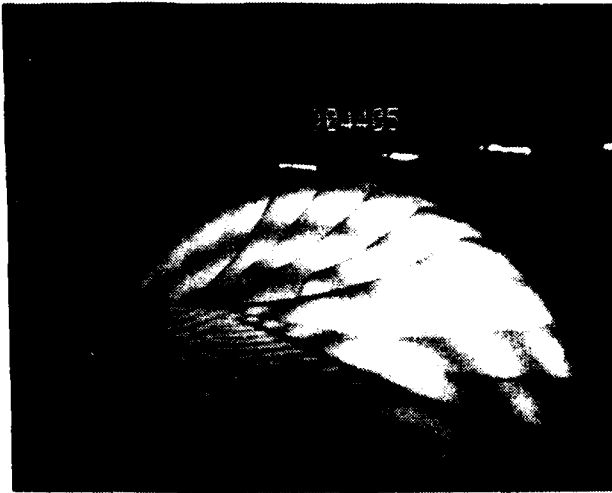
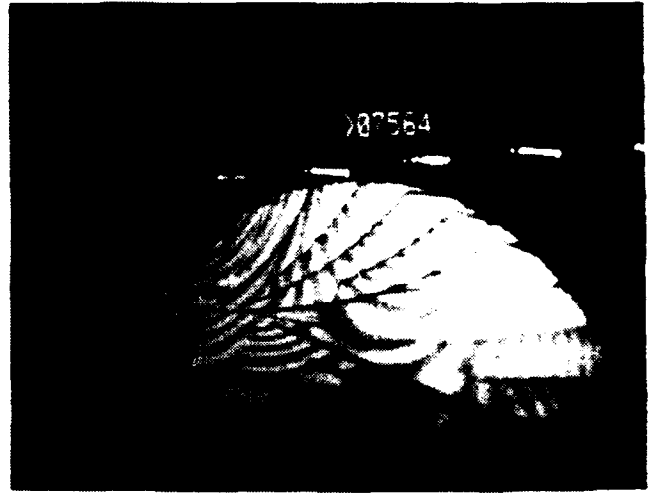


Figure 17. NASA 2-lb/Sec Scaled Compressor Main Blade Holography Campbell Diagram.



MODE 1



MODE 2 (BACKPLATE)



MODE 3 (BLADE MODE 2)



MODE 4 (BLADE MODE 3)

Figure 18. NASA 2-lb/Sec Scaled Compressor Blade Mode Shapes.



MODE 5 (BLADE MODE 4)



MODE 6 (BLADE MODE 5)



MODE 7 (BLADE MODE 6)



MODE 8 (BLADE MODE 7)

Figure 19. NASA 2-lb/Sec Scaled Compressor Blade Mode Shapes.



MODE 9 (BLADE MODE 8)



MODE 10 (BLADE MODE 9)



MODE 11 (BLADE MODE 10)



MODE 12 (BLADE MODE 11)

Figure 20. NASA 2-lb/Sec Scaled Compressor Blade Mode Shapes.

TABLE 2. ACOUSTIC TEST RESULTS: NASA 2-LB/SEC SCALED COMPRESSOR, ALL BLADES AND BACKPLATE DAMPED EXCEPT BLADE UNDER TEST.

Resonant Freq. 70F, ORPM				
Blade	Mode 1 (Hz)	Mode 2 (Hz)	Mode 3 (Hz)	Mode 4 (Hz)
1	5100	10650	12850	14900
2	5200	10450	13200	15300
3	5200	10650	13050	15050
4	5250	10650	13050	14850
5	5200	10700	13200	15100
6	5100	10450	12900	14650
7	5250	10750	12400	14600
8	5250	10750	13050	14950
9	5200	10600	13000	14600
10	5100	10450	12800	14700
11	5200	10550	12800	14750
12	5150	10450	12750	14600
13	5300	10750	13100	15100
14	5250	10850	13350	15300
15	5250	10650	13050	15050
16	5200	10750	13150	15100
17	5350	10800	13350	15100
18	5100	10450	12850	14600
19	5050	10450	12950	14650
20	5150	10750	12850	14800

Conversion From 0 RPM, 70F To 100-speed Operating Conditions

Mode	Correction Factor	Frequency Range	New Frequency Range	Expected Excitation Order
1	670	5050-5350	5720-6020	4.2-4.4
2	363	10450-10850	10813-11213	8.0-8.3
3	407	12400-13350	12807-13757	9.45-10.15
4	638	14600-15300	15238-15938	11.0-11.78

test results for the first four blade modes for all blades and correction factors to convert that data from laboratory conditions to 100-percent speed operating conditions. The final Campbell diagram is shown in Figure 21, which also relates the difference in calculated and tested natural frequencies above the first mode. The blade inspection revealed the reason for the disagreement. The blades, as cut, are thicker in local areas than the tooling layouts and corresponding tolerances allowed. While this is acceptable aerodynamically, the thickness variations observed account for the difference in calculated and measured frequencies. Additionally, since the thickness variations are not uniform, and occur in local areas only, the fundamental mode is less likely to be affected than are higher order modes.

An examination of Figure 21 reveals interferences at 100-percent speed on 8/rev and 10/rev excitation.

Since the inlet of the 2-lb/sec test rig has two inlet probes, and harmonics of these could excite 8/rev and 10/rev, a study was initiated to determine the harmonics excited by the two survey probes and three inlet struts. The probe and strut circumferential locations are shown in Figure 22.

The orientation and drag characteristics of the probes and struts were input into the GTEC Aerodynamics Group Computer Program "WAKE" which predicts pressure drop and angular extent of objects in a flow path. The resulting  $P/P_{iN}$  vs. angular position is shown in Figure 23 for three struts and for both probes in the flow path. The resulting harmonics and normalized magnitudes from a Fourier analysis performed on this and two other inlet configurations are shown in Table 3.

Table 2 shows no advantages to running with one probe at a time, since there is little difference in 8/rev levels, and 5 and 9/rev levels are smaller with two probes. While the absolute

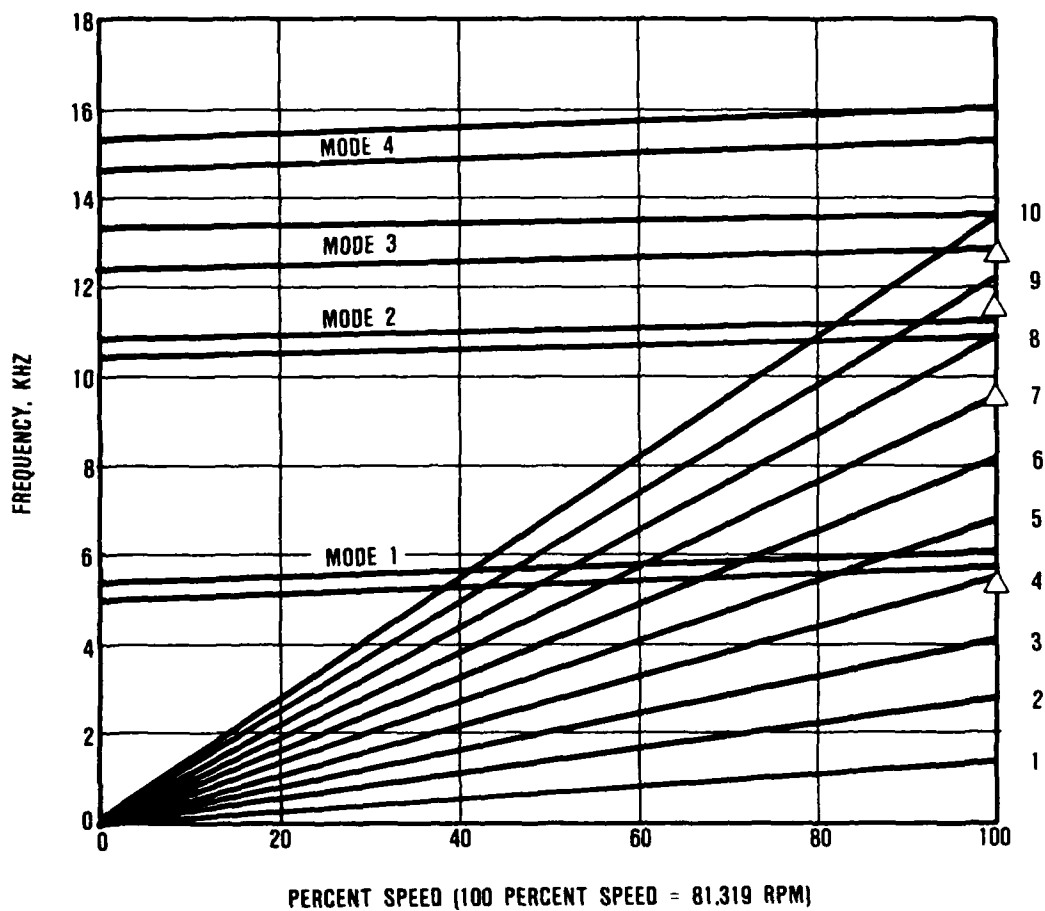


Figure 21. NASA 2-lb/Sec Scaled Compressor Acoustic Test Results.

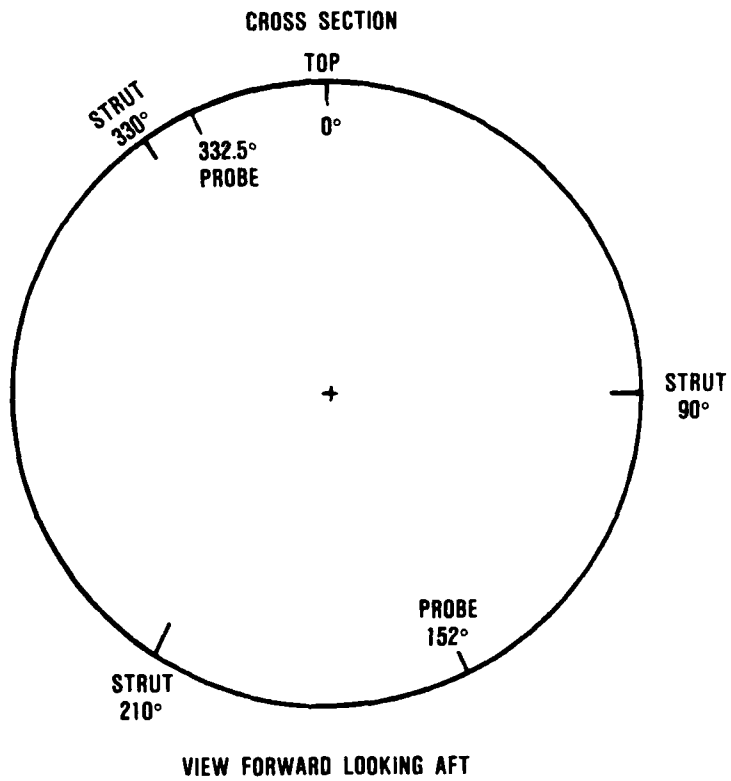


Figure 22. Probe and Strut Circumferential Locations.

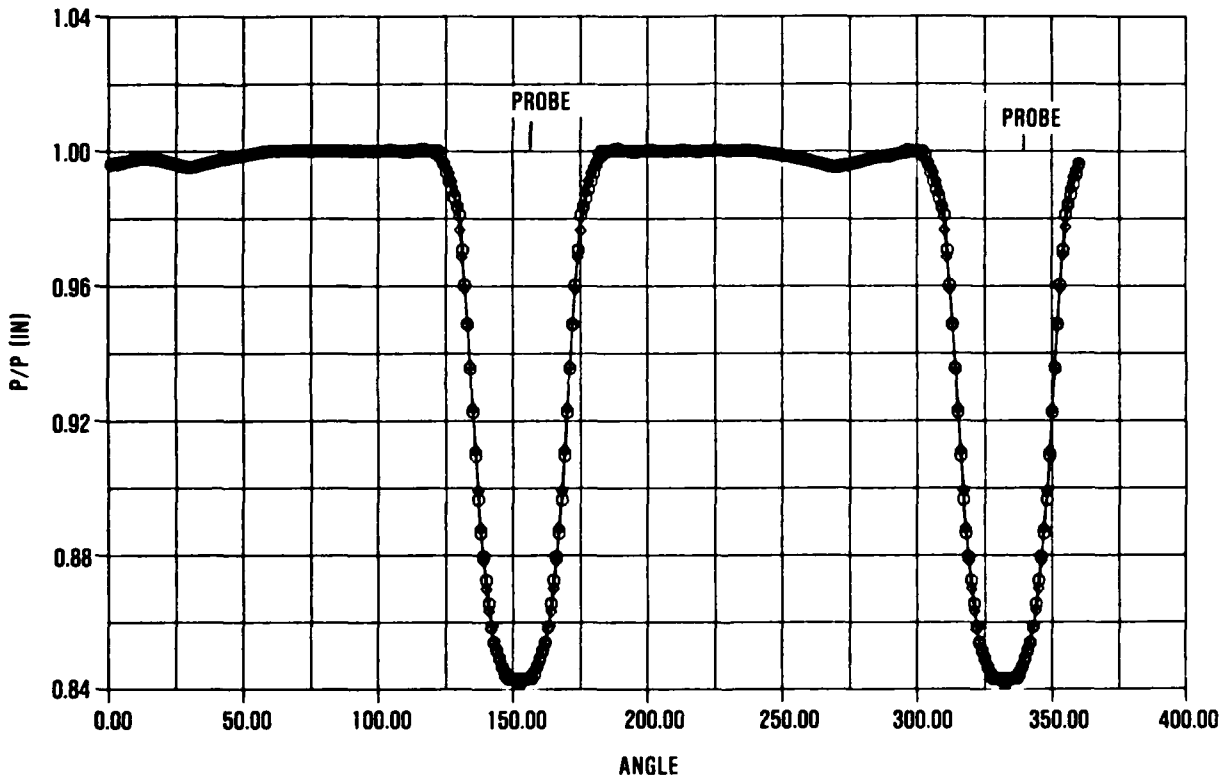


Figure 23. Pressure Drop Vs. Circumferential Angle at Blade Leading Edge.

TABLE 3. FOURIER ANALYSIS OF THE NASA 2-LB/SEC RIG INLET STRUT AND PROBE CONFIGURATION.

Both Probes Normalized Harmonic Content		One Probe at 152.5 Normalized Harmonic Content		One Probe at 332.5 Harmonic Content Content	
Order	Magnitude	Order	Magnitude	Order	Magnitude
2	1.000	1	1.000	1	1.000
4	0.7820	2	0.9432	2	0.9442
6	0.5164	3	0.9178	3	0.7937
8	0.2293	4	0.7395	4	0.7431
14	0.1042	5	0.6090	5	0.6137
16	0.8256E-01	6	0.5061	6	0.5108
12	0.7456E-01	7	0.3384	7	0.3437
18	0.4135E-01	8	0.2158	8	0.2204
10	0.3103E-01	9	0.1214	9	0.1039
3	0.2329E-01	14	0.9887E-01	14	0.9987E-01
24	0.2135E-01	13	0.9433E-01	13	0.9554E-01
26	0.17788E-01	15	0.8864E-01	15	0.9531E-01
1	0.1462E-01	16	0.7764E-01	16	0.7658E-01
22	0.1436E-01	12	0.7111E-01	12	0.7188E-01
28	0.8261E-02	17	0.5963E-01	17	0.5721E-01
20	0.7134E-02	18	0.34619E-01	18	0.3490E-01
5	0.6210E-02	11	0.3464E-01	11	0.3448E-01
7	0.4663E-02	10	0.2673E-01	10	0.2886E-01
15	0.3388E-02	19	0.2328E-01	24	0.1927E-01
30	0.2973E-02	24	0.2004E-01	19	0.1893E-01
11	0.2505E-02	25	0.2002E-01	23	0.1853E-01
19	0.2344E-02	26	0.1788E-01	25	0.1768E-01
9	0.2253E-02	23	0.1753E-01	22	0.1479E-01
17	0.2029E-02	27	0.1435E-01	26	0.1451E-01
13	0.1694E-02	22	0.1215E-01	27	0.1018E-01
23	0.1589E-02	28	0.9018E-02	21	0.6959E-02
27	0.1513E-02	20	0.8278E-02	28	0.6222E-02
25	0.1436E-02	21	0.4451E-02	30	0.4965E-02
21	0.1411E-02	29	0.3402E-02	20	0.3816E-02
29	0.1314E-02	30	0.2082E-02	29	0.3089E-02

magnitude of the forcing function that will excite 8/rev and 10/rev is not known, the normalized magnitude of this 10/rev is sufficiently low to be of no major concern. The normalized magnitude of the 8/rev harmonic, although also low, may be sufficiently high to cause possible blade damage from resonances of the second mode at or near 100-percent speed. This is unlikely, however, because the inlet circumferential distortion index (CDI) is well below current GTEC production engine standards. Since the rig was not designed for the inclusion of strain gages, it will be impossible to determine if this mode is excited during rig testing.

A normalized vibratory stress analysis indicates that the peak vibratory stress for the second mode is in an area of high steady-state stress. However, without knowing the magnitude of the vibratory stress, life prediction is impossible. The steady state and normalized vibratory stress plots for the first three modes are shown in Figures 24 and 25. With these steady-state stress levels, the failure level for vibratory stress is approximately  $\pm 40$  ksi for  $10^7$  cycles.

In conclusion, no options exist to completely eliminate the potential second mode resonance excited by 8/rev near 100-percent. Data from the acoustic test indicate only six full blades have natural frequencies which fall on 8/rev at 100-percent speed. Although the potential of exciting the second mode during testing is present, the probability of this occurring is extremely small.

### 3.3 Rough-Cut Impeller Blade Holographic and Acoustic Analyses

The objective of these analyses was to determine whether the acoustic and holographic test results for the 2-lb/sec rough-cut impeller agree with the results for the 2-lb/sec impeller referenced in Section 3.2.

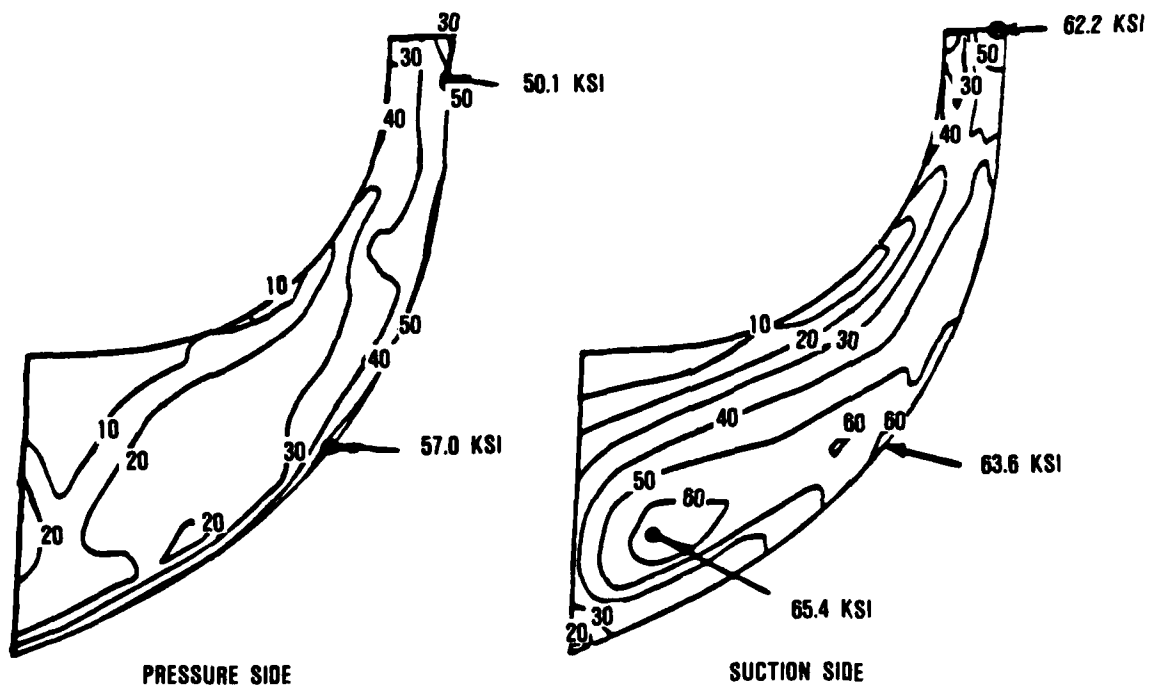
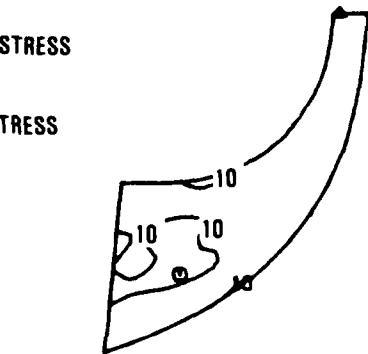


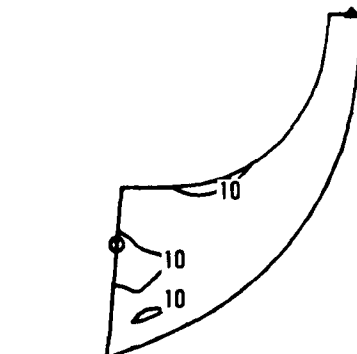
Figure 24. NASA 2-lb/Sec Scaled Compressor Steady-State Stress - 81,319 rpm.

○ PEAK STRESS

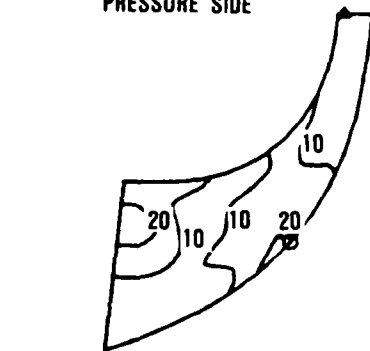
△ MIN STRESS



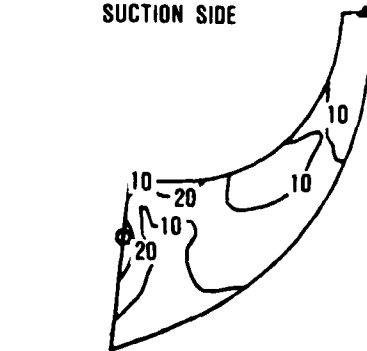
R X  
SIGMA(E)  
MODE 1  
PRESSURE SIDE



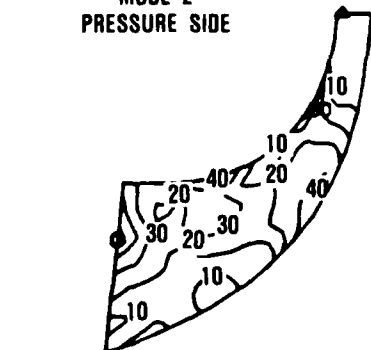
R X  
SIGMA(E)  
MODE 1  
SUCTION SIDE



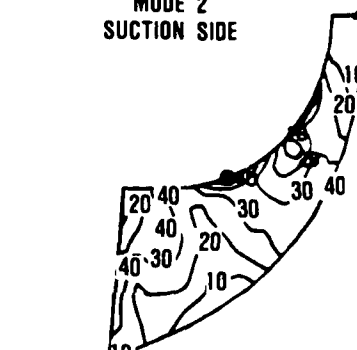
R X  
SIGMA(E)  
MODE 2  
PRESSURE SIDE



R X  
SIGMA(E)  
MODE 2  
SUCTION SIDE



R X  
SIGMA(E)  
MODE 3  
PRESSURE SIDE



R X  
SIGMA(E)  
MODE 3  
SUCTION SIDE

Figure 25. NASA 2-lb/Sec Compressor Normalized Vibratory Stress.

The acoustic tests were conducted on all blades. Each blade was excited at the inlet while all other blades and the disk backplate were damped. The holography tests were conducted on a single blade, with all other blades and the disk in damped and in undamped states. Undamped disk frequencies were also excited.

Table 4 contains all the blade frequencies obtained during these tests. Figure 26 shows the Campbell diagram with the acoustic test frequency range for all the blades.

Acoustic tests indicate blade-to-blade variations on the natural frequencies, as expected. Since the blade profile tolerances are higher, relative to blade size, the frequency ranges are higher.

Holography tests were conducted on a single blade with all other blades and the disk damped. The first six modes occur at discrete frequencies (Table 4) and agree well with acoustic test frequencies. The mode shapes are shown in Figures 27 and 28. In an undamped state, the blade has many more mode shapes due either to disk coupling or to the influence of other blades. Figure 29 shows the Campbell diagram for holography test results on the blade.

The 2-lb/sec rough-cut impeller acoustic and holographic test results are similar to that for the 2-lb/sec impeller referenced in Section 3.2. This is not surprising, considering that both impellers were manufactured by the same vendor and that the only major difference between the two is the surface finish.

TABLE 4. 2-LB/SEC ROUGH-CUT IMPELLER BLADE FREQUENCIES  
OBTAINED DURING ACOUSTIC AND HOLOGRAPHY TESTS.

One Blade Undamped; the Rest Damped (Hz)	Undamped Blades and Disk		Blades' Frequency Range by Acoustic Test (Hz)
	Blade Frequency (Hz)	Comment	
5,154	4,378	First Mode	5,125-5,375
	5,051	First Mode	
	5,094	First Mode	
	5,209	First Mode	
	6,349	Disk Coupled	
	7,506	Disk Coupled	
	9,816	Disk Coupled	
10,534	10,342	Second Mode	10,250-10,875
	10,452	Second Mode	
	10,567	Second Mode	
	11,557	Disk Coupled	
	12,401	Third Mode	
12,661	12,674	Third Mode	12,500-13,375
	13,447	Disk Coupled	
	14,360	Fourth Mode	
14,670	14,675	Fourth Mode	14,125-15,750
16,885	16,882	Fifth Mode	
17,428	17,176	Sixth Mode	17,250-18,500
	17,785	Sixth Mode	
	17,943	Sixth Mode	
	18,277	Sixth Mode	

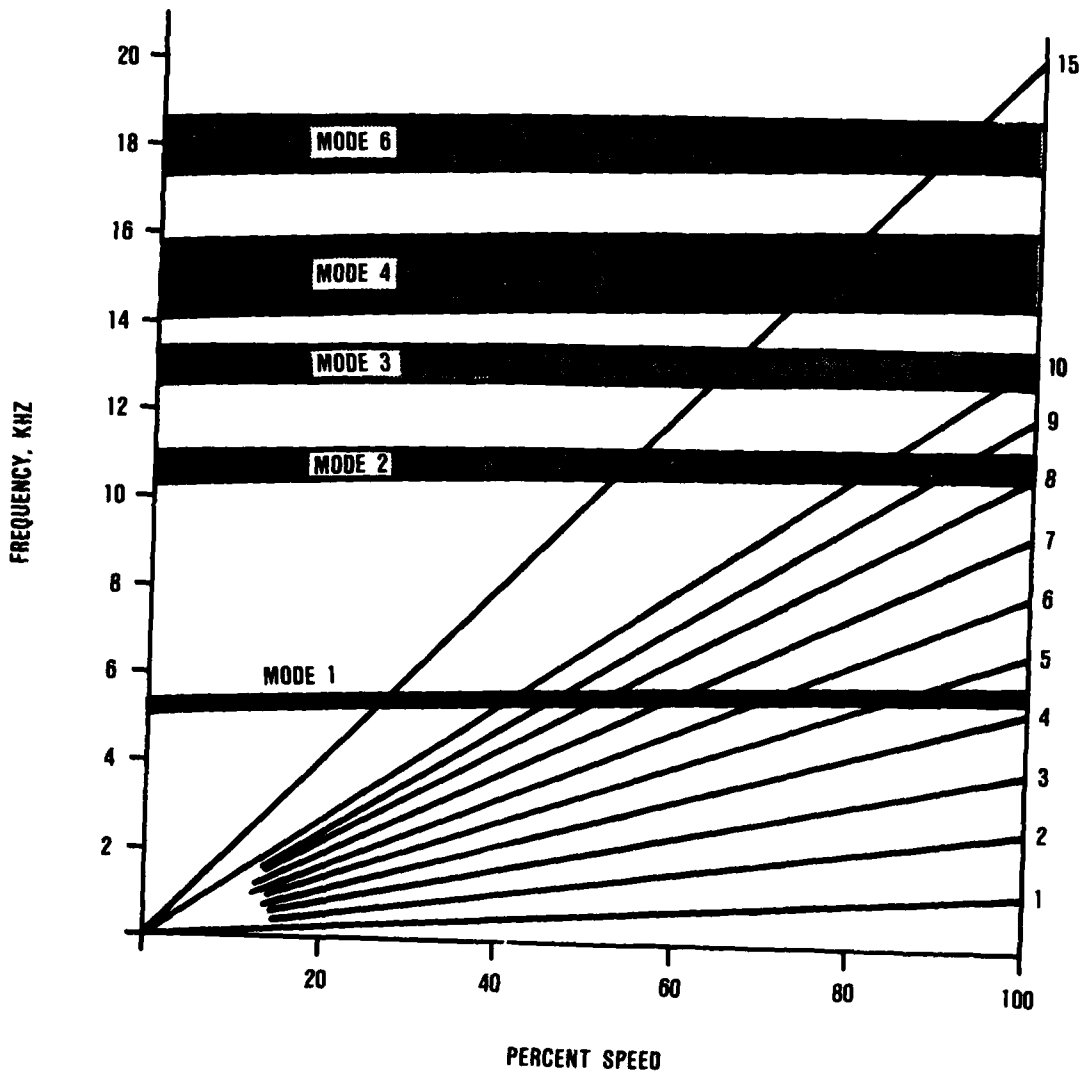


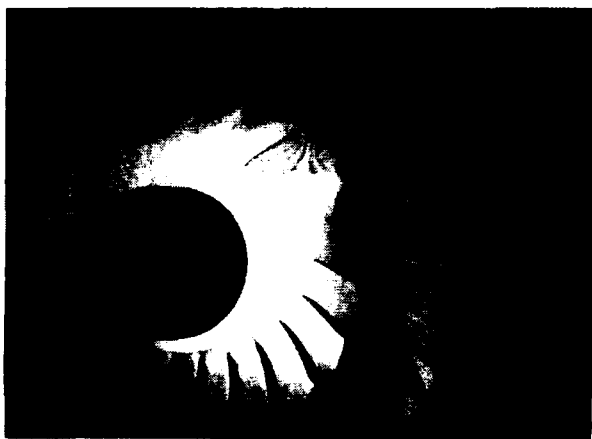
Figure 26. NASA 2-lb/Sec Rough-Cut Impeller Acoustic Test Results.



MODE 1



MODE 2



MODE 3



MODE 4

Figure 27. NASA 2-lb/Sec Rough-Cut Impeller Blade Mode Shapes.



MODE 5



MODE 6

Figure 28. NASA 2-lb/Sec Rough-Cut Impeller Blade Mode Shapes.

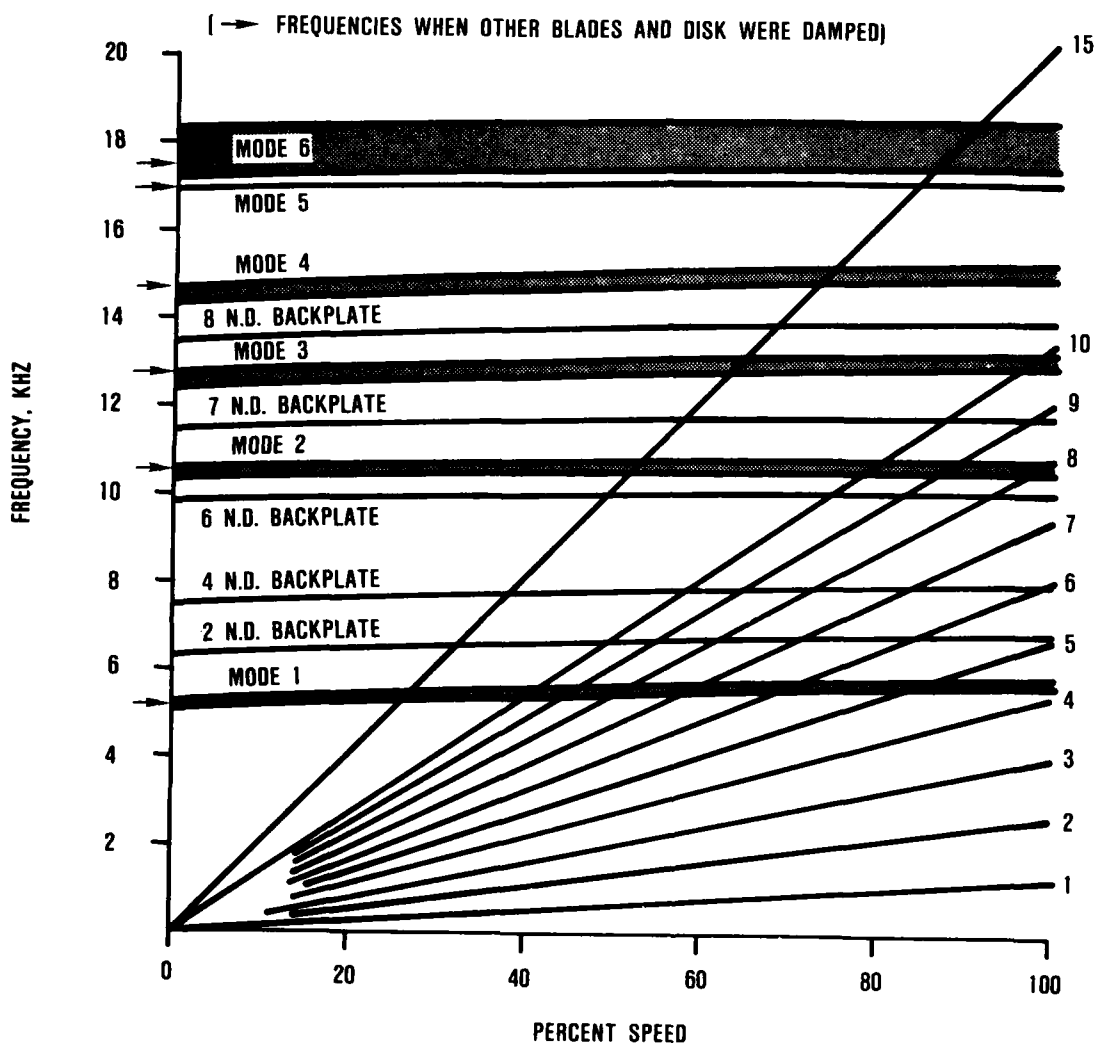


Figure 29. NASA 2-lb/Sec Rough-Cut Impeller Holography Test Results.

### 3.4 Impeller Backplate Vibration Analysis

The impeller backplate vibration resonant speeds are designed to occur above the rig operating speeds. A stiffening ring, located at 2.4175 radius, is used to provide a 25-percent speed margin on backplate vibration.

Backplate vibration frequencies have been calculated using an axisymmetric finite-element analysis. Only the portion of the disk that vibrates is modelled, as shown in Figure 30. An axisymmetric model, without the blades, is sufficiently accurate since test experience has shown that the lowering of the backplate natural frequency due to the blade-mass tends to be cancelled by the added stiffness the blades contribute to the disk. Centrifugal stiffening has also been included in the calculation. The frequencies for each mode are shown in an interference diagram in Figure 31. The final backplate design has a 25-percent speed margin on the lowest backplate vibration frequency.

### 3.5 Impeller Backplate Holographic Test Results

The disk backplate resonant frequencies were determined using the same setup and technique as the blade testing. The Campbell diagram in Figure 32 shows test results and the test data corrected analytically to 100-percent speed operating conditions. Corrected test results indicate a 33-percent frequency margin at operating conditions. Photographs of the first nine nodal diameters are shown in Figures 33, 34, and 35. As the disk becomes highly active above 15,000 Hz it is difficult to determine which modes are excited. However, the higher frequency modes are not expected to cross the 100-percent speed line as the trend in Figure 32 is away from 100-percent speed.

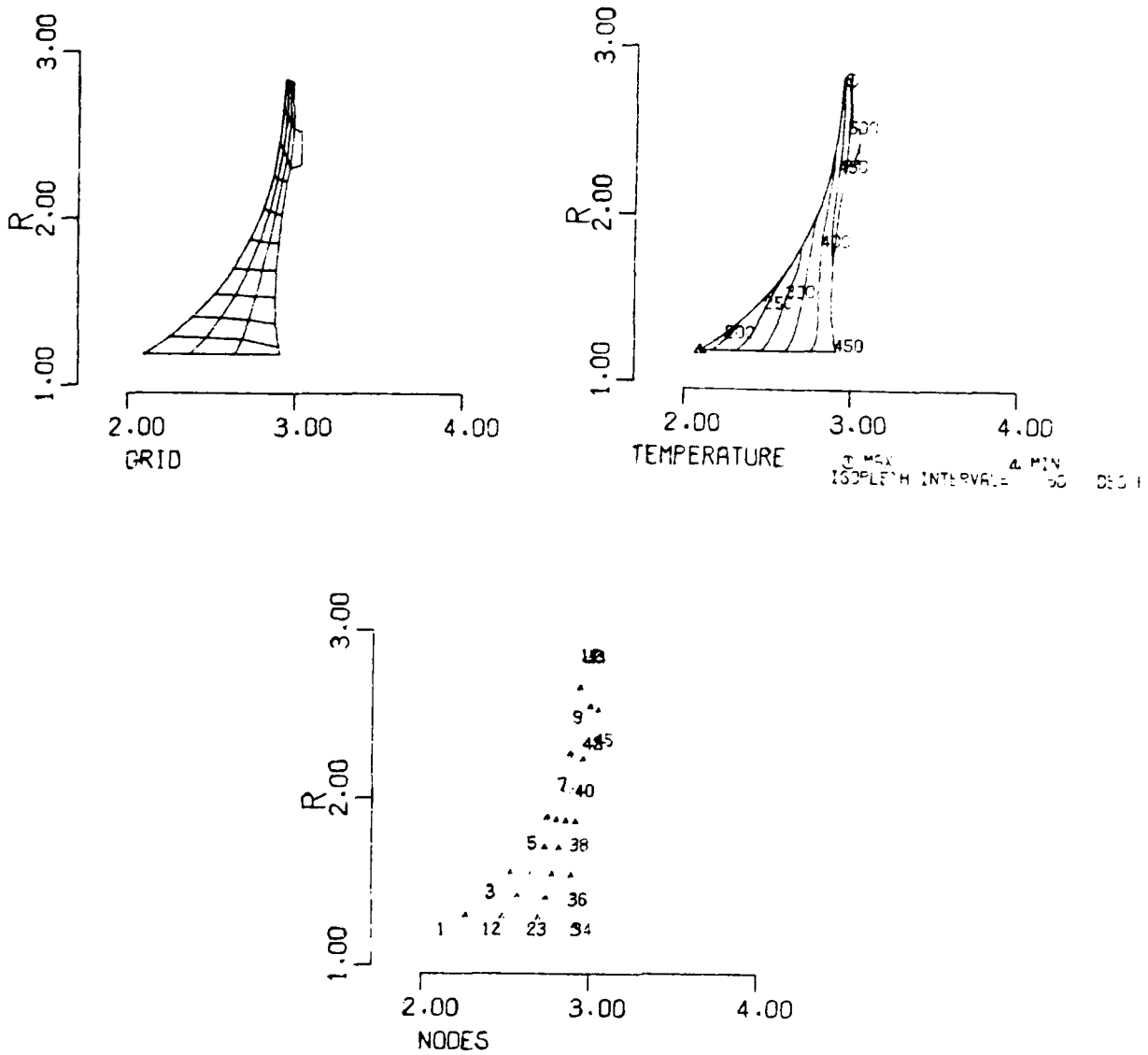


Figure 30. NASA 2-lb/Sec Impeller Backplate Vibration Model.

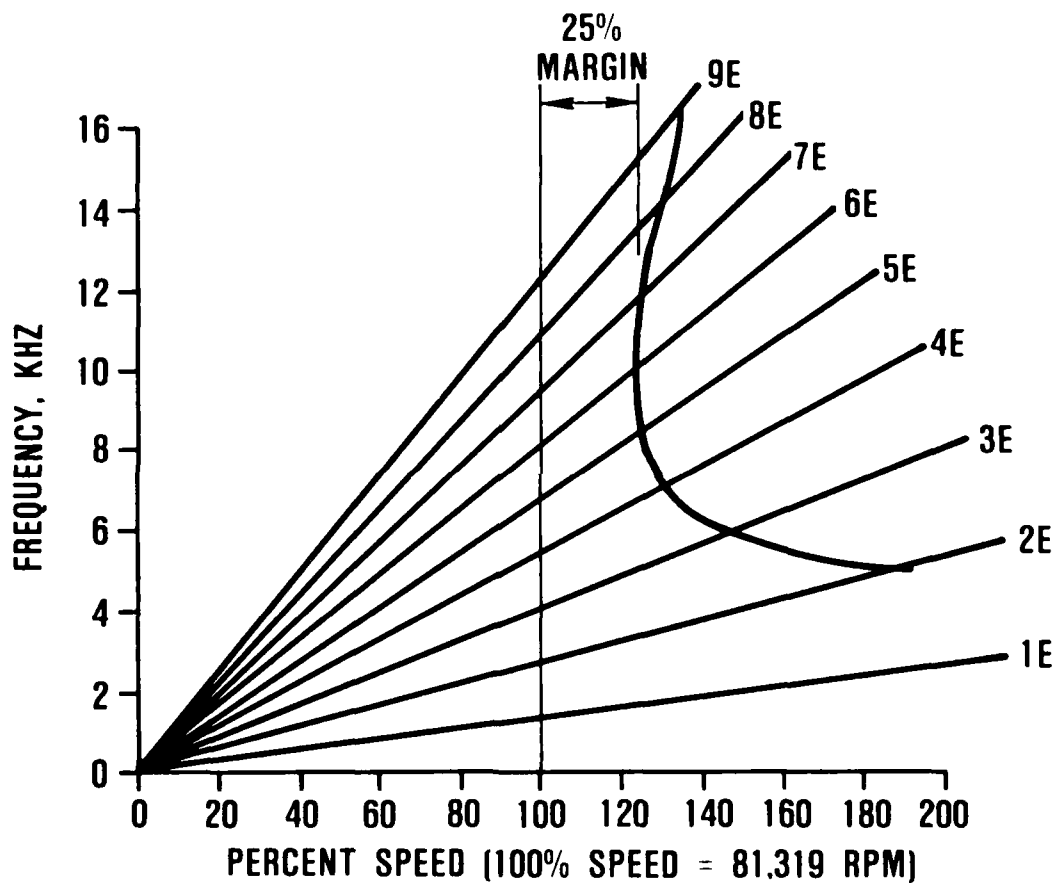


Figure 31. NASA 2-lb/Sec Compressor Backplate Vibration Campbell Diagram.

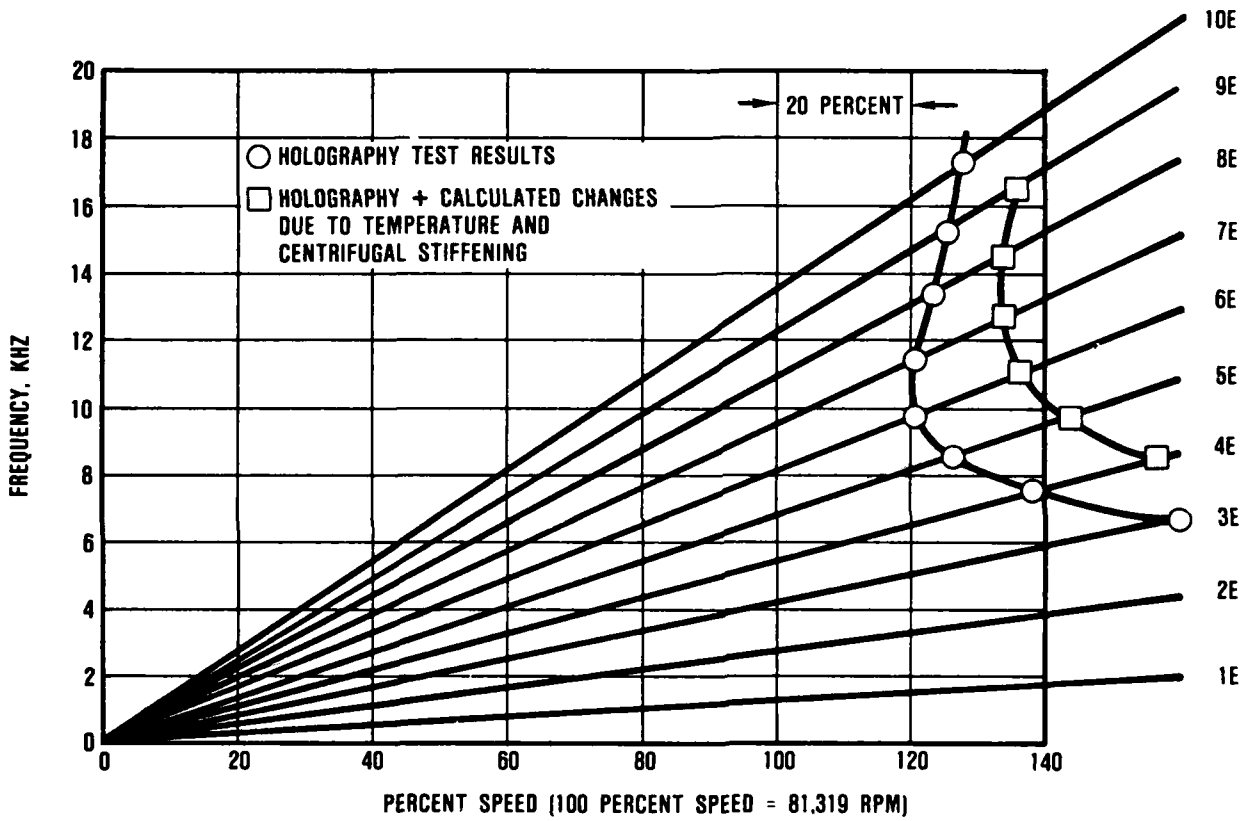
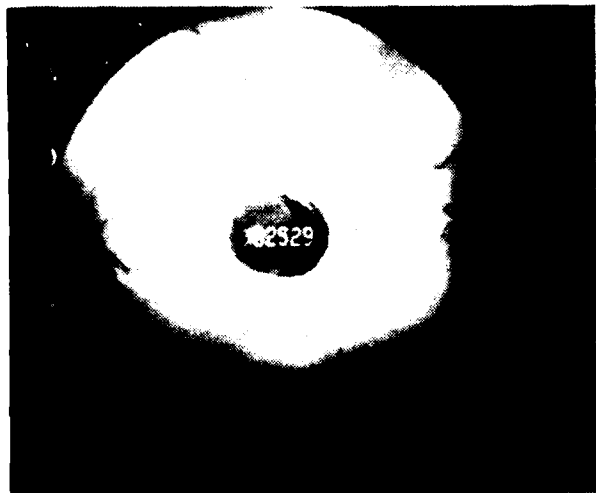
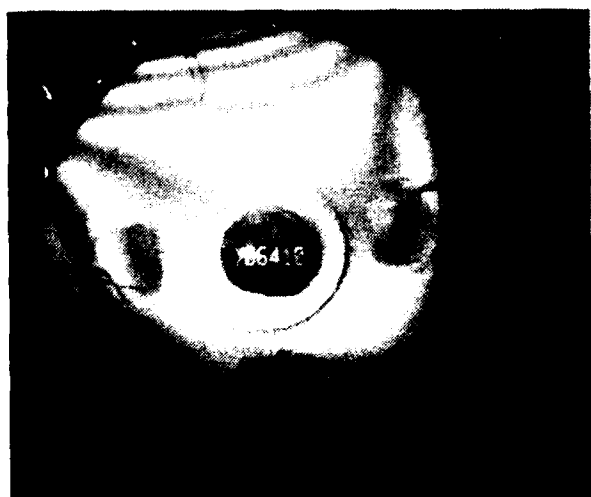


Figure 32. NASA 2-lb/Sec Impeller Backplate Holography Results.



UMBRELLA MODE



2 NODAL DIAMETERS

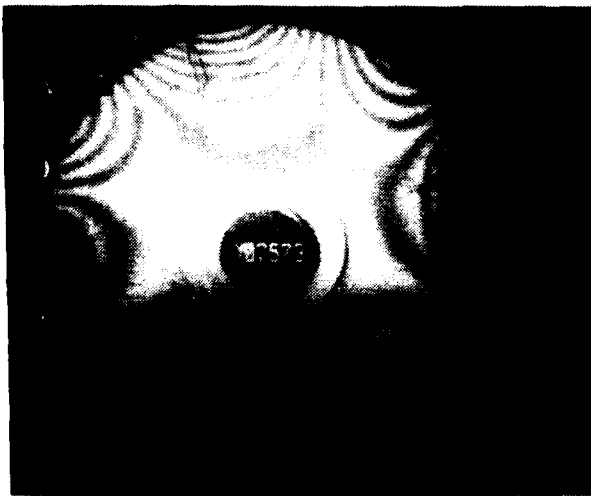
Figure 33. NASA 2-1b/Sec Scaled Compressor Holography Test Results.



3 NODAL DIAMETERS



UMBRELLA MODE

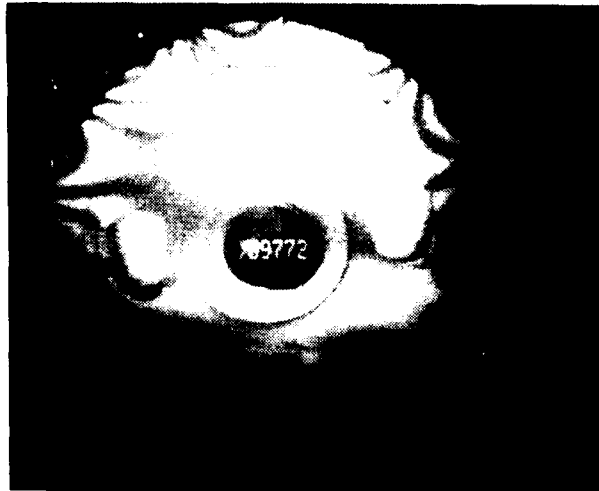


4 NODAL DIAMETERS



5 NODAL DIAMETERS

Figure 34. NASA 2-lb/Sec Scaled Compressor Holography Test Results.



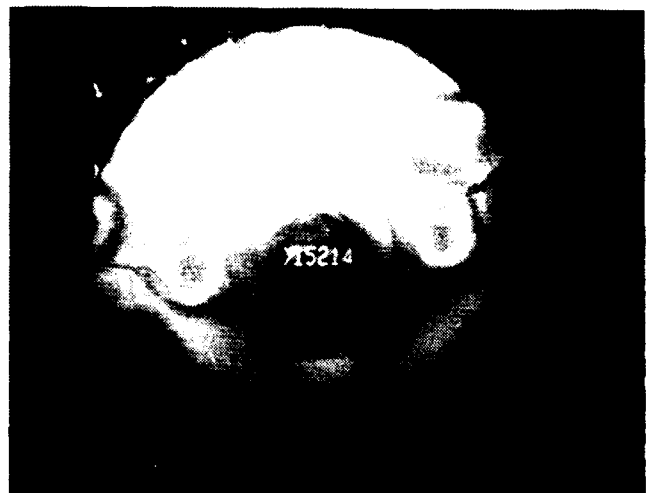
6 NODAL DIAMETERS



7 NODAL DIAMETERS



8 NODAL DIAMETERS



9 NODAL DIAMETERS

Figure 35. NASA 2-lb/Sec Scaled Compressor Holography Test Results.

### 3.6 Rough-Cut Impeller Backplate Holographic Test Results

The disk backplate resonant frequencies were determined using the same setup and technique as the blade testing. The Campbell diagram in Figure 36 shows test results. The disk frequencies have at least a 20-percent margin at room temperature. The margin is even greater at operating conditions. Photographs of several disk modes are shown in Figures 37 and 38. As the disk becomes highly active above 15,000 Hz, it is difficult to determine which modes are excited. However, the higher frequency modes are not expected to cross the 100-percent speed line, as the trend in Figure 36 is away from 100-percent speed.

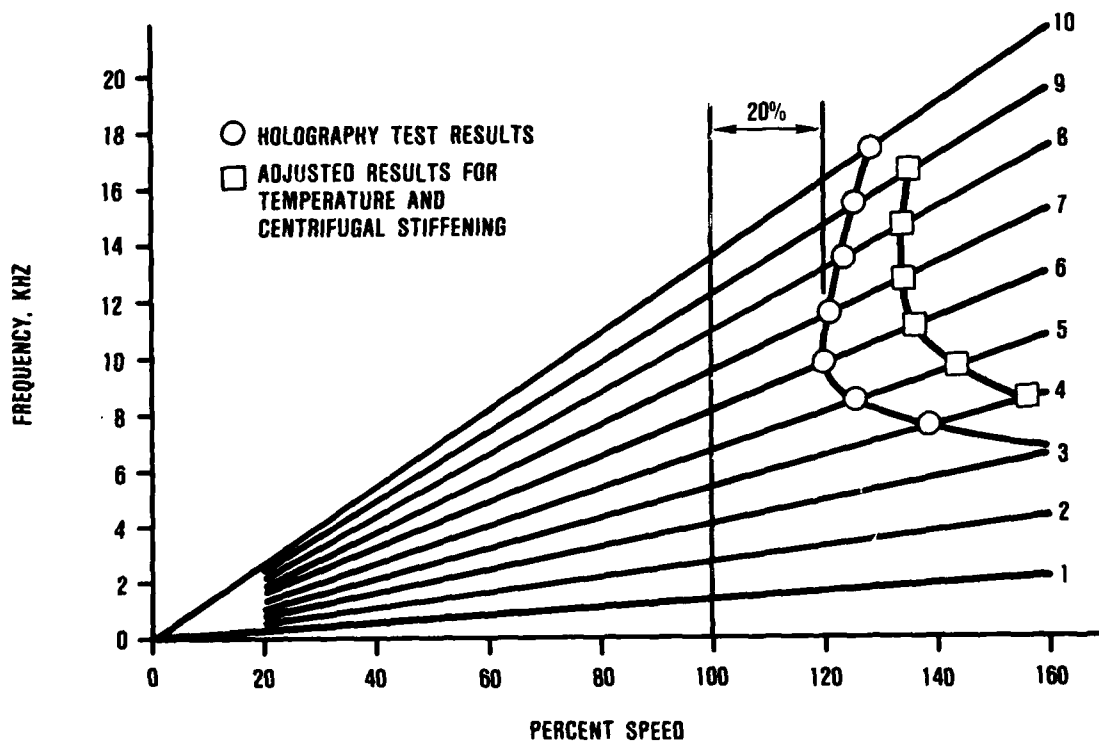
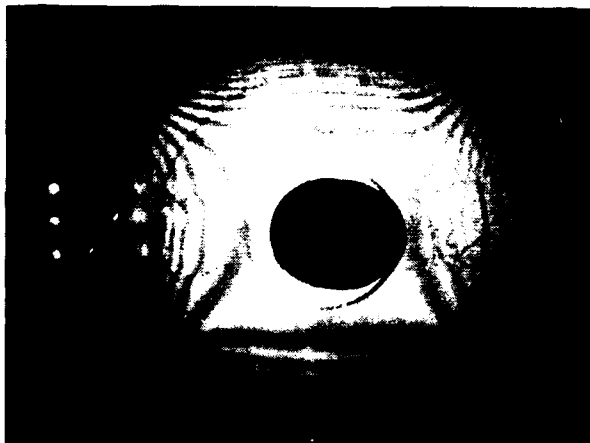
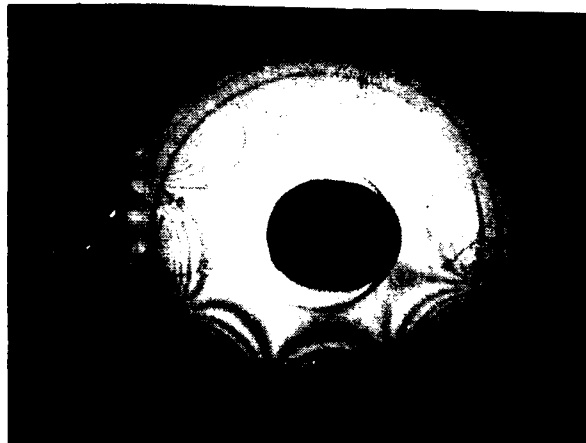


Figure 36. NASA 2-lb/Sec Rough-Cut Impeller Backplate Vibration Campbell Diagram.



2 NODAL DIAMETERS



4 NODAL DIAMETERS



6 NODAL DIAMETERS

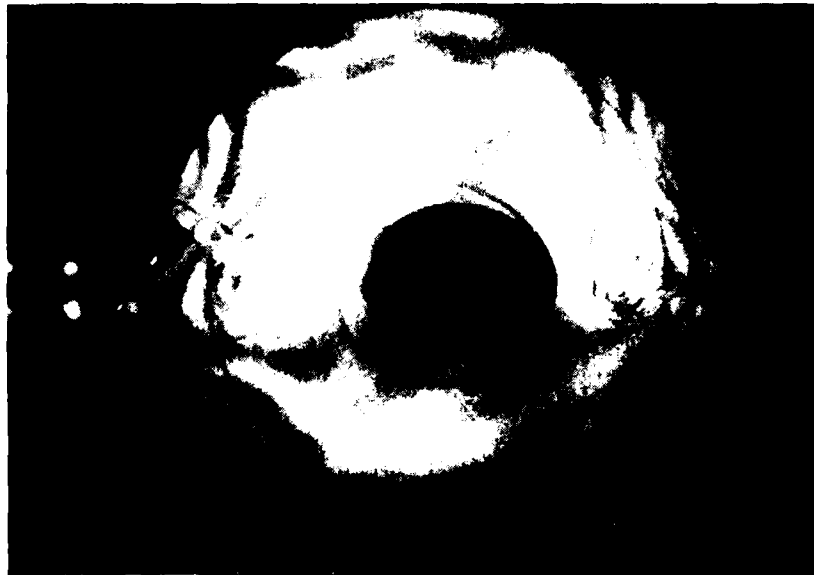


7 NODAL DIAMETERS

Figure 37. NASA 2-lb/Sec Rough-Cut Impeller Holography Test Results.



DISK MODE  
(COUPLED WITH BLADES  
FIRST NATURAL FREQUENCY)



DISK MODE  
(COUPLED WITH BLADES  
SECOND NATURAL FREQUENCY)

Figure 38. NASA 2-lb/Sec Rough-Cut Impeller Holography Test Results.

#### 4.0 2-LB/SEC ROTATING COMPONENT ANALYSIS

The 2-lb/sec compressor has been designed to fit within the existing rig with minimal modifications. It must also meet the design requirements listed below:

- o Burst margin >25 percent
- o Maximum bore Effective stress = 100 percent of yield strength
- o Average bore Effective stress = 85 percent of yield strength
- o Maximum effective Backplate stress = 80 percent of yield strength
- o Disk cycles >5000 cycles

Elliptical fillets at the impeller blade root provide a smooth stress transition from the blade to the disk. The impeller blades and disk have been analyzed with finite-element methods; therefore, stress concentration factors do not apply.

#### 4.1 2-Lb/Sec Impeller Stress and Burst Speed Analysis

The impeller stress and burst speed calculations were accomplished with the finite-element model shown in Figure 39. The blade inertias are simulated by plane stress elements of appropriate thickness. The disk stiffness is simulated by full-hoop axisymmetric elements.

The impeller material is Ti-6-4. The temperature distribution shown in Figure 40 is that which was calculated for the existing 10-lb/sec scaled impeller (P/N 3553023). The 2-lb/sec impeller should run cooler than the 10-lb/sec impeller at 100-percent speed, but this difference is not thought to be enough to warrant a full thermal analysis.

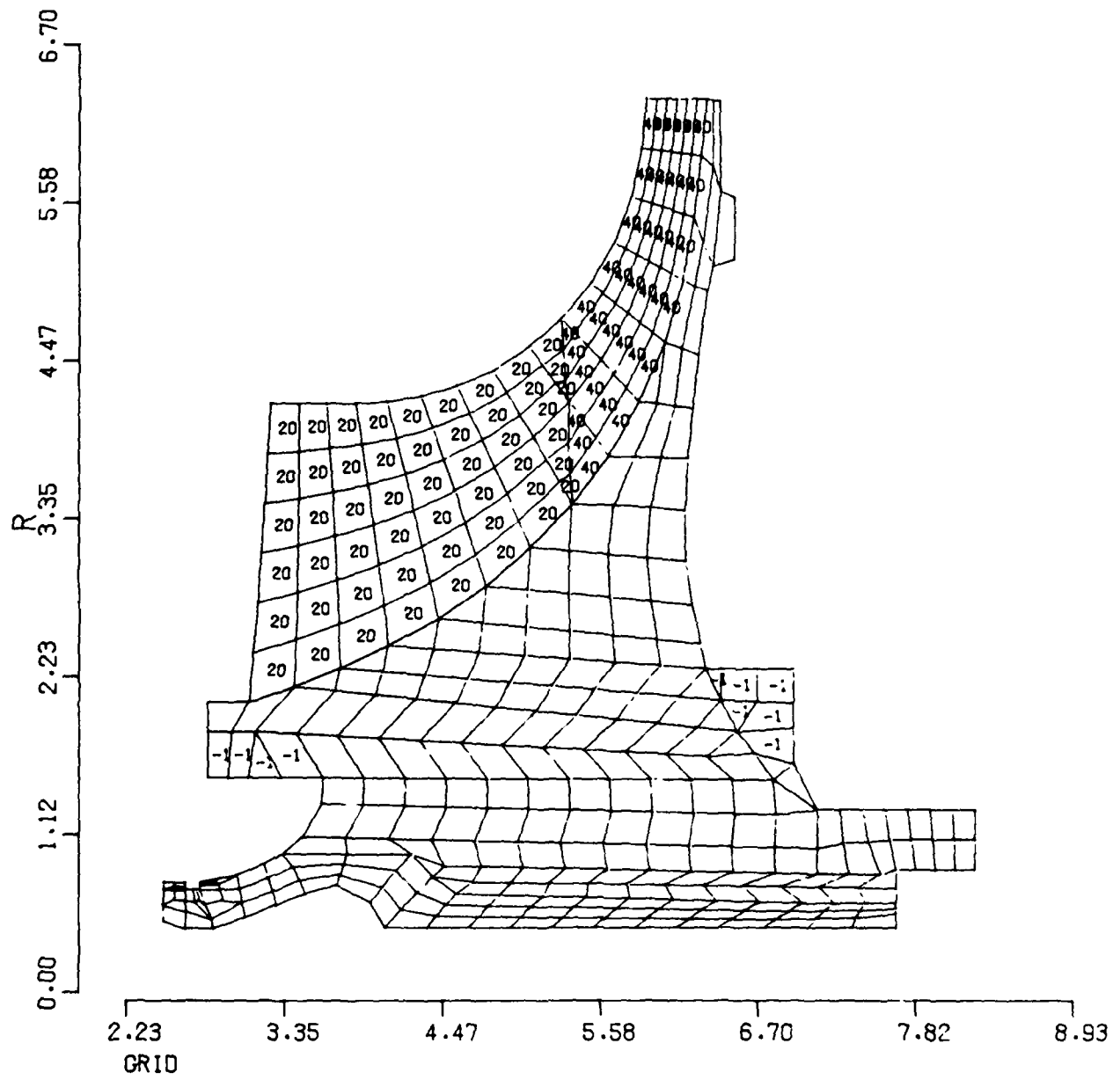
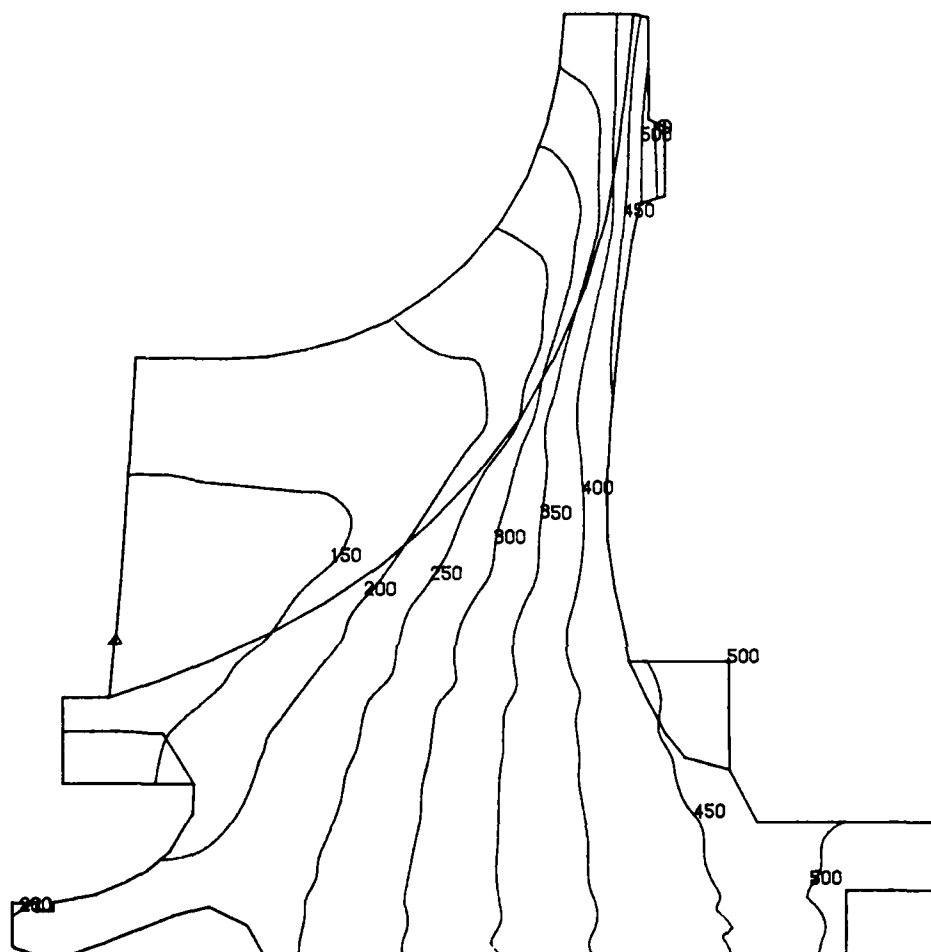


Figure 39. NASA 2-LB/Sec Impeller Finite Element Model.



TEMP DEG F

○ MAX=581.7    ▲ MIN=106.3  
ISOPLETH INTERVAL= 50

Figure 40. Temperature Distribution of 10-Lb/Sec Scaled Impeller.

Figures 41 through 43 show the various stress distributions at 105-percent speed. The effective stress distribution (Figure 41) shows the maximum stress levels per the design criteria. This is also summarized in tabular form in Table 5, which compares the design stress levels in the impeller disk with the actual yield-strength test results from the forging to be machined into the 2-lb/sec compressor. The design stress levels are within the maximum allowed, as shown in Table 5. Figure 44 shows the 2-D hub-line deflections at 105-percent speed (85,389 rpm). Figure 45 shows expected 3-D blade and hub deflections at 100-percent speed (81,319 rpm). All deflections have been calculated relative to the rear axial pilot surface.

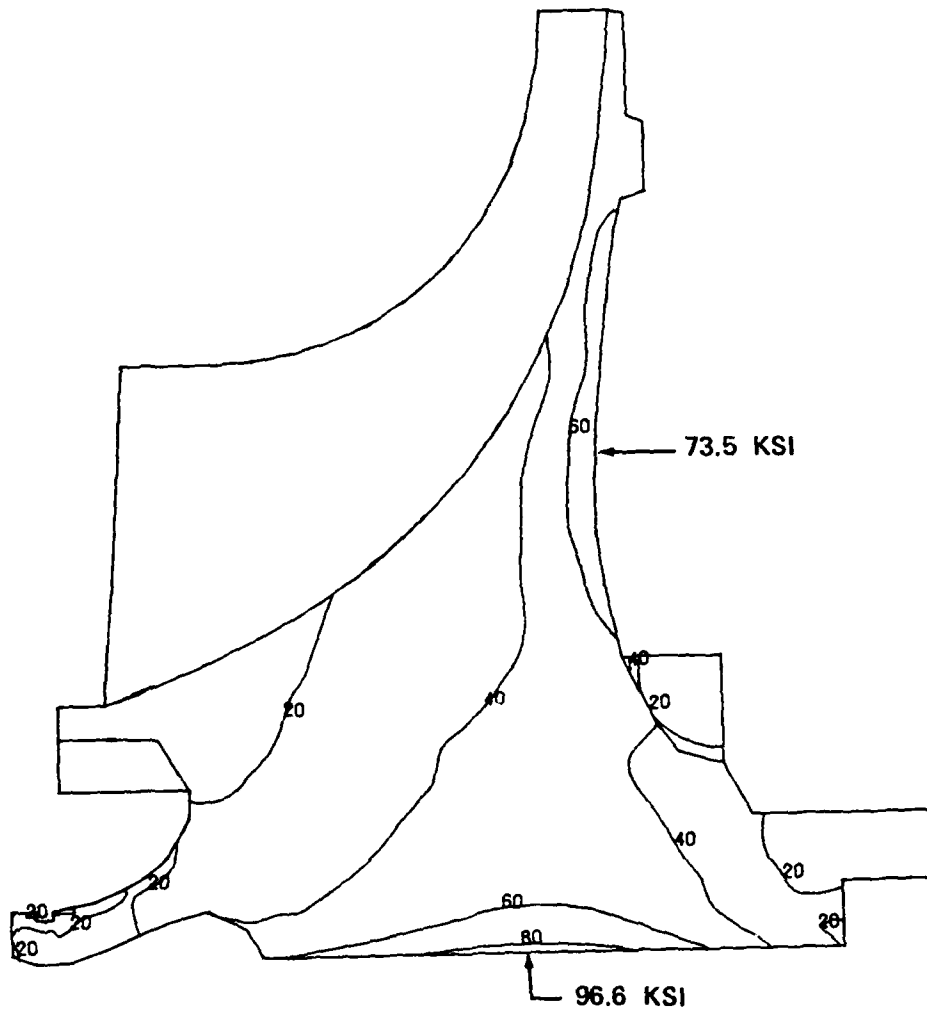
The average tangential stress calculation is based on integration of tangential stress in the disk elements. The tangential stress distribution is shown in Figure 42. The strength calculation is based on integrating the ultimate strength as a function of temperature.

For the impeller burst-speed calculation, 85 percent of the disk section is allowed to approach the ultimate material strength before burst.

Burst speed calculation:

$$\text{Burst Speed} = \sqrt{0.85 \frac{\sigma_{\text{ult}}}{\sigma_{\text{avg}}} \left( N_{100\% \text{ speed}} \right)}$$

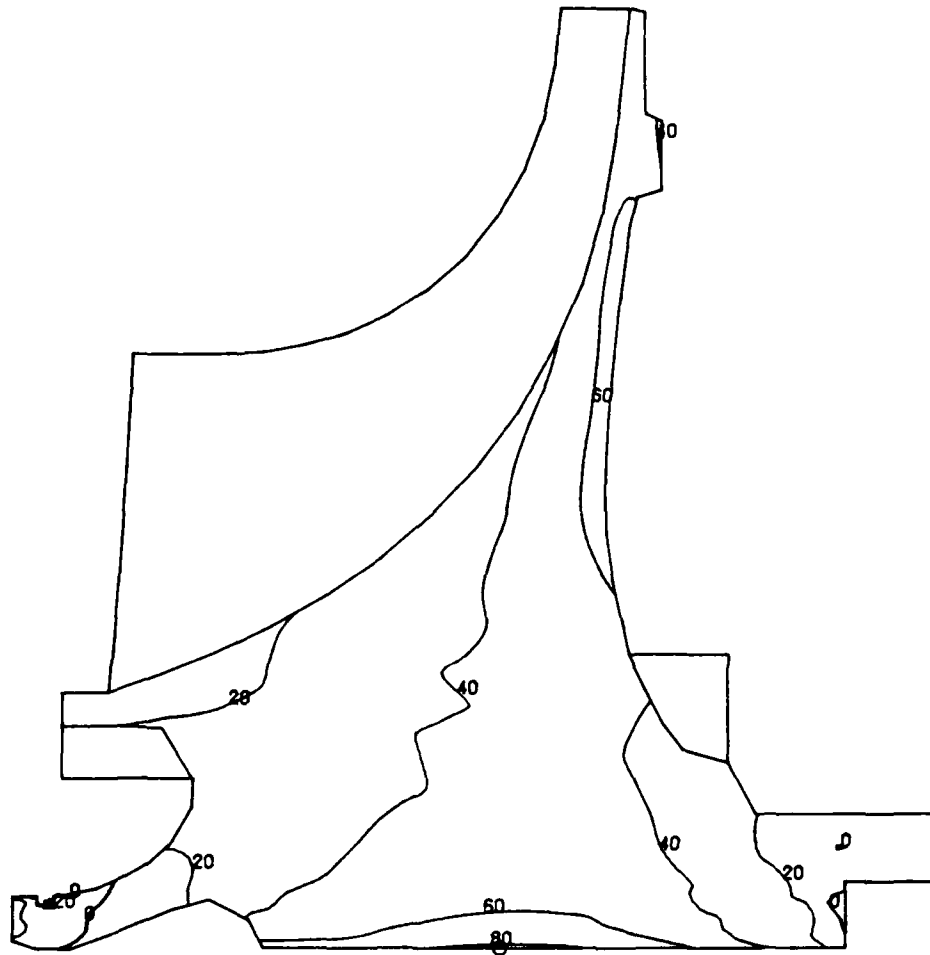
where  $\sigma_{\text{ult}}$  = ultimate material strength (minimum)  
 $\sigma_{\text{avg}}$  = average tangential stress  
 100-percent speed = 81,319 rpm



SIGMA(E)

ISOPLETH INTERVAL= 20

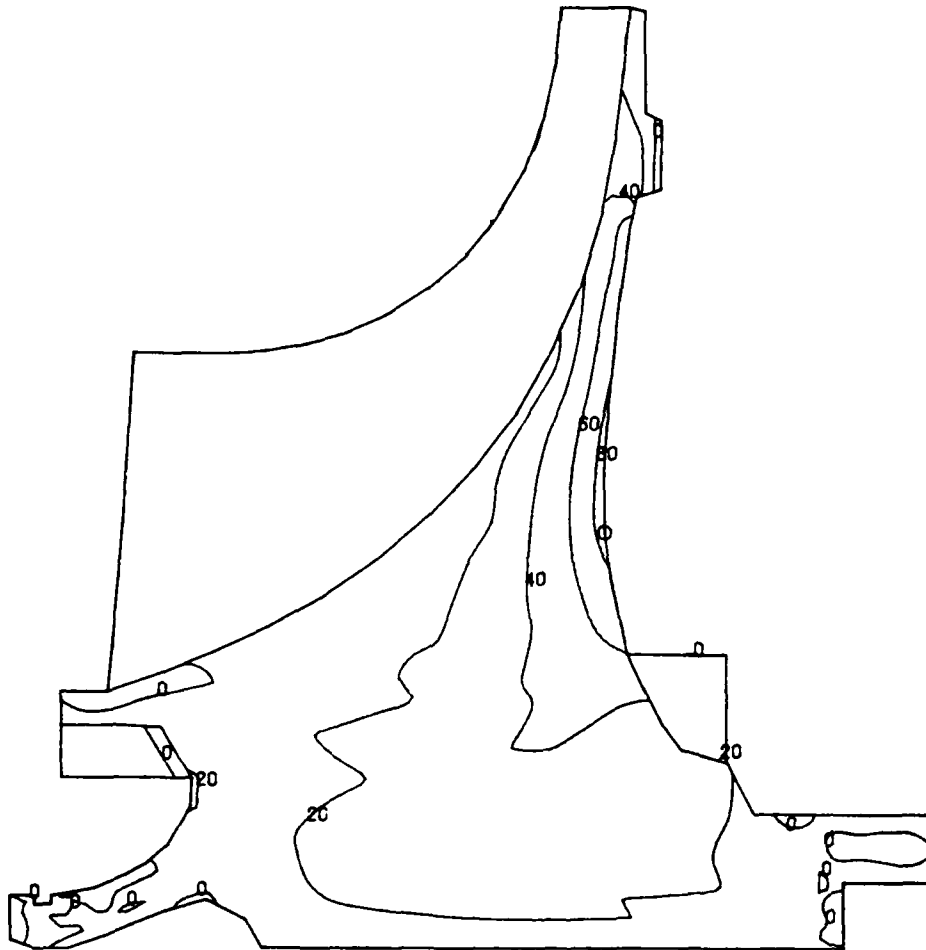
Figure 41. NASA 2-Lb/Sec Scaled Compressor at 105-Percent Speed Effective Distribution.



SIGMA(T)

○ MAX=85.7    ▲ MIN=-24.3  
ISOPLETH INTERVAL= 20

Figure 42. NASA 2-Lb/Sec Scaled Compressor at 105-Percent Speed Tangential Stress Distribution.



SIGMA(R)

MAX=87.2  
ISOPLETH INTERVAL= 20

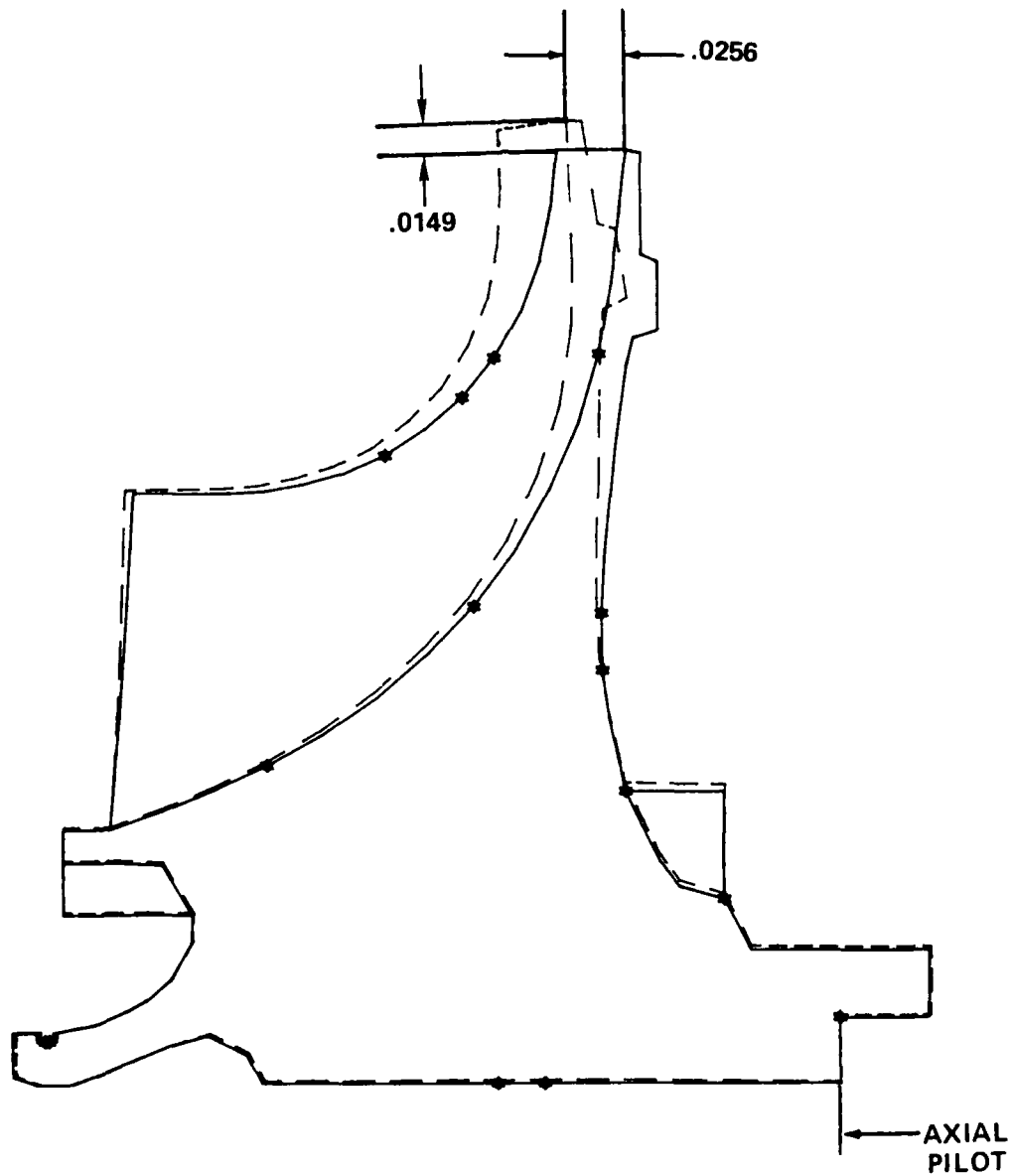
Figure 43. NASA 2-Lb/Sec Scaled Compressor at 105-Percent Speed Radial Stress Distribution.

TABLE 5. NASA 2-LB/SEC COMPRESSOR DISK ACTUAL AND ALLOWABLE STRESS LEVELS.

Criteria	Allowable	Temperature (F)	Average Tested Yield Strength (ksi)	Allowable Stress (ksi)	Actual	$\frac{\text{Allowable}}{\text{Actual}}$
Burst Margin.	>25%	-	-	-	56.9%	-
Bore, Max. Eff. Stress	100% of Yield Strength	376	105	105	96.6 ksi	1.09
Bore, Avg. Eff. Stress	85% of Yield Strength	339	107	90.9	84.2 ksi	1.08
Backplate Max. Eff. Stress	80% of Yield Strength	432	102	81.6	74.5 ksi	1.11
Disk LCF Cycles	>5000 Cycles	-	-	-	107 Cycles	-

Stress levels are at 105-percent speed (85,385 rpm)

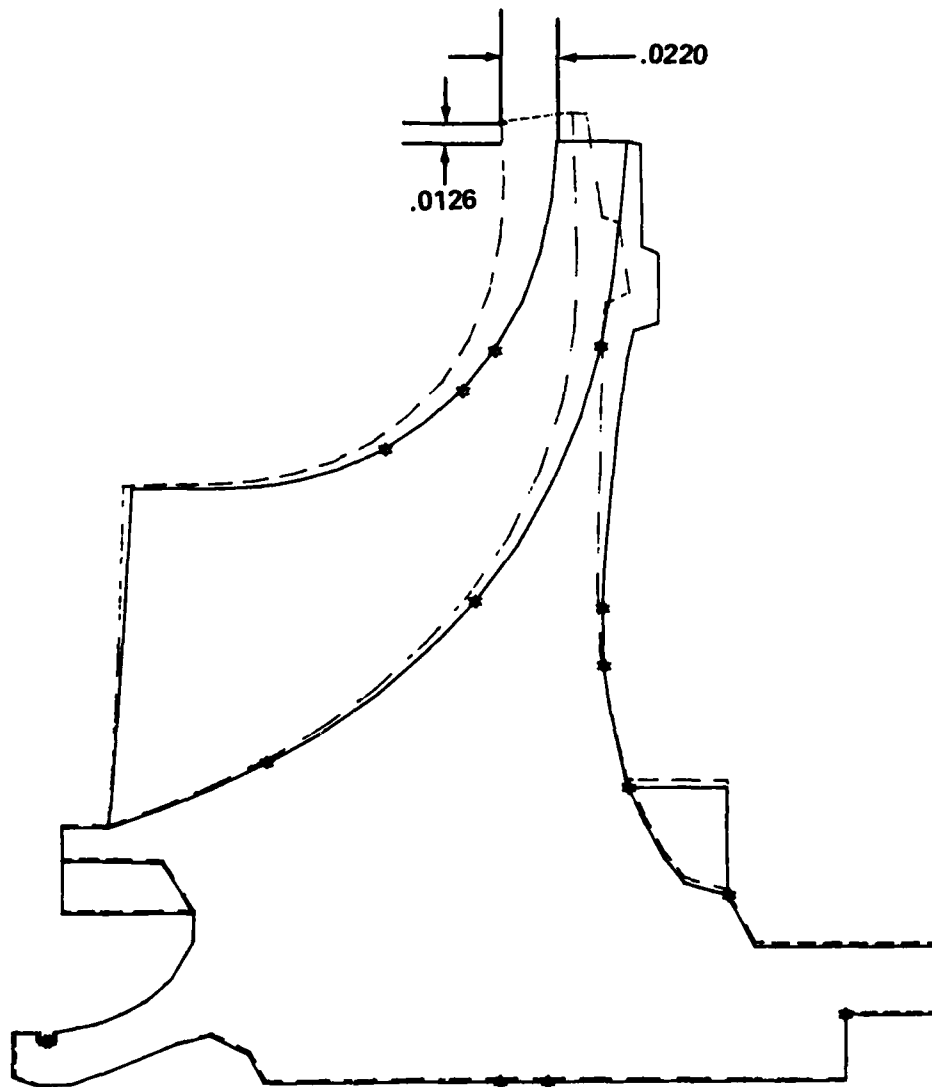
Material: Titanium 6-4



0.0200  
 0.0200 \* DISPLACEMENTS, MAGNIFIED  
 \* NODE APPEARS IN SUMMARY

ZMX 0.02657  
 RMX 0.01481

Figure 44. NASA 2-Lb/Sec Scaled Compressor at 105-Percent Speed 2-D Hubline Deflection.



0.0200  
 0.0200 L DISPLACEMENTS, MAGNIFIED ZMX 0.02488  
 \* NODE APPEARS IN SUMMARY RMX 0.01394

Figure 45. NASA 2-Lb/Sec Scaled Compressor at 100-Percent Speed 3-D Blade Displacements, 81,319 rpm.

therefore:

$$\begin{aligned} \text{Burst Speed} &= \sqrt{0.85 \frac{109.4}{34.1} (81,319)} \\ &= 134,287 \text{ rpm} \end{aligned}$$

#### 4.2 Calculation of Moment of Inertia

Inertial properties are calculated within the finite-element analysis program used to evaluate impeller stresses. The calculation is an integration of the element inertias. The results of the computer analysis are shown in Table 6 and are summarized as follows:

	<u>Blades</u>	<u>Disk</u>	<u>Total</u>
Weight (lb)	0.2711	1.662	1.933
Polar moment of inertia (lb-in.-sec <sup>2</sup> )	0.0016	0.0071	0.0087
Diametral moment of inertia (lb-in.-sec <sup>2</sup> )	0.0008	0.0044	0.0053

#### 4.3 2-Lb/Sec Test Rig Rotor Dynamics Analysis

The existing NASA 2-lb/sec compressor rig rotating group has been modified to reduce the possibility of the stacking tolerance of the components, combining in such a way as to shift the center of gravity of the impeller. The new tieshaft features a clamping load only through the impeller. The portion of the tieshaft aft of the impeller is loaded by the wavy washers near the bearing.

Other modifications include the addition of a spring-cage support at the forward bearing with a stiffness of 20,000 lb/in. in parallel with a squeeze-film damper. The squeeze-film damper

TABLE 6. COMPUTER MECHANICAL ANALYSIS NASA SCHEDULE 2-LB/SEC IMPELLER.

HUB AREA PROPERTIES--AREA	1.9873 IN**2	MASS PROPERTIES--MASS	.0043 LB-SEC2/IN
RBAR	.8268 IN	WEIGHT	1.6621 LB
ZBAR	2.4190 IN	I(P)	.0071 LB-IN-SEC2
		I(D)	.0044 LB-IN-SEC2
		RBAR	0.0000 IN
		ZBAR	2.4509 IN
BLADE AREA PROPERTIES--AREA	1.1129 IN**2	MASS PROPERTIES--MASS	.0007 LB-SEC2/IN
RBAR	1.6364 IN	WEIGHT	.2711 LB
ZBAR	2.0940 IN	I(P)	.0016 LB-IN-SEC2
		I(D)	.0008 LB-IN-SEC2
		RBAR	1.4008 IN
		ZBAR	2.1747 IN
(MASS PROPERTIES ARE FOR ALL BLADES)			
TOTAL PROPERTIES-----MASS	.0050 LB-SEC2/IN	KINETIC ENERGIES	
WEIGHT	1.9332 LB	-ALL BLADES	62600. IN-LB
I(P)	.0067 LB-IN-SEC2	-----DISC	284600. IN-LB
I(D)	.0053 LB-IN-SEC2	-----TOTAL	347200. IN-LB
RBAR	1.1725 IN		
ZBAR	2.4122 IN		

SPEED OF ROTATION = 65361 RPM

should have a land length of 0.45 inch and a radial clearance of 0.0023 inch. The rear bearing is to be hard-mounted with no damper.

The rotor schematic and rotor dynamics model used for the analysis are shown in Figures 46a and 46b.

The final support stiffnesses used to determine the critical speed margin have been determined by combining bearing, structural, damper, and spring-cage stiffnesses. The front structural support is assumed to be extremely stiff compared to the spring cage. Additionally, the spring cage and damper are in parallel; therefore, the minimum front bearing support is the 20,000 lb/in. spring-cage stiffness. The rear bearing radial stiffness is 500,000 lb/in., while the rear structural stiffness at the bearing location has been calculated to be between 500,000 lb/in. and  $1.2 \times 10^6$  lb/in. Combining the bearing and structural stiffness in series, the total support stiffness at the rear is between 250,000 lb/in. and 355,000 lb/in. The higher value has been used in all the unbalance response calculations, except in the nominal case where an average value of 300,000 lb/in. has been assumed. The margin above full speed on the flexural critical speed is over 60 percent, assuming 20,000 lb/in. front and 250,000 lb/in. rear support stiffness. The relationship between critical speed and front and rear support stiffness is shown in Figure 47. The first four mode shapes are shown in Figure 48.

Unbalance response calculations assumed 0.001-inch eccentricity on each wheel, both in- and out-of-phase. The minimum damper radial clearance was 0.0023 inch and the land length was 0.45 inch. The oil was assumed to be MIL-L-7808 (Type I), 150F.

The combination of 0.001-inch eccentricity unbalance and damper characteristics has maintained a maximum bearing radial

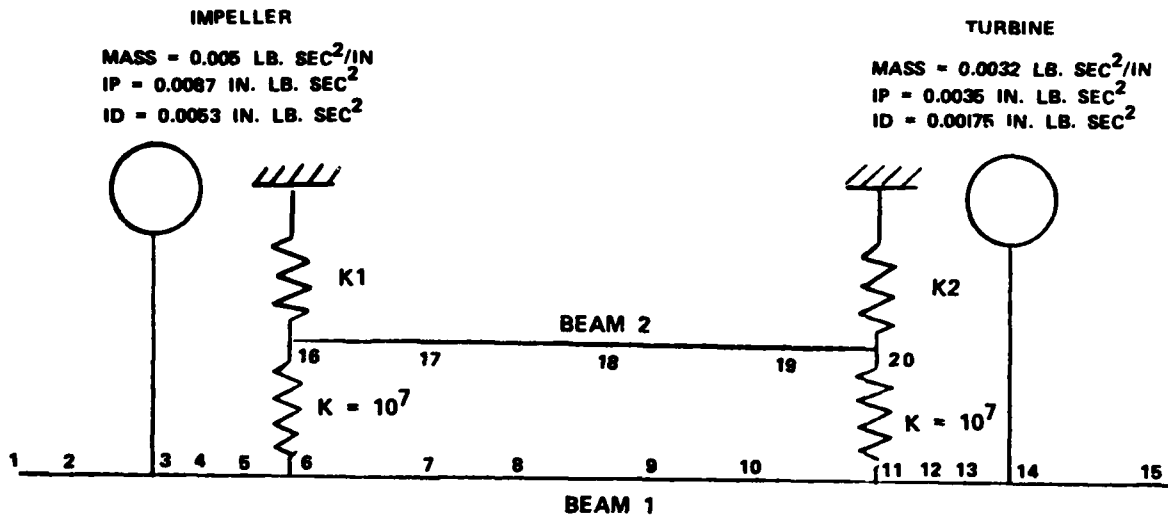


Figure 46a. 2-Lb/Sec Compressor Rig Rotor Dynamics Schematic.

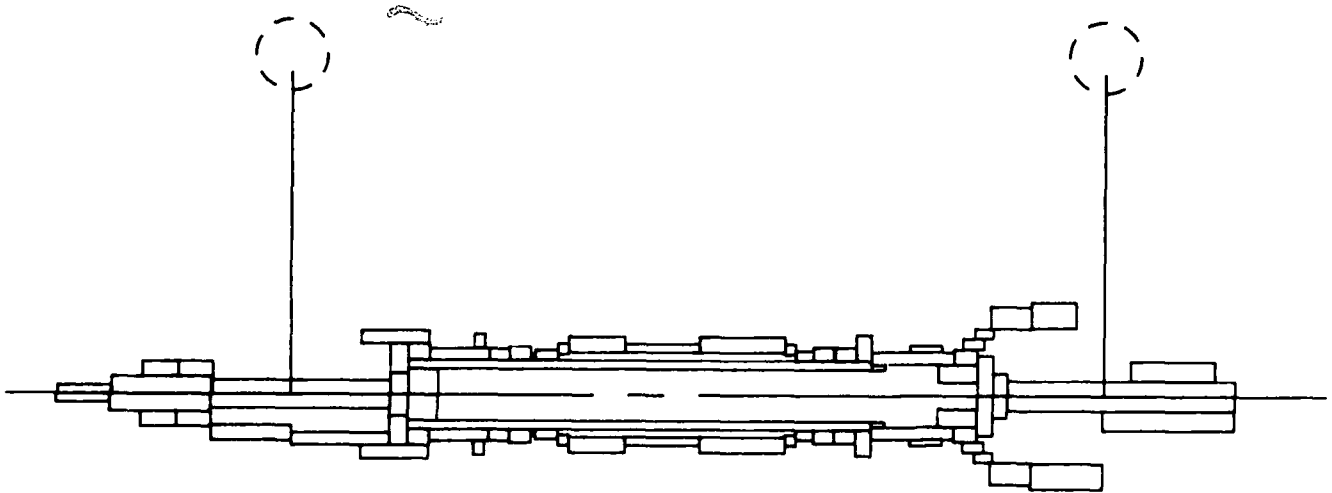


Figure 46b. 2-Lb/Sec Compressor Rig Rotor Dynamics Analysis Model.

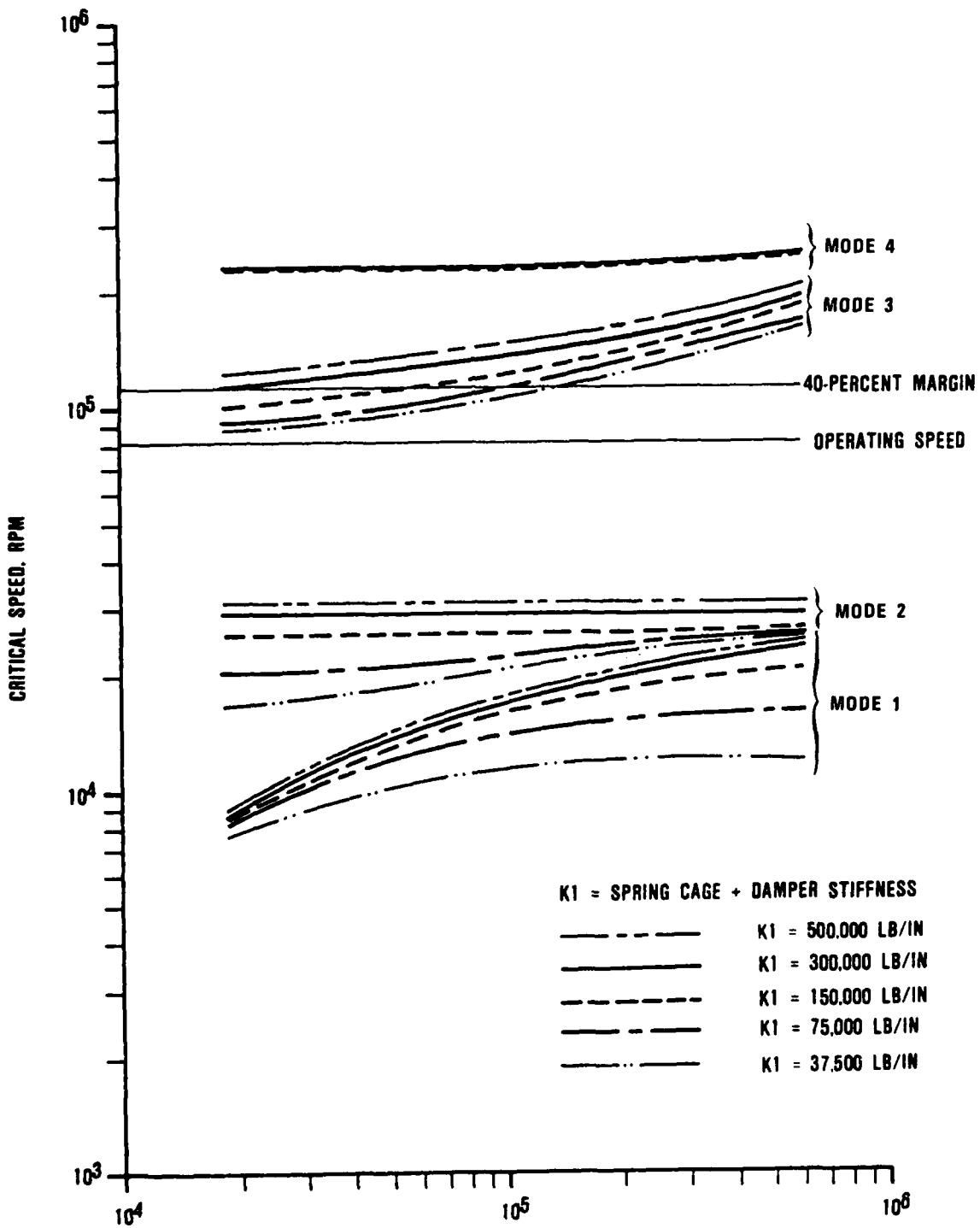


Figure 47. Structural Stiffness Versus Critical Speed.

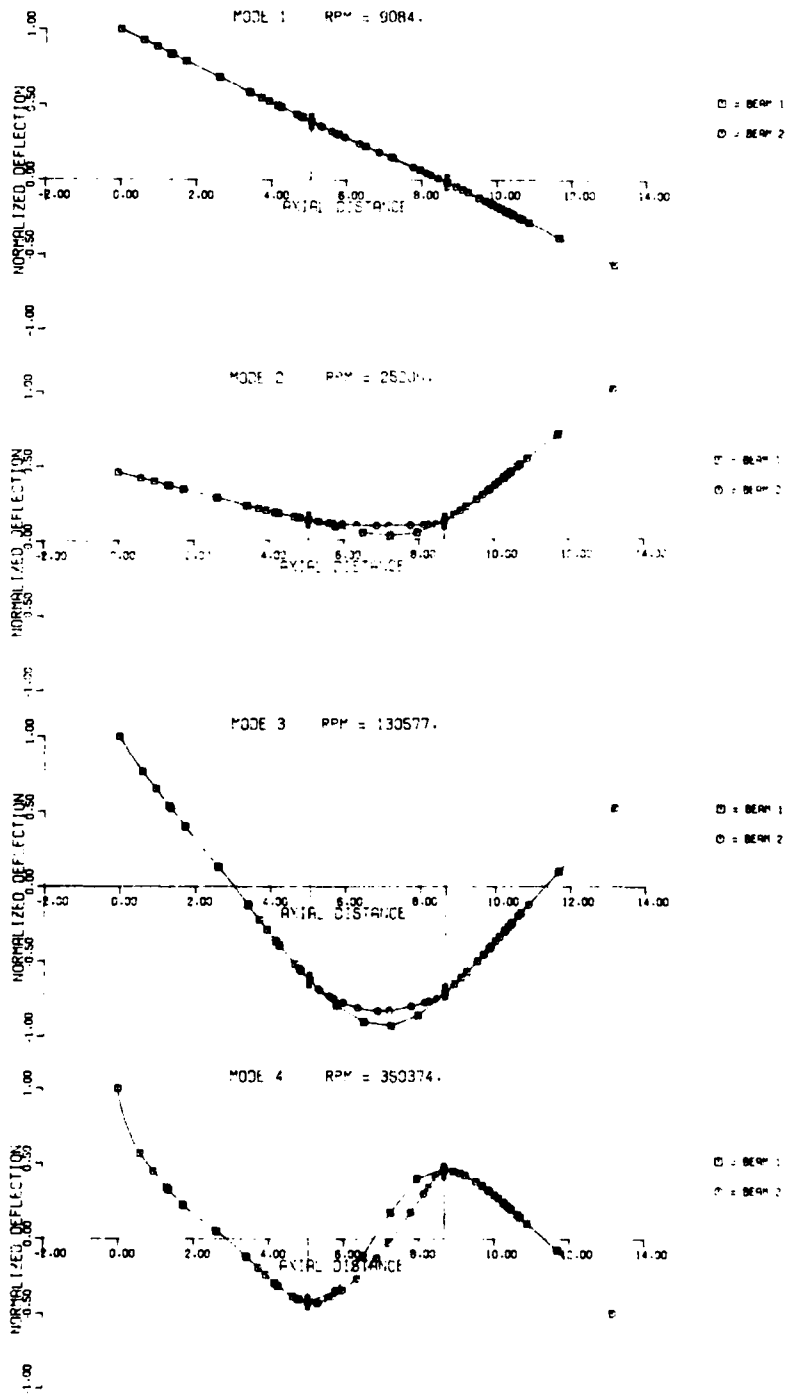


Figure 48. Deflection Vs. Axial Distance, Modes 1 to 4.

load of under 390 pounds. This is well below the maximum allowable transient load of 600 pounds. Plots of load and displacement-versus-speed for in-phase and out-of-phase unbalances are shown in Figures 49 through 52.

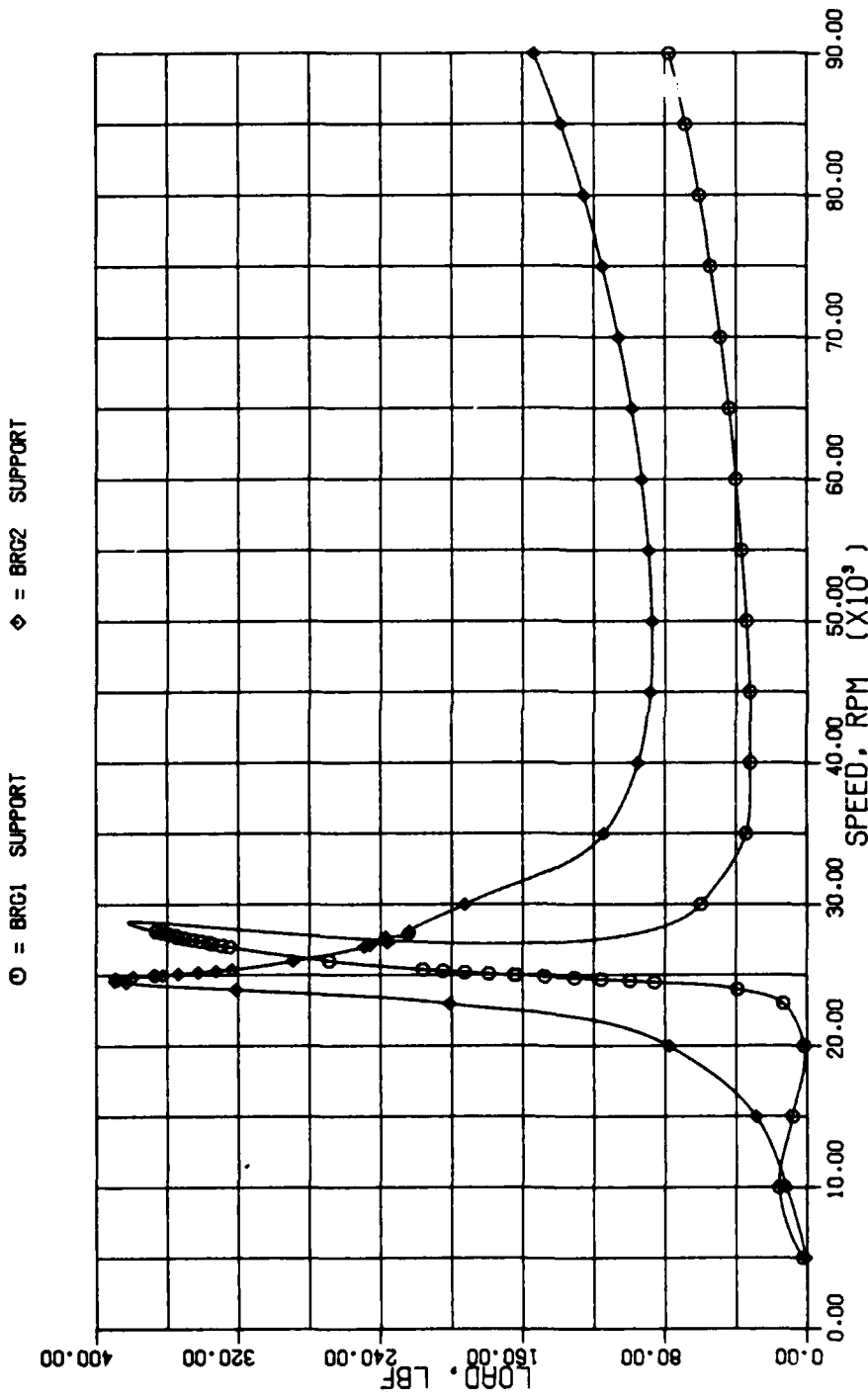
Figures 53 through 56 show similar responses, but for a nominal eccentricity of 0.0005 inch on each wheel, and an average rear-support stiffness of 300,000 lb/in. Peak transient loads under nominal unbalance are expected to be less than 340 pounds at the rear support and less than 160 pounds at the front bearing. One-hundred-percent speed bearing radial loads should be less than 35 and 70 pounds for the front and rear bearings, respectively.

The damper clearance has been set by the assumption of 0.001-inch eccentricity as a worst-case condition. Decreasing the clearance for lower levels of unbalance will result in lower 100-percent speed bearing loads at the expense of higher transient loads. Similarly, if higher than a 0.001-inch eccentricity unbalance is expected, increasing the damper clearance will result in lower transient loads, but higher bearing loads at operating speed, with an associated decrease in bearing life.

#### 4.4 2-Lb/Sec Impeller Weight Study

At NASA's request, a study was conducted to determine the effect of varying impeller weight on the rotor dynamics of the 2-lb/sec test rig. Bearing loads and critical speeds were determined as a function of varying the impeller mass and inertia. The impeller (Part No. 3554664) mass and inertia were increased and decreased by 50 percent of the respective design values. The support and squeeze-film damper parameters are listed below:

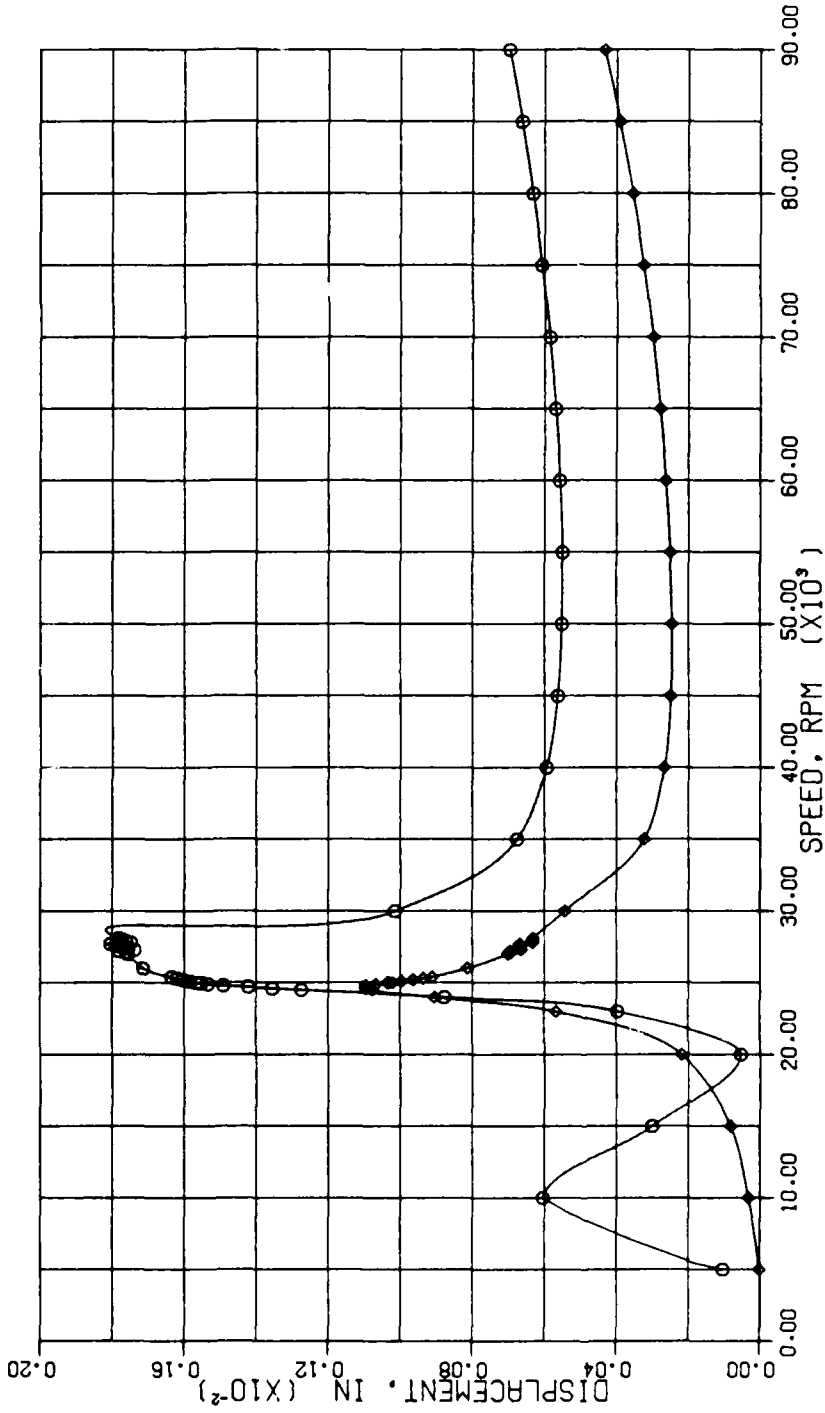
Forward support stiffness	20,000 lb/in.
Rear support stiffness	355,000 lb/in.



.0023 IN CLEARANCE ON DAMPER,.001 IN PHASE,K1=20K,K2=355K,TYPE1,150F OIL,L=.45

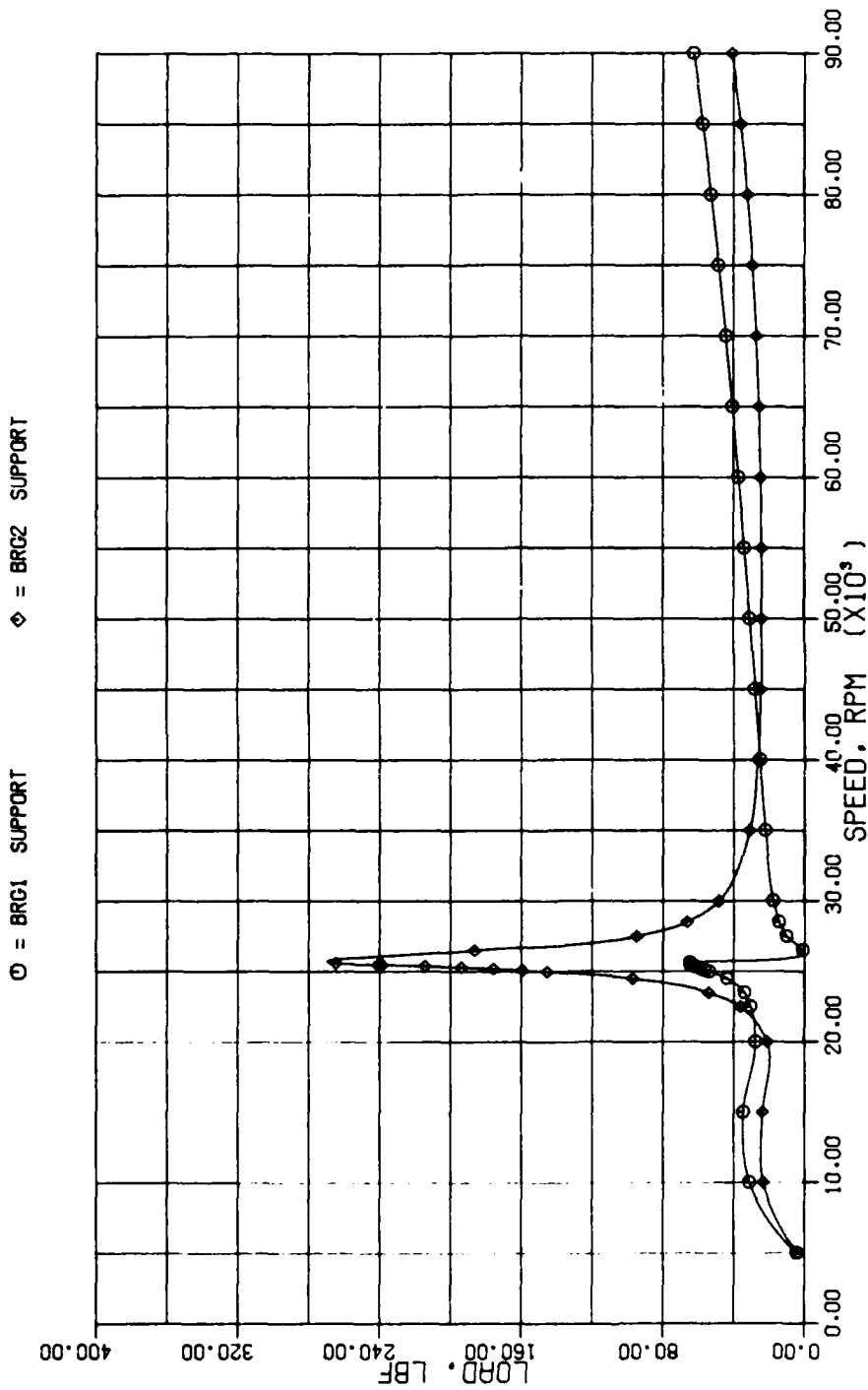
Figure 49. Unbalance Condition Load Vs. Speed, In-Phase.

○ = BRG1 SUPPORT      ◇ = BRG2 SUPPORT



.0023 IN CLEARANCE ON DAMPER..001 IN PHASE,K1=20K,K2=355K,TYPE1,150F OIL,L=-.45

Figure 50. Unbalance Condition Displacement Vs. Speed, In-Phase.



.0023 IN CLEARANCE ON DAMPER .001 OUT PHASE .K1=20K .K2=355K .TYPE1,150F OIL .L=.45

Figure 51. Unbalance Condition Load Vs. Speed, Out-Of-Phase.

AD-A174 001

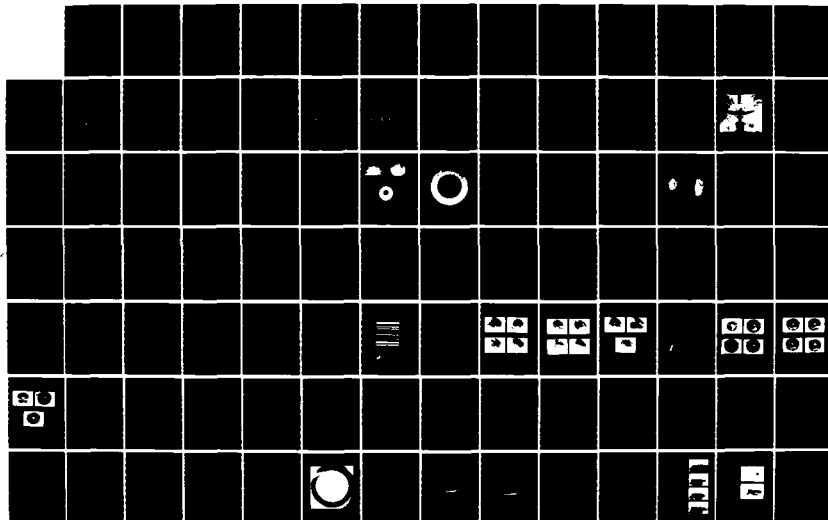
SCALED CENTRIFUGAL COMPRESSOR PROGRAM(U) GARRETT  
TURBINE ENGINE CO PHOENIX AZ G CARGILL ET AL.  
31 OCT 96 21-5464 NASA-CR-174912 NAS3-23277

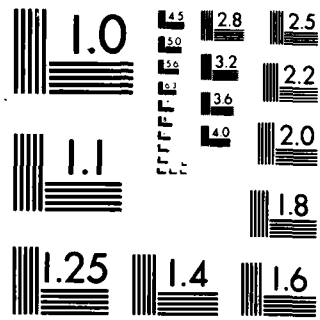
2/3

UNCLASSIFIED

F/G 21/5

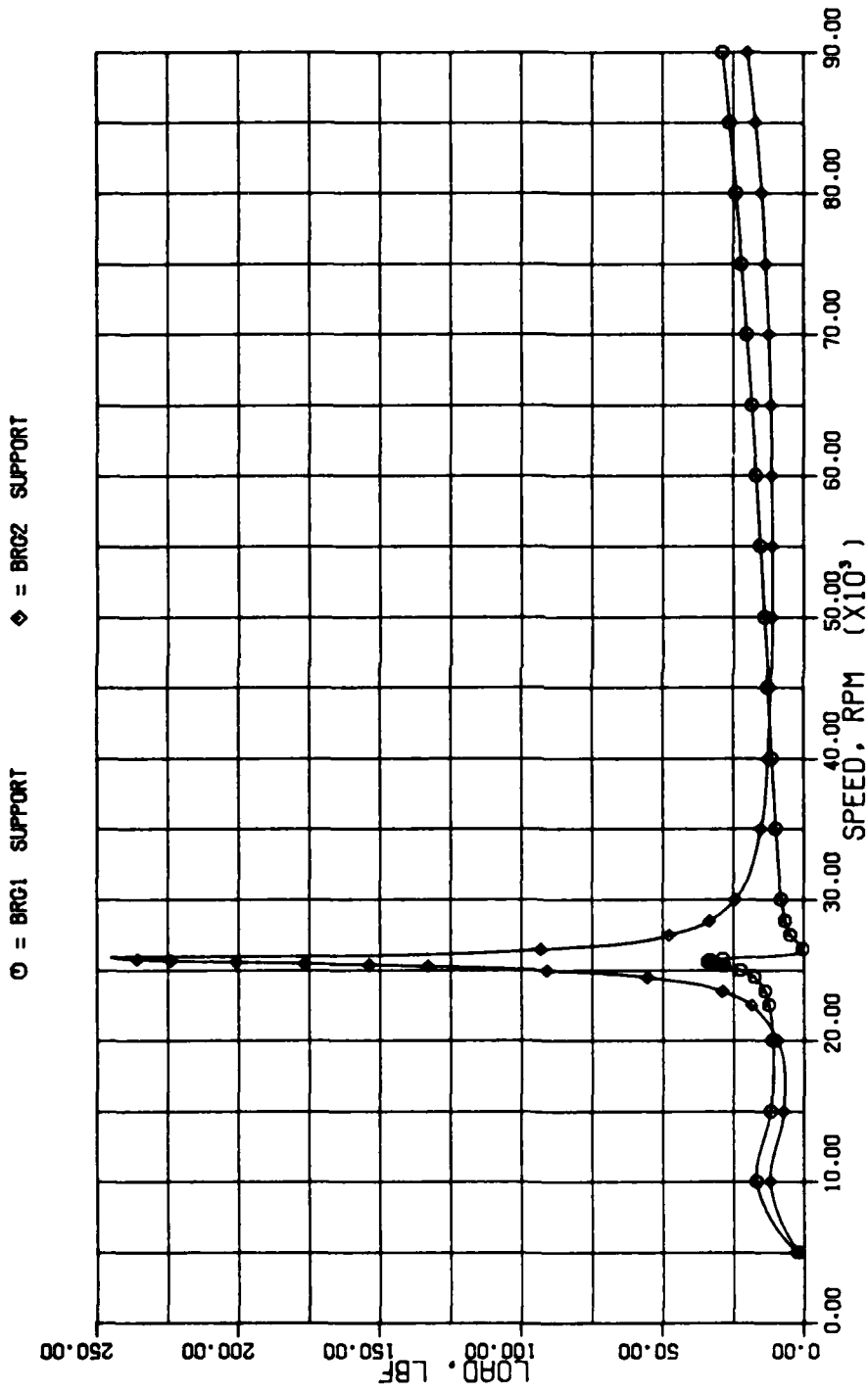
NL





MICROCOPY RESOLUTION TEST CHART  
NATIONAL BUREAU OF STANDARDS-1963-A

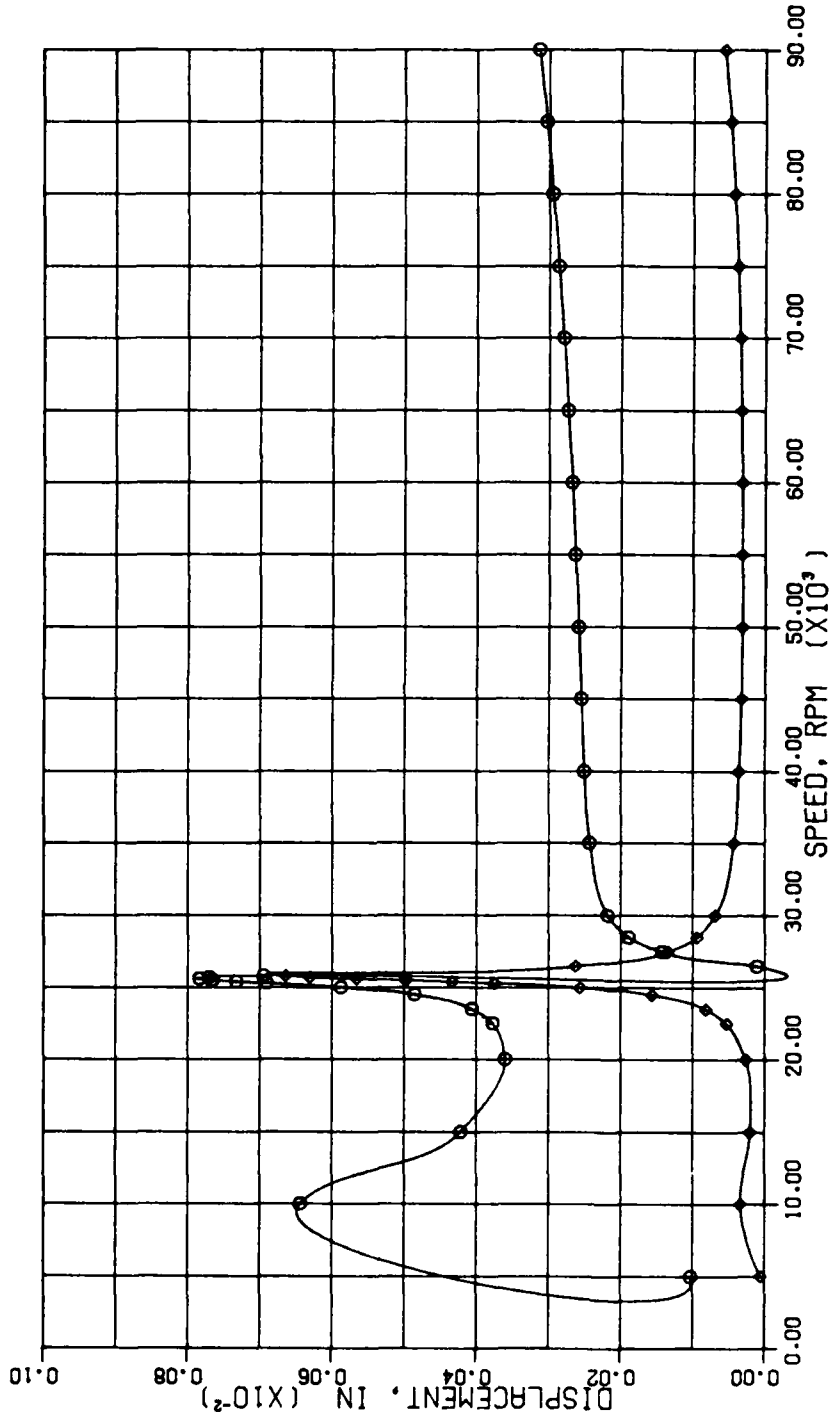




.0023 OUT CLEARANCE ON DAMPER .0005 OUT PHASE .K1=20K .K2=355K .TYPE1 .150F OIL .L=.45

Figure 53. Unbalance Condition Load Vs. Speed, Out-Of-Phase.

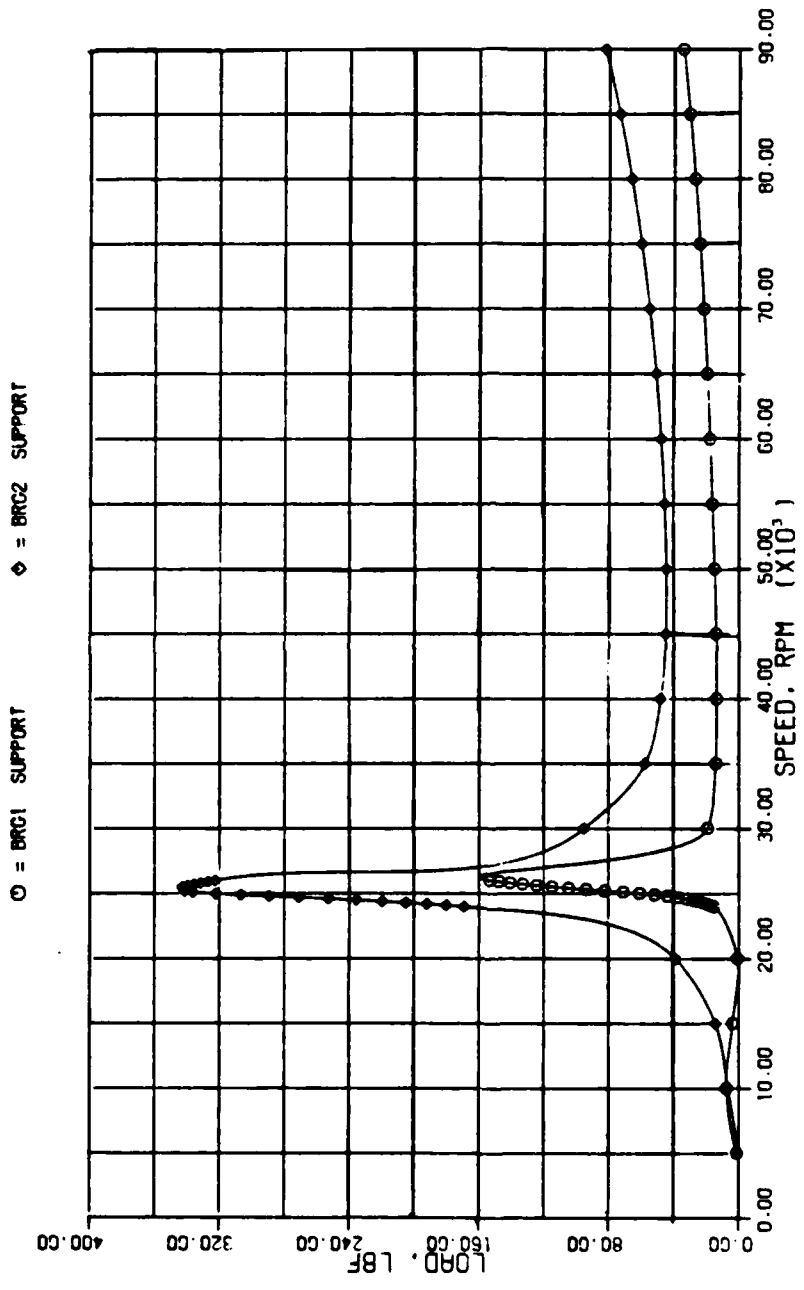
○ = BRG1 SUPPORT      ◇ = BRG2 SUPPORT



.0023 OUT CLEARANCE ON DAMPER, K1=20K, K2=355K, TYPE 1, 150F OIL, L=.45

Figure 54. Unbalance Condition Displacement Vs. Speed, Out-Of-Phase.

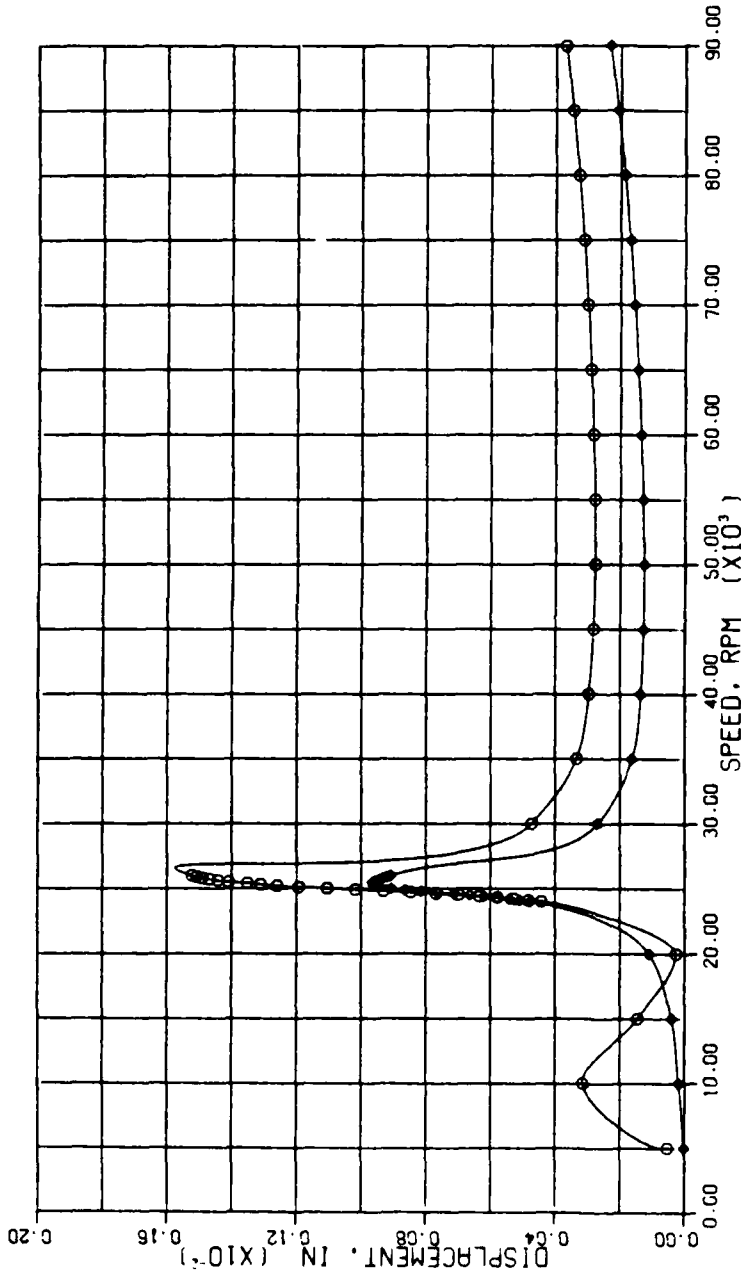
0 100 200 300 400 500 600 700 800 900 1000 1100 1200 1300 1400 1500 1600 1700 1800 1900 2000 2100 2200 2300 2400 2500 2600 2700 2800 2900 3000 3100 3200 3300 3400 3500 3600 3700 3800 3900 4000 4100 4200 4300 4400 4500 4600 4700 4800 4900 5000 5100 5200 5300 5400 5500 5600 5700 5800 5900 6000 6100 6200 6300 6400 6500 6600 6700 6800 6900 7000 7100 7200 7300 7400 7500 7600 7700 7800 7900 8000 8100 8200 8300 8400 8500 8600 8700 8800 8900 9000 9100 9200 9300 9400 9500 9600 9700 9800 9900 10000



.0023 IN CLEARANCE ON DAMPER. COOS IN PHASE. M1=20K. M2=355K. TYPE1. 'SDP' OIL. I=.45

Figure 55. Unbalance Condition Load Vs. Speed, In-Phase.

○ = BRC1 SUPPORT      ◇ = BRC2 SUPPORT



.0023 IN CLEARANCE ON DAMPER .K1=20K .K2=355K .TYPE1.150F OIL.L=.45

Figure 56. Unbalance Condition Displacement Vs. Speed, In-Phase.

Oil type, temperature	Type 1, 150F
Damper clearance	0.0023-inch radial
Damper length	0.45 inch
Unbalance eccentricity	0.0005 inch, in-phase

The results of this study indicate that the critical speed is not significantly affected by varying impeller mass. Figure 57 presents the critical-speed change as a function of the impeller-mass change, i.e., the ratio of new impeller mass to Part No. 3554664 impeller mass.

The study results also indicate that bearing loads can be significantly affected by varying impeller weight. The maximum transient radial load capability of the bearing is 600 pounds. A transient radial load of 580 pounds could be produced as the rotating group passes through the second critical speed (24,800 rpm) by an impeller with a mass 1-1/2 times that of Part No. 3554664. This condition is presented in Figure 58. Figures 59 and 60 present bearing loads-versus-speed for nominal (Part No. 3554664) impeller mass and 1/2-nominal impeller mass. The maximum bearing loads as a function of varying impeller mass are summarized in Figure 61.

The results of this study conclude that an impeller with a mass up to 1-1/2 times that of Part No. 3554664 can be used in this test rig. However, extra attention must be used to balance the rotating group precisely to minimize bearing load.

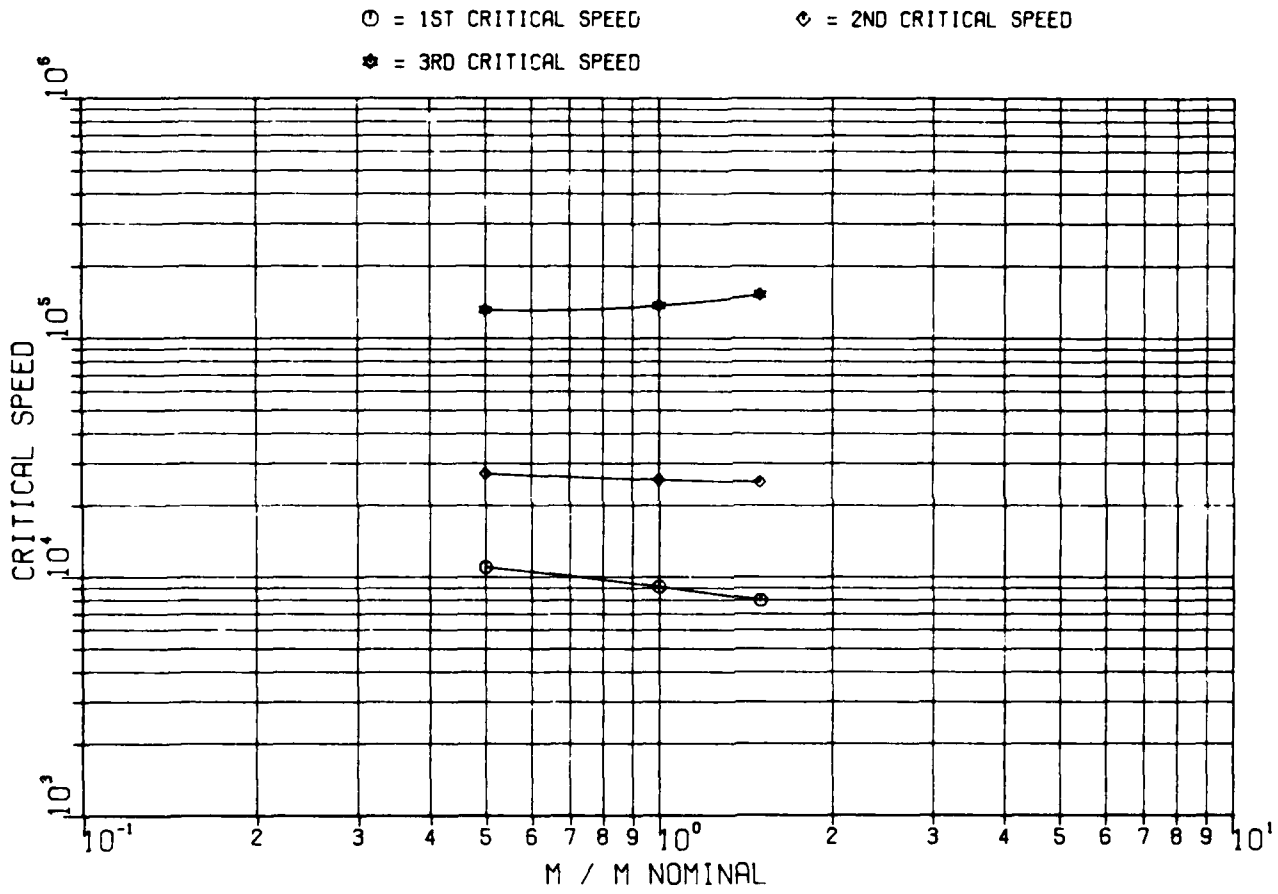


Figure 57. 2-Lb/Sec Compressor Rig; Effect of Mass and Inertia on Critical Speed.

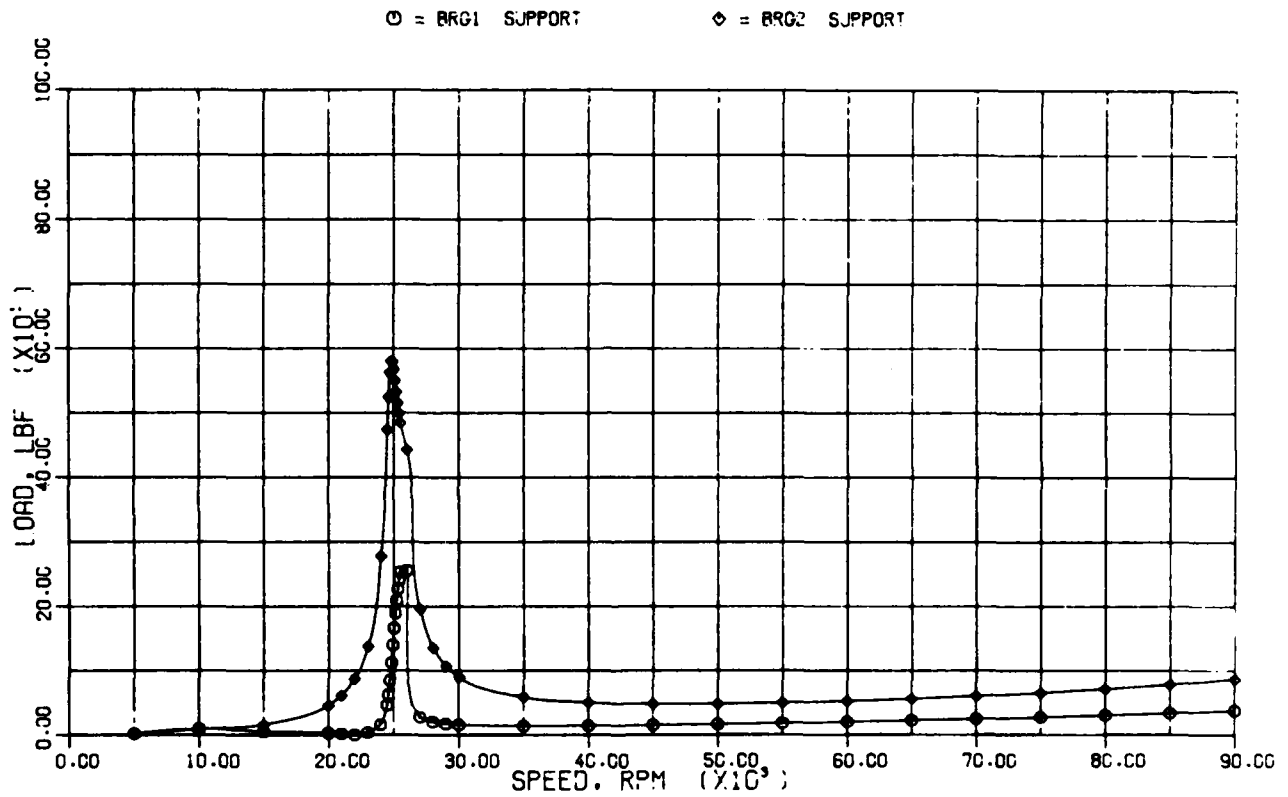


Figure 58. NASA 2-Lb/Sec Compressor Rig Unbalance Response With 1.5 Times Nominal Impeller Mass.

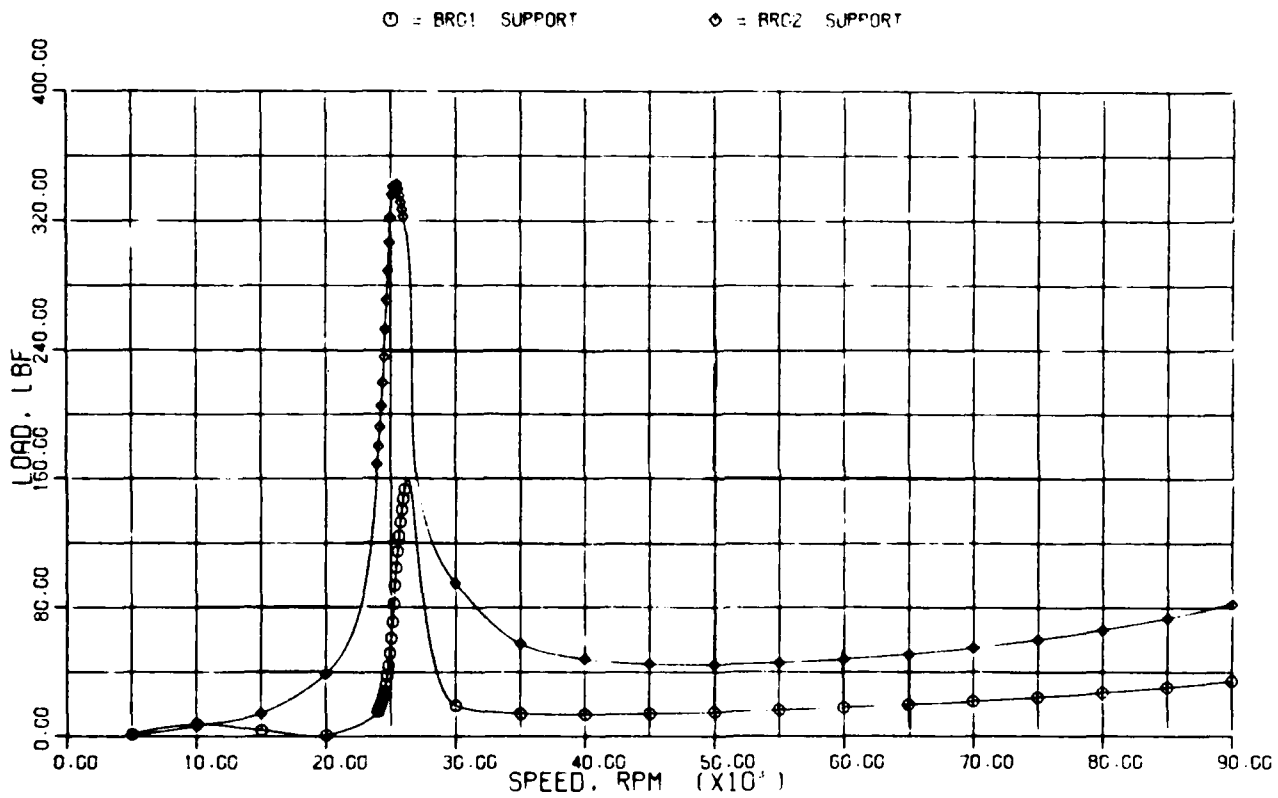


Figure 59. NASA 2-Lb/Sec Compressor Rig Unbalance Response with Nominal Impeller Mass.

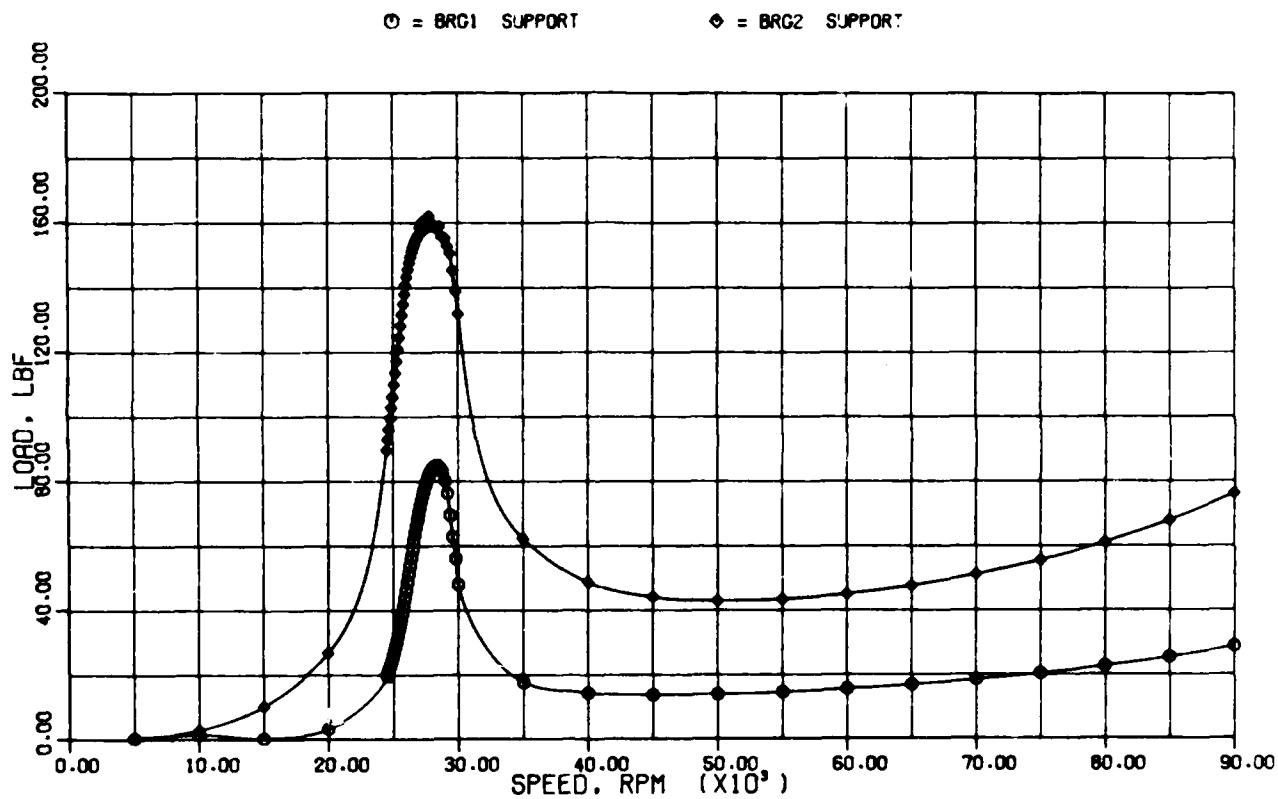


Figure 60. NASA 2-Lb/Sec Compressor Rig Unbalance Response with One-Half Nominal Impeller Mass.

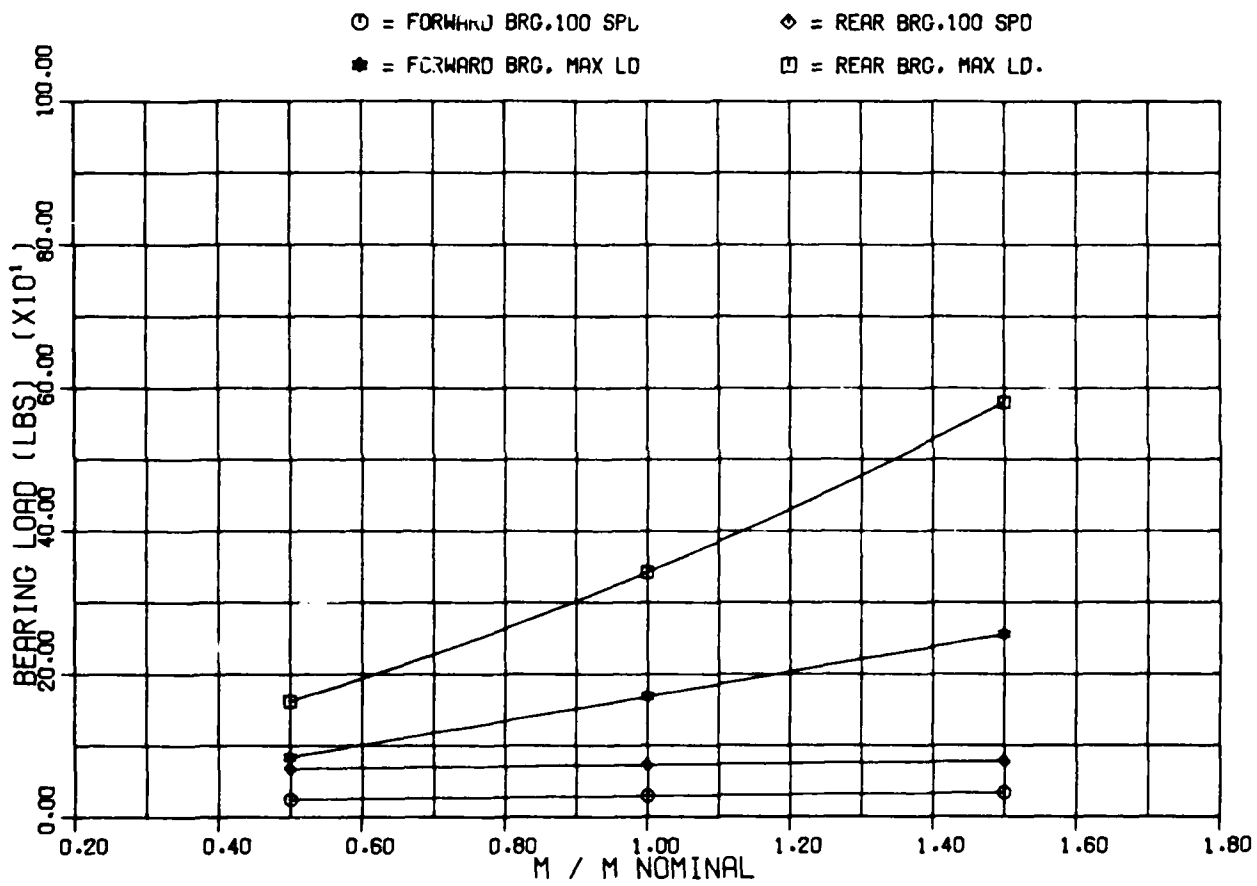


Figure 61. NASA 2-Lb/Sec Compressor Rig; Effect of Mass and Inertia on Maximum Bearing Load.

## 5.0 2-LB/SEC STATIC COMPONENT ANALYSIS

A detailed finite-element thermal and stress analysis performed on the compressor shroud and diffuser housings indicates that all design parameters will be met.

The finite-element model of the static structure is shown in Figure 62. The analysis assumed that all hardware is CRES 347. The static structure thermal distribution is shown in Figure 63. These values are for 100-percent design speed and are based on a compressor inlet temperature of 59F and a compressor discharge temperature of 560F. The magnified thermal deflection of the static structure is shown in Figure 64. In steady state, the outer diameter of the shroud moves 0.01881 inch toward the impeller due to temperature, and 0.00071 inch away from the impeller due to pressure.

GTEC emphasizes that the 2-lb/sec compressor shroud is not a thermal scale of the 10-lb/sec compressor shroud. NASA should be aware that the additional material thickness of the 2-lb/sec shroud (required to meet structural design criteria) could unfavorably affect compressor performance.

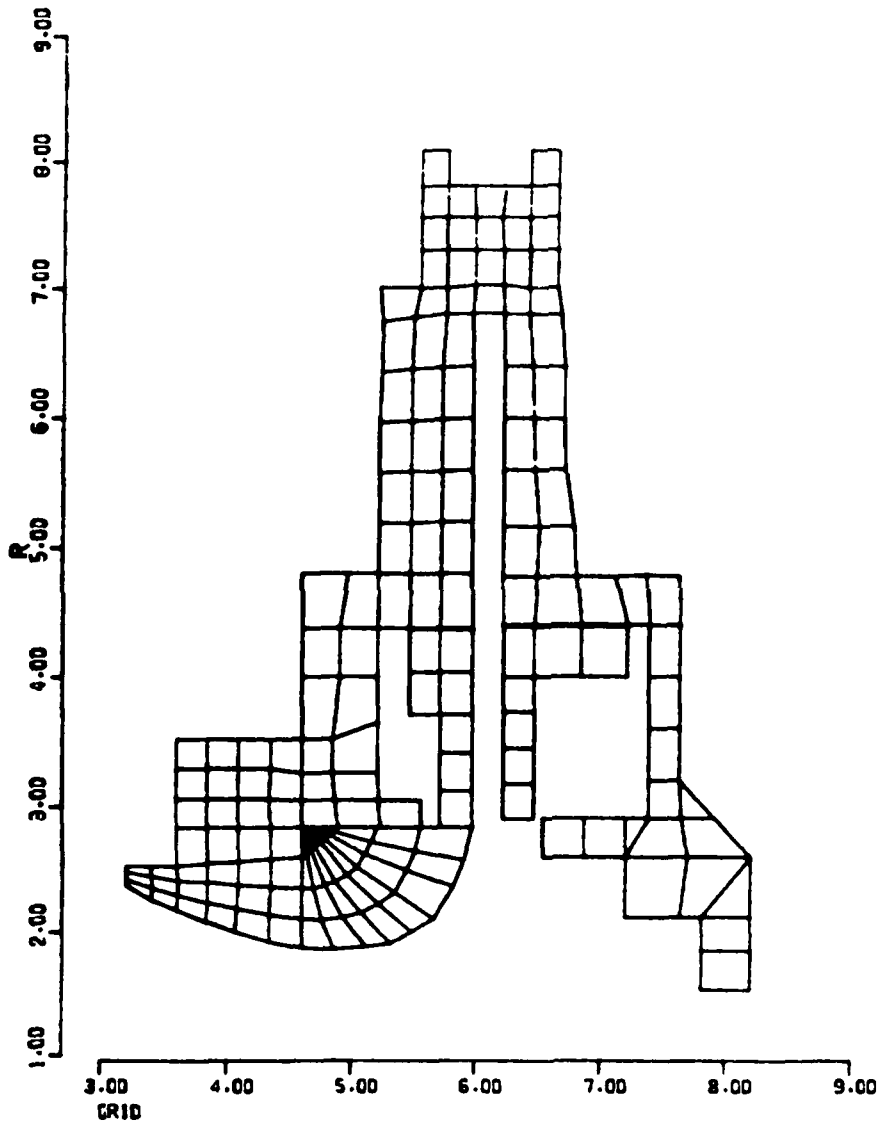


Figure 62. 2-lb/Sec Test Rig Static Structure Finite Element Model.

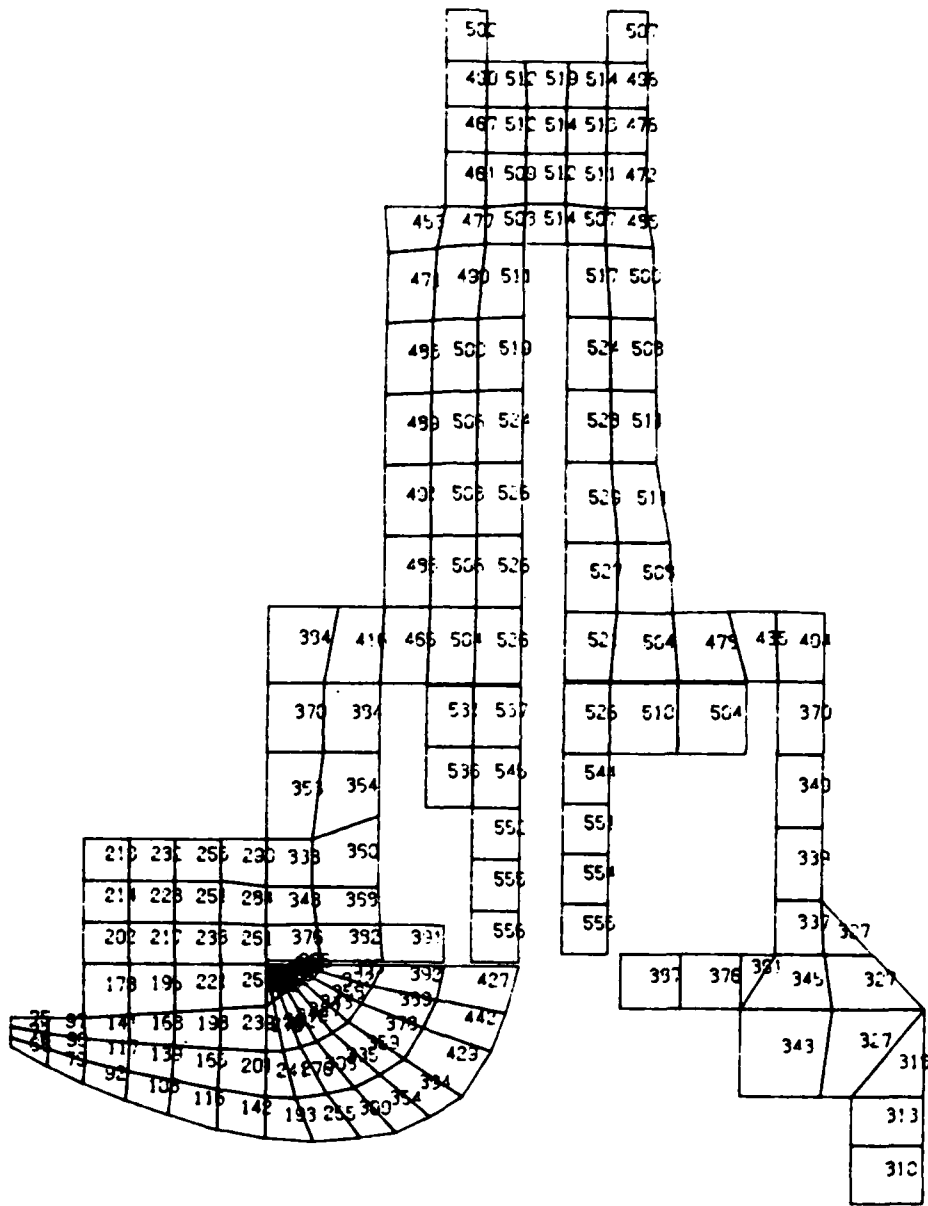


Figure 63. 2-lb/Sec Test Rig Static Structure Thermal Distribution at 100-Percent Speed.

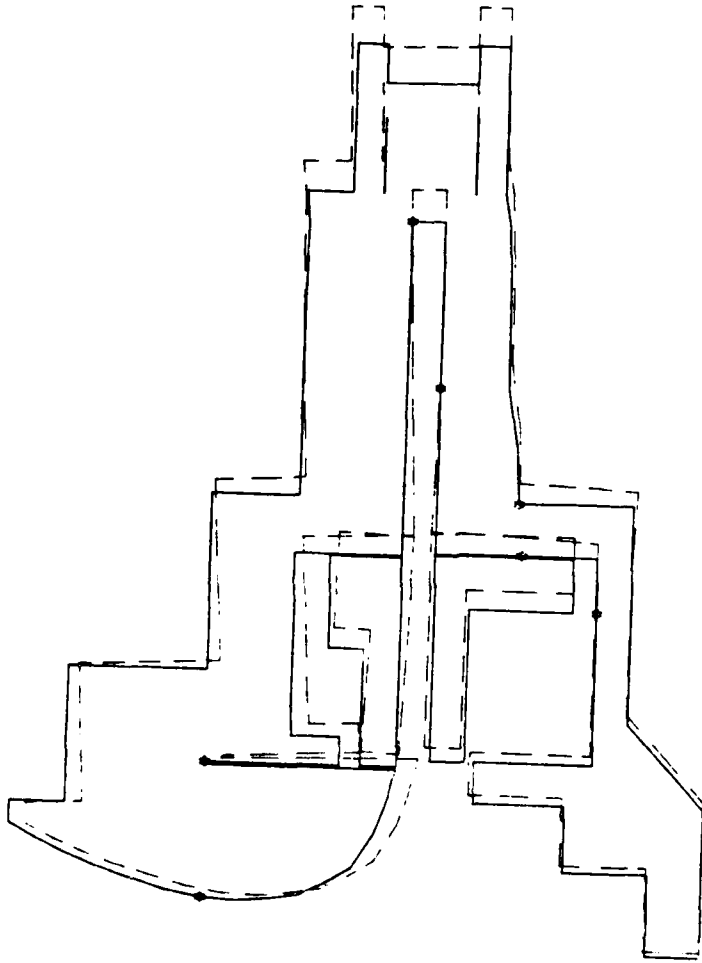


Figure 64. Magnified Thermal Deflection of 2-lb/Sec Test Rig Static Structure (100-Percent Speed).

## 6.0 2-LB/SEC TEST RIG DESCRIPTION

The NASA 2-lb/sec test rig (Figure 1), which will operate in a vertical position, is a modification of a previous NASA compressor rig. It is a two-bearing arrangement with the centrifugal compressor overhung on the forward (top) side and a single-stage drive turbine overhung on the aft (bottom) side of the bearings. A thrust balance system is used to maintain a constant load in the compressor direction on the thrust (aft) bearing. Instrumentation locations (shown in Figure 65) are provided to monitor impeller-to-shroud clearance, thrust load, shaft excursion, compressor speed, bearing outer race temperatures, flow-path static pressures, and air-seal pressures. Compressor performance is determined by total temperature (Figure 66) and total pressure (Figure 67) performance rakes located at the diffuser exit.

The objectives of the 2-lb/sec test rig modification were to incorporate the 2-lb/sec compressor into the test rig, scale the impeller-to-shroud running clearance to 0.004 inch, and provide a durable, high integrity test rig.

These objectives were met only by redesigning certain inadequacies of the existing test rig design. The areas of concern to GTEC included the impeller-to-tie-shaft interface, the direction of thrust loading during operation, the design of the labyrinth seal immediately downstream of the impeller, and the reduced critical speed margin due to heavy, massive shafting and excessive impeller overhang. GTEC addressed each of these concerns and incorporated solutions into the test rig layout shown in Figure 68.

The improved impeller-to-tie-shaft interface controls the center of gravity for the rotating group by reducing the number of parts that are included in the stretch load. As shown in

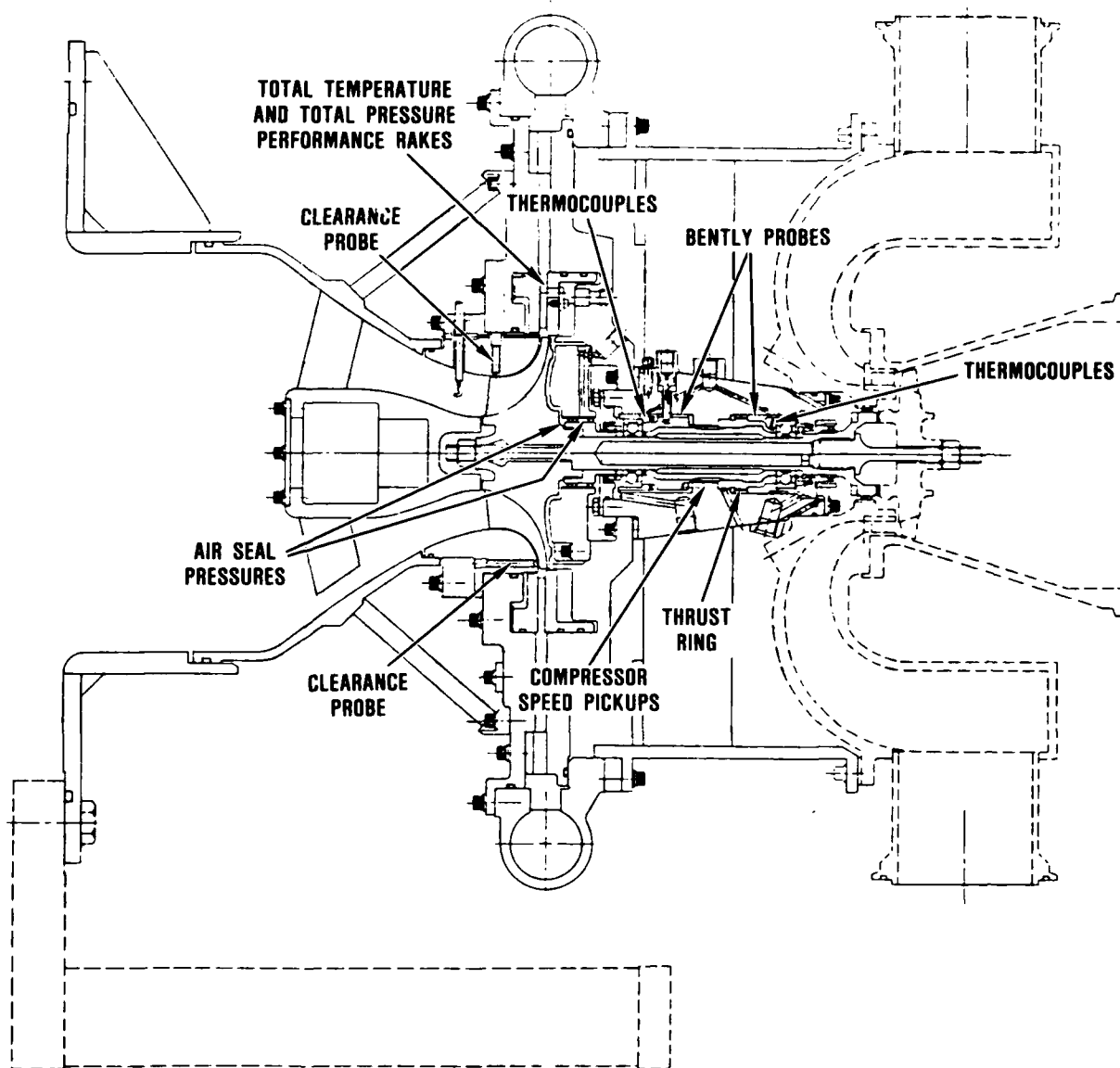


Figure 65. Test Rig Instrumentation Summary.

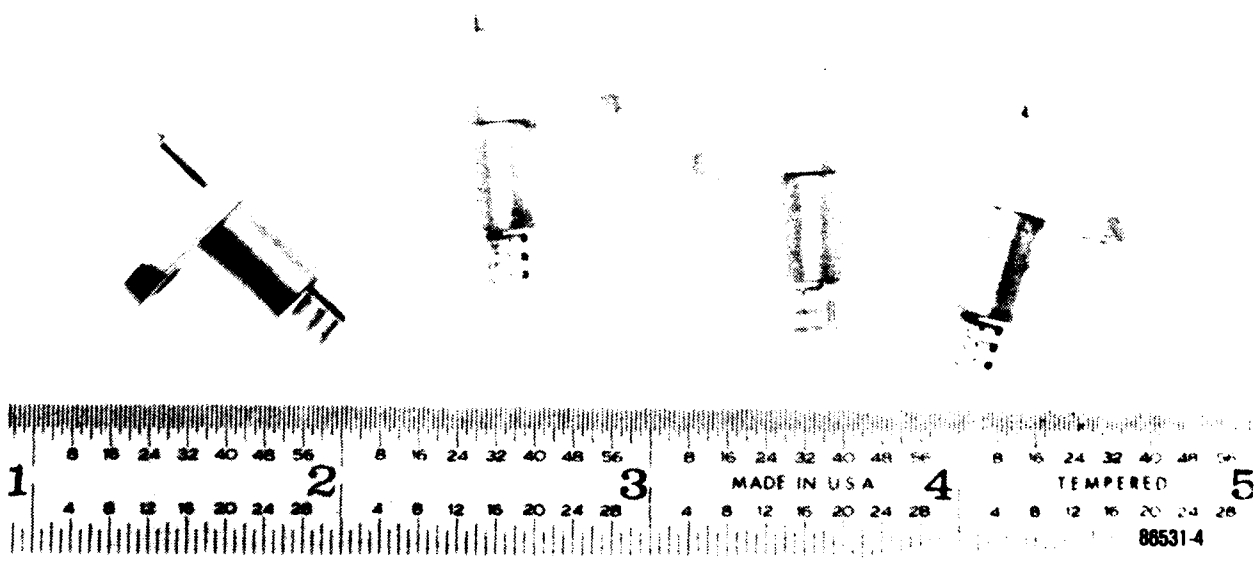


Figure 66. Total Temperature Performance Rakes.

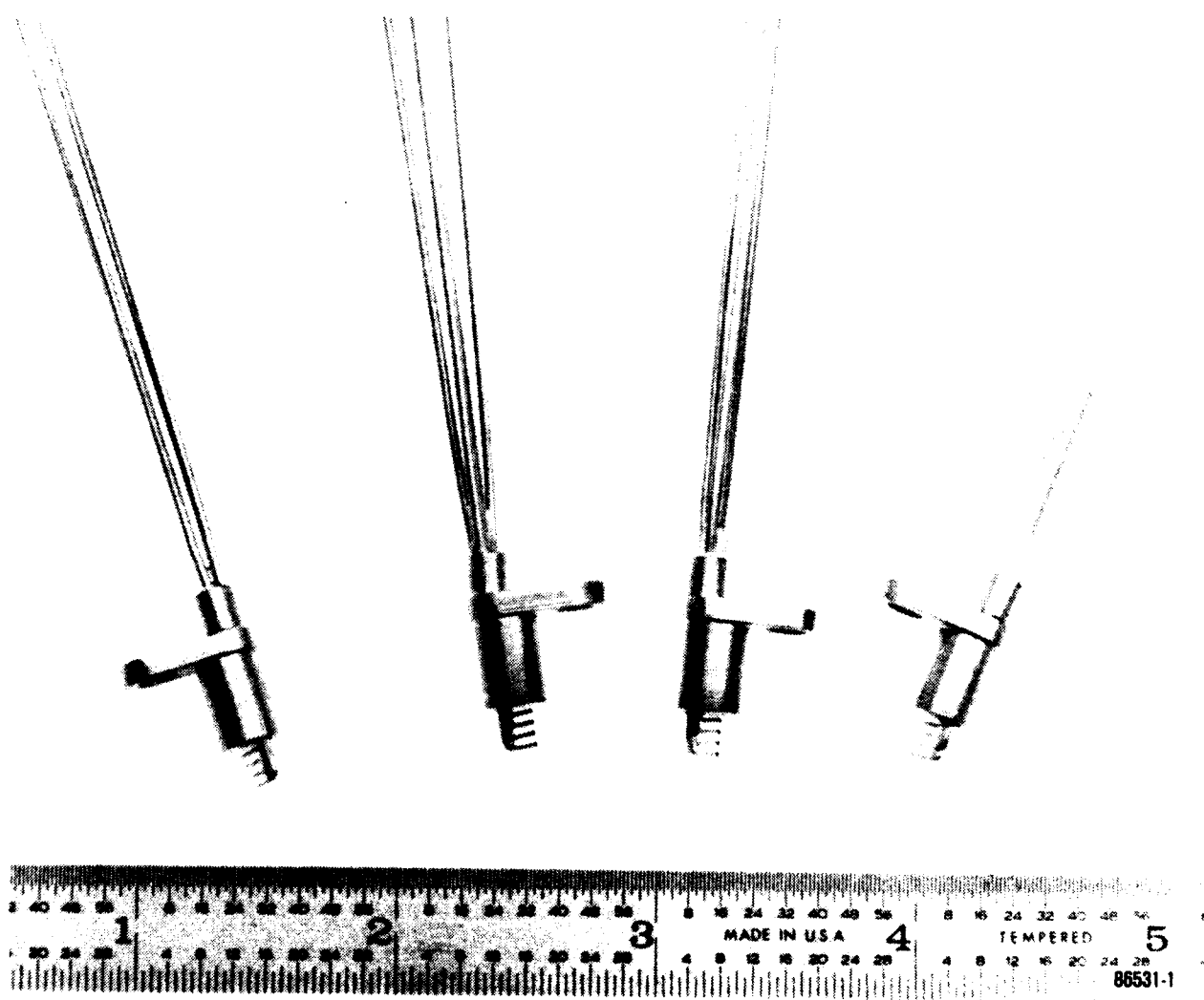


Figure 67. Total Pressure Performance Rakes.

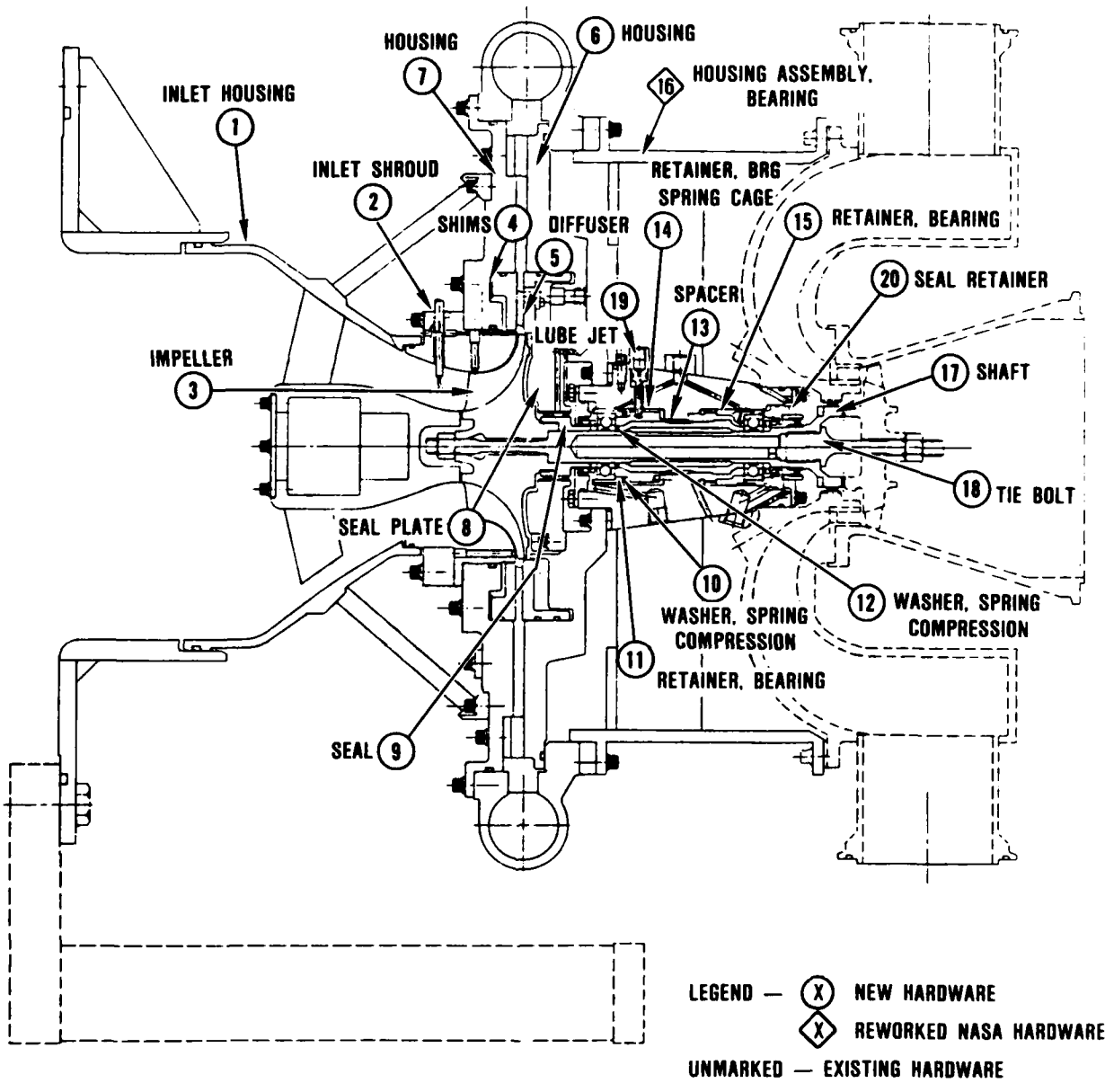


Figure 68. Modified NASA 2-lb/Sec Centrifugal Compressor Test Rig Layout.

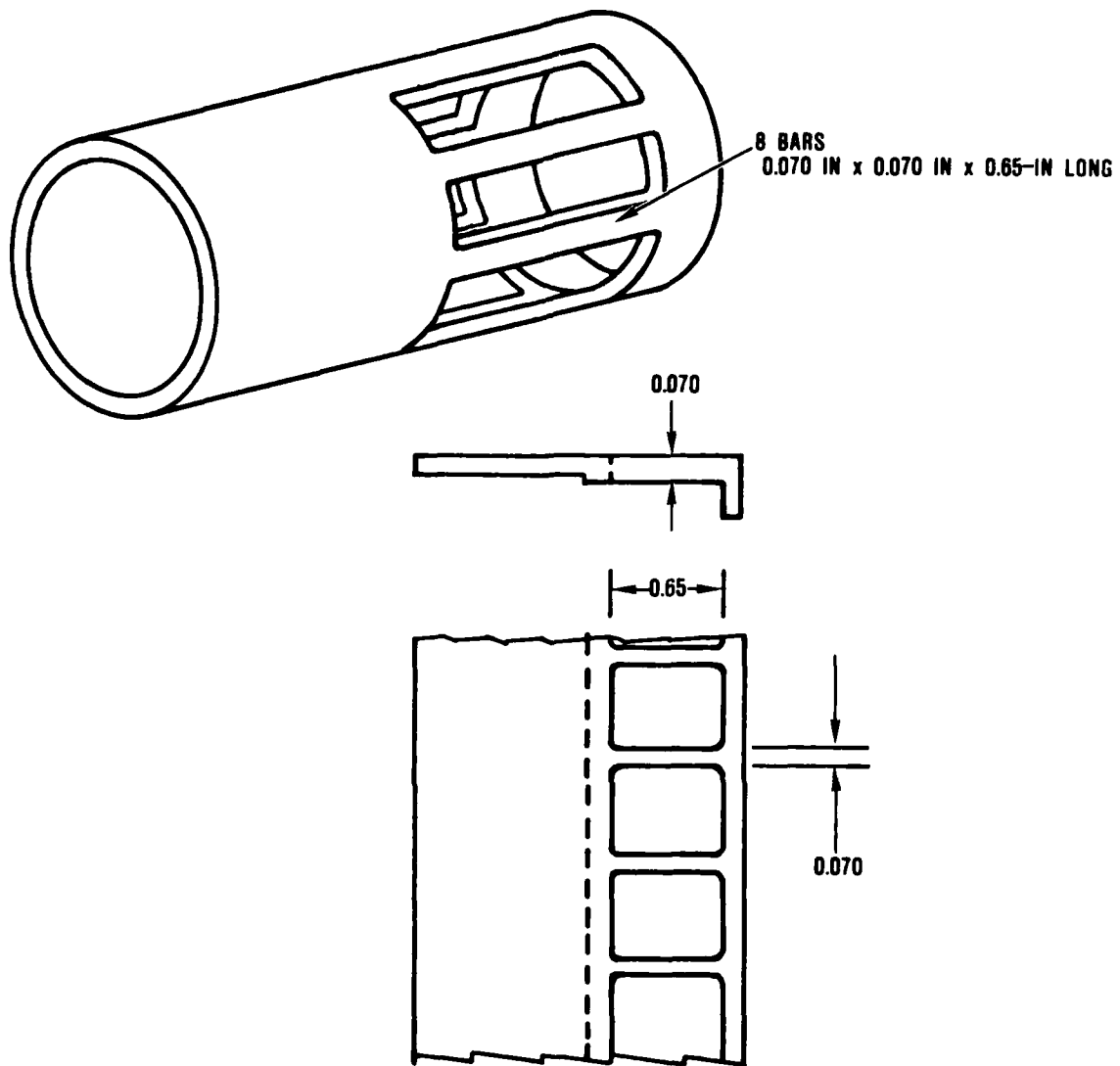
Figure 68, the impeller has a close tolerance fit at two locations on the inner diameter to control dimensional runout. The impeller is shouldered against the drive shaft, providing a simple load path for the tie shaft that includes only two pieces of hardware - the impeller and the tie shaft.

The spring cage (Find No. 20, Figure 69) has been designed in conjunction with the upstream bearing mount (Figure 70). The spring cage will allow the structural stiffness of this bearing mount to be precisely designed. It will also center the rotating group (relative to the shroud) within the bearing hydraulic mount clearances. The spring cage is surrounded by the hydraulic mount.

The direction of thrust during operation for the test rig shown in Figure 68 is toward the impeller. This change in thrust is the opposite direction from previous NASA operation and is necessary to prevent shroud rub during emergency shutdown conditions. The bearings have approximately 0.008 inch of axial "free-play," allowing the impeller to move axially by 0.008 inch during emergency conditions. Since the design running clearance between the impeller and shroud is only 0.004 inch, the impeller would rub the shroud without a redesigned thrust direction. However, the impeller will now move away from the shroud by 0.008 inch during emergency shutdown because of the change in the direction of thrust.

The design of the labyrinth seal (Find No. 15) immediately downstream of the impeller has been improved. The seal is piloted on the drive shaft and is a loose fit around the impeller. This will eliminate the possibility of the seal damaging the impeller as could happen with the original design.

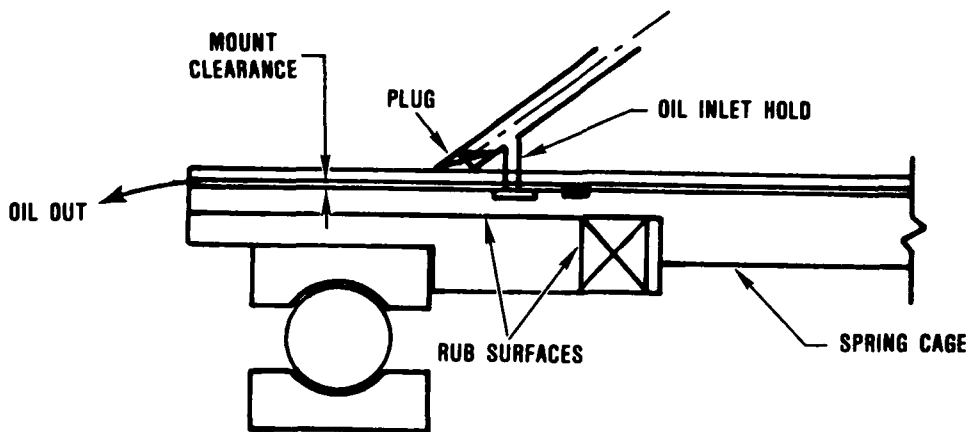
The critical speed margin of the test rig has been increased by incorporating a lighter weight bearing spacer (Find No. 21), a



**DESIGN DATA:**

SPRING CONSTANT — 20,000 LB/IN  
 MAXIMUM DEFLECTION (DAMPER CLEARANCE) — 0.0023 IN  
 MAXIMUM BENDING STRESS (0.0023 DEFLECTION) — 66.3 KSI  
 CRITICAL BUCKLING LOAD — 10,700 LBS  
 TRANSLATIONAL NATURAL FREQUENCY — 7250 HZ  
 MATERIAL — 4340 AMS 6415

Figure 69. Spring Cage Design.



BEARING TYPE	BALL
BEARING PART NUMBER	3606004-1
BEARING BORE DIAMETER	0.78 IN
OIL TYPE	MIL-L-7808 (TYPE 1)
OIL INLET TEMPERATURE	150° F
OIL PRESSURE	50 PSIG

**HYDRAULIC MOUNT**

DIAMETER	1.76 IN
LENGTH	0.45 IN
RADIAL CLEARANCE	0.0023 IN
RADIAL EXCURSION	0.00029 IN AT 85,000 RPM
OIL INLET HOLE DIAMETER	0.0465 — 0.0505 IN
RECIRCULATING ANNULUS AREA	0.0034 IN <sup>2</sup> — 0.0040 IN <sup>2</sup>
SPRING LOAD	23.4 — 31.2 LBS
THEORETICAL PUMPING FLOW	0.267 GPM

**DRAWING NOTES**

- 1) ALL RUB SURFACES IN CONTACT WITH THE BEARING OUTER RACE MUST BE RC 50 MIN AND 16 RMS MAX
- 2) SPRING CAGE BORE MUST BE CIRCULAR TO WITHIN 0.0002 INCH
- 3) THRUST FACE ON SPRING CAGE MUST BE NORMAL TO BORE WITHIN 0.0003 INCH

Figure 70. Compressor Bearing Hydraulic Mount Design.

lighter weight drive shaft (Find No. 24), a spring cage (Find No. 20), and less impeller overhang.

The test rig layout also incorporates the following NASA requests:

- o A scaled 10-lb/sec inlet
- o Elimination of the impeller exit bleed provisions while retaining a nonfunctional slot to simulate the 10-lb/sec rig, no bleed condition
- o A cavity with reduced volume behind the diffuser
- o A minimized cavity volume around the tiebolt nut along with a minimized axial gap between the impeller and the inlet hubline
- o An inlet interface with the existing NASA inlet plenum

The test rig layout has incorporated the NASA survey actuators at the impeller inlet, however, interference with the scaled inlet prohibits surveys at the diffuser exit.

The test rig layout design also includes new positions for the thrust ring, Bently probes, and speed pickup.

Final assembly of the test rig was witnessed at GTEC by NASA personnel. The assembled rig (Figure 71) was delivered to NASA-Lewis Research Center on February 8, 1985, to undergo testing in the NASA facilities. The assembly of the test rig is described in detail in the assembly procedures, GTEC Report 21-5411.



Figure 71. NASA 2-lb/Sec Scaled Compressor Test Rig.

## 7.0 2-LB/SEC TEST RIG MECHANICAL INTEGRITY

### 7.1 Test Rig Operating Conditions

The maximum operating speed of the 2-lb/sec test rig is 85,383 rpm (105-percent speed).

At 100-percent speed (81,319 rpm), the design running clearance between the impeller and the shroud is 0.0043 inch.

The maximum expected air temperature at 105-percent speed (with 100F inlet) is 686F. The maximum expected pressure is 126 psia.

The maximum bearing temperature is 350F. The load on the thrust ring should be maintained between 150 and 175 lbs in the compressor direction. Under no circumstances should the thrust level exceed 500 lbs.

The test rig service conditions are summarized in Table 7.

TABLE 7. TEST RIG SERVICE CONDITIONS.

Parameter	Operating Condition	Maximum Allowable
Oil Inlet Temperature	150F	200F
Oil Inlet Pressure	50 psig	65 psig (Max Flow=0.672 gpm)
Thrust Balance Air	As required	125 psig (Max Flow=0.5 lb/sec)
Buffered Labyrinth Seal Air	As required	75 psig (Max Flow=0.5 lb/sec)

## 7.2 Hardware Inspection

Inspection results are presented for the following hardware:

<u>Description</u>	<u>P/N</u>	
Compressor Shroud	3554662-1	Figure 72
Diffuser	3554663-1	Figure 73
Impeller, hub, and shroud	3554664-1	Figure 74

Figure 75 illustrates the inspection criteria for the diffuser. All 42 passage throat widths were measured, as summarized in Table 8.

The impeller and diffuser (prior to braze) are shown in Figure 76 and 77, respectively. A review of the inspection results indicated no major concerns.

The 2-lb/sec "rough-cut" impeller surface finish was between 50 and 65 microinches in the inducer region and between 60 and 80 microinches in the exducer region. This compares with a measured surface finish of 24 to 30 microinches for the standard 2-lb/sec impeller.

## 7.3 Balance Results

The 2-lb/sec impeller was balanced to the following specifications (balance plane locations shown in Figure 78):

<u>Balance Plane</u>	<u>Final Balance, oz-in.</u>	<u>Limits, oz-in.</u>
G	0.0020	0.0023
H	0.0025	0.0038

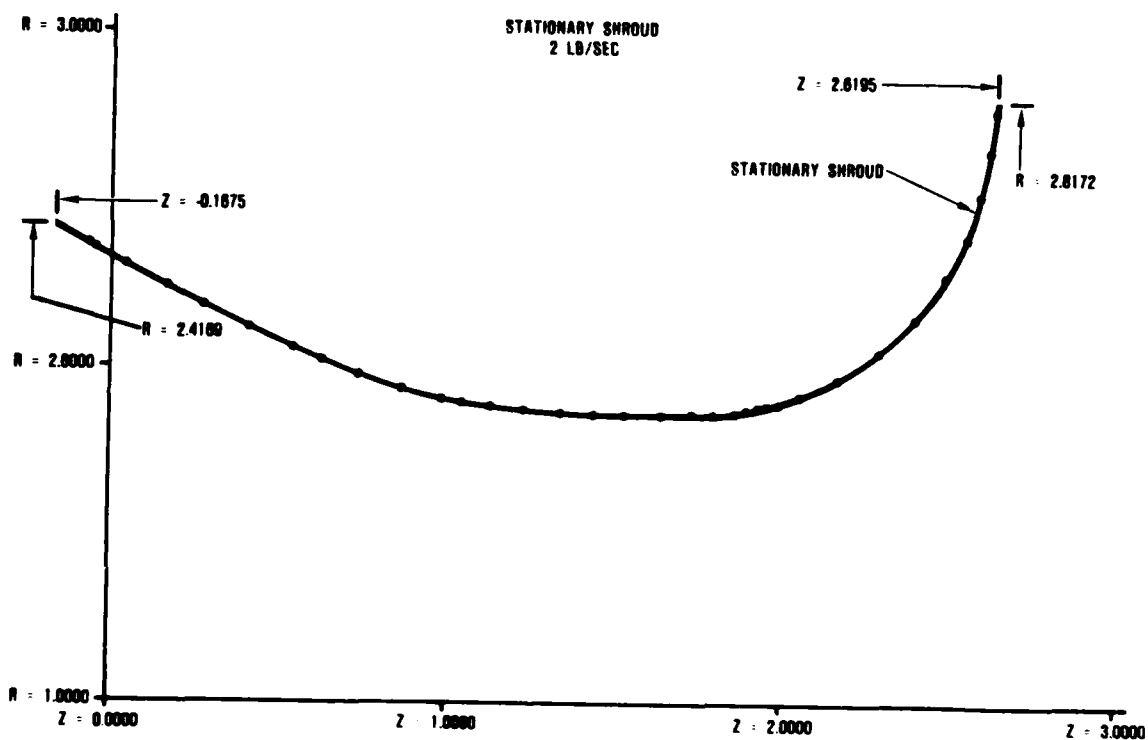


Figure 72. 2-lb/Sec Shroud Contour Inspection Results (P/N 3554662-1).



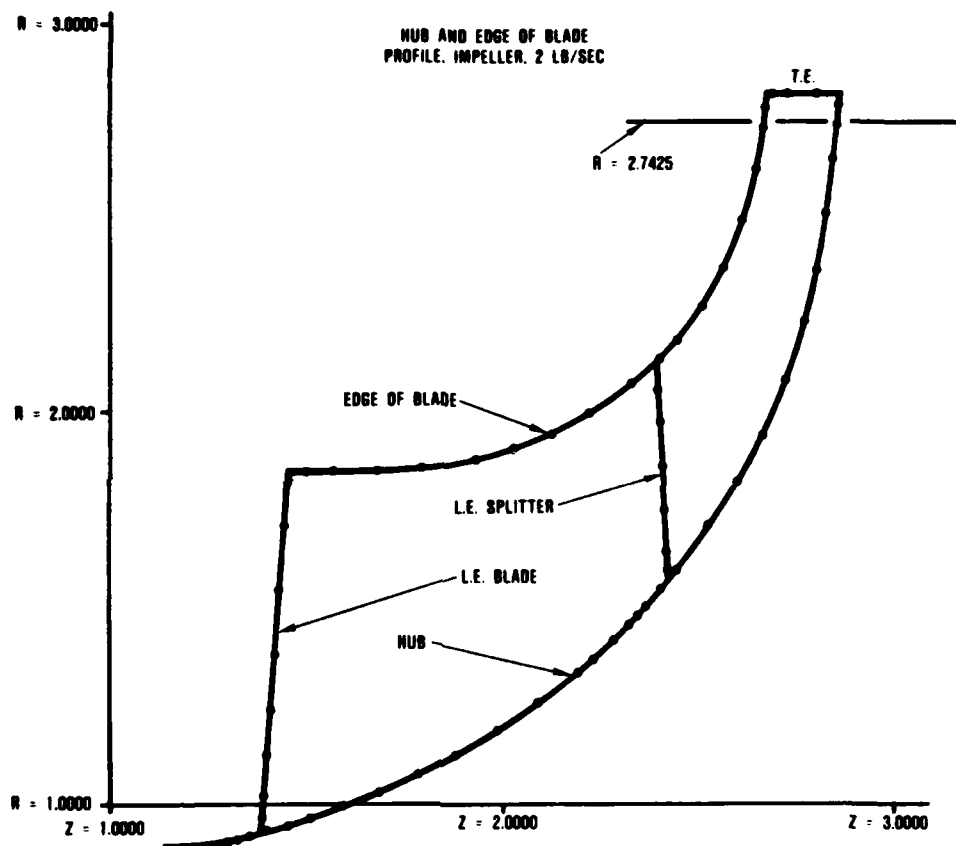


Figure 74. 2-lb/Sec Impeller Inspection Results (P/N 35554664-1), Hub and Shroud Profile.

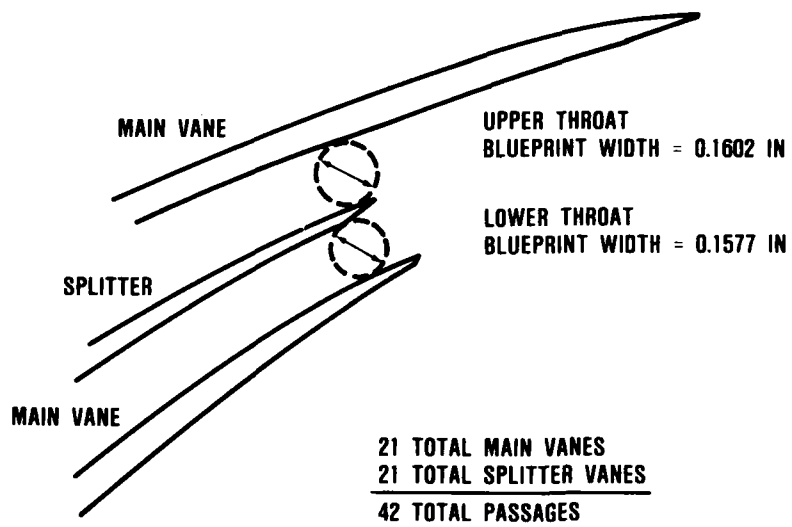
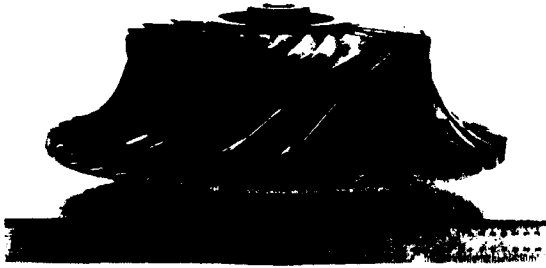


Figure 75. Vane Diffuser Throat Area.

TABLE 8. SUMMARY OF MEASURED THROAT WIDTHS.

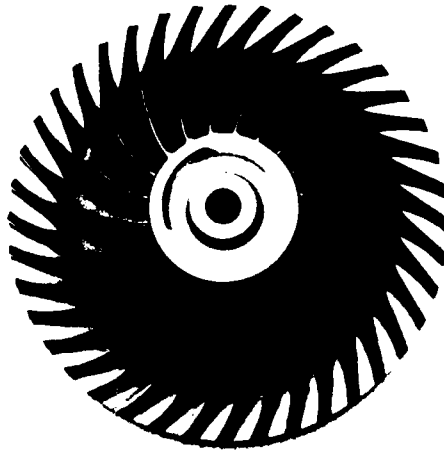
Upper (Blueprint = 0.1602 Inch)		Lower (Blueprint = 0.1577 Inch)	
Passage	Diameter	Passage	Diameter
2	0.159	1	0.157
4	0.160	3	0.156
6	0.160	5	0.157
8	0.160	7	0.158
10	0.160	9	0.156
12	0.160	11	0.158
14	0.160	13	0.154
16	0.159	15	0.157
18	0.160	17	0.155
20	0.159	19	0.157
22	0.160	21	0.157
24	0.160	23	0.157
26	0.160	25	0.157
28	0.161	27	0.157
30	0.160	29	0.158
32	0.161	31	0.156
34	0.159	33	0.156
36	0.160	35	0.157
38	0.160	37	0.157
40	0.160	39	0.157
42	0.160	41	0.158



88993-1

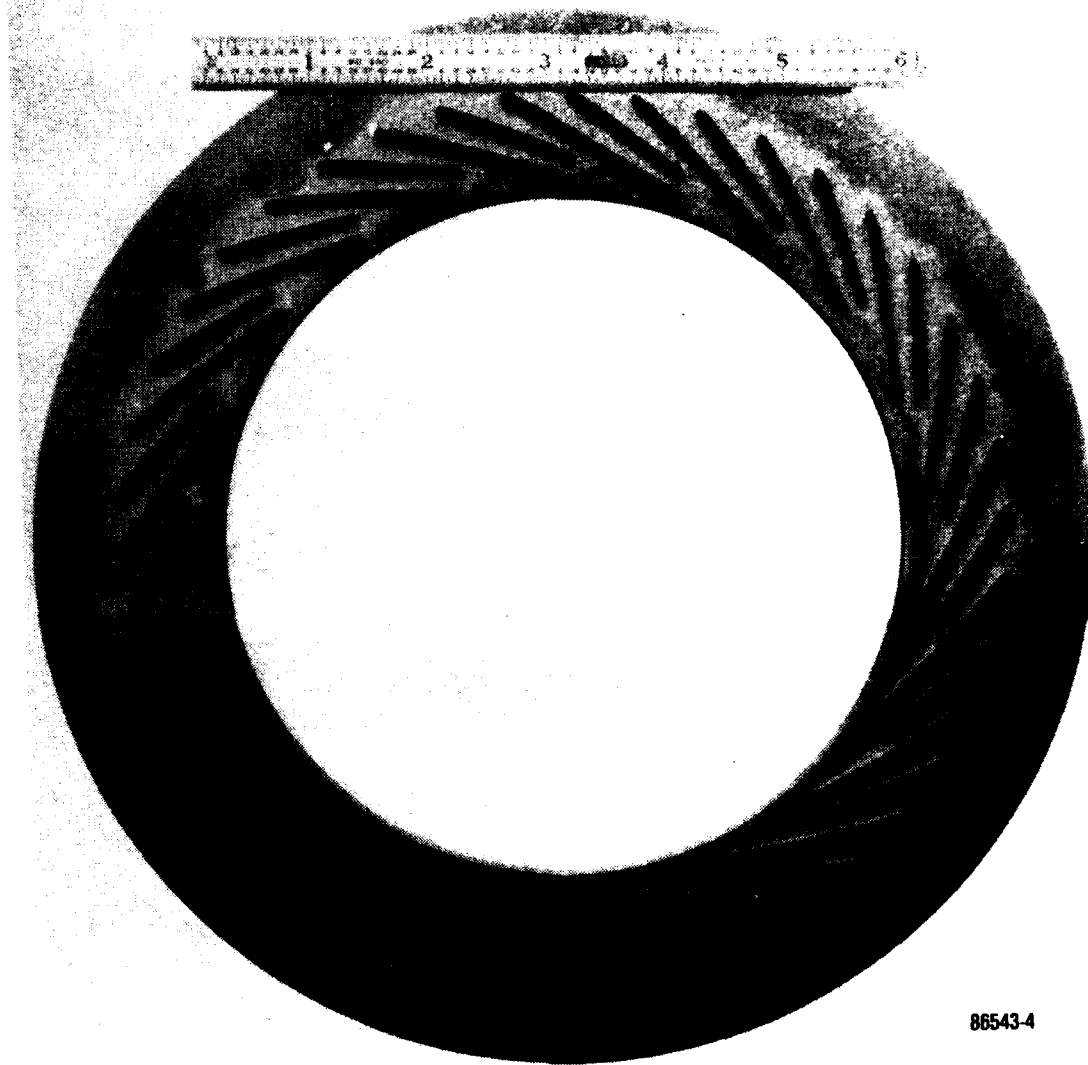


88993-2



88993-3

Figure 76. NASA 2-lb/Sec Impeller.



86543-4

Figure 77. NASA 2-lb/Sec Diffuser Prior to Braze.

<b>BALANCE PLANE G</b>	<b>BALANCE PLANE H</b>
<b>0.0019 OZ-IN ACTUAL</b>	<b>0.0015 OZ-IN ACTUAL</b>
<b>0.0037 OZ-IN OR LESS REQUIRED</b>	<b>0.0023 OZ-IN OR LESS REQUIRED</b>

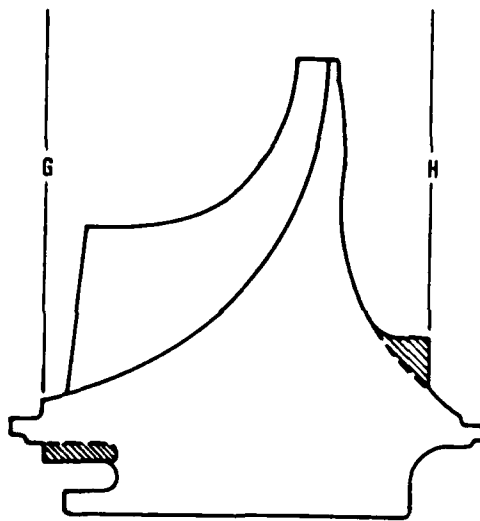


Figure 78. 2-lb/Sec Impeller Balance Plane Locations.

Similarly, the 2-lb/sec "rough-cut" impeller was balanced to the following specifications:

<u>Balance Plane</u>	<u>Final Balance, oz-in.</u>	<u>Limits, oz-in.</u>
G	0.0015	0.0023
H	0.0019	0.0038

The NASA-supplied drive turbine rotor for the 2-lb/sec test rig was balanced to GTEC specifications, as shown in Figure 79.

The 2-lb/sec rotating group, consisting of the impeller (P/N 3554664-1), shaft (P/N 3554667-1), tie bolt (P/N 3554678-1), and NASA drive turbine, was assembled and checked for runouts. This assembled rotating group is shown in Figure 80. These runouts were measured with the rotating group supported at the bearing locations. The results are acceptable and are shown in Figure 81.

The 2-lb/sec rotating group was check-balanced at the balance plane locations shown in Figure 82. Roller supports were located between planes A and B to record the unbalance at planes A and B. Roller supports were located at planes A and B to record the unbalance at planes C and D. The results are as follows:

<u>Balance Plane</u>	<u>Imbalance, oz-in.</u>	<u>Angle (degrees)</u>
A	0.0134*	56
B	0.0193**	178
C	0.0080	117
D	0.0078	177

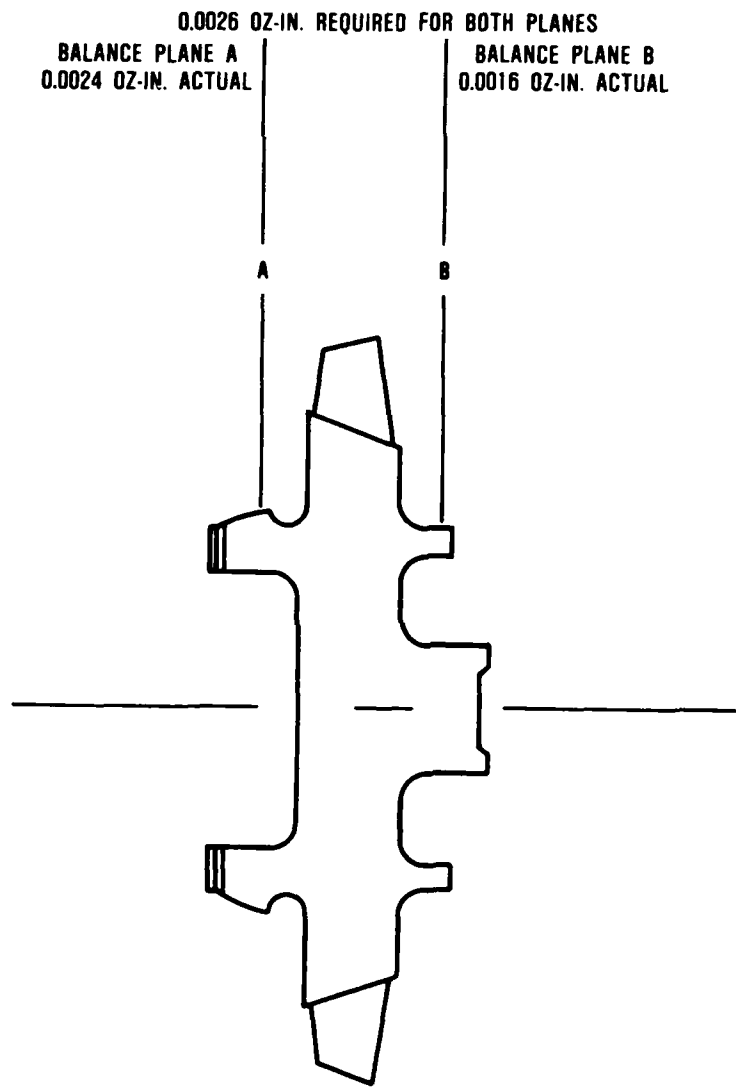


Figure 79. NASA Drive Turbine Rotor Balance Results.

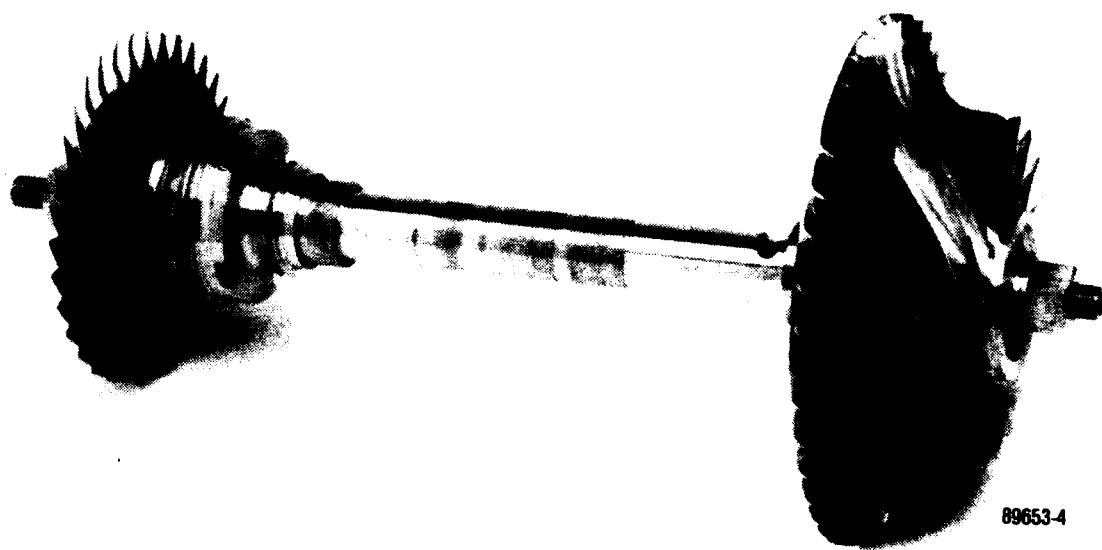


Figure 80. NASA 2-lb/Sec Rotating Group.

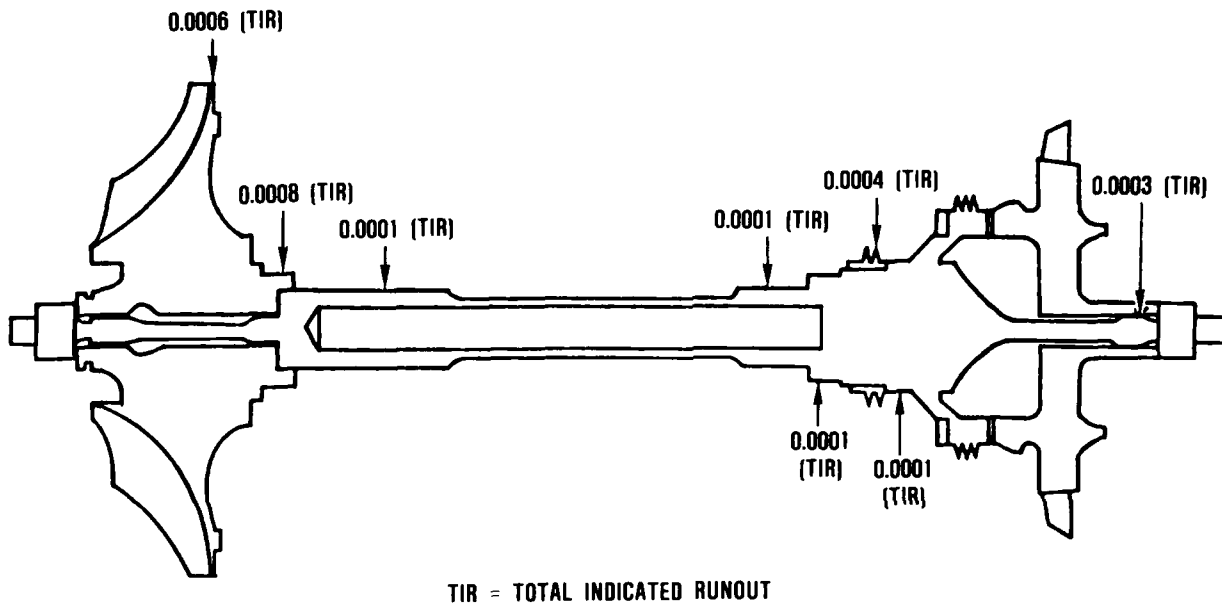


Figure 81. NASA 2-lb/Sec Rotating Group Runouts.

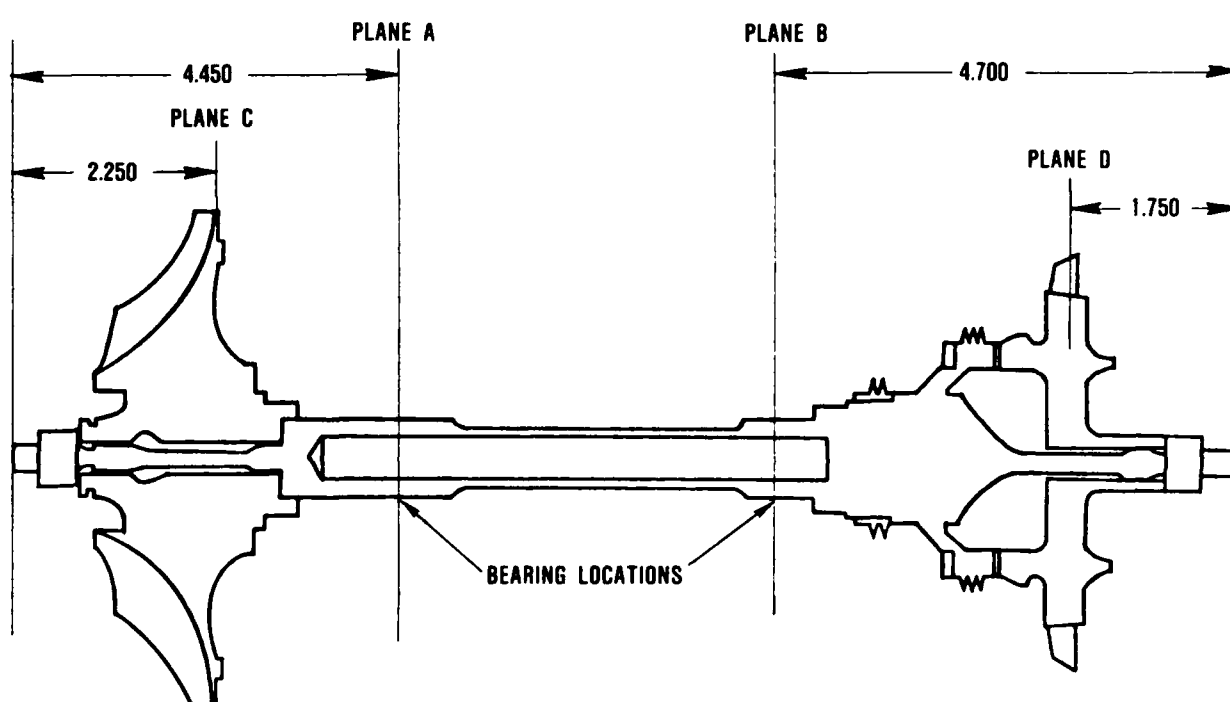


Figure 82. NASA 2-lb/Sec Rotating Group Balance Plane Locations.

Similarly, the 2-lb/sec "rough-cut" rotating group, consisting of the "rough-cut" impeller (P/N 3554664-1), shaft (P/N 3554667-1), tie bolt (P/N 3554678-1), and NASA drive turbine, was assembled and check-balanced at the balance plane locations shown in Figure 82. The results are as follows:

<u>Balance Plane</u>	<u>Imbalance, oz-in.</u>	<u>Angle (degrees)</u>
A	0.0058*	282
B	0.0132**	179
C	0.0012	303
D	0.0049	142

All the above rotating group balance limits assumed 0.0005 inch c.g. eccentricity, a common assumption for rotating group balance. The balance results for the 2-lb/sec rotating groups were satisfactory.

#### 7.4 Test Rig Instrumentation Calibrations

Calibration information for the 2-lb/sec thrust ring is shown in Figures 83 and 84.

The 2-lb/sec compressor test rig Bently probe calibration curves are shown in Figures 85 through 88.

The thermocouple wire used to make the 2-lb/sec test rig total temperature rakes was calibrated at GTEC. The results are presented in Table 9.

\*Limit is 0.028  
 \*\*Limit is 0.031

**STRAIN GAGE INSTALLATION INFORMATION SHEET**

TECH F. Belungi C.I. JOB NO. 223  
 DATE 10-29-84 R.I. JOB NO. \_\_\_\_\_  
 S.I. JOB NO. \_\_\_\_\_

**ENGINEERING DATA**

Lab. Engineer JEFFREY O. CLARK Ext 2781  
 Proj. Engineer GREG CARROLL Ext 7006  
 LWO 100517  
 Unit Name NASA 2N/SEC Compressor Rg S/N \_\_\_\_\_  
 Part Name BEARINGS RETAINER S/N \_\_\_\_\_  
 Part Matl. 4340 STEEL P/N 35,466  
 Photographs Requested Yes (NO)  
 Mail Photos To: \_\_\_\_\_ Dept \_\_\_\_\_

**LABORATORY DATA**

**STRAIN GAGE** SA-06-062TT-120 Lot \_\_\_\_\_  
 Gage Type SA-06-062TT-120 S 1384046  
 Gage Factor 2.005 Res. 120.0  
 Adhesive Type 8112  
 Covering Type \_\_\_\_\_  
 Mithra  Rokide  
 CER 1000  Armadillo  
 Denex 2  Gagekote  
 Gagekote Type \_\_\_\_\_

**APPLICATION**

- Thrust  Dynamic
- Torque  Static
- Stress  Rotating
- Other \_\_\_\_\_

**LEADWIRE**

Gage to Terminator #38 HFI FormVar  
 Terminator Out #32 Teflon 4-C shield  
 Solder Type S/N 96 Temp 430 °F  
 Armadillo

**STRAIN GAGE**

Gage Type SA-06-062TT-120  
 Max Temp 300 °F No. of Gages \_\_\_\_\_

**IDENTIFICATION**

- Notches (.020 MGO.)
- Wire Marker
- Standard Color Code
- Gage Location Data Attached

**LEADWIRE**

Max Temp 250 °F Length 5 feet  
 Type #32 Tef shield 4-c Gage 32

**FINAL RESISTANCE COMPLETED PART**

Gage	Res	Gnd	Gage	Res	Gnd
1			13		
2			14		
3			15		
4			16		
5			17		
6			18		
7			19		
8			20		
9			21		
10			22		
11			23		
12			24		

**CIRCUIT**

- Full Bridges  Half Bridge
- Single  2 Wire  3 Wire

**FULL BRIDGE CALIBRATION**

Calib Range 0-500 lb Cal Points x-y plot  
 No. of Temp Cycles As required  
 Temp Cycle Range Amb. °F to 300 °F  
 Temp Cycle Increments 50

**GAGE POSITION VERIFICATION**

Engineering \_\_\_\_\_

**ISA STANDARD**

Compression - Negative  
 Tension - Positive

**CALIBRATED INSTRUMENTATION**

Strain Indicator Type SR 4 S/N 98  
 C.I. Identification  
 Bridge Identification  
 Temp Cycle Data Attached  
 Bridge No. 1 Unloaded 10-1430 AG  $\mu$ E  
 Bridge No. 2 Unloaded 10-0850 AB  $\mu$ E

**COMMENTS**

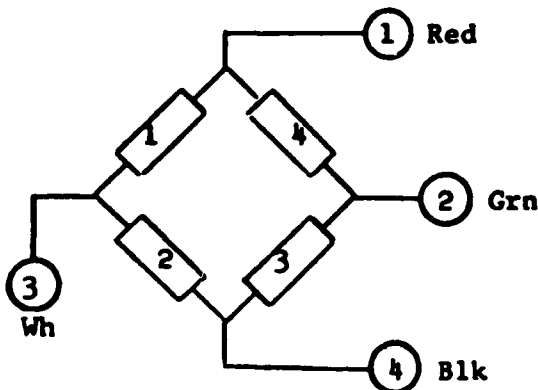


Figure 83. Strain Gage Installation Information Sheet.

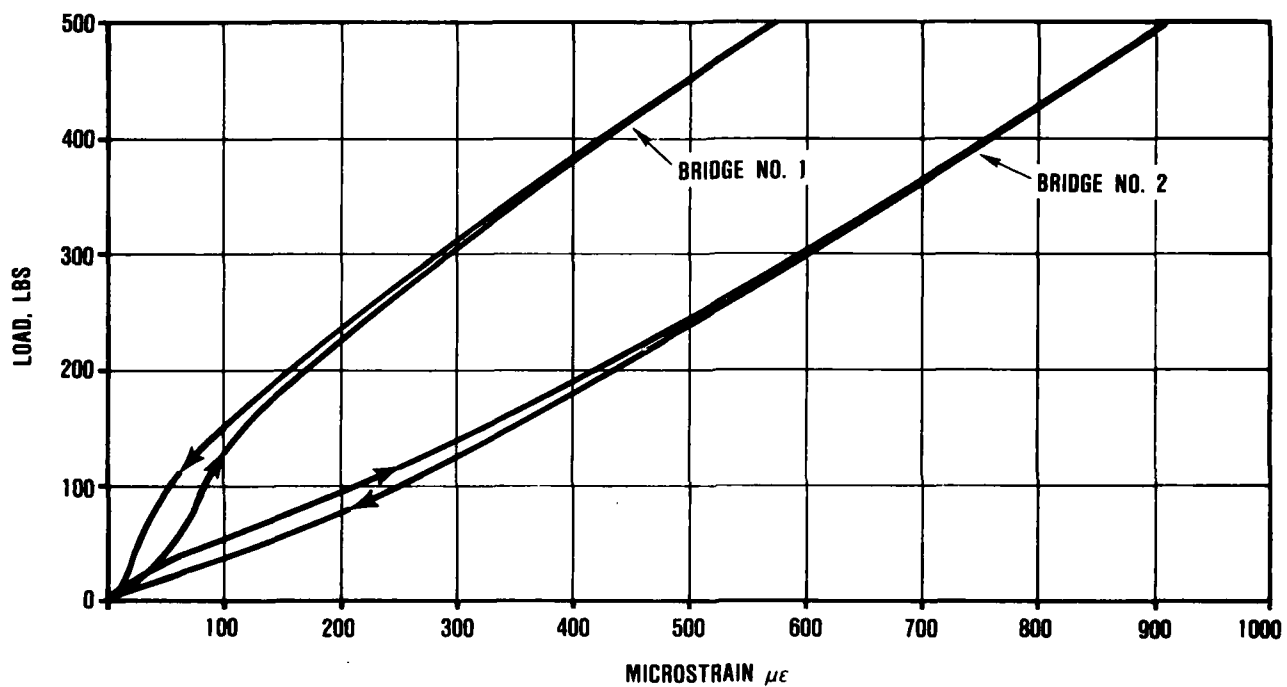


Figure 84. Thrust Ring Strain Gage Calibration.

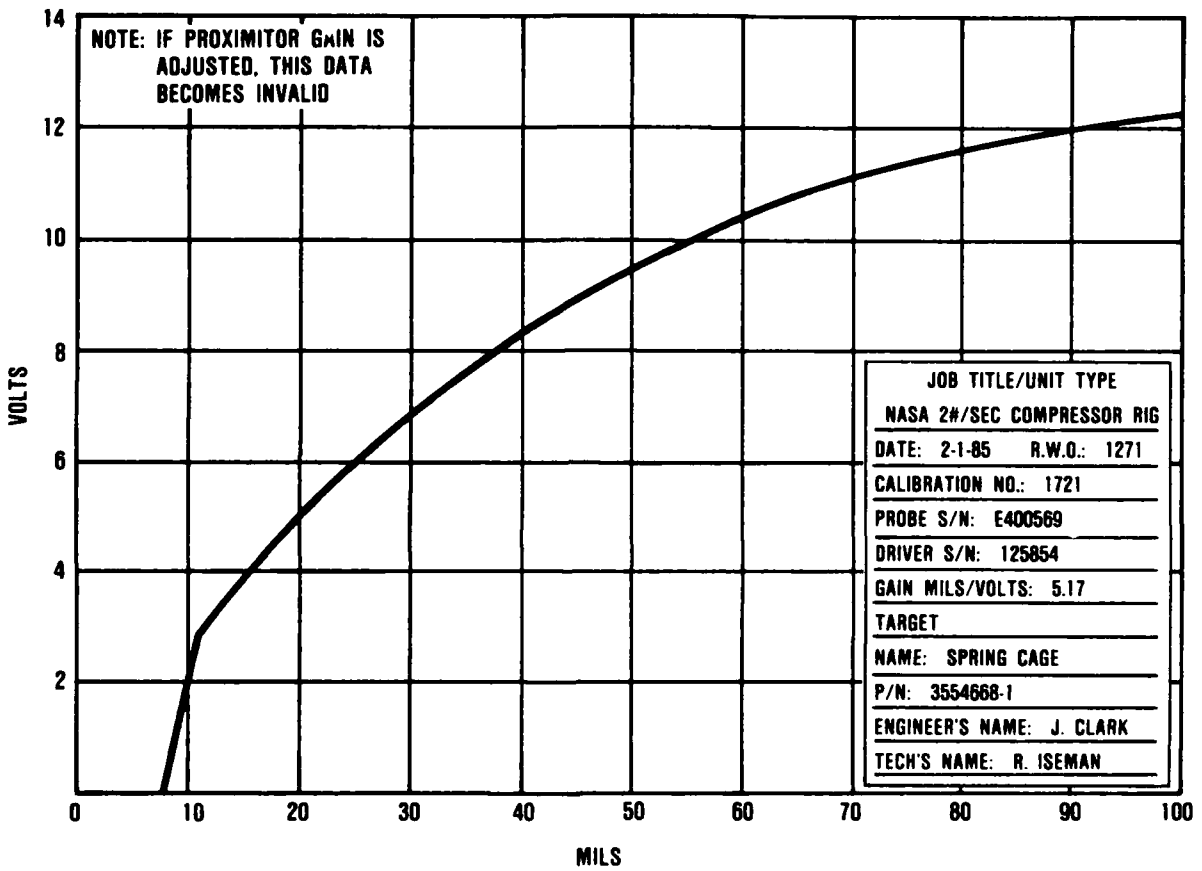


Figure 85. Forward Bently Probe Calibration - Vertical.

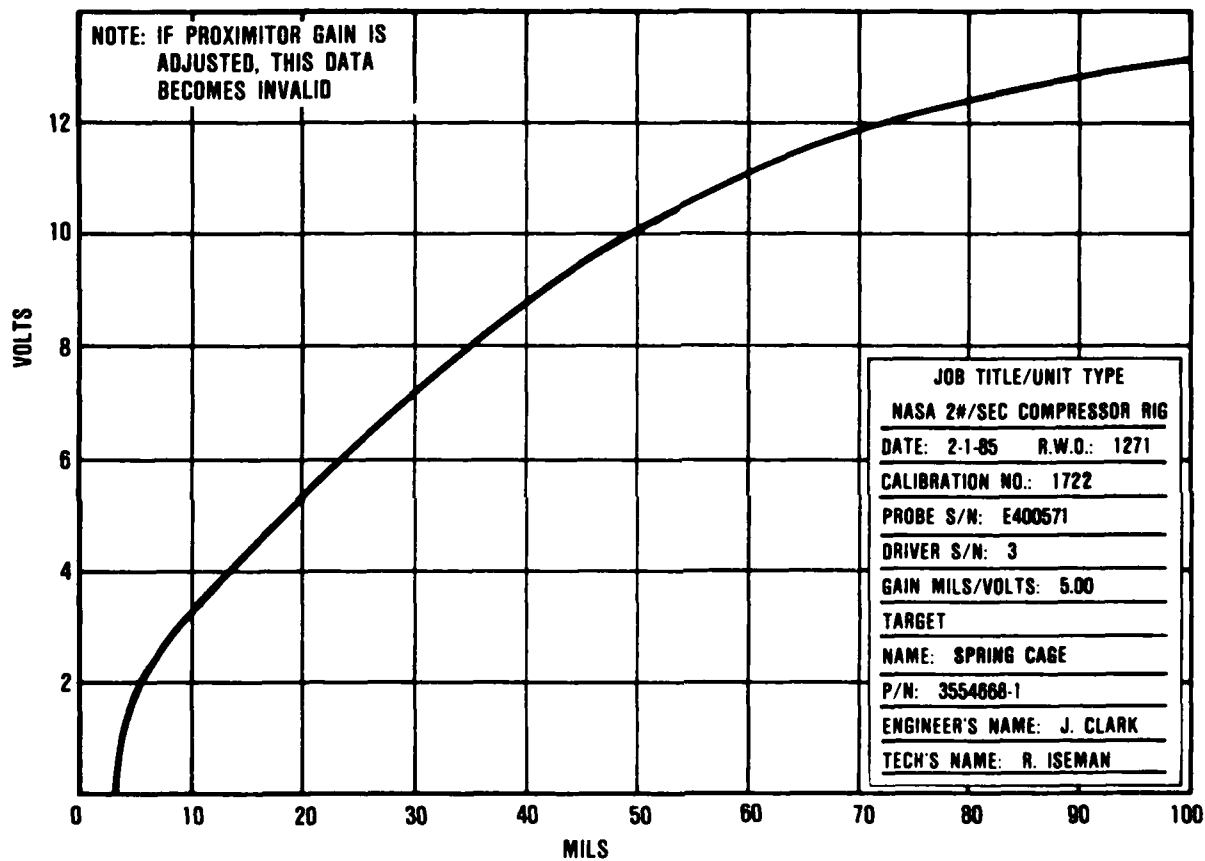


Figure 86. Forward Bently Probe Calibration - Horizontal.

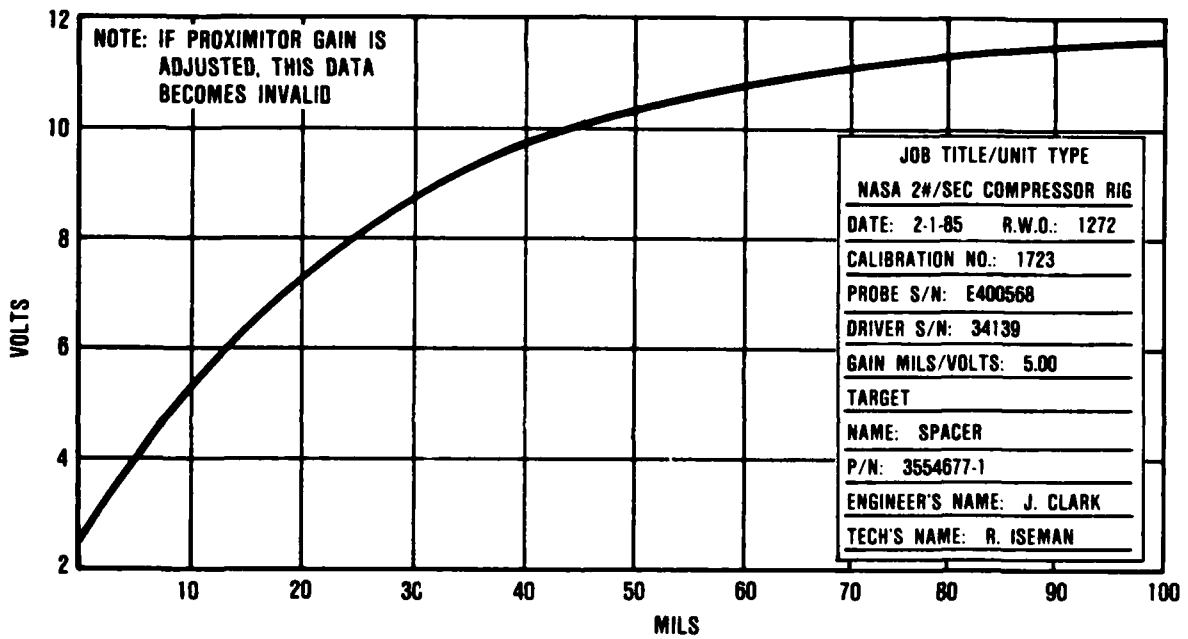


Figure 87. Aft Bently Probe Calibration - Vertical.

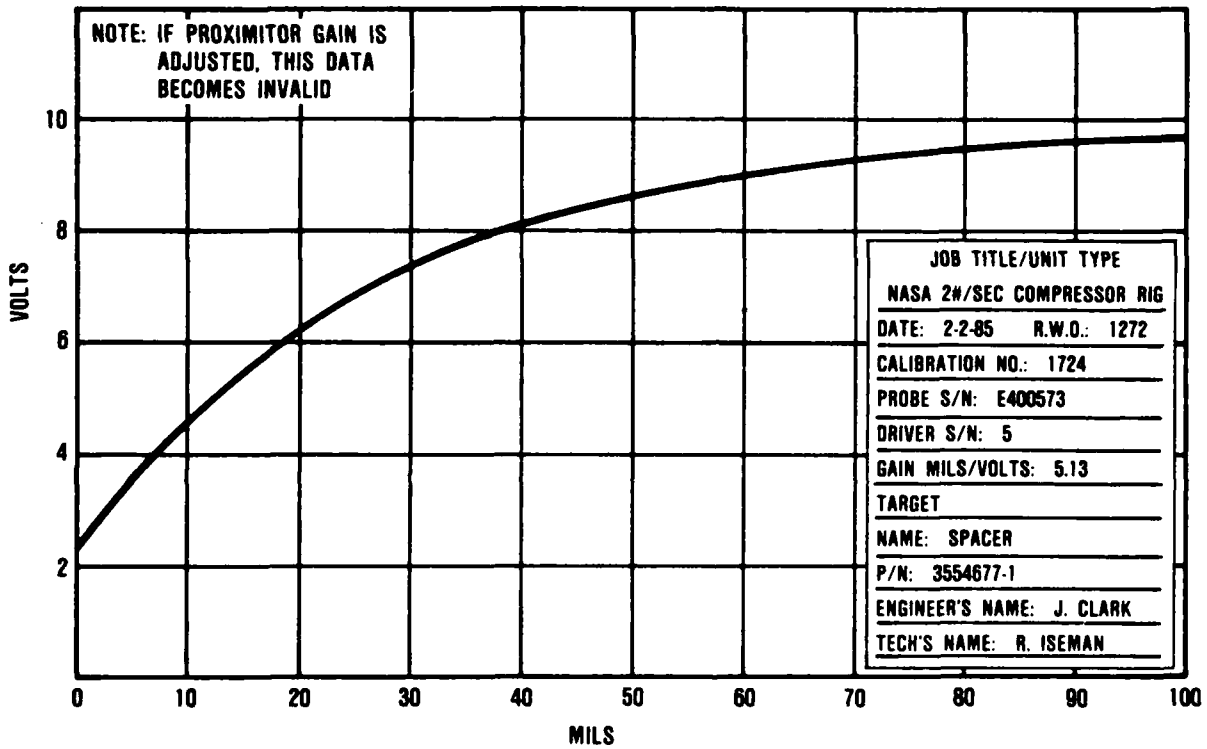


Figure 88. Aft Bently Probe Calibration - Horizontal.

TABLE 9. THERMOCOUPLE CALIBRATION RESULTS.

Time (Minutes)	Deviation from Reference Temperature, F		
	Ref. Temp = 449.54F	Ref. Temp = 621.50F	Ref. Temp = 786.56F
2	4.45	5.49	7.40
3	2.76	4.15	6.00
4	0.93	3.15	4.72
5	-0.90	2.98	3.61
6	-2.81	2.98	2.63
7	-4.77	2.98	1.83
8	-6.78	2.98	1.91
9	-8.78	2.94	1.78
10	-5.93	2.89	1.74
11	1.33	2.85	1.78
12	2.54	2.85	1.70
13	2.85	2.85	1.70
14	2.94	2.85	1.66
15	2.98	2.81	1.66
16	2.98	2.81	1.66
17	2.98	2.76	1.66
18	2.98	2.72	1.57
19	2.98	2.68	1.66
20	2.98	2.68	1.57
21	2.89	2.68	1.66
22	2.98	2.59	1.61
23	2.98	2.59	1.66
24	2.98	2.51	1.57
25	2.98	2.51	1.57
26	2.98	2.51	1.49
27	2.98	2.51	1.61
28	2.98	2.46	1.14
29	2.98	2.46	1.57
30	2.98	2.42	1.53
31	2.98	2.38	1.57
32	2.71	2.42	1.57
33	2.94	2.33	1.53
34	2.94	2.33	1.53
35	2.89	2.29	1.49
36	2.67		1.53
37	2.76		1.53
38	2.62		1.53
39	2.49		1.49
40	2.22		1.44

## 8.0 10-LB/SEC ROTATING COMPONENT ANALYSIS

Rotating components were designed for a margin of safety based on allowable yield and ultimate strengths. The yield-allowable stress is 80 percent of the  $-3\sigma$  yield, and the ultimate allowable stress is 64 percent of  $-3\sigma$  ultimate. A stress concentration factor ( $K_t$ ) of 1.56 is used for all curvic couplings. Elliptical fillets at the impeller blade root provide a smooth stress transition from the blade to the disk. The impeller blades and disk are analyzed with finite element methods; therefore, stress concentration factors do not apply.

### 8.1 Rotor Burst Speed Calculation

The impeller burst speed calculations were accomplished with the finite-element model shown in Figure 89. Annealed Ti-6Al-4V is the material from which the impeller is made. The blade inertias are simulated by the plane stress elements of appropriate blade thickness. The disk stiffness is simulated by full-hoop axisymmetric elements.

The average tangential stress calculation is based on integration of tangential stress in the disk elements. The 105-percent speed tangential stress distribution is shown in Figure 90. The effective stress distribution at 105-percent speed is shown in Figure 91.

For the impeller burst speed calculation, 85 percent of the disk section is allowed to approach the ultimate material strength before burst. The strength calculation is based on integrating the variation of ultimate strength with temperature.

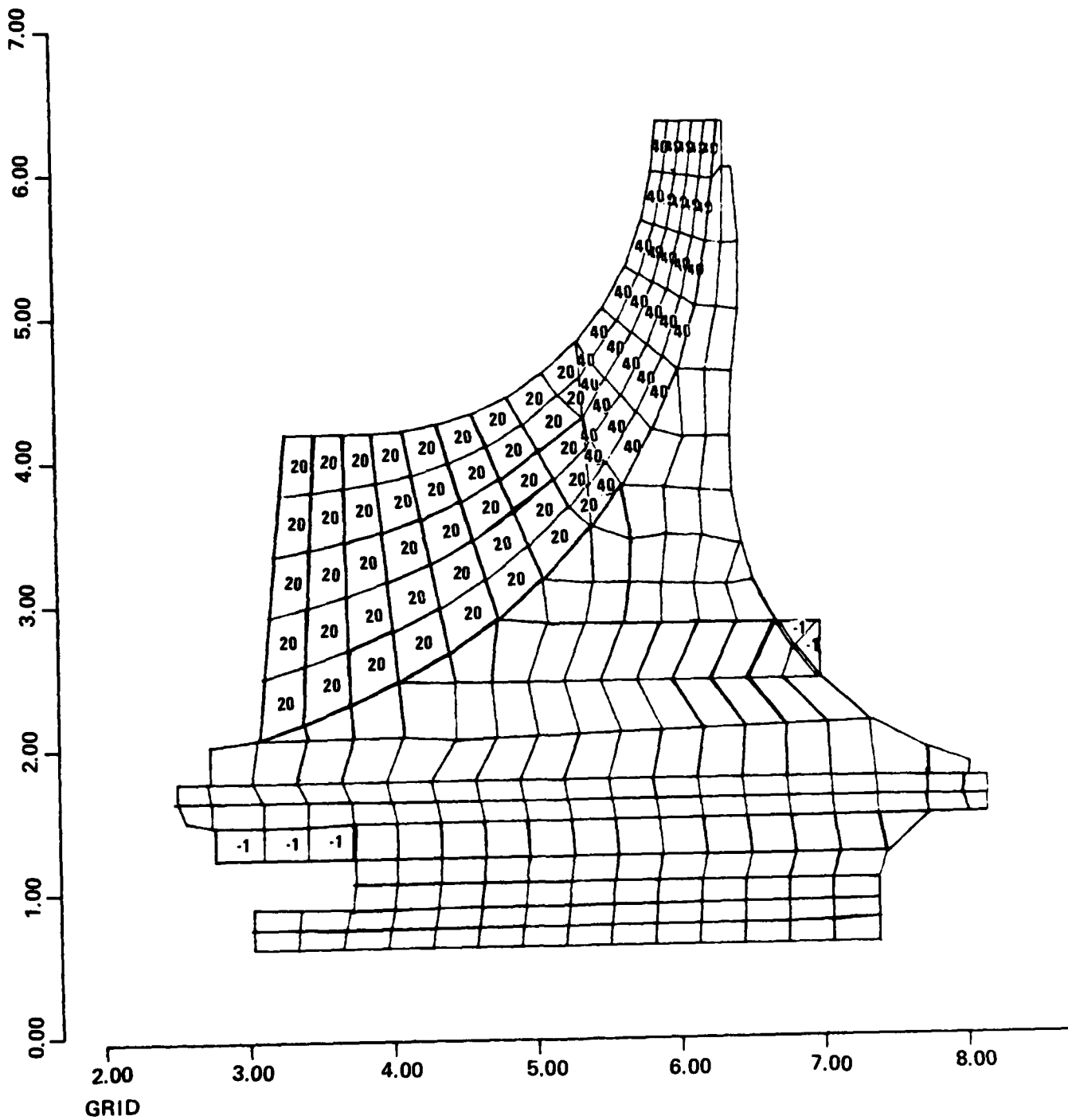


Figure 89. Finite-Element Model.

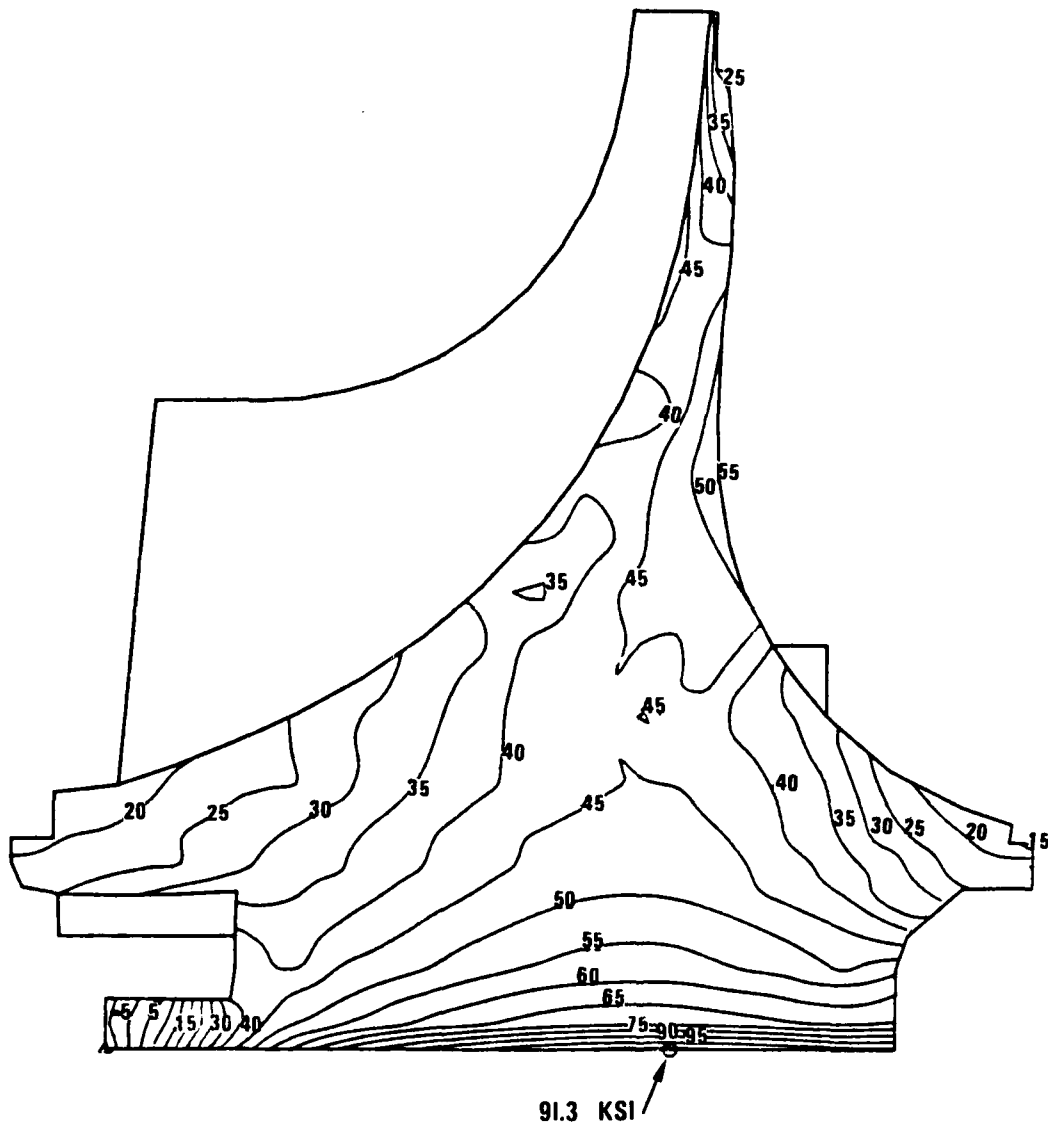


Figure 90. Tangential Stress Distribution at 105-Percent Speed.

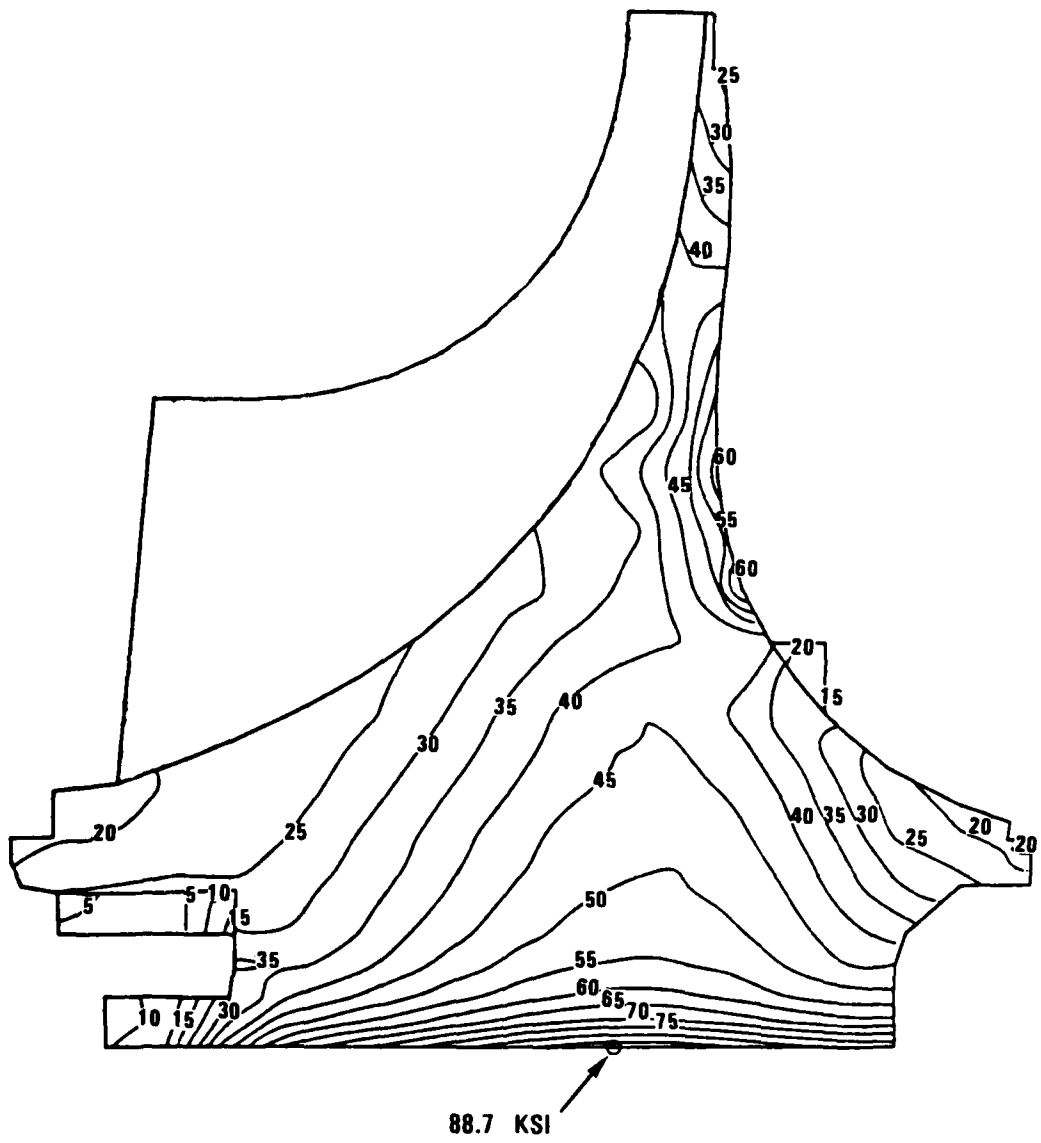


Figure 91. Effective Stress Distribution at 105-Percent Speed.

Burst calculation:

$$\text{Burst Speed} = \sqrt{0.85 \left( \frac{\sigma_{\text{ult}}}{\sigma_{\text{avg}}} \right)^N (100\% \text{ speed})}$$

where  $\sigma_{\text{ult}}$  = ultimate material strength (minimum)  
 $\sigma_{\text{avg}}$  = average tangential stress  
 100-percent speed = 36,366 rpm

therefore:

$$\begin{aligned} \text{Burst Speed} &= \sqrt{(0.85) \frac{108.8}{38.1} (36,366)} \\ &= 56,647 \text{ rpm} \end{aligned}$$

Stress margins have been calculated for the impeller disk. These values are shown in Table 10.

TABLE 10. IMPELLER DISK STRESS MARGINS

Stress Parameter	Minimum Requirement	Temp (F)	Yield (-3 $\sigma$ ) (ksi)	Allowable Stress (ksi)	Actual	<u>Allowable</u> <u>Actual</u>
Burst Margin	>1.25	-	-		1.484	-
Bore $\sigma_E$ Max	100% of YLD*	377	88.9	88.9	88.7 ksi	1.0
Bore $\sigma_E$ Avg	85% of YLD	343	91.76	78.0	71.3 ksi	1.09
Disk $\sigma_E$ Max	80% of YLD	502	81.9	65.5	62.2 ksi	1.05

\*YLD = Yield Strength

## 8.2 Rotor Cyclic Life Calculation

The cyclic life of the impeller has been determined using the stress simulation results discussed earlier. The critical location of the impeller is the disk bore with a maximum effective stress of 88.7 ksi. The disk is the dominant area because of its highest peak stress.

Disk life has a minimum requirement of 5000 cycles. Below the proportional limit, the loading is purely cyclic, ranging from 0 ksi to 88.7 ksi back to 0 ksi. Figure 92 illustrates the life diagram for 600F Ti-6Al-4V and reveals a life in excess of 10,000 cycles. The impeller disk bore will reach an approximate temperature of 400F while operating. The fatigue strength of titanium at 400F is higher than at 600F.

## 8.3 Calculation of Moment of Inertia

Inertial properties calculated within the finite-element analysis program are shown in Table 11 and summarized below:

	<u>Blades</u>	<u>Disk</u>	<u>Total</u>
Weight	3.1504	22.654	25.805
Polar moment of inertia (lb-in.-sec <sup>2</sup> )	0.1130	0.4808	0.5938
Diametral moment of inertia (lb-in.-sec <sup>2</sup> )	0.0581	0.3072	0.3712

## 8.4 Backplate Vibration Analysis

A finite-element model vibration analysis was performed on the impeller disk. Figure 93 illustrates the results. The final backplate design is a trade-off on backplate thickness (to obtain

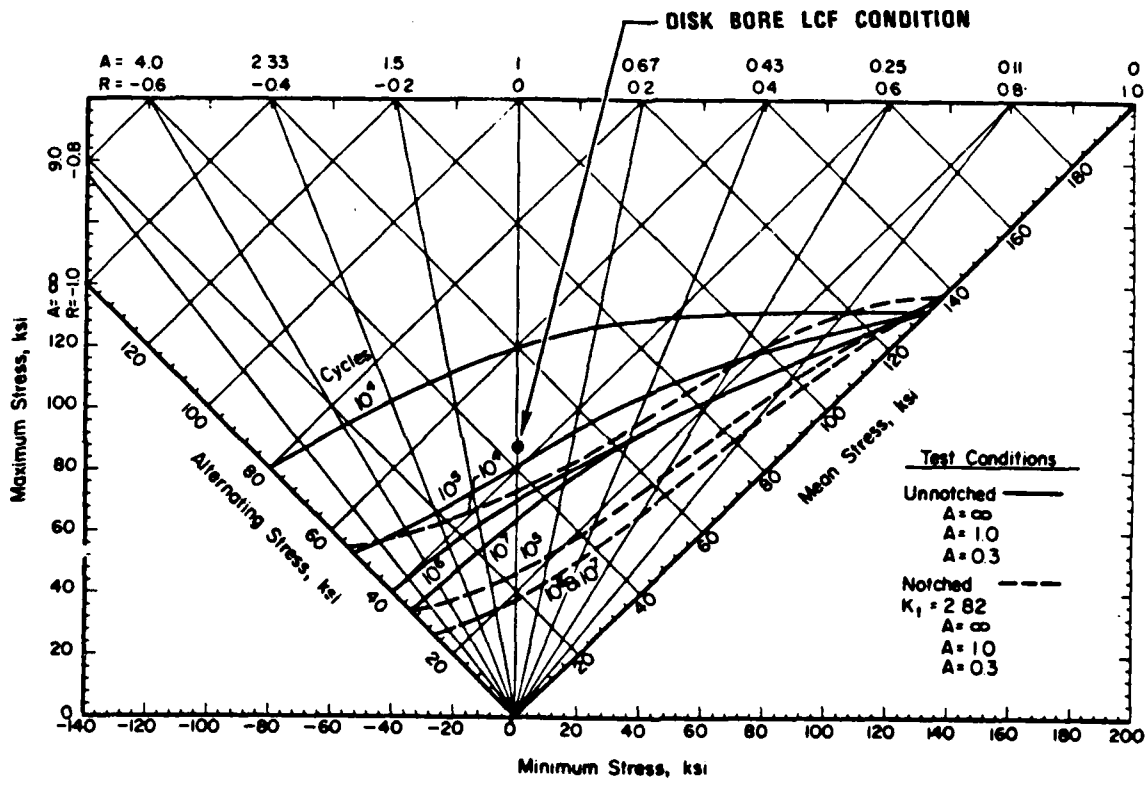


Figure 92. Titanium 6-4 Life Diagram.

TABLE 11. INERTIA PROPERTIES COMPUTER PRINTOUT.

NASA 2LB/SEC IMP SCALE) TO 1DLB/SEC FOR 20 DISK MODEL HANK-SYTIME. 9999.000 SFC RPM= 36366.00

HUB AREA PROPERTIES--AREA	10.9540 IN**2	MASS PROPERTIES--MASS	.0587 LB-SEC2/IN
W1A4	2.0443 IN	WEIGHT	22.6543 LB
ZBAR	5.5260 IN	I(P)	.4908 LB-IN-SEC2
		I(D)	.3072 LB-IN-SEC2
		RRAR	0.0000 IN
		ZBAR	5.6401 IN

BLADE AREA PROPERTIES--AREA	5.3000 IN**2	MASS PROPERTIES--MASS	.0082 LB-SEC2/IN
Z1A4	3.7254 IN	WEIGHT	3.1504 LB
ZBAR	4.6095 IN	I(P)	.1130 LB-IN-SEC2
		I(D)	.0581 LB-IN-SEC2
		RRAR	3.5306 IN
		ZBAR	4.7316 IN

(MASS PROPERTIES ARE FOR ALL BLADES)

TOTAL PROPERTIES-----MASS	.0668 LB-SEC2/IN	KINETIC ENERGIES	
WEIGHT	25.8048 LB	-ALL BLADES	819400. IN-LB
I(P)	.5938 LB-IN-SEC2	-----DISC	3486100. IN-LB
I(D)	.3712 LB-IN-SEC2	-----TOTAL	4305500. IN-LB
RRAR	2.7040 IN		
ZBAR	5.5292 IN		

SPEED OF ROTATION = 36366 RPM (100%)

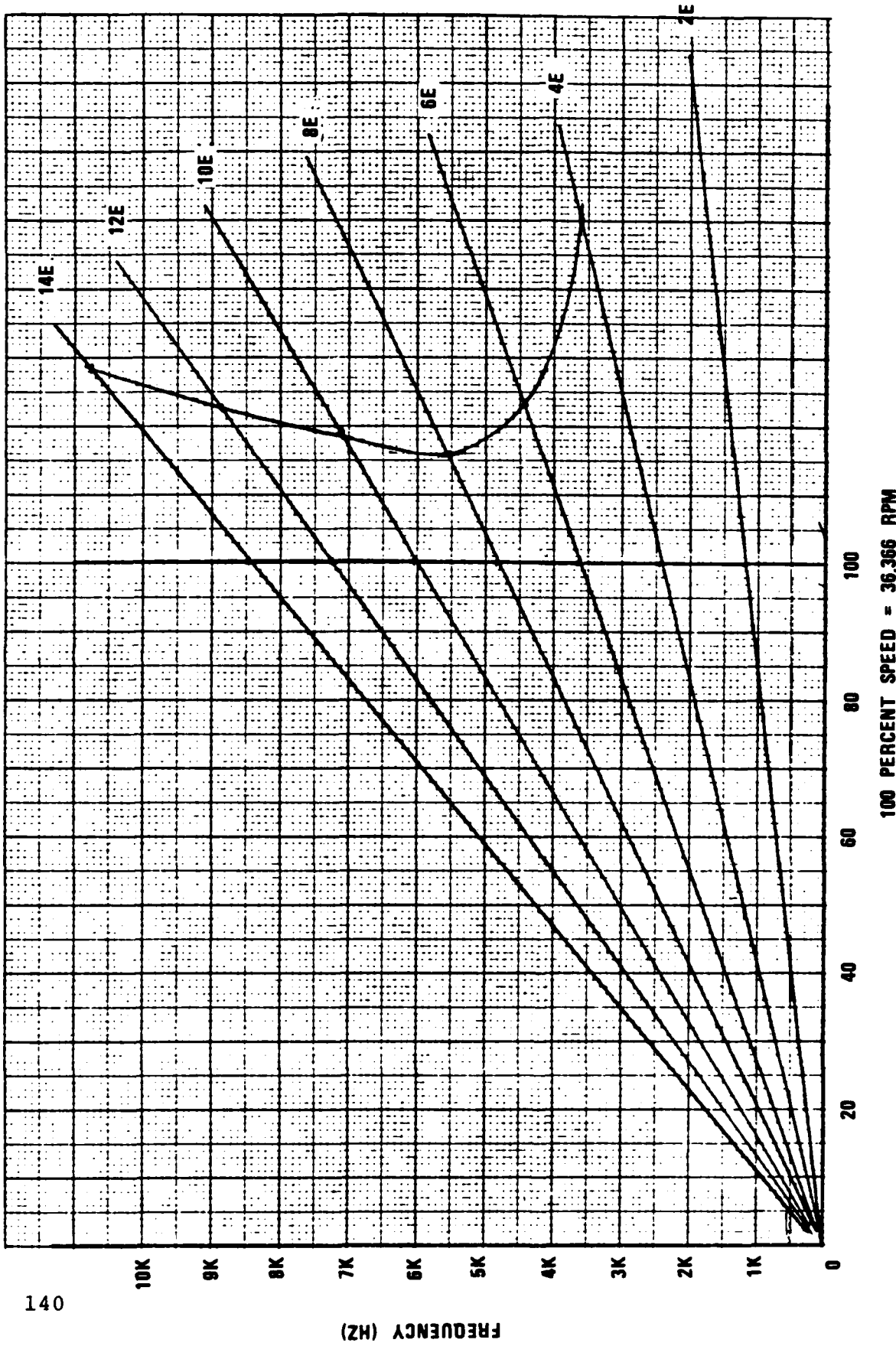


Figure 93. Backplate Model Vibration Analysis.

adequate frequency margin), flowpath deflection (to obtain the same shroud contour as the previous 10-lb/sec impeller), and bore stress. The final design met the design goals with a 16-percent frequency margin at 100-percent speed.

#### 8.5 Compressor Rig Compatibility

The 10-2-10-lb/sec scaled compressor must not vary the rotor dynamic characteristics of the rig. To ensure the rotor dynamic characteristics remain unchanged with the new compressor, the rotor unbalanced response was reanalyzed with the mass and inertia of the new 10-lb/sec compressor. As shown in Figures 94 and 95, bearing loads for the two compressors do not differ significantly.

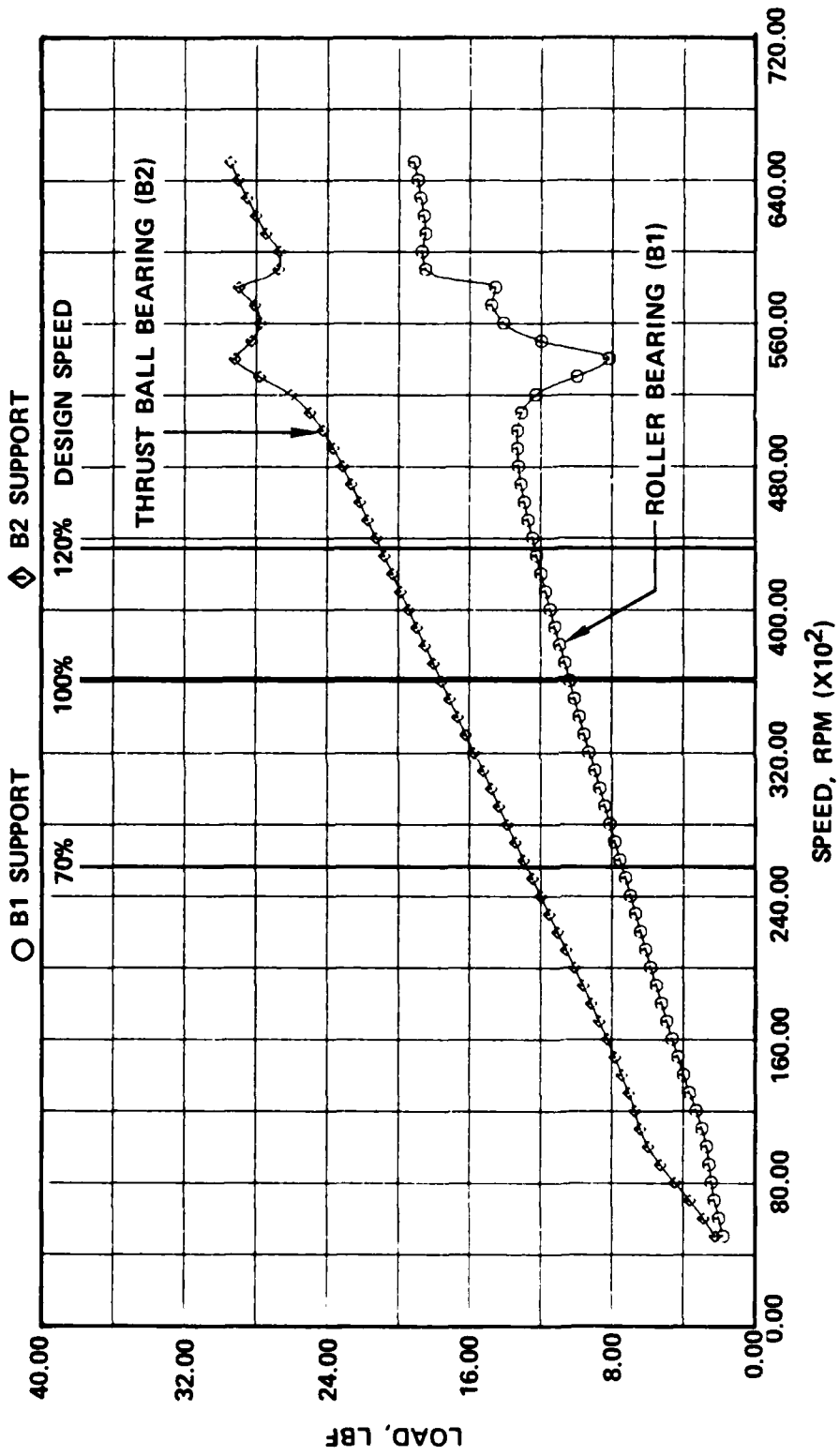
#### 8.6 Impeller Holographic Test

Holography testing was performed to determine the vibratory characteristics of the NASA 10-lb/sec impeller. Blade and disk backplate natural frequencies were determined for the 0 to 30,000 Hz range. The maximum frequency reported is 13 kHz range. The maximum frequency reported is 13 kHz, which includes the diffuser vane interference of 21/rev at 100 percent speed (36,366 rpm).

Figure 96 is a Campbell diagram showing the impeller full-blade natural frequencies. The blade modes are plotted at constant frequency without the blade centrifugal stiffening and thermal effects.

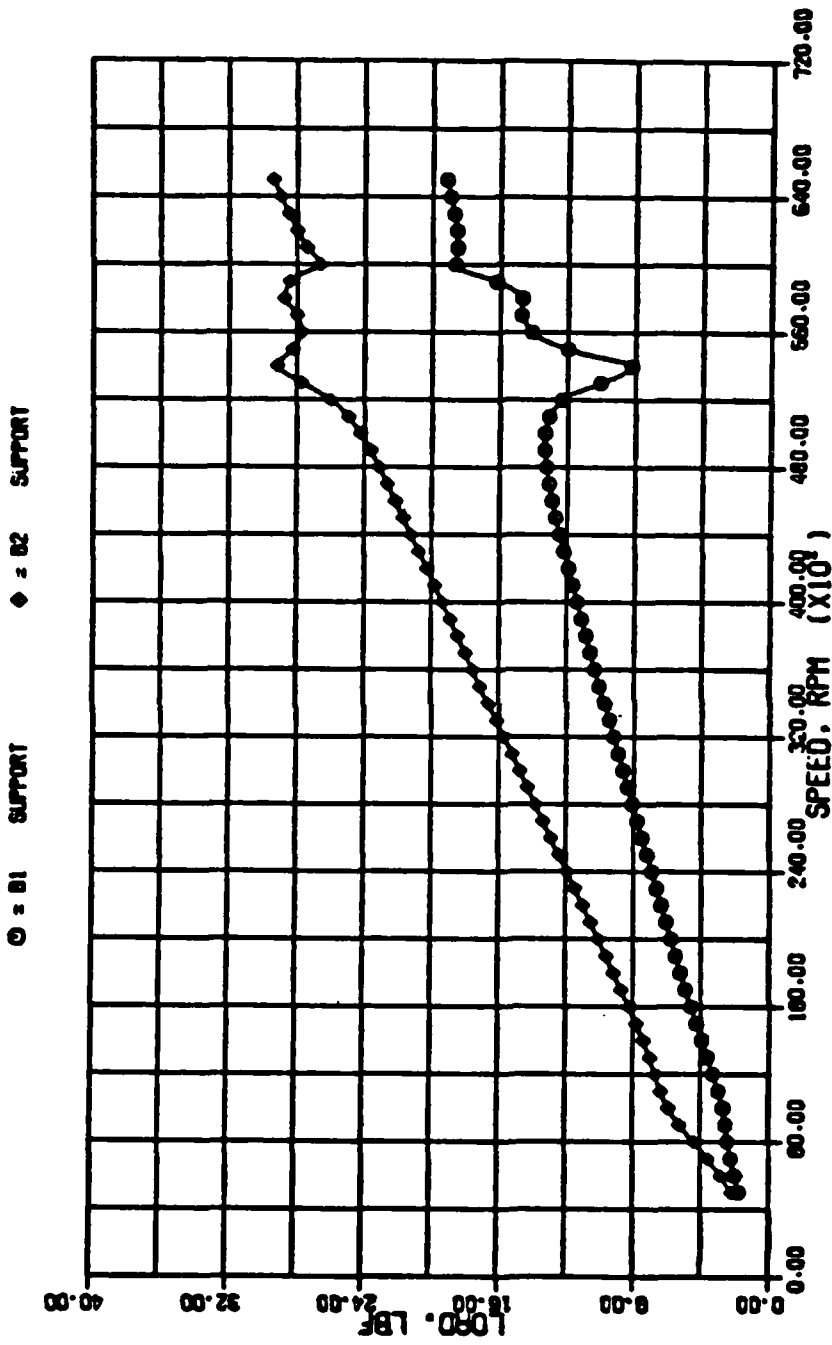
The first blade mode shows 4/rev interference above 90-percent speed. However, incorporating the centrifugal stiffening and thermal effects from a similar 10-lb/sec impeller shows that the first mode is above 4/rev at 100-percent operating speed. Figure 91 also shows that several modes have a frequency range (the observed blade is transmitting the frequencies of other blades and/or the active disk backplate) and that some higher

ECCENTRICITY OF IMPELLER AND SHAFTS ±0.0005 INCH



23-SVG1213-25

Figure 94. 10-Lb/Sec Compressor Rig Unbalance Response with Original 10-Lb/Sec Compressor.



02-12-1945

Figure 95. 10-Lb/Sec Compressor Rig Unbalance Response with 10-2-10-Lb/Sec Scaled Compressor.

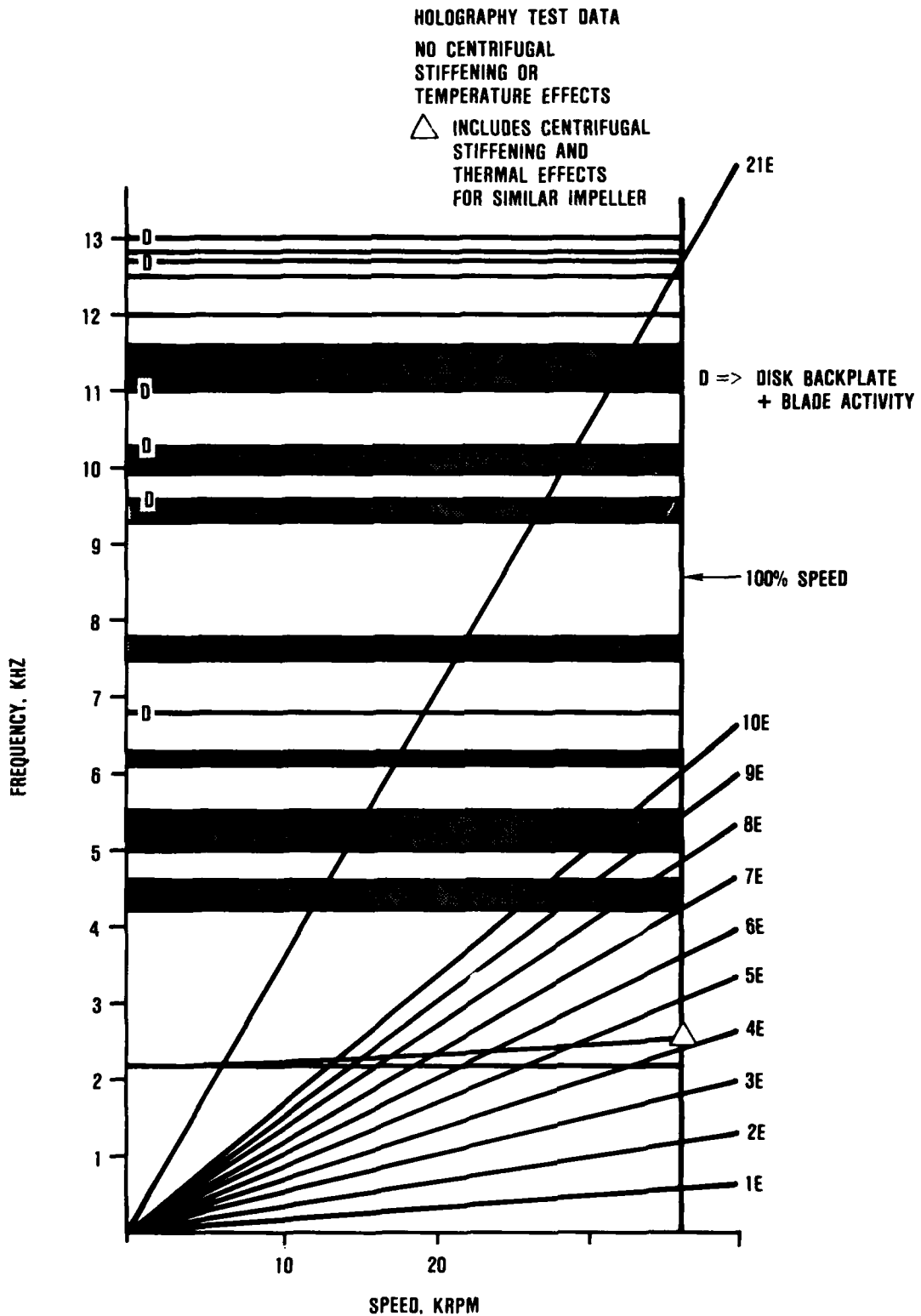


Figure 96. Full-Blade Campbell Diagram from Holographic Testing.

order modes cross 21E (diffuser vane count) near 100-percent speed. Higher order modes are generally low in energy, and it is felt that they should present no problems. Figure 96 shows some modes with the letter D to designate significant disk backplate activity. Figures 97, 98, and 99 show the first 11 blade modes obtained from holography.

Holography testing was also performed to determine disk backplate modes. Figure 100 is a Campbell diagram which shows that the backplate has 30-percent margin on 100-percent speed (11 nodal diameter - 11E crossing). This margin is sufficient to prevent significant blade-disk coupling within the operating speed range. Figures 101, 102, and 103 show the first 12 nodal diameters obtained from holography testing.



MODE 1



MODE 2



MODE 3



MODE 4

Figure 97. NASA 10 Lb/Sec Impeller Holographic Blade Modes.



MODE 5



MODE 6



MODE 7



MODE 8

Figure 98. NASA 10-Lb/Sec Impeller Holographic Blade Modes.



MODE 9



MODE 10



MODE 11

Figure 99. NASA 10-Lb/Sec Impeller Holographic Blade Modes.

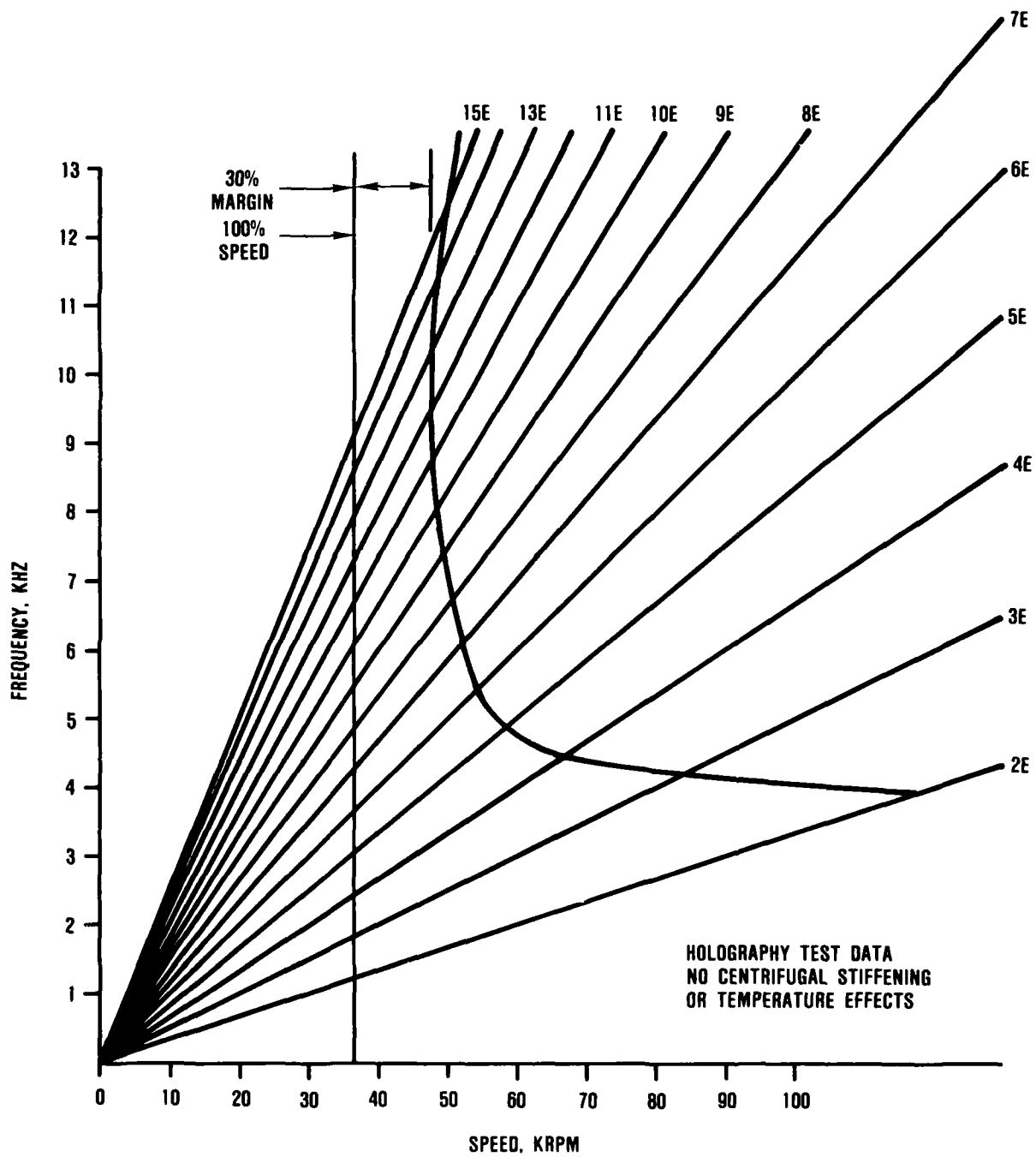
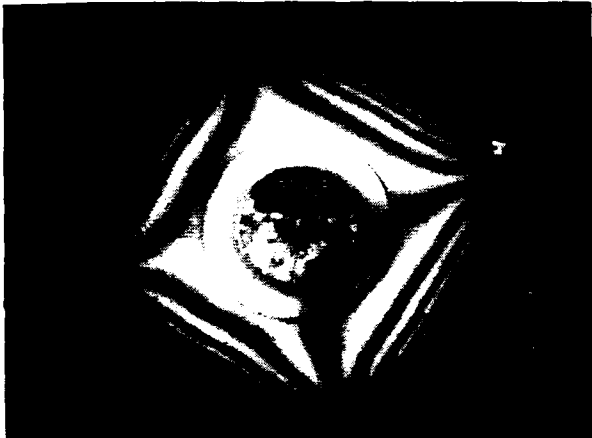


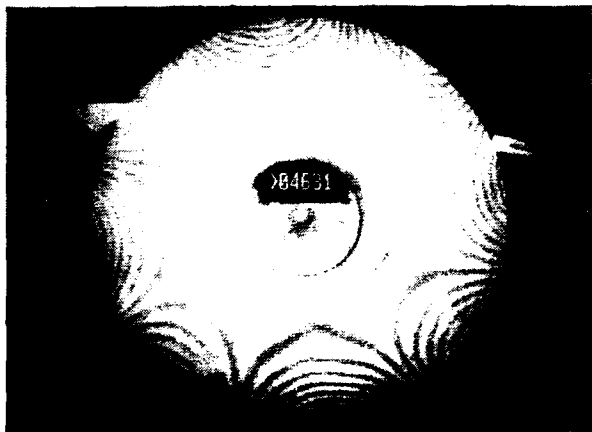
Figure 100. Back Plate Campbell Diagram from Holographic Testing.



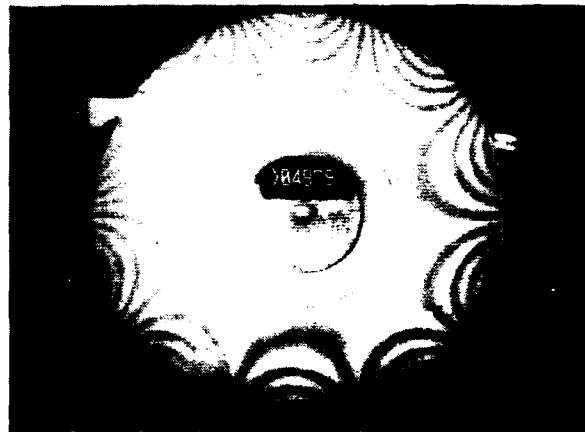
2 NODAL DIAMETERS



3 NODAL DIAMETERS

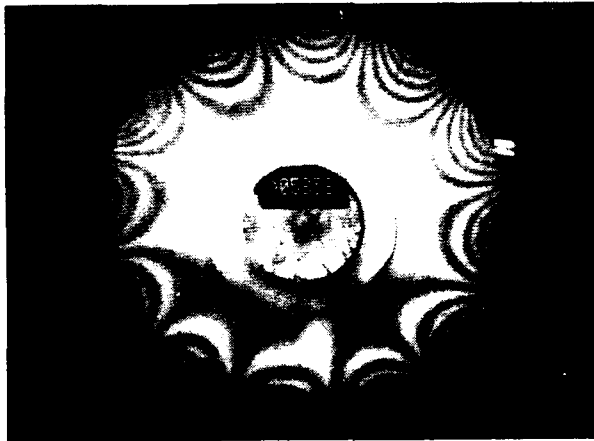


4 NODAL DIAMETERS



5 NODAL DIAMETERS

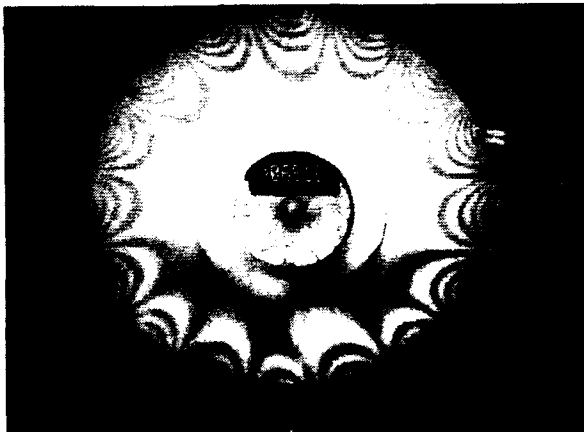
Figure 101. NASA 10-Lb/Sec Impeller Holographic Results.



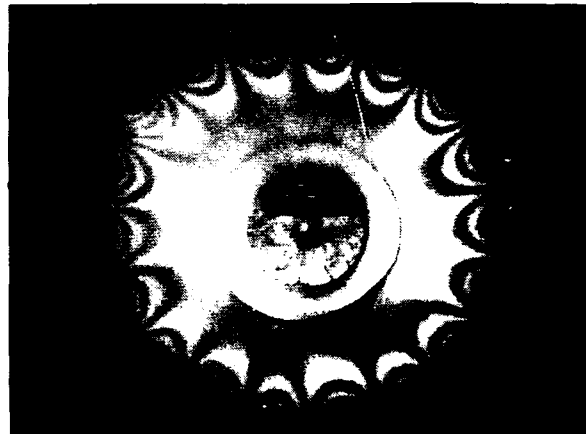
6 NODAL DIAMETERS



7 NODAL DIAMETERS



8 NODAL DIAMETERS



9 NODAL DIAMETERS

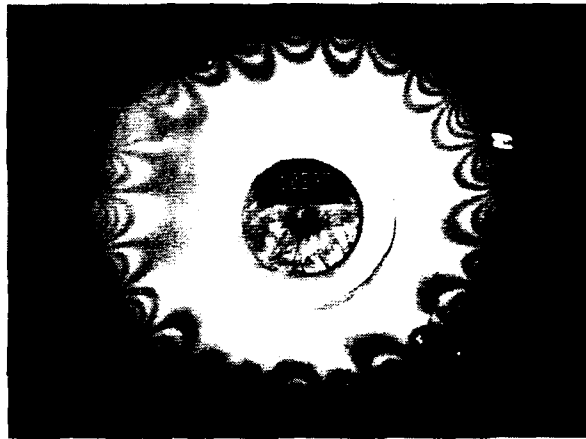
Figure 102. NASA 10-Lb/Sec Impeller Holography Results.



10 NODAL DIAMETERS



11 NODAL DIAMETERS



12 NODAL DIAMETERS

Figure 103. NASA 10 Lb/Sec Impeller Holography Results.

## 9.0 10-LB/SEC STATIC COMPONENT ANALYSIS

### 9.1 Component Definition

Two 10-lb/sec static impeller shrouds were required in this program. The two shrouds will be interchangeable with the Part Number (P/N) 3553028 shroud supplied under Contract NAS3-22431. The existing 10-lb/sec shroud (P/N 3553028) is not a thermal scale of the baseline 25-lb/sec shroud, but was designed to contain a blade failure as requested by NASA. The two new shrouds will be thermally scaled from the baseline 25-lb/sec shroud design (GTEC P/N 3551000). One of the new shrouds supplied under this contract will be for aerodynamic performance evaluation and the other for Laser Doppler Velocimeter (LDV) activities. Again, all three 10-lb/sec shrouds will be interchangeable on the test rig as well as with the existing P/N 3553023 10-lb/sec impeller and the new P/N 3553144 10-lb/sec impeller.

### 9.2 Baseline (25 Lb/Sec) Shroud Thermal Analysis

The 10-lb/sec compressor shrouds for this program were designed to be thermally scaled from the 25-lb/sec compressor shroud. Thermal scaling is defined as identical temperature increase (or decrease) of the compressor airflow as a function of flow path length. The temperature increase (or decrease) is due to conduction from the hot exit gas into the shroud, then from the shroud into the colder gas at the compressor inlet.

A thermal model of the 25-lb/sec compressor shroud is shown in Figure 104. The shroud inside heat-transfer coefficients are calculated from results published in General Electric Technical Report AFAPL-TR-73-46 entitled "Advanced Turbine Engine Seal Design." The calculated shroud metal temperatures resulting from analytical gas path air temperatures furnished by the Compressor

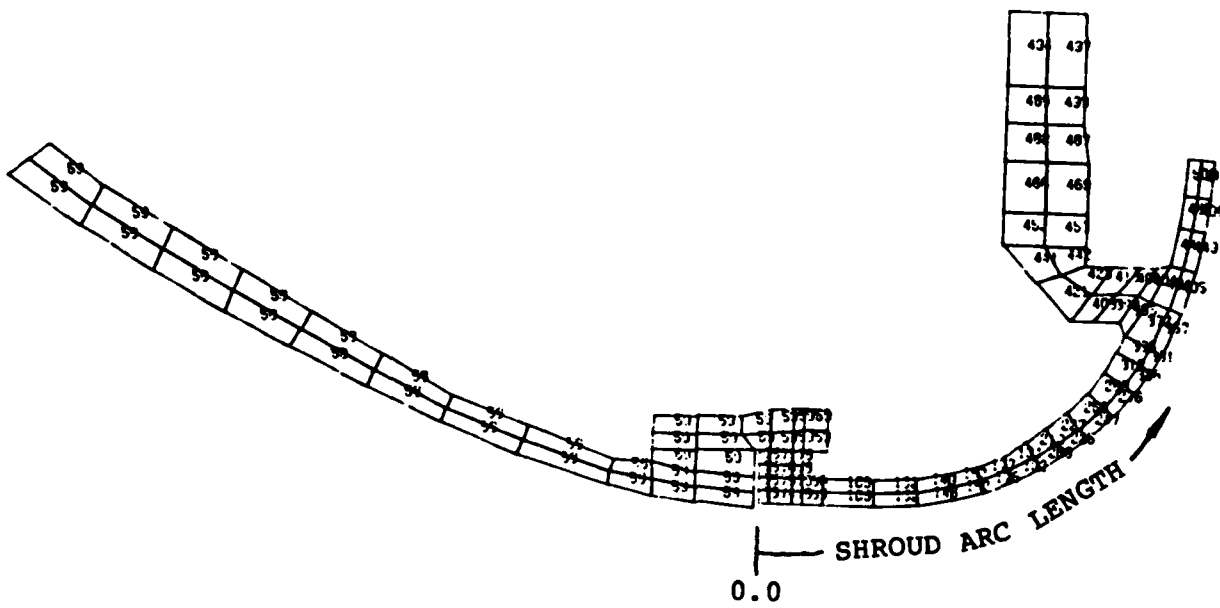


Figure 104. Baseline (25-Lb/Sec) Shroud and Inlet Duct Metal Temperatures (F).

Aerodynamics Group are shown in Figure 105. Shroud metal temperatures are observed to closely follow the gas path air temperatures. The heat flux per unit of mass flow is shown in Figure 106. Figure 106 also includes a plot of cumulative bulk gas temperature increase (from shroud-heat conduction) as a function of shroud-arc length. The net effect of shroud-heat conduction for the baseline shroud is to raise the gas temperature 0.04F.

An examination of other heat-transfer mechanisms in the 25-lb/sec compressor rig indicates that the heat-conduction effect along the shroud is only one of the possible paths by which heat can be conducted from the hot compressor exit gas to the colder inlet air. A schematic of other possible heat-transfer paths is shown in Figure 107. The figure shows that heat conduction within the compressor rotor from exit to inlet is a second significant mechanism by which heat may be transferred to the inlet air. In fact, computer thermal calculations have indicated that the effects of rotor conduction are even greater than conduction along the shroud. In addition, the figure also indicates that heat is exchanged from the back side of the compressor to the rear shroud. Neither of these two mechanisms are likely to scale directly since they are dependent on convection heat transfer from the surfaces to the adjacent gas.

A comparison of shroud and rotor heat-flux rates for a similar GTEC single-stage centrifugal compressor is shown in Figure 108. These results indicate that the heat-flux magnitudes between the gas flow and the rotor are significantly greater than between the gas flow and the shroud. In addition, it is apparent that heat transfer on the back side of the rotor due to viscous-heating effects and impeller discharge air results in a net heat addition to the gas flow along the entire rotor flow path.

### 9.3 10-Lb/Sec Shroud Thermal Design

A thermal analysis was performed on the existing P/N 3553028 shroud to determine how near (or far) it is from a thermal scale of

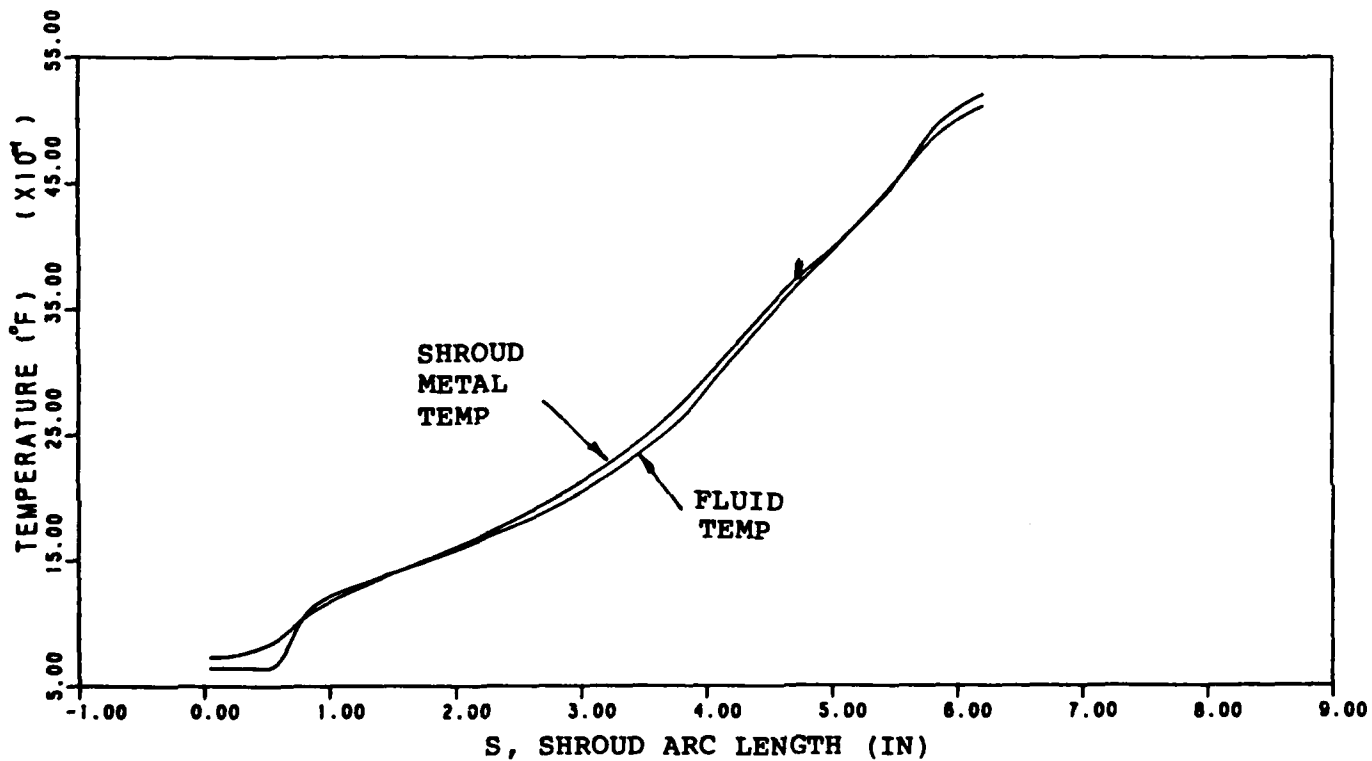


Figure 105. Baseline (25-Lb/Sec) Shroud and Fluid Stream Temperatures (F).

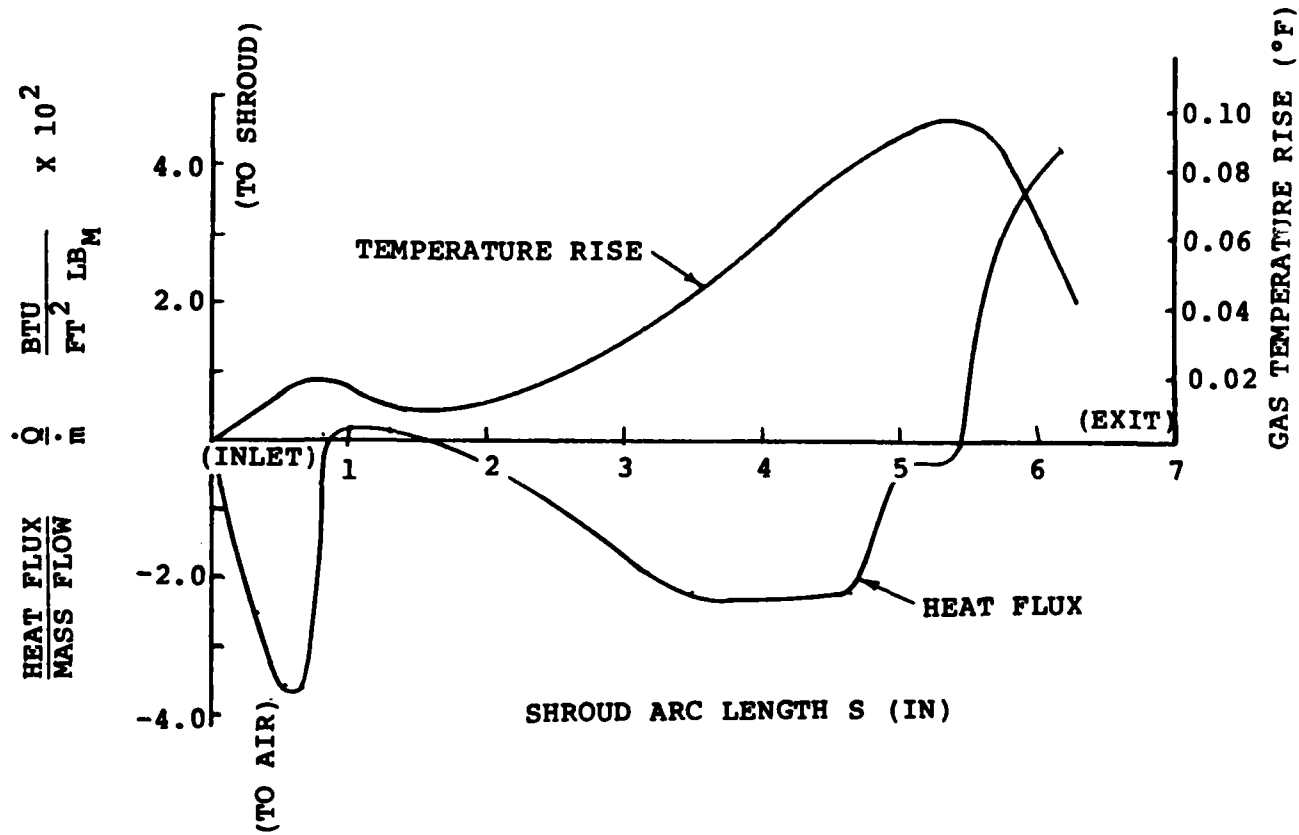
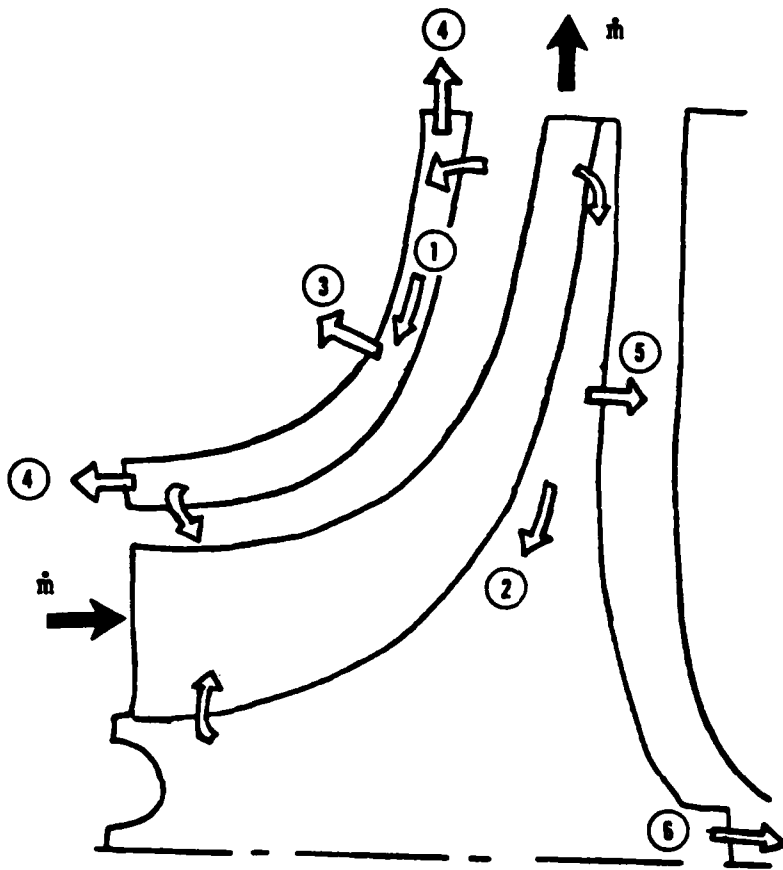


Figure 106. Shroud Heat Flux, Baseline Compressor (25-Lb/Sec).



• Thermal scale implies

$$\frac{\dot{q}}{\dot{m}} - \text{constant}$$

where:

$\left(\frac{\dot{q}}{\dot{m}}\right)_1$  = Shroud transfer from exit to inlet

$\left(\frac{\dot{q}}{\dot{m}}\right)_2$  = Compressor rotor transfer from exit to inlet

$\left(\frac{\dot{q}}{\dot{m}}\right)_3$  = Convection and radiation loss from shroud to surroundings

$\left(\frac{\dot{q}}{\dot{m}}\right)_4$  = Conduction loss from shroud to supports

$\left(\frac{\dot{q}}{\dot{m}}\right)_5$  = Connection and radiation loss from rotor to back shroud

$\left(\frac{\dot{q}}{\dot{m}}\right)_6$  = Conduction loss from rotor through shroud

Figure 107. Thermal Scaling of Compressor Rotor and Shroud.

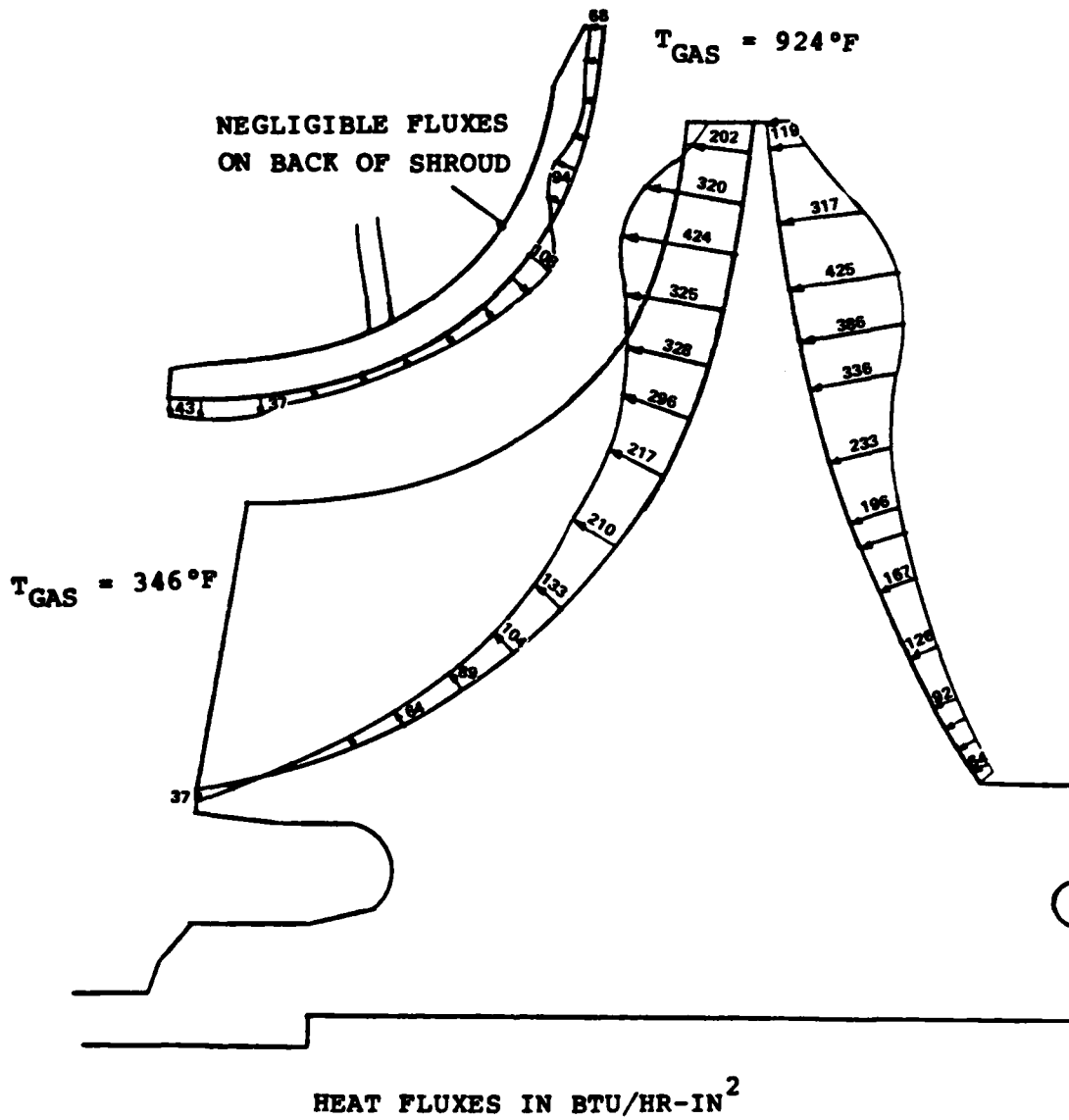


Figure 108. Comparison of Shroud and Rotor Heat Flux Rates for a Similar GTEC Centrifugal Compressor.

the 25-lb/sec shroud. The results of this analysis are shown in Figures 109, 110, and 111. The heat flux per mass flow ( $\dot{Q}/\dot{m}$ ) and bulk fluid temperature rise are plotted against the dimensionless length of the flowpath in Figures 109 and 110. Figure 111 presents a comparison of metal temperatures and fluid temperatures for the two shrouds.

Figure 110 compares the bulk-fluid temperature rise for the two shrouds. At the impeller exit, the 25-lb/sec shroud will increase the fluid temperature by 0.05F and the 10-lb/sec shroud will increase the fluid temperature by 0.25F. This data shows that the 10-lb/sec shroud is not a thermal scale of the 25-lb/sec shroud; however, GTEC views the difference in temperature increase of 0.20F between the two shrouds as being within the measuring accuracy of typical performance thermocouples.

The 25-lb/sec shroud design was then geometrically scaled to 10-lb/sec. The material was also changed from Inco-600 (25-lb/sec shroud) to CRES-347 (new 10-lb/sec shrouds). The thermal design process shown in Figure 112 was used to complete the design of the 10-lb/sec shroud. A comparison of the 10-lb/sec and 25-lb/sec shroud metal temperatures is shown in Figure 113. The 10-lb/sec shroud is 11F cooler at the impeller exit due to material thickness required for instrumentation probes. The 25-lb/sec shroud is 3F warmer near the impeller inlet because of an assembly joint which resembles an adiabatic surface.

#### 9.4 Shroud Mechanical Design

The 10-lb/sec performance shroud (P/N 3553145) effective stress distribution is shown in Figure 114. As indicated, the peak stress is 65.2 ksi at compressor design point conditions. The thermal and stress analyses (deflections) were applied to the shroud contour to provide the proper tooling layout coordinates for fabrication.

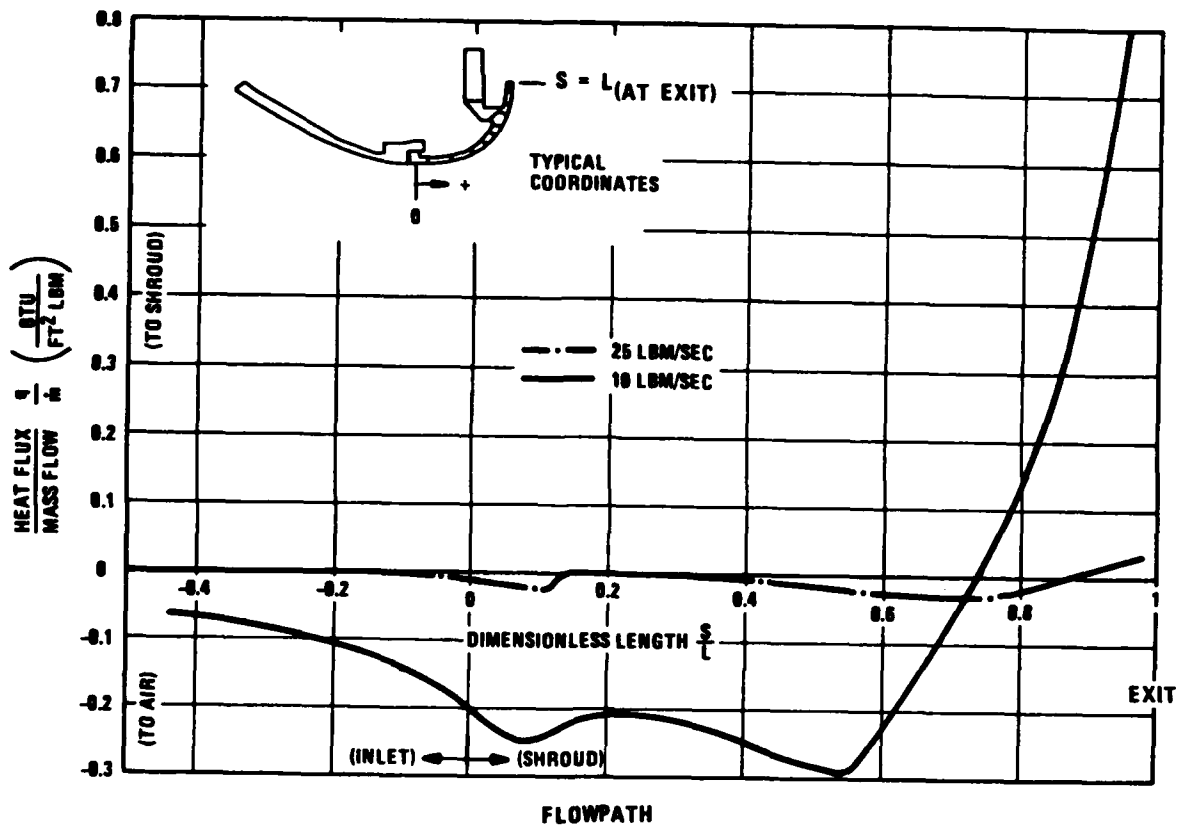


Figure 109. Comparison of the Shroud (25-Lbm/Sec and P/N 3553028 10-Lbm/Sec) Conductivity.

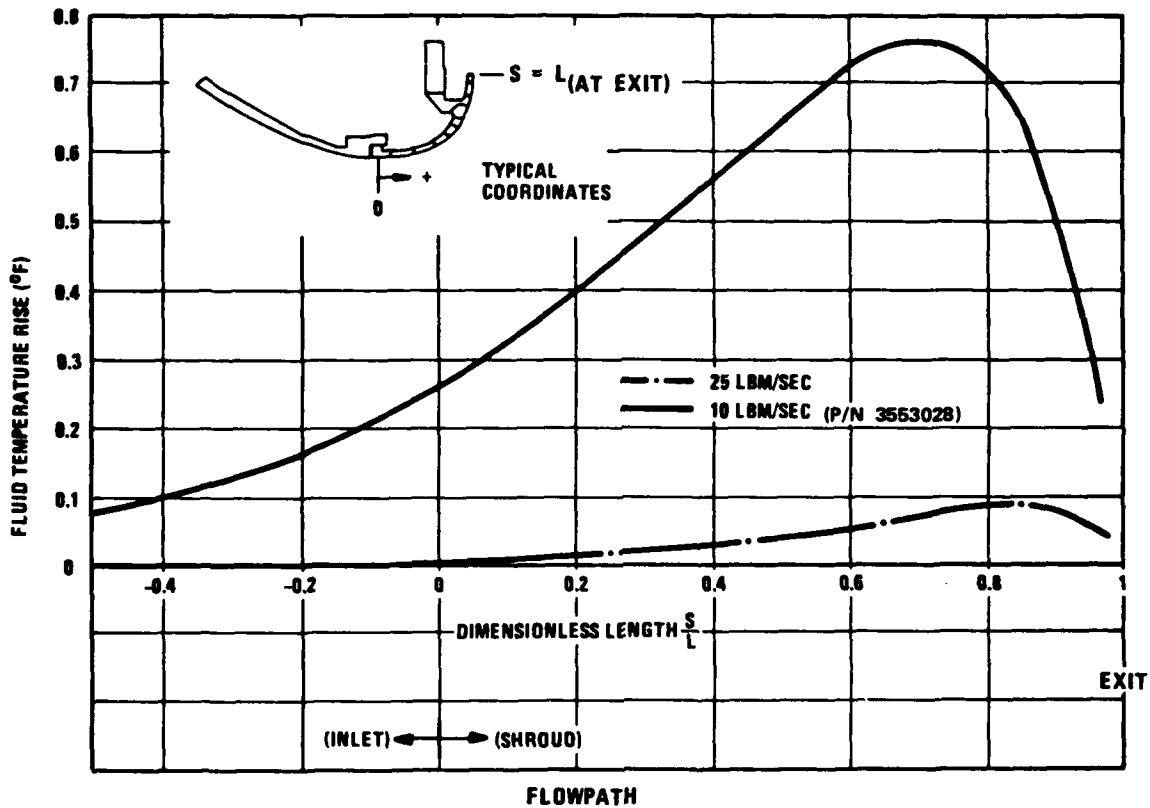
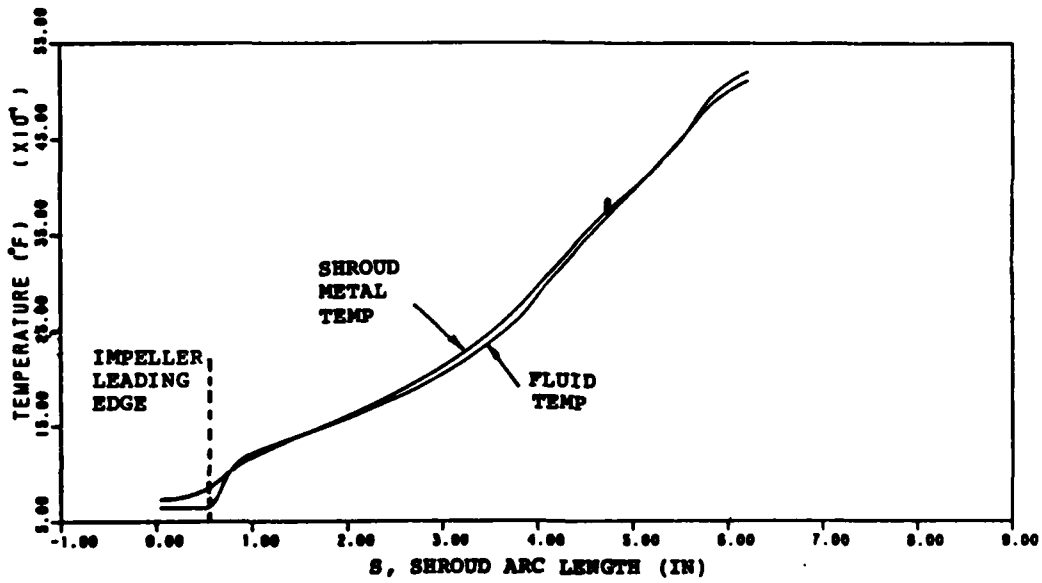
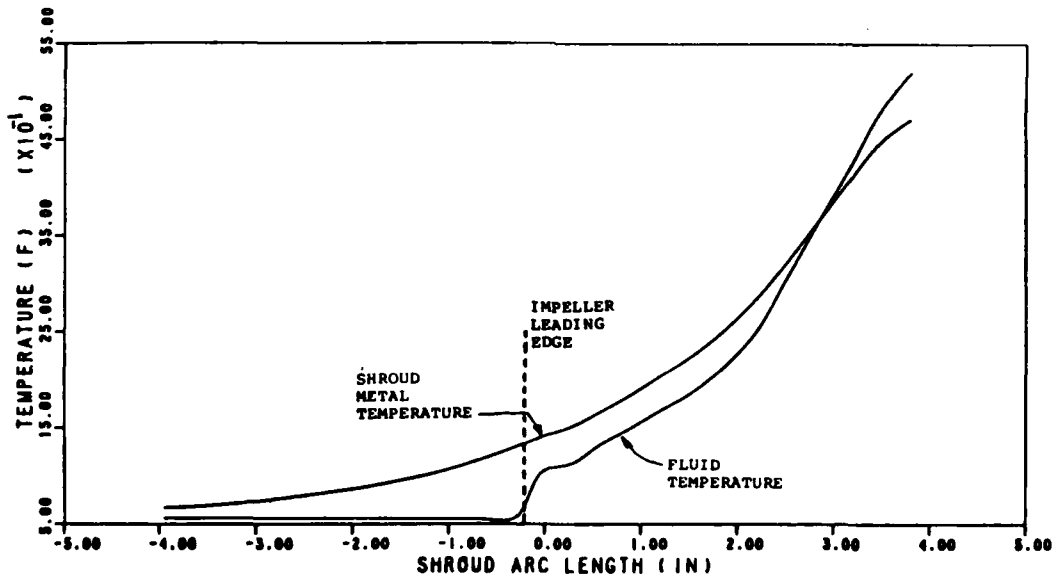


Figure 110. Bulk-Fluid Temperature Rise Due to Shroud Conductivity.



25-LBM/SEC COMPRESSOR (BASELINE)



10-LBM/SEC COMPRESSOR (P/N 3553028 Shroud)

Figure 111. Metal and Fluid Temperature Comparison of the Two Shrouds.

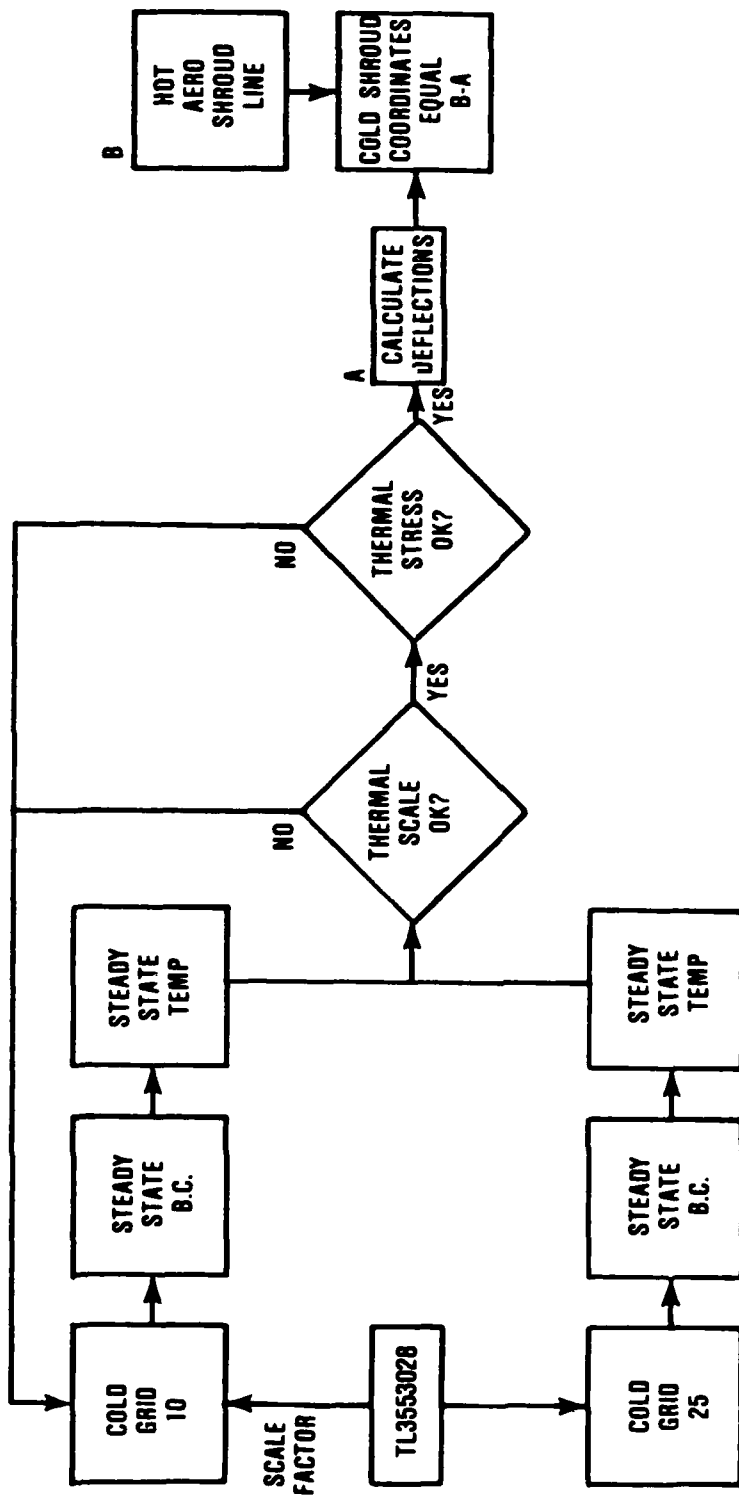


Figure 112. Thermal Design Process.

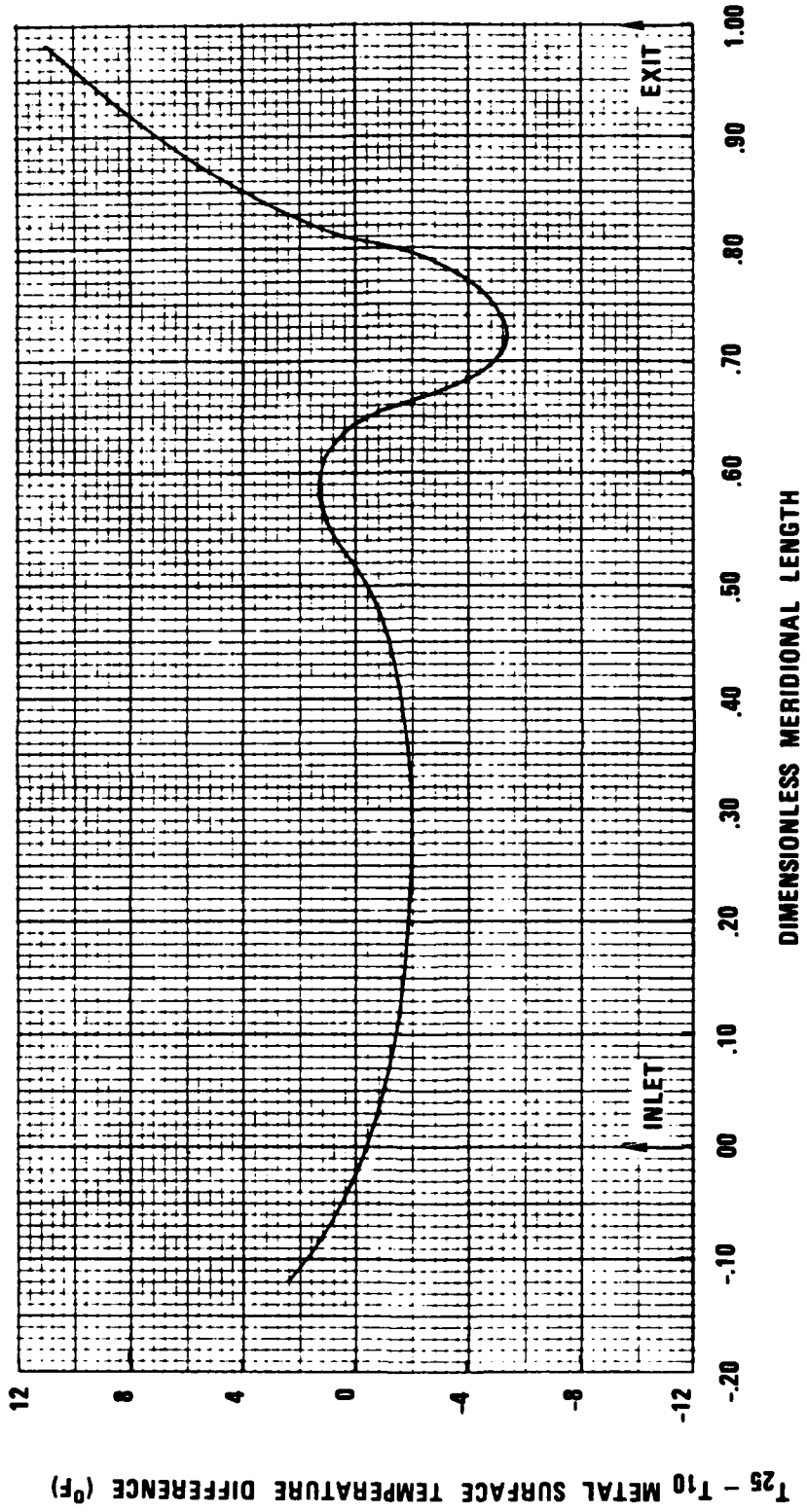
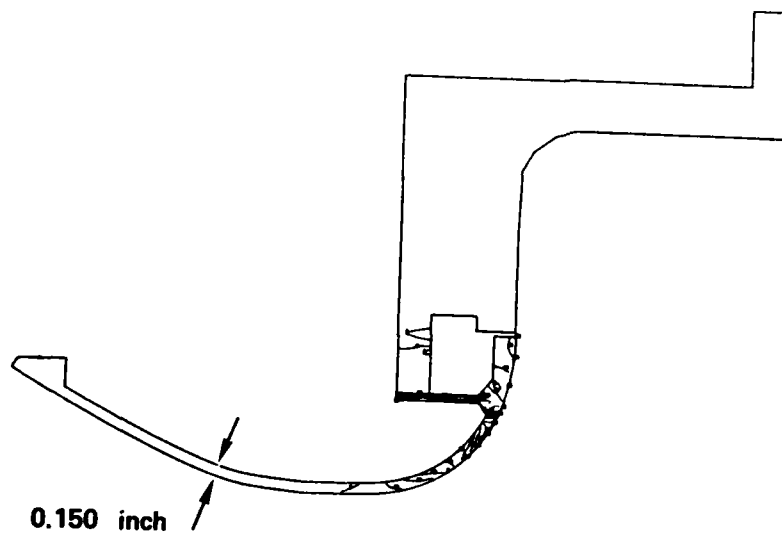


Figure 113. Metal Temperature Comparison Between Baseline 25-Lb/Sec Shroud and Thermally Scaled 10-Lb/Sec Shroud (P/N 3553145).



(DETAIL)

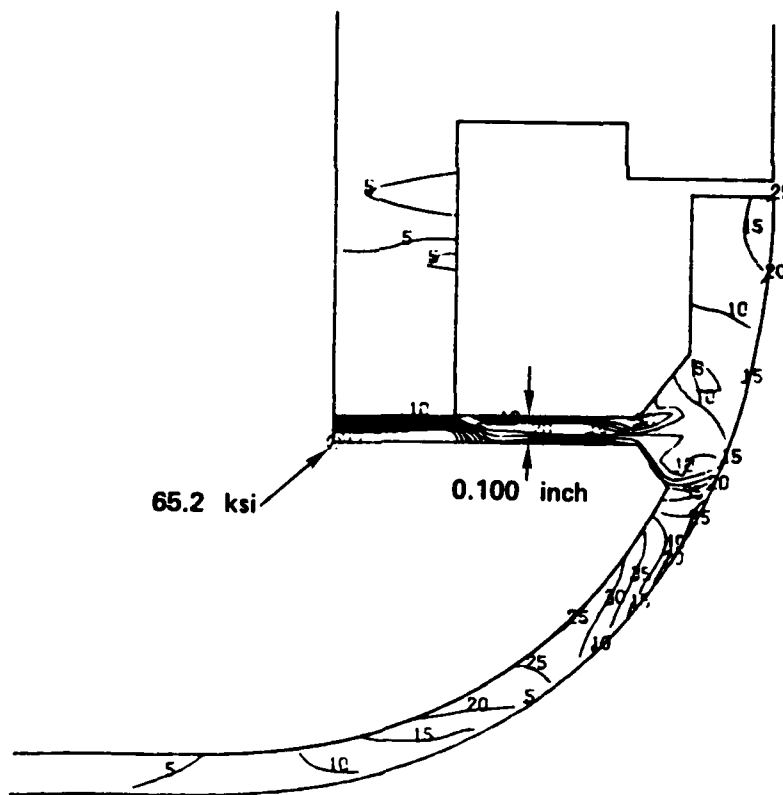


Figure 114. 10-lb/sec Performance Shroud (P/N 3553145)  
Stress Distribution.

The 10-lb/sec LDV shroud (P/N 3553146) required more detailed 3-dimensional analysis to ensure acceptable stress and deflection characteristics. The model used for the design analysis is shown in Figure 115. The final design incorporated additional material thickness above a direct scale in order to control deflections. The knee window was also removed to help maintain dimensional stability.

The LDV shroud deflection tends to be oblong or egg-shaped because of the local cutouts for the windows. The intent of the shroud design was to control the deflections to a point where reasonable running clearances were possible with a minimum risk of the impeller contacting the shroud. A cross section of the shroud in the window region is shown in Figure 116. Circumferential meridional sections (e.g., 9, 10, 11...) were taken from inlet to exit of the shroud for deflection analysis. The "worst case" point in each section -- that is, the point around the shroud that deviated most from a circular deflection -- has been plotted in Figure 117. This deflection is considered aerodynamically acceptable and will provide adequate clearance to avoid impeller to shroud contact.

#### 9.5 10-Lb/Sec LDV Diffuser Design

Certain vanes in the LDV diffuser (Figure 118) were cantilevered. An analysis was performed to calculate the natural frequencies of the "worst case" cantilevered vane and splitter to determine if the blade passing frequency could be a source of excitation. This analysis was supplemented by holographic testing of the diffuser.

The first five natural frequencies of the vane and splitter were calculated and are shown in Table 12. Figures 119 and 120 display the Campbell diagrams for the cantilevered vane and splitter, respectively. The vane Campbell diagram shows that it

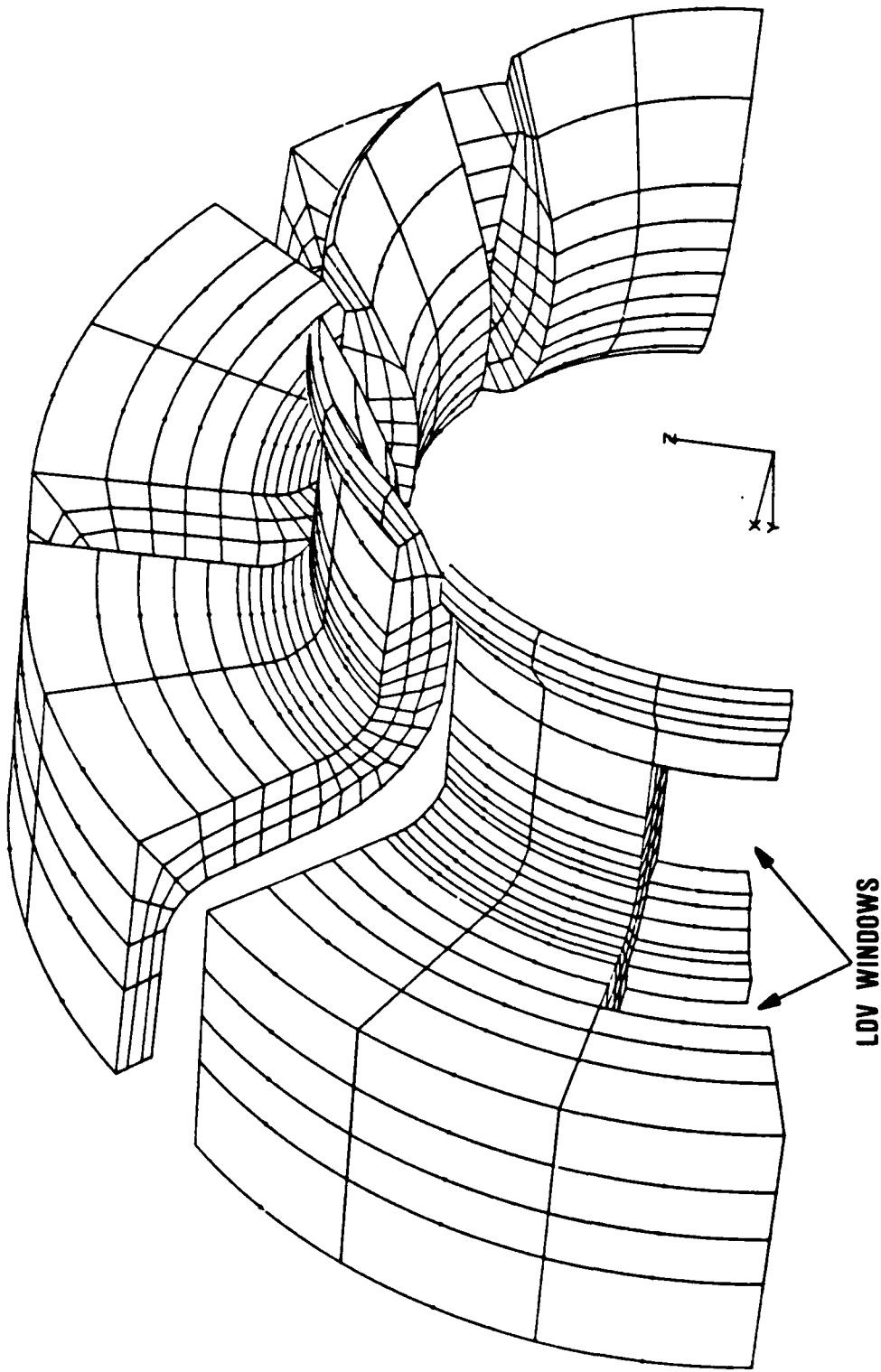


Figure 115. LDV Shroud Design Model.

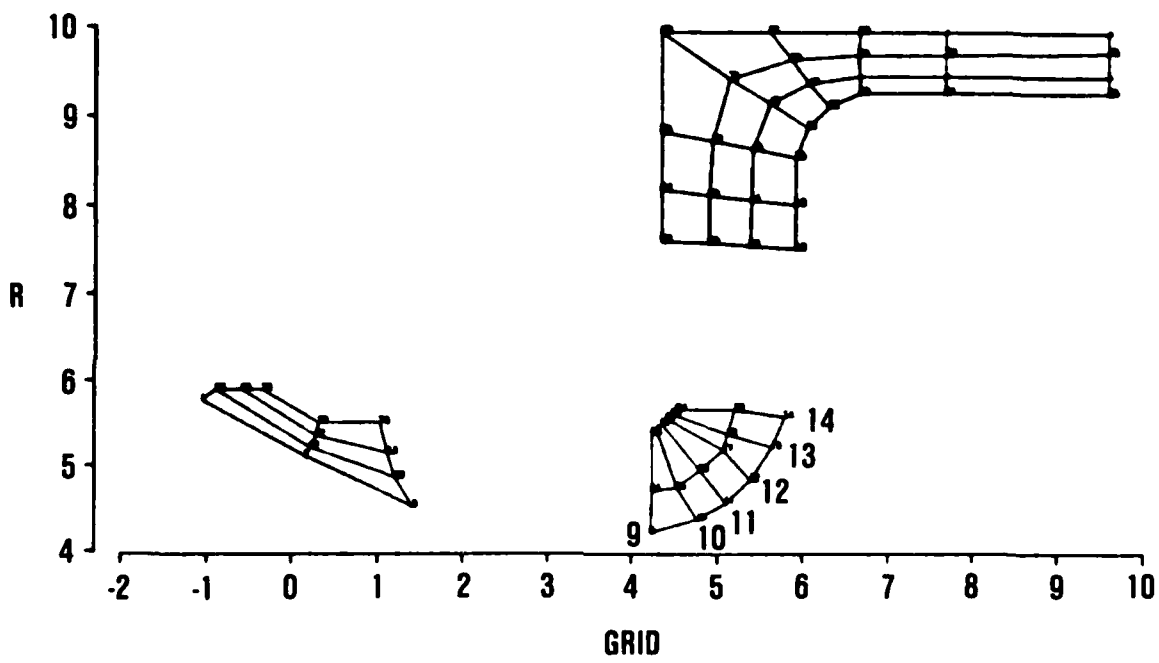


Figure 116. LDV Shroud Cross Section.

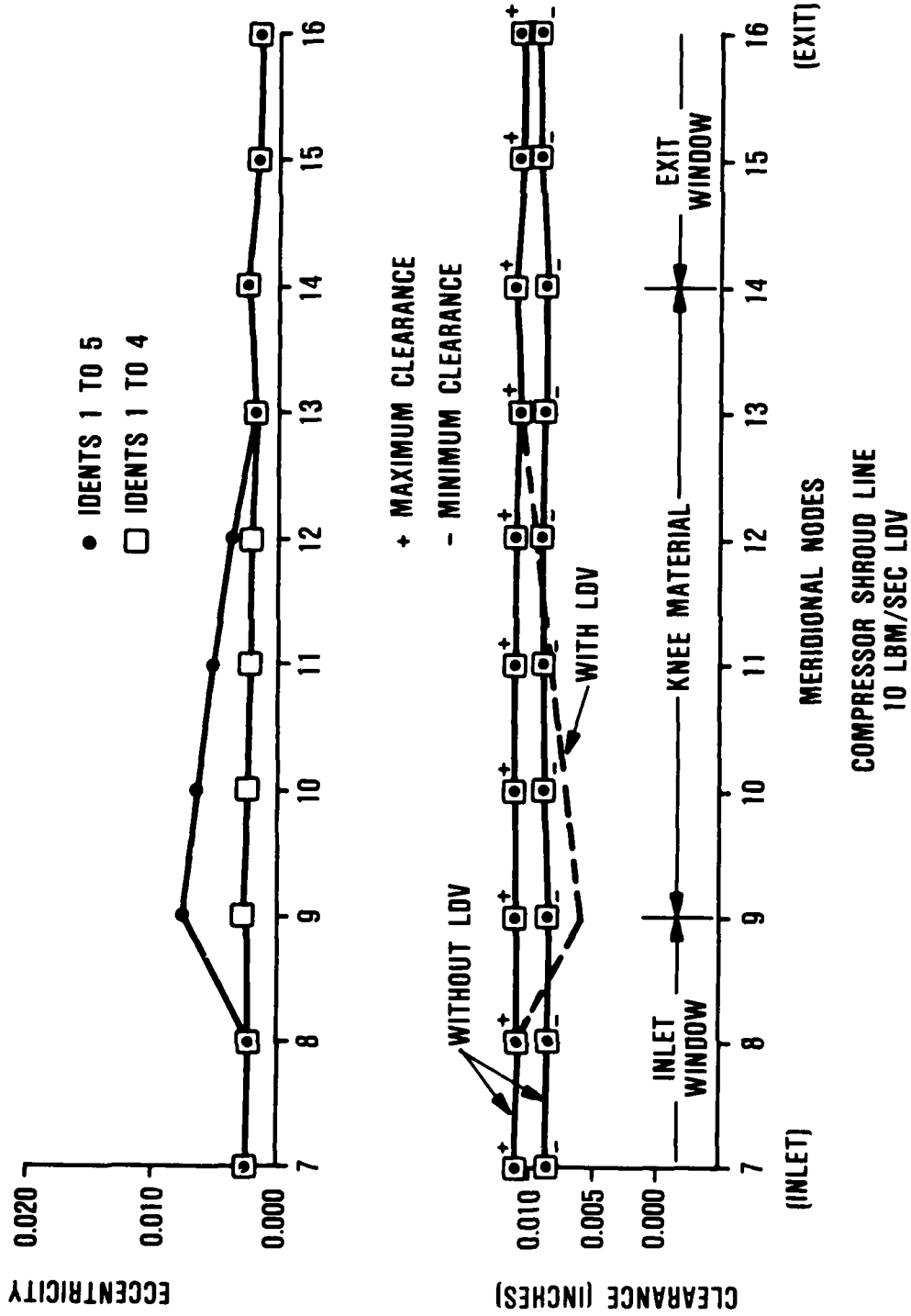


Figure 117. LDV Shroud Deflection (P/N 3553146).

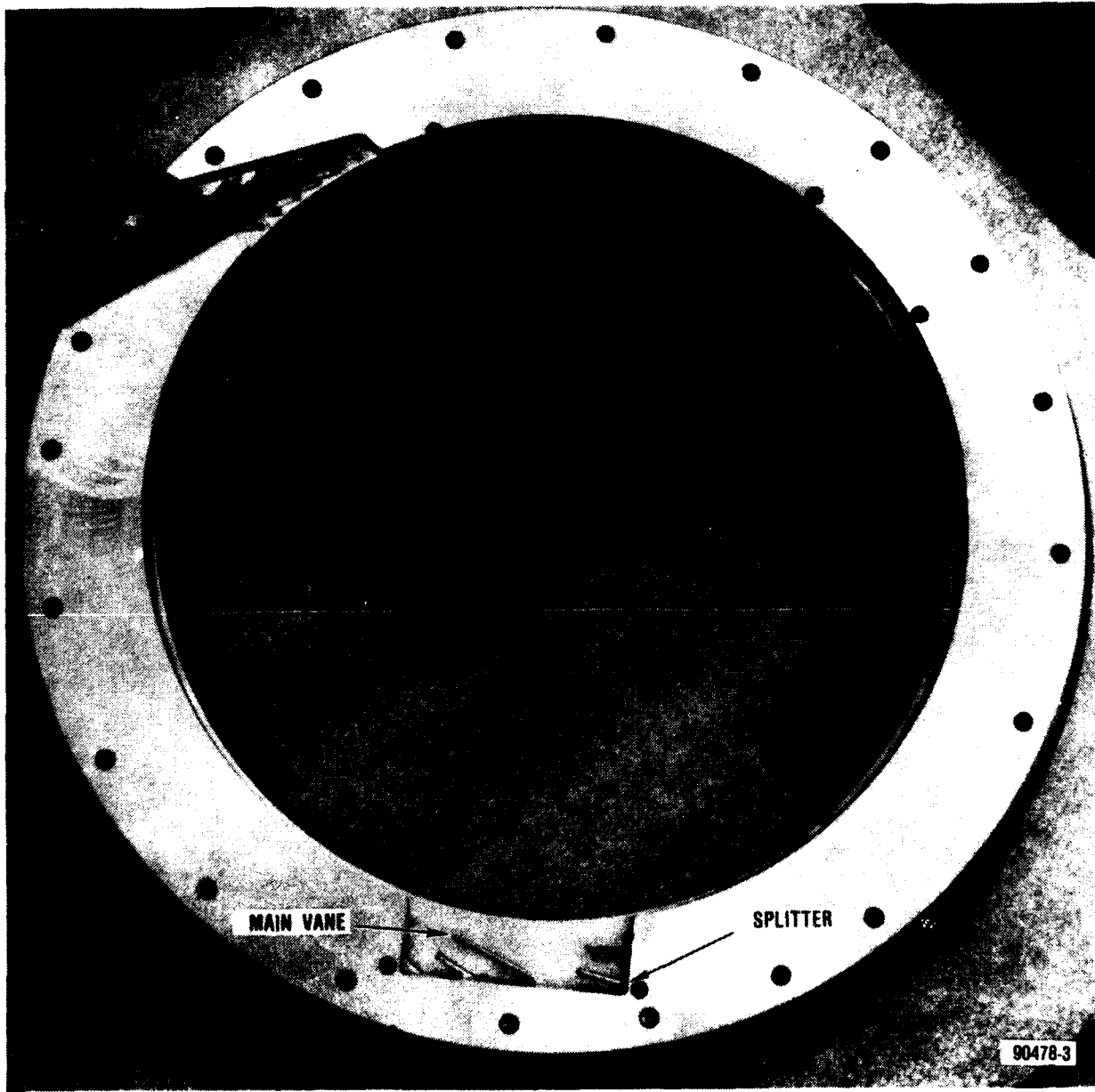


Figure 118. 10-Lb/Sec LDV Diffuser (P/N 3553147-2).

TABLE 12. SUMMARY OF VIBRATION ANALYSIS.

Frequency (hz)	Vane		Splitter	
	Fully Supported	Cantilevered	Fully Supported	Cantilevered
f <sub>1</sub>	37,163	11,039	38,230	14,479
f <sub>2</sub>	59,218	14,201	70,758	21,599
f <sub>3</sub>	66,285	19,313	72,931	36,780
f <sub>4</sub>	67,900	30,143	75,936	47,616
f <sub>5</sub>	70,721	39,552	88,472	72,119

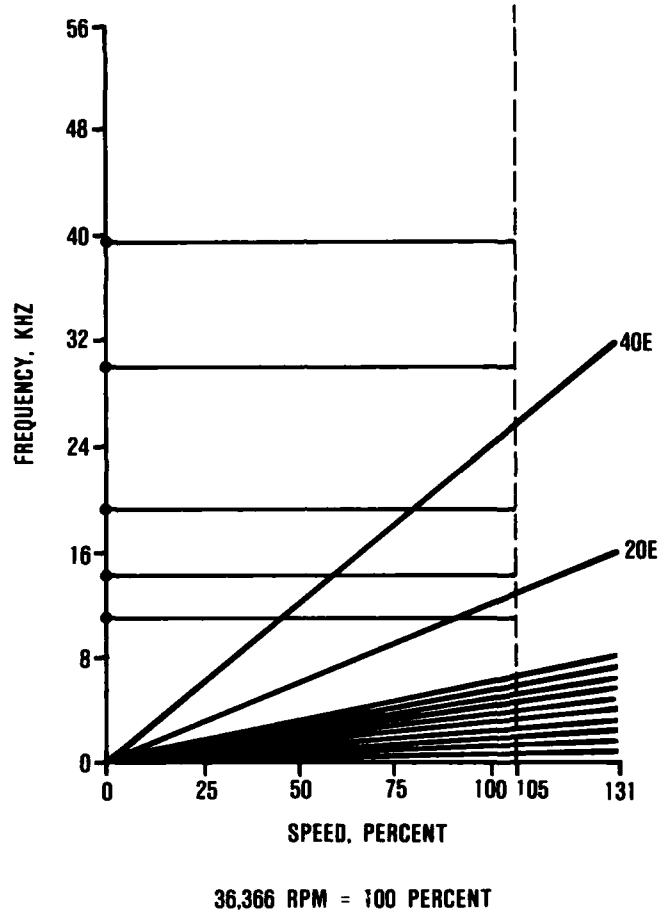


Figure 119. Campbell Diagram for Cantilevered Vane.

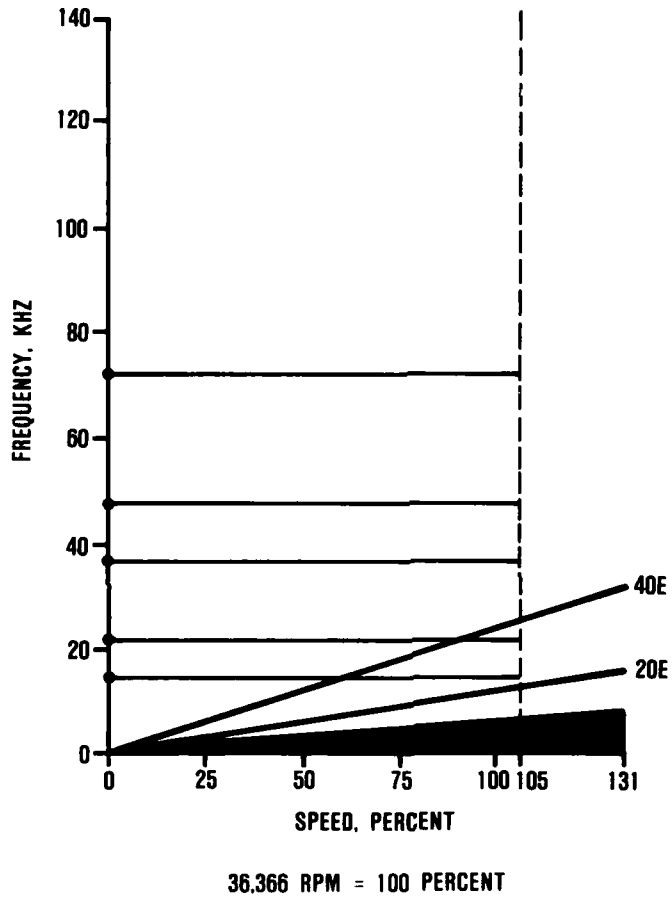


Figure 120. Campbell Diagram for Cantilevered Splitter.

is possible to excite mode 1 with a 20E excitation (20 full blades on the impeller) at 91-percent speed. The splitter Campbell diagram shows that it is possible to excite mode 2 with a 40E excitation (20 full blades and 20 splitter blades on the impeller) at 91-percent speed. The splitter Campbell diagram shows that it is possible to excite mode 2 with a 40E excitation (20 full blades and 20 splitter blades on the impeller) at 89-percent speed.

The vane and splitter natural frequencies determined from a holography test on the diffuser are summarized in Table 13. The difference between the calculated natural frequencies and those determined from holography can be attributed to the tolerance band on the diffuser vanes and to the inability to exactly duplicate the 10-lb/sec test rig boundary conditions. Based on the holography test, the vane mode 1 could be excited at approximately 70-percent speed (from 20E) and vane mode 2 could be excited at approximately 102-percent speed (from 20E). The splitter mode 1 could be excited at approximately 99-percent speed (from 20E) and at approximately 65-percent speed (from 40E). Both calculated and holographic mode shapes are shown in Figures 121 and 122.

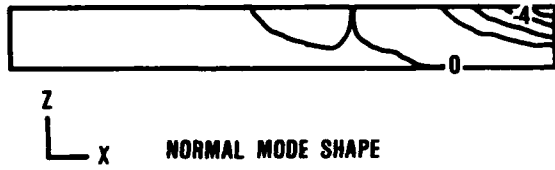
The absolute magnitude of the forcing function that will excite 20/rev and 40/rev is unknown. However, no options exist to eliminate the potential resonance of the vane and splitter modes previously discussed. It was agreed between NASA and GTEC to install strain gages on the cantilevered vanes and to monitor the gage response during the mechanical check run. The strain gages will be removed prior to testing for aerodynamic data.

TABLE 13. HOLOGRAPHY RESULTS

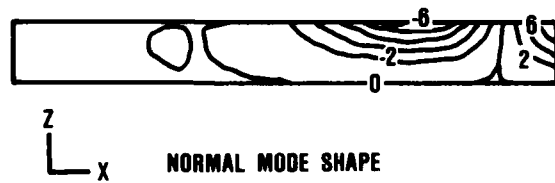
Frequency (hz)	Cantilevered Vane		Cantilevered Splitter	
	Calculated Frequency	Holography Results	Calculated Frequency	Holography Results
$f_1$	11,039	9,022 (8,384)	14,479	12,856(11,947)
$f_2$	14,201	13,355 (12,411)	21,599	28.351(26,347)
$f_3$	19,313	20,293 (18,859)	36,780	--
$f_4$	30,143	30,702 (28,531)	47,616	--

Note: Numbers in parenthesis are corrected from room temperature to 680F.

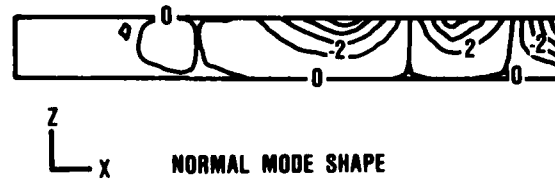
HOLOGRAPHIC



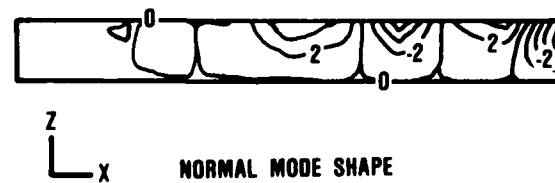
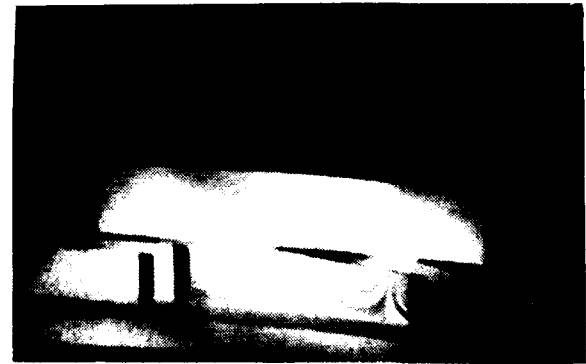
MODE 1



MODE 2



MODE 3



MODE 4



Figure 121. Cantilevered Vane Mode Shapes.

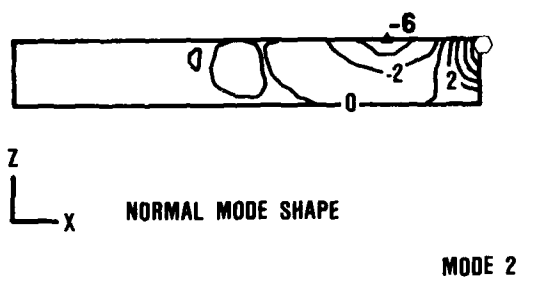
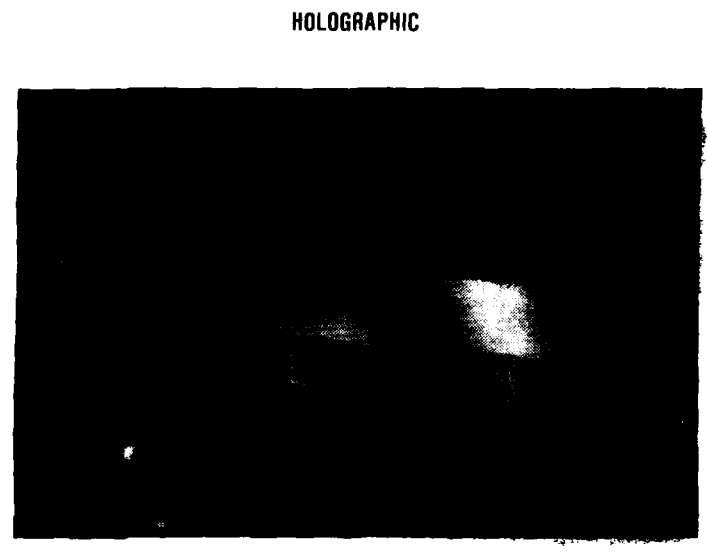
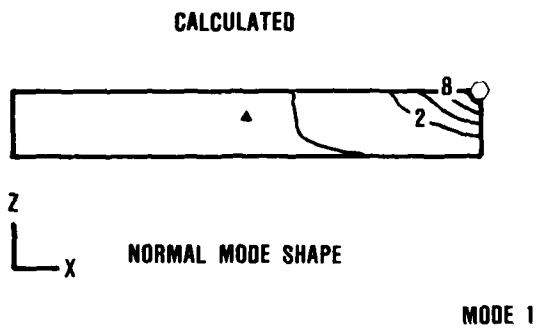


Figure 122. Cantilevered Splitter Mode Shapes.

## 10.0 10-LB/SEC HARDWARE MECHANICAL INTEGRITY

### 10.1 Hardware Inspection

The 10-lb/sec impeller (Figure 123) inspection results were satisfactory. The hub and shroud line contours are shown in Figure 124.

The performance diffuser and LDV diffuser vane contour inspection results (prior to braze) were acceptable and are shown in Figure 125. The LDV diffuser (prior to braze) is shown in Figure 126.

The performance shroud inspection results, which were acceptable, are shown in Table 14. The performance shroud and diffuser assembly is pictured in Figure 127.

Inspection results of the LDV shroud revealed that the flow-path contour was offset axially 0.004 inch from blueprint datums. However, the contour itself was excellent. This was not considered to be a problem since the 10-lb/sec test rig is equipped with a clearance control spindle. The LDV diffuser (P/N 3553147-2) was trimmed 0.004 inch axially to maintain the proper axial offset between shroud and diffuser. Inspection results of the shroud contour with respect to the shroud trailing edge are shown in Table 15.

### 10.2 Impeller Balance

The 10-lb/sec impeller was balanced to the specifications shown in Figure 128.

AD-A174 001

SCALED CENTRIFUGAL COMPRESSOR PROGRAM(U) GARRETT  
TURBINE ENGINE CO PHOENIX AZ 8 CARGILL ET AL.  
31 OCT 86 21-5464 NASA-CR-174912 NAS3-23277

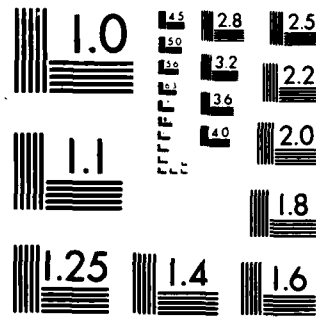
3/3

UNCLASSIFIED

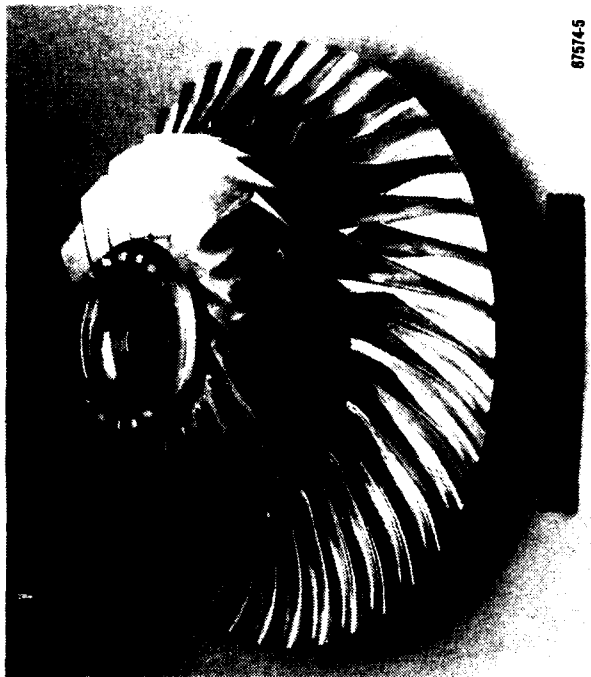
F/G 21/5

NL





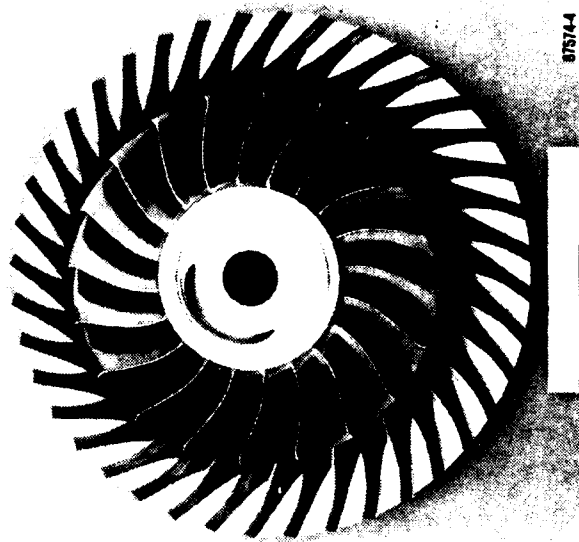
MICROCOPY RESOLUTION TEST CHART  
NATIONAL BUREAU OF STANDARDS 1963 A



875745



875743



875744

Figure 123. NASA 10-Lb/Sec Impeller (P/N 3553144-1).

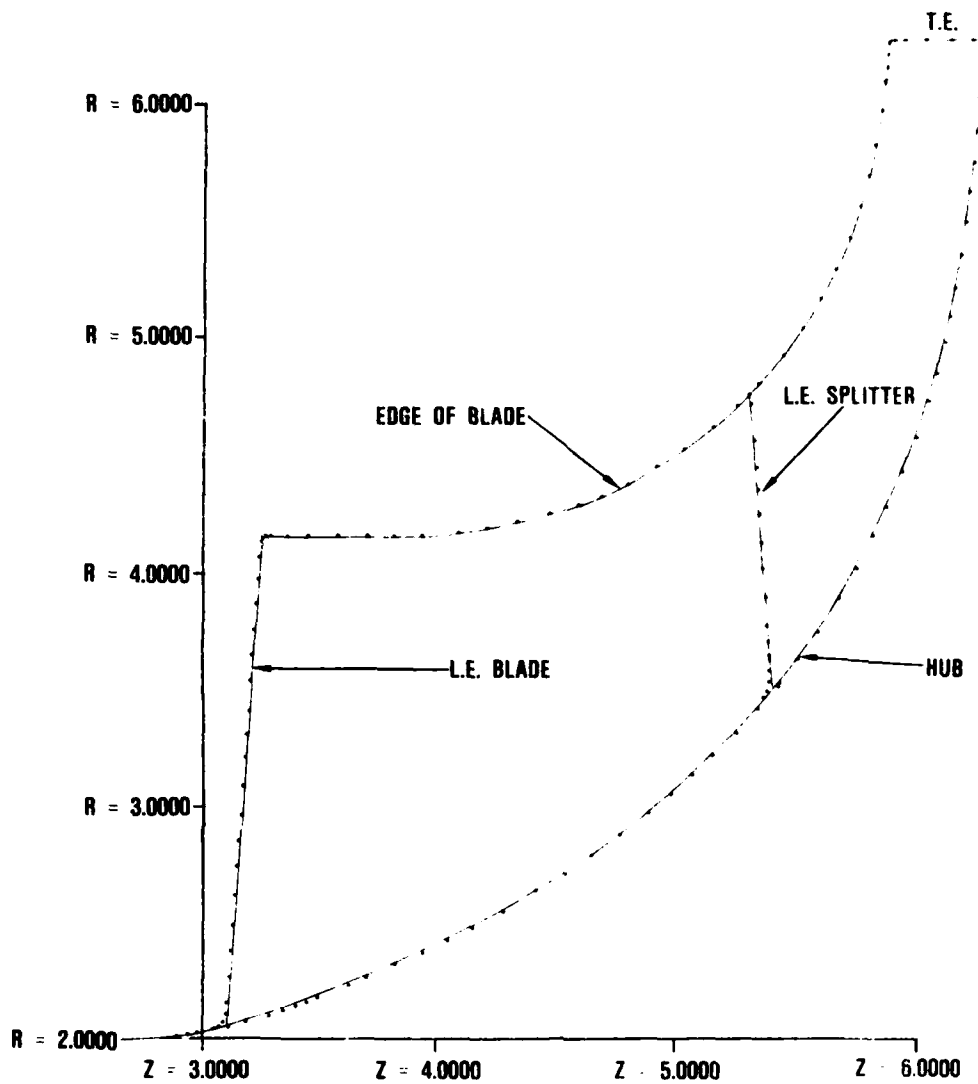


Figure 124. 10-Lb/Sec Impeller Inspection Results  
(P/N 3553144-1) Hub and Shroud Contour.

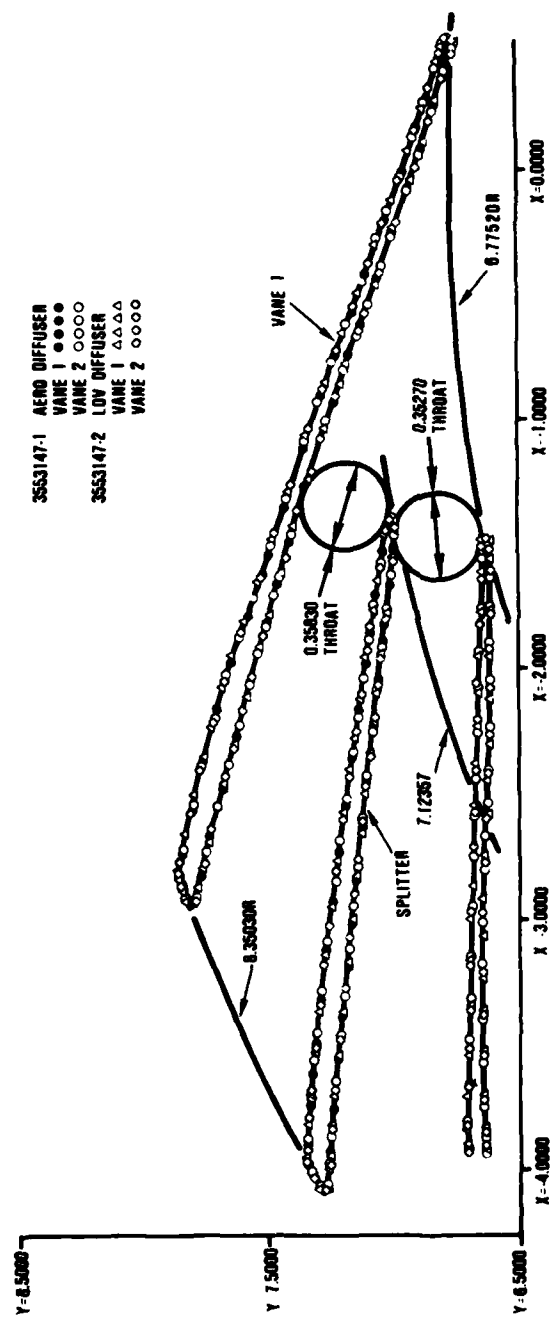


Figure 125. Diffuser Inspection Results.



Figure 126. 10-Lb/Sec LDV Diffuser Prior to Braze.

TABLE 14. PERFORMANCE SHROUD CONTOUR INSPECTION (P/N 3553145-1)

Set -Z- To Nominal, and Measure -R-			
-Z- Nominal	-R- Nominal	-R- Actual	-R-Deviation
003.1082	004.1739	004.1748	000.0009
003.0682	004.1749	004.1750	000.0001
002.9546	004.1817	004.1811	-000.0006
002.8293	004.1927	004.1920	-000.0007
002.6623	004.2075	004.2068	-000.0007
002.5372	004.2200	004.2190	-000.0010
002.3293	004.2458	004.2456	-000.0002
002.1643	004.2764	004.2751	-000.0013
002.0010	004.3145	004.3125	-000.0020
001.8801	004.3489	004.3469	-000.0020
001.6818	004.4168	004.4143	-000.0025
001.4862	004.4919	004.4894	-000.0025
001.2924	004.5717	004.5693	-000.0024
001.0620	004.6726	004.6700	-000.0026
000.8717	004.7603	004.7573	-000.0030
000.6827	004.8511	004.8480	-000.0031
000.4577	004.9633	004.9600	-000.0033
000.2712	005.0589	005.0559	-000.0030
000.0856	005.1562	005.1532	-000.0030
-000.1363	005.2748	005.2723	-000.0025
-000.3204	005.3748	005.3716	-000.0032
-000.5407	005.4963	005.4933	-000.0030
-000.7235	005.5987	005.5958	-000.0029
-000.9421	005.7231	005.7200	-000.0031

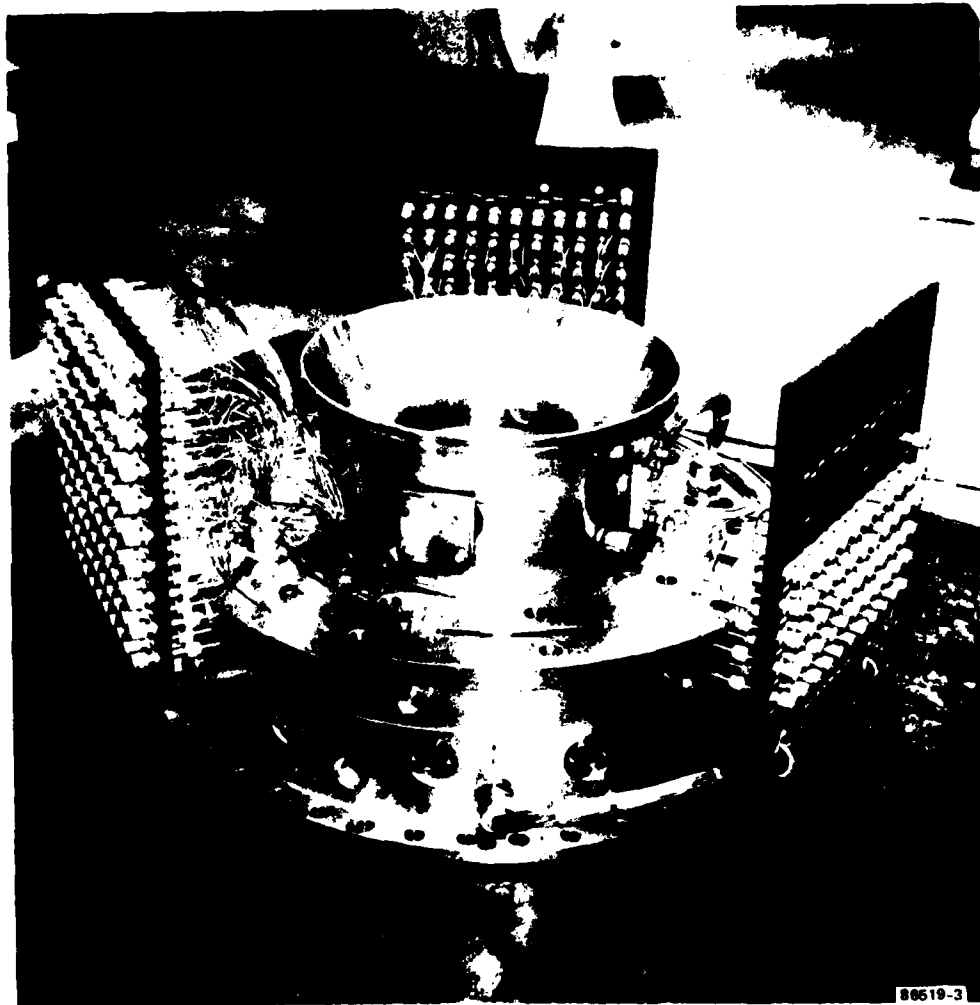


Figure 127. Performance Shroud and Diffuser Assembly.

TABLE 15. 10-LB/SEC LDV SHROUD (P/N 3553146-1)  
FLOW PATH INSPECTION RESULTS.

SET -R- TO NOMINAL, AND MEASURE -Z-			
-R- Nominal	-Z- Nominal	-Z- Actual	-Z- Deviation
006.3861	005.9233	005.9233	-000.0000
006.2058	005.9120	005.9113	-000.0007
006.0811	005.8994	005.8985	-000.0009
005.9371	005.8794	005.8779	-000.0015
005.8290	005.8594	005.8580	-000.0014
005.7347	005.8394	005.8373	-000.0021
005.6540	005.8194	005.8165	-000.0029
005.5843	005.7994	005.7970	-000.0024
005.5216	005.7794	005.7779	-000.0015
005.4661	005.7594	005.7590	-000.0004
005.4131	005.7394	005.7394	000.0000
005.3627	005.7194	005.7192	-000.0002
005.3149	005.6994	005.6996	000.0002
005.2607	005.6794	005.6752	-000.0042
005.2270	005.6594	005.6598	000.0004
005.1588	005.6244	005.6249	000.0005
005.0919	005.5844	005.5850	000.0006
005.0293	005.5444	005.5456	000.0012
004.9710	005.5044	005.5050	000.0006
004.9167	005.4644	005.4652	000.0008
SET -Z- TO NOMINAL, AND MEASURE -R-			
-Z- Nominal	-R- Nominal	-R- Actual	-R- Deviation
005.4244	004.8663	004.8649	-000.0014
005.3844	004.8189	004.8176	-000.0013
005.3444	004.7748	004.7740	-000.0008
005.2994	004.7290	004.7275	-000.0015
005.2394	004.6716	004.6706	-000.0010
005.1794	004.6192	004.6186	-000.0006
005.1194	004.5721	004.5715	-000.0006
005.0594	004.5279	004.5273	-000.0006
004.9944	004.4833	004.4829	-000.0004
004.9144	004.4336	004.4332	-000.0004
004.8344	004.3908	004.3901	-000.0007
004.7394	004.3450	004.3450	000.0000
004.6344	004.3010	004.3006	-000.0004
004.5044	004.2580	004.2581	000.0001
004.3294	004.2148	004.2152	000.0004
004.1094	004.1820	004.1822	000.0002
003.8894	004.1688	004.1691	000.0003
003.6694	004.1680	004.1678	-000.0002
003.4494	004.1672	004.1672	000.0000
003.3345	004.1667	004.1666	-000.0001

BALANCE (0.0341 OZ.-IN. ACTUAL)  
PLANE F (0.037 OZ.-IN. REQUIRED)

BALANCE (0.0319 OZ.-IN. ACTUAL)  
PLANE G (0.049 OZ.-IN. REQUIRED)

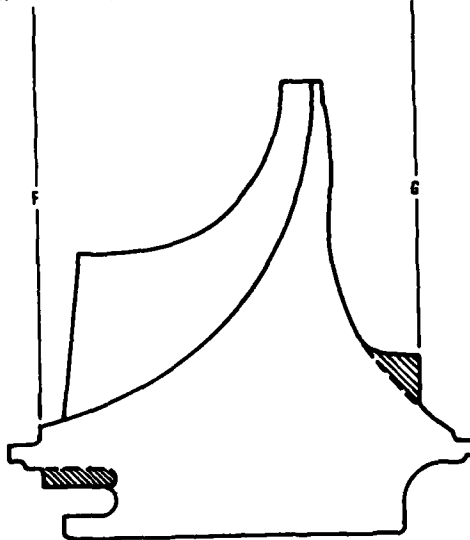


Figure 128. 10-Lb/Sec Balance Plane Results.

## 11.0 CONCLUSIONS AND RECOMMENDATIONS

The modifications that were made to the 2-lb/sec test rig will provide NASA with a safe and durable test rig capable of operating with a 0.004 inch impeller-to-shroud clearance. GTEC strongly recommends that the 0.004-inch operating clearance be approached in gradual increments (i.e., 0.015-inch clearance, 0.010 inch clearance, 0.007 inch clearance, etc.).

The 2-lb/sec compressor duplicates (within the design constraints) the aerodynamic design of the baseline compressor. The 10-lb/sec impeller is an exact scale of the 2-lb/sec impeller. Both 10-lb/sec shrouds are thermal scales of a baseline 25-lb/sec shroud designed for the U.S. Air Force under Contract F33615-74-C-2006. Both the 2-lb/sec and the 10-lb/sec hardware furnished under this contract will facilitate the acquisition of meaningful test data that will fulfill the overall program objectives.

## REFERENCES

1. Hermann Schlichting, Boundary Layer Theory, (Translated by J. Kestin.) 4th Edition, New York, McGraw-Hill, 1960.
2. J.A. Broadstone, Control of Surface Quality, Unpublished Paper Available from Surface Checking Gage Company, Hollywood, California.

DISTRIBUTION LIST

NASA Lewis Research Center  
21000 Brookpark Road  
Cleveland, OH 44135  
Attn: G.J. Skoch, 77-6  
A.A. Spence, 500-305  
M. Tharp, 86-1  
Report Control, 60-1  
Library, 60-3

NASA Scientific and  
Technical Information  
Facility  
Attn: Accessioning Dept.  
P.O. Box 8757  
Balt./Wash./Int'l Airport  
MD 21240

Director  
Propulsion Directorate, 77-12  
US Army Aviation Research and  
Technology Activity-AVSCOM  
21000 Brookpark Road  
Cleveland, OH 44135-3127

Director  
Aviation Applied Technology  
Directorate  
US Army Aviation Research  
and Technology Activity-  
AVSCOM  
Attn: SAVRT-TY-AT  
Ft. Eustis, VA 23604-5577

Director  
US Army Aviation Research  
and Technology Activity-  
AVSCOM  
Attn: SAVRT-R, 207-5  
Ames Research Center  
Moffett Field, CA 94035-1099

Director  
US Army Aviation Research  
and Technology Activity-  
AVSCOM  
Attn: SAVRT-M, 206-4  
Ames Research Center  
Moffett Field, CA 94035-1099

Commander  
US Army Aviation Systems Command  
Attn: AMSAV-N (Titus)  
4300 Goodfellow Blvd  
St. Louis, MO 63120-1798

Commander  
US Army Aviation Systems Command  
Attn: AMSAV-EQP  
4300 Goodfellow Blvd  
St. Louis, MO 63120-1798

Commander  
US Army Troop Support Command  
Attn: AMSTR-DIL (Ms Feng)  
4300 Goodfellow Blvd  
St. Louis, MO 63120-1798

Commander  
US Army Mobility Equip. R&D  
Command  
Attn: STRBE-ZT, Mr. Dinger  
Ft. Belvoir, VA 22060

Commander  
US Army Tank-Automotive R&D  
Command  
Attn: AMSTA-RGE, Mr. Whitcomb  
Warren, MI 48090

Dr. Donald Dix  
Staff Specialist for  
Propulsion  
OSD/OUSDR&E(ET)  
Rm 1809, The Pentagon  
Washington, D.C. 20301

Commander  
Army Research Office  
Attn: Dr. R. Singleton  
P.O. Box 12211  
Research Triangle Park,  
NC 27709

Commandant  
US Military Academy  
Attn: Chief, Dept. of  
Mechanics  
West Point, NY 10996

DISTRIBUTION LIST

Commander  
Southwest Research Institute  
US Army Fuels & Lubricants  
Research Laboratory  
P.O. Drawer 28510  
San Antonio, TX 78284

Department of the Army  
Aviation Systems Division  
ODCSRDA (DAMA-WSA, R. Ballard)  
Room B454, The Pentagon  
Washington, D.C. 20310

US Army Materiel Systems  
Analysis Activity  
Attn: DRXSY-MP  
(Mr. Herbert Cohen)  
Aberdeen Proving Grd.,  
MD 21005-5055

Director, Turbopropulsion  
Laboratory  
Code 67Sf  
Naval Postgraduate School  
Monterey, CA 93940

Mr. Richard Alpaugh  
US DOE  
1000 Independence Ave  
Washington, D.C. 20585

Mr. Bill Cleary  
Associate Division Director  
ORI, Inc.  
1375 Piccard Drive  
Rockville, MD 20850

END

12-86

DTIC